LINGO proteins - novel inactivating regulatory subunits of BK channels

A thesis submitted to the

School of Health & Science,

Dundalk Institute of Technology

For the degree of **Doctor of Philosophy**

By

Shruti G. Kulkarni M.Sc.

July 2022

Under the supervision of **Prof. Mark A. Hollywood** &

Co-supervision of **Prof. Keith D. Thornbury**

Declaration

We, the undersigned declare that this thesis entitled LINGO proteins - novel inactivating regulatory subunits of BK channels is entirely 2 own work and has not been taken from the work of others, except as cited and acknowledged within the text.

The thesis has been prepared according to the regulations of Dundalk Institute of Technology and has not been submitted in whole or in part for an award in this or any other institution.

Author Name: Shruti G. Kulkarni

Author Signature: 

Date: 07/07/2022

Supervisor Name: Prof. Mark A. Hollywood

Supervisor Signature: 

Date: 07/07/2022

Acknowledgements

I would like to express my sincere gratitude to my project supervisor, Prof. Mark Hollywood for his continuous support, guidance, motivation and invaluable insight over the last 4 years. I would also like to thank Prof. Keith Thornbury and Prof. Gerard Sergeant for their support and invaluable suggestions on this project.

I am deeply grateful to our post-doctoral researchers Dr. Roddy Large, Dr. Srikanth Dudem and Dr. Nicholas Mullins who provided excellent training during my time in the lab. I am very grateful to Dr. Nicholas Mullins for synthesising countless peptides for my experiments. I would like to offer a special thanks to Dr. Srikanth Dudem and Dr. Roddy Large for their experimental contributions in this thesis. I would like to extend my sincere thanks to Billie McIlveen, who provided great technical and emotional support throughout this project.

I am very grateful to have worked alongside Leanna, Nicole, Rabab, Ritu, Ruth, Tuleen and Vishakha through every stage of this project. Thank you for the excellent craic, encouragement, and friendship over the years. I am extremely thankful to my housemates Abira and Poorani for their friendship and support. I would also like to extend my thanks to Maeve and Patrick for making me feel at home in Ireland.

I am very grateful to my mentor Dr. Mahendra Sonawane and my friends Aditya, Antara and Indraneel for their guidance and support in my early days as a researcher at Tata Institute of Fundamental Research, India. I am extremely thankful to my friends Abhijeet, Adwait, Ketakee, Pooja, Rujuta and Swapnil for their friendship and immense support.

Most importantly, my warm and heartfelt thanks go to my family, my grandparents, my aunts and uncles, my parents Girija and Gururaj and to my brother Shreyash for their unconditional, unequivocal and loving support. Last but not the least, I am enormously thankful to my dear husband Kunal for his encouragement and loving support.

Table of Contents

Glossary

Å	Angstrom
aa	Amino acid
Ac	Acylated
Ac-Am	Acylated-amidated
AHR	Airway hyperactivity
AMIGO	Amphoterin-induced gene and ORF
ANOVA	Analysis of variance
ASM	Airway smooth muscle
Ba^{2+}	Barium ion
BK	Big potassium
BK_L	BK like
BLAST	Basic local alignment search tool
Bp	Base-pairs
C-terminus (COOH)	Carboxy terminus
C_{10}	Decyltriethylammonium
Ca^{2+}	Calcium ion
cDNA	Complimentary DNA
Cl^-	Chloride ion
CNG	Cyclic nucleotide-gated
CNS	Central nervous system
COPD	Chronic obstructive pulmonary disease
Cryo-EM	Electron cryomicroscopy
CTD	Cytosolic tail domain
CTX	Charybdotoxin
DHA	Docosahexaenoic acid
DHS-I	Dehydrosoyasaponin1
DiBAC	Bis-(1,3-dibutylbarbituric acid) trimethine oxonol
DMEM	2 2 2
DMSO	Dimethylsulfoxide
dNTPs	Deoxyribonucleotide triphosphates
dsDNA	Double stranded DNA

dSlo	Drosophila slowpoke
DTT	Dithiothreitol
E. coli	Escherichia coli
EAQ	Ether-a-go-go-related
EBP	Enhanced ball peptide
EDTA	Ethylenediaminetetraacetic acid
EGF	Epidermal growth factor
eGFP	Enhanced Green fluorescent protein
EGFR	Epidermal growth factor receptor
eLRRs	Extracellular leucine rich repeats
Erb-B2	Receptor Tyrosine Kinase 2
FBS	Fetal Bovine serum
FN3	Fibronectin type-3
FV	Fluorescence-Voltage
G(V)	Conductance versus voltage
GPCR	G-protein-coupled receptors
G_{max}	Maximal conductance
HA	Horrigan-Aldrich
HCS	Highly conserved segment
HEK	Human embryonic kidney
Hz	Hertz
I	Current
IbTX	Iberiotoxin
IC_{50}	Half maximal inhibitory concentration
Ig	Immunoglobulin
IK	Intermediate-conductance potassium
I_{max}	Maximal control current
ISLR	Immunoglobulin superfamily containing leucine-rich repeat
IV	Current-Voltage relationship
K^+	Potassium ion
K2p	Two-pore domain background potassium
KATP	Adenosine triphosphate sensitive potassium

K_{Ca}	Calcium-activated potassium
kDa	Kilodalton
kHz	Kilohertz
K_{ir}	Inward rectifier potassium
K_v	Voltage-gated potassium
K_vLQT	Voltage-gated potassium long QT
LB	Luria-Bertani
LINGO	Leucine Rich Repeat and Ig domain-containing, Nogo Receptor-interacting protein
LNCaP	Lymph node carcinoma of the prostate
LRR	Leucine Rich Repeat
LRRC	Leucine Rich Repeat containing
LRRCT	Leucine Rich Repeat C-terminal domain
LRRNT	Leucine Rich Repeat N-terminal domain
M	Molar
MAG	Myelin-associated glycoprotein
MEM	Minimum essential medium
Mg^{2+}	Magnesium ion
l	Microlitres
M	Micromolar
ml	Millilitres
mM	Millimolar
mRNA	Messenger RNA
ms	Millisecond
MS	Multiple sclerosis
MthK	Methanobacterium thermoautotrophicum potassium
mV	Millivolt
m	Milliohm
N-terminal	Amino terminus
nA	Nanoampere
Na^+	Sodium ion
NCAM	Neural cell adhesion molecule
NCBI	National Center for Biotechnology Information

NFW	Nuclease-free water
NGL	Netrin-G ligand
NgR	Nogo receptor
NH_4^+	Ammonium ion
NLRR	Neuronal leucine rich repeat
nM	Nanomolar
ns	not statistically significant
OAB	Overactive bladder
ºC	Degree Celsius
Oligo Calc	Oligonucleotide Properties Calculator
OMgp	Oligodendrocyte-myelin glycoprotein
P_0	Open probability
pA	Picoampere
PCR	Polymerase chain reaction
PD	2
PDB	Protein database
PGD	Pore gating domain
pH	Potential of hydrogen
pS	Picosiemens
Q-PCR	Quantitative PCR
QA	Quaternary ammonium
R	Resistance
R_a	Access resistance
Rb^+	Rubidium ion
RCK	Regulator of K^+ conductance
RI	Ribonuclease inhibitor
R_p	Pipette resistance
rpm	Revolutions per minute
R_s	Series resistance
RT	Room temperature
RT-PCR	Reverse transcriptase polymerase chain reaction
SALM	Synaptic adhesion-like molecules
ShB	Shaker ball peptide

SK	Small potassium
Slo	Slowpoke
SOC	Super optimal broth with catabolite repression
Sr^{2+}	Strontium ion
STOCs	Spontaneous transient outward K^+ currents
TAE	Tris Acetate-EDTA
TBA	Tetrabutylammonium
TEA	Tetraethylammonium
Tl^+	Thallium ion
TLE	Temporal lobe epilepsy
TM	Transmembrane
TP	Tail peptide
TPAB	Tetrapentylammonium bromide
TrkB	Tropomyosin receptor kinase B
TRP	Transient receptor potential
U	Units
UV	Ultraviolet
V	Volts
$V_{1/2}$	Half maximal activation voltage
VDCC	Voltage dependent calcium channel
VSD	Voltage sensing domain
WT	Wildtype
	Micro
	Alpha
	Beta
	Gamma
$_{inact}(\ _i)$	Time constant of inactivation
$[Ca^{2+}]_i$	Intracellular calcium concentration
$[K^+]$	Potassium ion concentration

Publications

Scientific papers in various peer reviewed journals:

Dudem, S., Large, R. J., Kulkarni, S., McClafferty, H., Tikhonova, I. G., Sergeant, G. P., Thornbury, K. D., Shipston, M J., Perrino, B. A., and Hollywood M. A. (2020). LINGO1 is a novel regulatory subunit of large conductance, Ca^{2+}-activated potassium channels. *Proceedings of the National Academy of Sciences of the USA, 117*(4), 2194-2200.

The work related to this thesis was presented at different national and international scientific meetings:

Posters:

1) Kulkarni S**,** Dudem S, Large RJ, Sergeant GP, Thornbury KD, & Hollywood MA. Novel putative regulatory subunits of BK channels. BREATH annual conference, 19-20 June 2018, Dundalk, Ireland.
2) Kulkarni S, Dudem S, Large RJ, Martin L, Rehill J, Sergeant GP, Thornbury KD, & Hollywood MA. Lingo Proteins Novel Regulatory Subunits of BK Channels? Irish Thoracic Society, 23-24 November 2018, Belfast, Northern Ireland.
3) Kulkarni S**,** Dudem S, Large RJ, Sergeant GP, Thornbury KD and Hollywood MA. LINGO proteins - novel inactivating regulatory subunits of BK channels. FASEB Smooth Muscle Conference, 13-19 July 2019, West Palm Beach, Florida, USA.
4) Kulkarni S, Dudem S, Large RJ, Mullins N, Martin SL, Reihill J, Sergeant GP, Thornbury KD & Hollywood MA. LINGO1 inactivation of BK channels depends on positively charged residues in the LINGO1 intracellular tail. Irish Thoracic Society, 22-23 November 2019, Galway, Ireland.

Oral Presentations:

1) Novel putative regulatory subunits of BK channels at BREATH annual conference, 19-20 June 2018, Dundalk, Ireland.
2) Lingo Proteins - Novel Regulatory Subunits of BK Channels? Irish Thoracic Society, 23-24 November 2018, Belfast, Northern Ireland.
3) LINGO proteins - novel regulatory subunits of BK channels at BREATH annual conference 19-21 June 2019, Belfast, Northern Ireland.
4) LINGO1 inactivation of BK channels depends on positively charged residues in the LINGO1 intracellular tail at Irish Thoracic Society meeting held on 22-23 November 2019, Galway, Ireland.
5) Assessing the contribution of individual residues in the LINGO1 tail peptide to inactivation of BK channels at the annual BREATH conference held virtually from 15-17 June 2020.
6) The effects of LINGO1 tail peptide are reduced by mutations in the S6 helix of BK channels at the annual BREATH conference held virtually from 21-23 June 2021.

Abstract

LINGO proteins - novel inactivating regulatory subunits of BK channels

Large-conductance, voltage- and Ca^{2+}-regulated potassium (BK) channels are widely expressed across several tissues including smooth muscle, brain, kidney and thymus (Butler *et al.* 1993; Garcia-Calvo *et al.* 1994; Pallanck and Ganetzky 1994). These channels consist of tetrameric subunits and associated auxiliary or subunits, which can modulate their biophysical and pharmacological properties (Orio *et al.* 2002; Gessner *et al*. 2005; Latorre *et al.* 2017). Since the four subunits are Leucine Rich Repeat (LRR) proteins, we examined if other LRR proteins such as LRR and Ig domain-containing, Nogo Receptor-interacting protein, LINGO1, and its subtypes modulated BK channels. The aim of this study was to investigate the interacting partners between BK and LINGO proteins. In order to achieve this, we 1) examined the effects of the LINGO tail peptides on the BK channels, 2) investigated the effect of LINGO1 tail residues on BK channel inactivation, 3) elucidated the role of net positive charge and positively charged residues in LINGO1 tail peptide-mediated inactivation of BK channels.

Patch-clamp experiments in the inside-out configuration were performed with LINGO tail peptides to determine their effects on BK channels. Site-directed mutagenesis was used to examine if the BK pore mutants altered the interaction with LINGO1 tail peptide. Additionally, the transcriptional expression of the LINGO subtypes in murine bronchial tissue and brain was examined using RT-PCR.

The key findings of my study are:

1. mRNA expression for all four LINGO subtypes was detected in murine airway and brain.

2. The synthetic tail peptides of LINGO1 and LINGO2 inactivated BK currents. However, LINGO4 tail peptide blocked but did not inactivate BK currents.

3. The net positive charge and the position of positive charges in the LINGO1 tail peptide affected its ability to inactivate BK channels.

4. LINGO1 tail peptide appears to insert itself into the pore of the BK channel and may compete with quaternary ammonium ions for a common binding site.

5. The positively charged residues of LINGO1 tail peptide may interact with negatively charged residues in the S6 helix of the BK channel.

In conclusion, the results of this thesis indicated that the last 8-residues of LINGO1 protein mimic the inactivation of the full-length LINGO1 protein, co-expressed with BK . Furthermore, these data suggest that LINGO peptides interact with BK channels and inactivation may occur by a mechanism involving charged and uncharged residues of the BK channel pore.

1. Review of the literature

1.1 Ion channels

Ion channels form macromolecular pores in cell membranes and play a critical role in both excitable and non-excitable cells by permitting the selective movement of ions through these aqueous pores. Ion channels are selectively permeable to a limited class of ions whose direction of flow through the ion channel depends on the electrochemical gradients. The main types of channel include Na^+, K^+, Ca^{2+}, Cl^- and TRP ion channels all of which have distinct ion selectivities. These channels can respond to a variety of stimuli either evoked by a change in membrane potential or a ligand, which can open or close the channel and thereby modulate cellular activity. They play central roles in physiological processes as diverse as modulation of blood pressure, secretion of hormones, release of neurotransmitters, regulation of membrane potential and excitability, modulate the shape of action potentials, trigger muscle contraction, control exocytosis and help regulate cell volume (Hille, 2001; Di Resta and Becchetti, 2010).

1.1.1 K^+ channels

K^+ channels are a diverse family of membrane proteins, abundantly found in excitable and non-excitable cells and are selectively permeable to K^+ ions. In the human genome, at least 90 genes code for the potassium channel subunits (Tian *et al.* 2014). These pore forming subunits are broadly classified into four structural classes (Wei *et al.* 1996; González *et al.* 2012; Figure 1.1). Firstly, the inward rectifier K^+ channels (K_{ir}), which contains two transmembrane (TM) domains and their subunits assemble as tetramers (González *et al.* 2012). Secondly, the two-pore four TM domains K^+ channels (K2p), which contains four TM domains and their subunits assemble as dimers (González *et al.* 2012). Thirdly, six TM domains K^+ channels which can be divided into four families of which, voltage-gated potassium channels (K_v), voltage-gated KCNQ-type (KCNQ) are gated by voltage, ether-a-go-go (Eag) is gated by voltage and cyclic nucleotides and small-conductance K^+ channels (SK) are gated by calcium (González *et al.* 2012). Finally, the members of the *Slo* family of potassium channels some of which have seven TM domains (Meera *et al.* 1997) and are gated by both voltage and calcium or pH (Schreiber *et al.* 1998).

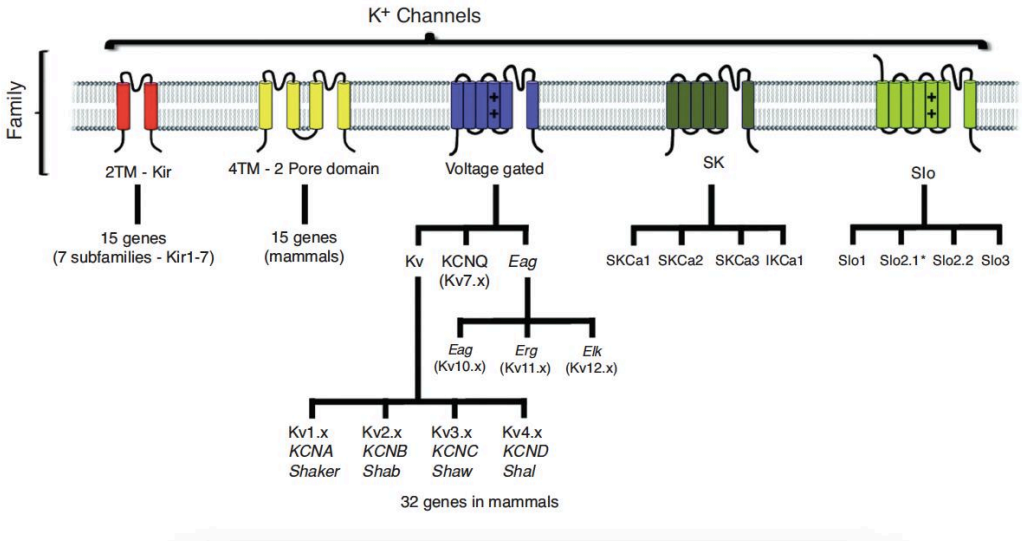

Figure 1.1: Classification of potassium channel families based on structure.
Potassium channel families are broadly classified into 4 groups namely, two transmembrane segments (2TM; Kir), 4TM (2-pore domain), 6TM (voltage gated and SK), and 7TM (Slo). Note that for the sake of simplicity the large-conductance Slo channel family includes the Slo2.x channels, which have only six transmembrane domains (Adapted from González *et al.* 2012).

The K_{ir} channels have seven subfamilies called $K_{ir}1$-$K_{ir}7$. They are further grouped into four categories based on their functional roles *viz.* 1) classical K_{ir} ($K_{ir}2.x$) which are constitutively active, 2) G-protein-gated K_{ir} channels that are regulated by G-protein-coupled receptors (GPCR), 3) ATP-sensitive K^+ channels (KATP) which are involved in cellular metabolism and 4) K^+ transport channels ($K_{ir}1.x$, $K_{ir}4.x$, $K_{ir}5.x$ and $K_{ir}7.x$) (Nichols *et al*. 1997; Grover *et al.* 2000).

The K2p channels have 16 members and they are further grouped into 6 main structural and functional classes namely, 1) tandem of P domains in weak inwardly rectifying TWIK-1, TWIK-2 and KCNK7 channels, 2) mechano-gated and arachidonic acid-activated TWIK-related TREK-1, TREK-2 and TRAAK channels, 3) TWIK-related acid-sensitive TASK-1, TASK-3 and TASK-5 channels, 4) tandem PD halothane-inhibited THIK-1 and THIK-2 channels, 5) TWIK-related alkaline-pH-activated TALK-1, TALK-2 and TASK-2 channels and 6) TWIK-related spinal cord TRESK channel, which is regulated by intracellular calcium (Tian *et al.* 2014).

K_v channels are the most diverse members of the K^+ ion channel family. These proteins are encoded by 40 genes in humans and are subdivided into 12 subfamilies, of which K_v1-K_v4, K_v7, K_v10, K_v11 and K_v12 can form the pore forming subunits. However, K_v5, K_v6, K_v8 and K_v9 subunits act as regulators of K_v channels and can, for example, interact with K_v2 to modify their functional role (Grizel *et al.* 2014; Bocksteins, 2016).

The K_{Ca} channels are activated by intracellular calcium levels and consist of eight members including the big-conductance K_{Ca}1.1 (BK, Slo1), small-conductance K_{Ca}2.1 (SK1), K_{Ca}2.2 (SK2) and K_{Ca}2.3 (SK3), along with intermediate-conductance K_{Ca}3.1 (IK / SK4) and includes the subfamilies K_{Ca}4.1 (Slo2.2), K_{Ca}4.2 (Slo2.1) and K_{Ca}5.1 (Slo3). However, not all the members of the subfamilies are activated by intracellular calcium levels, as exemplified by the K_{Ca}4 and K_{Ca}5 channels which are activated by Na^+ and Cl^- ions (Tian *et al.* 2014).

1.2 BK channel structure

BK channels are frequently referred to in the literature as BK_{Ca}, Maxi K^+, KCNMA1, Slo1 or K_{Ca}1.1 channels. As their name suggests, these channels have a remarkably large single channel conductance (~100-300 pS in symmetrical 100 mM K^+), yet they have an exquisite selectivity for K^+ ions over other cations (Blatz *et al.* 1984; Latorre *et al.* 2017). The channel is made up of subunits, which are encoded by the *KCNMA1* gene. These subunits tetramerise to form functional BK channels (Butler *et al.* 1993; Quirk *et al.* 2001). The hydrophobicity profile illustrated that the subunit of the BK channels has seven TM domains and four cytosolic tail domains (Meera *et al.* 1997; Quirk *et al.* 2001).

The subunit has three distinct functional domains, called the voltage sensing domain (VSD), the pore gating domain (PGD) and the cytosolic tail domain (CTD) (Horrigan, 2012; Cui *et al.* 2015; Miranda *et al.* 2018, Figure 1.2A). Early studies attempted to model the structure of the BK channel using homology models. One example is Figure 1.2B which shows a homology model of BK channels constructed using UCSF Chimera software, based on the combination of the CTD structure of the zebra fish BK channel (PDB ID:3U6N; Yuan *et al.* 2012) and the membrane spanning domain of the K_v1.2–K_v2.1 chimera structure (PDB ID:

2R9R; Long *et al.* 2007) which was then superimposed to the corresponding conserved regions of the MthK channel from *Methanobacterium thermoautotrophicum* (PDB ID: 1LNQ, Jiang *et al.* 2002a; Jiang *et al.* 2002b).

In 2017, Tao *et al.* determined the detailed subunit cryo-EM structure of the BK channel from *Aplysia californica* in the presence of Ca^{2+} and Mg^{2+} ions. Their solved structure measured approximately 110 Å x 130 Å x 130 Å and the bulk of the structure was taken up by the gating ring (PDB ID: 5TJ6, Tao *et al.* 2017, Figure 1.2C). As seen from Figure 1.2C, the side view of the tetrameric BK channel (extracellular side facing upwards) has three distinct regions: 1) transmembrane domain, 2) tandem regulator of K^+ conductance (RCK) domains RCK1 and 3) RCK2. Furthermore, the BK channel cryo-EM structure revealed that the VSD interacted with the pore domain of the same subunit and helped to confirm that the VSD in BK channels were not domain-swapped. Interestingly however, the CTD of each subunit was found to be domain swapped with the transmembrane domain of its neighbouring subunit (Tao *et al.* 2017).

In 2019, Tao and MacKinnon determined the human subunit (hSlo1) cryo-EM structure of the BK channel in the absence and presence of the auxiliary 4 subunit. The reported structures of hSlo1 had four different states of which, two were obtained in the Ca^{2+}-free and Ca^{2+}-bound subunit state and the other two were obtained with and without the subunit namely, Ca^{2+}-free (hSlo1 + 4) complex and Ca^{2+}-bound (hSlo1 + 4) complex and all structures had a resolution of ~4 Å (Tao and MacKinnon, 2019). The hSlo1 cryo-EM structure was, unsurprisingly, practically identical to the cryo-EM structure from *Aplysia californica* (Tao *et al.* 2017; Tao and MacKinnon, 2019). Figures 1.2D and E show the cryo-EM structure of the hSlo1 subunits with and without the 4 subunits, in the presence and absence of Ca^{2+} ions, respectively (Tao and MacKinnon, 2019).

Previous studies have demonstrated that the TM domain of the BK channel had an additional segment (S0) to which the extracellular N-terminal tail of the channel was attached (Wallner *et al.* 1996; Meera *et al.* 1997). Tao *et al.* (2017) demonstrated that the BK channel transmembrane domain consisted of 28 helices, which included the S0 segment, resulting from each of the 7 transmembrane helices in the tetramer. Moreover, the cryo-EM structure of the

BK channel from *Aplysia californica* also revealed that the S0 transmembrane segment was located at the periphery of the VSD (Tao *et al.* 2017). Previous studies demonstrated that the S0 segment was involved in interacting with subunits and modulated the activity of the channel (Wallner *et al.* 1996; Morrow *et al*. 2006; Liu *et al.* 2008; Liu *et al.* 2010). The cryo-EM structure of the BK channel from *Aplysia californica* also helped to confirm that the S0 segment had an extensive surface which faced the lipid membrane and suggested that this feature helped the S0 to interact with subunits (Tao *et al.* 2017).

As mentioned previously, in the BK channel, each subunit consists of three structural components, where 1) the S1-S4 segments form the voltage sensor domain (VSD), additional S0 segment is located before the VSD, 2) the S5-S6 segments form the pore gating domain (PGD), through which the K^+ ions permeate through the channel and 3) the large cytosolic tail domain (CTD) which creates a tetrameric gating ring of two high affinity Ca^{2+} binding sites per subunit (Latorre *et al*. 2006; Wang *et al.* 2009; Tao *et al.* 2017).

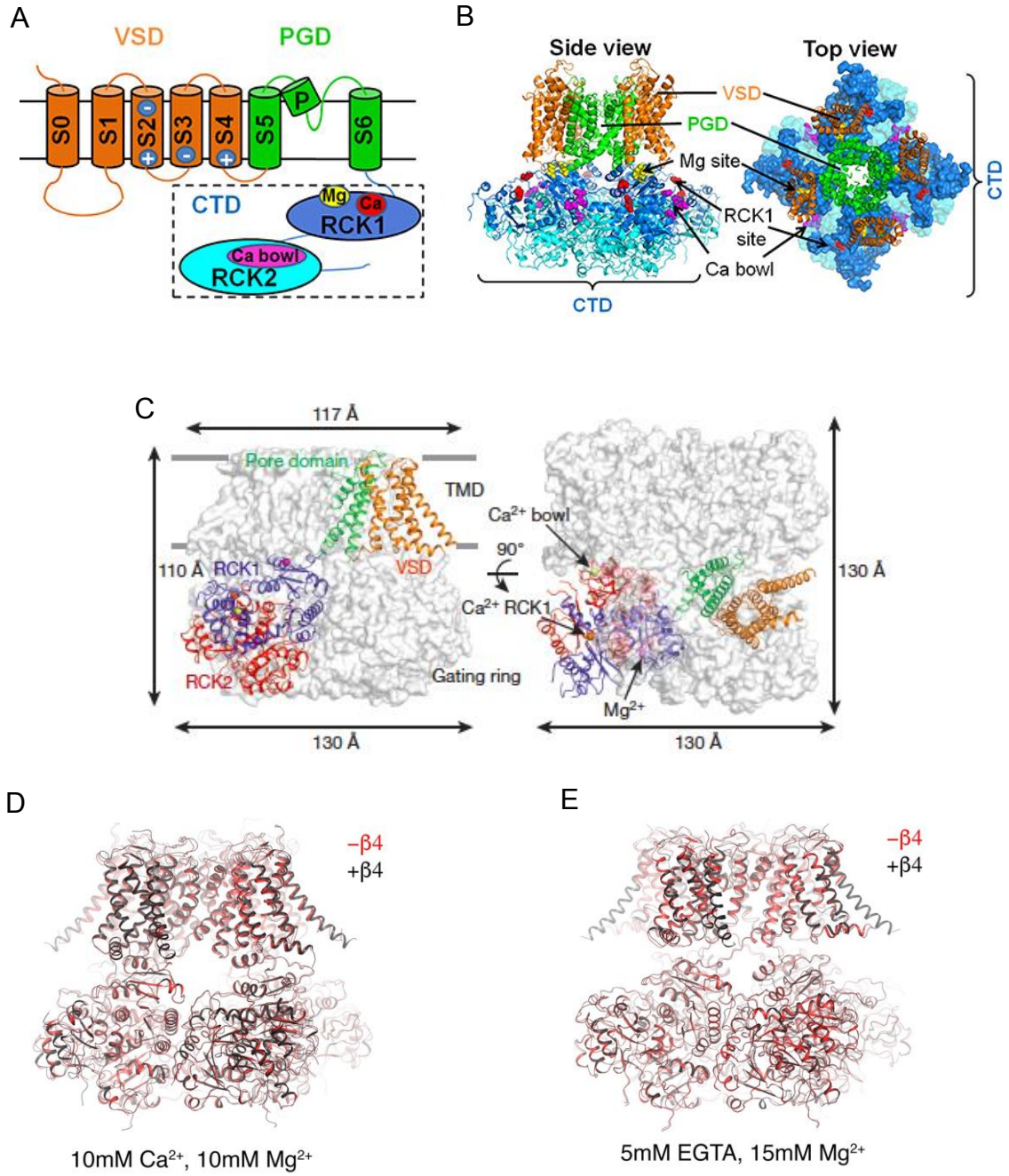

Figure 1.2: Schematic representation and the cryo-EM structure of BK channel.

A subunit of the BK channel showing the VSD, PGD and CTD domains. In the VSD, the blue highlighted charged residues are crucial for voltage sensing. The binding sites for Ca^{2+}, Mg^{2+} are present in the CTD. **B** The homology model of BK channel side and top views. **C** *Aplysia californica* BK tetramer top and side views. The coloured ribbon structures represent the VSD (orange), pore domain (green), RCK1 (blue) and RCK2 (red) whereas the other subunits of the channel are shown in grey. The superimposed structure of human Slo1 in the absence (red) and presence (black) of 4, **D** in Ca^{2+}-bound state and **E** in Ca^{2+}-free state (Adapted from Cui *et al.* 2015; Tao *et al*. 2017; Tao and MacKinnon, 2019).

1.2.1 Voltage sensing domain (VSD)

The construction of a homology model, based on the crystal structures of K_v1.2 - K_v2.1 chimera, along with superimposition of the MthK selectivity filter from *Methanobacterium thermoautotrophicum* and the BK channel gating ring, suggested that the BK VSD associated with PGD of the channel (Long *et al.* 2005; Long *et al.* 2007; Lee *et al.* 2010). This association was proposed to occur via physical connection of the VSD-PGD through the S4-S5 linker (Lu *et al.* 2002; Long *et al.* 2005; Long *et al.* 2007; Figure 1.3A), interaction of the S4-S5 linker with the cytosolic side of the S6 segment (Lu *et al.* 2001; Lu *et al.* 2002; Tristani-Firouzi *et al.* 2002) and interplay of the S4-S5 linker with the neighbouring subunits (Ledwell *et al.* 1999; Lu *et al.* 2001; Soler-Llavina *et al.* 2006).

The cryo-EM structure of the BK channel from *Aplysia californica* demonstrated that the VSD interacted with the pore domain of the same subunit and further confirmed that the VSD in BK channels was not domain-swapped. The S4-S5 linker was an ordered loop and was shorter, when compared to Shaker-like K_v channels, where the S4-S5 linker was an -helix (Tao *et al.* 2017). The study by Tao *et al.* (2017) also demonstrated that the BK channel S4 helix was tightly packed against the antiparallel S5 segment, whereas in Shaker-like K_v channels the S4 was separated from the S5.

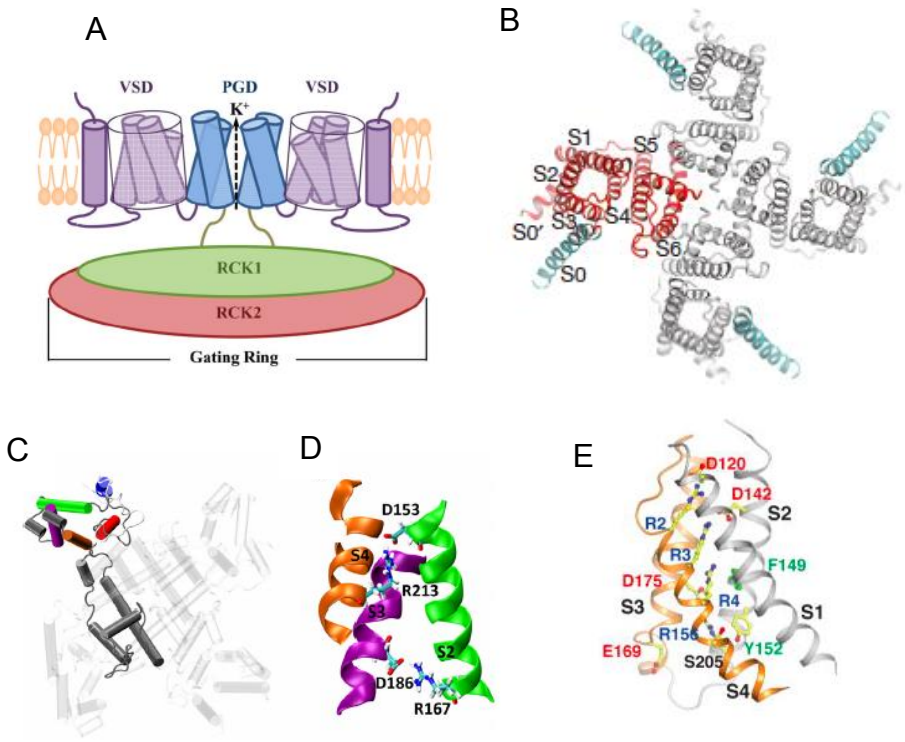

Figure 1.3: Topology and the cryo-EM structure of BK channel VSD.

A Cartoon of a functional BK channel where two opposing subunits are shown interacting with each other. **B** Top view of the transmembrane regions (S0-S6) of the *Aplysia californica* BK channel. **C** Voltage sensing domain of the BK channel showing S0 (blue), S1 (red), S2 (green), S3 (violet), S4 (orange), the linkers and pore of the same subunit in dark grey whereas the rest of the channel in light grey, **D** voltage sensing residues located in the S2, S3, S4 transmembrane segments. **E** Stereo view of the *Aplysia californica* BK channel VSD showing S3 and S4 (orange) and the rest of the channel in grey (Adapted from Lee *et al.* 2010; Latorre *et al.* 2017; Tao *et al.* 2017).

In Shaker-like K_v channels, the S4 segment contains six positively charged amino acid residues whereas, the BK channel contains only three positively charged arginine residues at positions 196, 199 and 202 (Tao *et al.* 2017). Previous studies proposed that the distribution pattern of these arginine residues in the S4 segment of the BK channel closely resembled the distribution of arginine residues in the S4 segment of K_v2.1 channels (Islas *et al.* 1999; Latorre *et al*. 2017). The Tao *et al.* (2017) study helped to confirm that the location of these three arginine residues (labelled R2, R3 and R4 in Figure 1.3E) corresponded to the location of the arginine residues in Shaker-like K_v channels. Previous studies used mutagenesis and demonstrated that the R213 in S4, D153 and R167 in S2, as well as D186 in the S3 segment of mouse BK channels were the main voltage

sensing residues (Diaz *et al.* 1998; Hu *et al.* 2003; Ma *et al.* 2006; Figure 1.3D). This accounts for the 'decentralised' distribution of sensing residues in the BK channel (Pantazis *et al.* 2010). Moreover, the cryo-EM structure of the BK channel also revealed that residues R2 and R3 formed strong hydrogen bonds with D120 and D142, respectively, near the extracellular side of the voltage sensor and R4 showed weak interactions with F145 and D175 on the S3 segment. In addition, D175 strongly interacted with R156 on the S2 segment (Tao *et al.* 2017). The S4 segment of the K_v channels contributed ~50% of the total gating charge, but in BK channels the functional gating charge was ~20% of that seen in Shaker-like K_v channels (Pantazis *et al.* 2010; Tao *et al.* 2017). Thus, the structural differences in the voltage sensors between BK and K_v channels appear to account for the large differences in the gating changes (Latorre *et al.* 2017).

1.2.2 Voltage-dependent activation

In the virtual absence of Ca^{2+}, depolarisation is sufficient to generate macroscopic BK currents, supporting the idea that BK channels can open independently of Ca^{2+} ions (Cui *et al.* 1997). This voltage-dependent activation stems from the VSD, which activates when the cell is depolarised to quite positive potentials (> +110 mV) in the complete absence of Ca^{2+} (Cui *et al.* 1997). Furthermore, a study has demonstrated that in a mutant BK channel construct, where the entire CTD of the channel was replaced with 11 amino acids of the K_v1.4 C-terminal sequence (Core-MT), channels opened in response to more positive membrane depolarisation steps and shifted the activation $V_{1/2}$ rightwards by 49.2 ± 3.0 mV. These results helped to confirm that the BK channels can open in the absence of a functional gating ring (Budelli *et al.* 2013).

With the use of voltage-clamp fluorometry, it has been confirmed that BK channels undergo voltage-dependent conformational changes in the S3-S4 segments (Mannuzzu *et al.* 1996; Cha *et al.* 1997; Savalli *et al.* 2006). In addition, Pantazis *et al.* (2010) demonstrated that at hyperpolarised membrane potentials, a tryptophan residue (W203) located in the extracellular end of the S4 segment moved away from S0 during channel activation. Furthermore, Pantazis *et al.* (2012) demonstrated that during the activation of the BK channel, the TM domains underwent rearrangement such that the S4 segment moved away from S1 and S2 while S2 moved closer to S1. In addition, Koval *et al.* (2007)

hypothesised that the S0 segment was involved in modulation of the equilibrium between resting and active conformations of the voltage sensors in the BK channel. Previous studies hypothesised that the VSD comprised of segments S0-S4, Figure 1.3C shows that S0 resided between S1 and S2 TM domains (Castillo *et al.* 2016; Latorre *et al.* 2017). However, the Tao *et al.* (2017) study demonstrated that the additional S0 transmembrane segment was located at the periphery of the VSD. In addition, it also confirmed that the extracellular loop of S0 interacted with the S5 and the turret connecting the S5 segment to the pore helix whereas, the cytoplasmic end had minimal interactions with the VSD (Tao *et al.* 2017).

1.2.3 Cytosolic tail domain (CTD)

The CTD is the primary chemical sensing domain of the BK channel and has multiple binding sites for intracellular ligands. The tail has two nonidentical Regulator of K^+ Conductance (RCK) domains (RCK1 and RCK2; Cui *et al.* 1997; Figure 1.4). These RCK domains help regulate the permeation of K^+ ions through the pore, upon binding of intracellular ligands (Jiang *et al.* 2001; Jiang *et al.* 2002a; Fodor and Aldrich, 2006). The sequence of the RCK1 domain is conserved across eukaryotic and prokaryotic species (Jiang *et al.* 2001). The X-ray crystal structure of the human BK CTD was predicted based on the sequence similarity with the prokaryotic-MthK channel (Wu *et al*. 2010; Yuan *et al*. 2010).
The tetrameric BK channel is comprised of eight RCK domains or four CTDs, which form a large gating ring structure connected to the PGD via a C-linker (Yang *et al.* 2015). In the prokaryote MthK channel, the CTD contains two indistinguishable RCK domains, whereas in the eukaryotic BK channel, the CTD contains two non-identical RCK domains (Wu *et al*. 2010). As shown in Figure 1.4, each RCK domain is subdivided into 3 distinct parts. The central core of the gating ring is called the Rossmann-fold subdomain (A- F), whereas the intermediate helix-crossover (F-turn- G) links the two RCK domains of a single subunit. Finally, the peripheral C-terminal (H-C-terminus) interacts with its corresponding partner in the adjacent RCK domain within the same subunit and helps maintain the integrity of the gating ring structure (Wu *et al*. 2010). These interactions with the helix-crossover and the peripheral C-terminus form a bi-

lobed structure of the two RCK domains in the BK channels (Wu *et al*. 2010). In addition, the inter-subunit interactions between RCK domains occurred in a head to tail manner at the 'assembly interface' which was formed by the hydrophobic interactions between the D and E helices from each RCK domain (Wu *et al*. 2010; Yuan *et al*. 2010; Yang *et al.* 2015; Figure 1.4D).

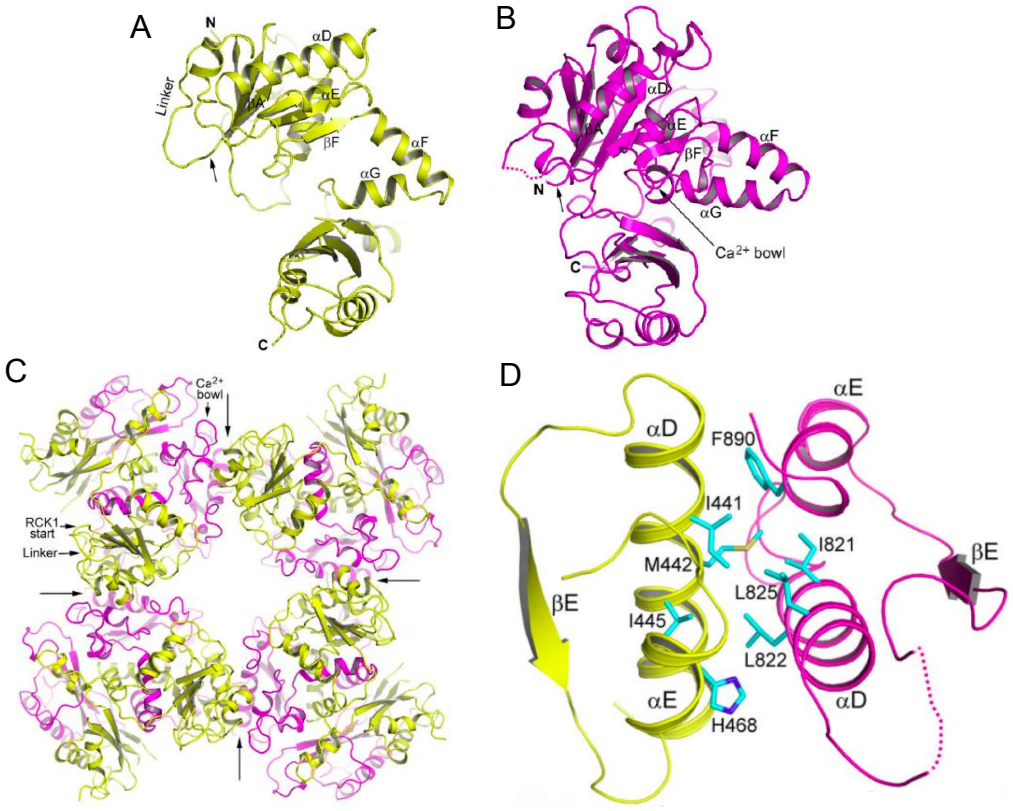

Figure 1.4: RCK1, RCK2 and gating ring structure. The individual structures of the two RCK domains of BK are shown, **A** is RCK1 (yellow) and **B** is RCK2 (magenta). The linker connects the RCK to the pore of the channel and the arrow specifies the start point of each RCK domain. **C** The assembled gating ring of tetrameric subunits of BK viewed down the 4-fold axis from the extracellular side. The point of interface of the four subunits is indicated by the long arrows which also define the boundary of each subunit. **D** A magnified view of the assembly interface comprising helices D and E from both RCK1 and RCK2 domains shown in yellow and magenta, respectively. The hydrophobic residues involved in protein-protein intercations are also shown. The disordered loop between D and E is shown as a dotted line (Adapted from Wu *et al*. 2010).

1.2.4 Calcium-dependent activation

Each subunit of the BK channel has at least two distinct Ca^{2+} binding sites, one each in the RCK1 and RCK2 domain, respectively. The RCK2 domain contains t h e - a h i f i g h i t y ' c a and consists of a 28-amino acid chain (E883 to Q910 in mouse BK) in which a string of five aspartic acid residues form the Ca^{2+} bowl (Schreiber *et al.* 1997). When these aspartic acid residues were neutralised, the BK channels showed a reduced sensitivity to Ca^{2+} (Bian *et al*. 2001). Moreover, when the aspartic acid residues between D895 to D903 were mutated to alanine, in mouse BK, Ca^{2+} sensitivity was reduced but not abolished. These experiments confirmed the presence of additional high-affinity sites distinct from the Ca^{2+} bowl (Bao *et al*. 2002).

However, when a methionine at position 513 in the RCK1 domain was mutated to an isoleucine, along with deletion of most of the Ca^{2+} bowl, the channels were rendered practically insensitive to Ca^{2+} (Bao *et al*. 2002). In 2002, Xia *et al.* demonstrated that neutralising two aspartate residues from the RCK1 domain (D362A/D367A) also resulted in markedly reduced Ca^{2+} sensitivity. In addition, when mutant constructs of RCK1 and RCK2 were designed (D362A/D367A-D5N5), the resultant BK channels only activated in the presence of very high Ca^{2+} concentrations (1 mM Ca^{2+}). Furthermore, when the point mutations D898A and D900A were performed on a M513I background, they practically abolished the BK channel Ca^{2+} sensitivity (Bao *et al*. 2004; Zhang *et al.* 2010).

Both the X-ray crystal structure of the human BK CTD and the cryo-EM structure of the full-length BK from *A. californica* helped confirm which residues were involved in Ca^{2+} sensing. They demonstrated that within the Ca^{2+} bowl, the side-chain carboxylates of D905 and D907 (D895, D897 in human BK) and main-chain carbonyl oxygen atoms of Q899 and D902 (Q889, D892 in human BK) favoured the direct binding of Ca^{2+} ions (Yuan *et al*. 2010; Tao *et al*. 2017; Figure 1.5B). Along with these previously known sites, Tao *et al*. (2017) demonstrated that a side-chain carboxylate of residue N438 was also crucial for Ca^{2+} binding in the Ca^{2+} bowl. However, a recent study by Li *et al.* (2018) demonstrated that although this residue may have been important for Ca^{2+} co-ordination in the Ca^{2+} bowl, it played little role in Ca^{2+} binding, since N449A mutant (N438 in *A. californica*) showed a Ca^{2+} sensitivity which was similar to WT BK channels. Li *et al.* (2018) also demonstrated that the neutralisation of E955 (E965 in *A. californica*), a

residue located at the inter subunit assembly interface, distal to the Ca^{2+} bowl resulted in reduced Ca^{2+} sensitivity. In addition, they demonstrated that when the charge neutralisations of R786 and R790 (R808 and R812 respectively, in *A. californica*) were performed on an E955Q mutant background, Ca^{2+} sensitivity was diminished. This suggested that there might be inter-subunit electrostatic interactions between E995 and both R786 and R790 from the other subunit (Li *et al.* 2018).

The cryo-EM density of the full-length *A. californica* BK channel also helped confirm the likely location of the Ca^{2+} binding sites in the RCK1 domain. As shown in Figure 1.5C, the Ca^{2+} binding is well co-ordinated by the main-chain carbonyl oxygen atoms of the R503 (R514 in human BK), G523 and E591 residues along with the side-chain carboxylates of D356 and E325 (D367 and E535 in human BK) residues (Yuan *et al*. 2010; Tao *et al*. 2017). However, the Tao *et al*. (2017) study demonstrated that neither the M513 nor D362 residues were directly involved in Ca^{2+} binding. Their study suggested that the mutation of either of these residues was likely to destabilise the Ca^{2+} binding sites by an allosteric mechanism.

1.2.4.1 Magnesium-dependent activation

In addition to having distinct Ca^{2+} binding sites in the CTD, BK channels also have a Mg^{2+} binding site in the RCK1 domain (Shi *et al.* 2002). Previous studies have shown that the residues E374, E399 and Q397 could form a putative Mg^{2+} binding site as the mutations of E374A, E399N, and Q397C abolished or reduced Mg^{2+} sensitivity of the BK channels (Shi *et al.* 2002). Yang *et al.* (2008) suggested that the Mg^{2+} binding site was formed at the interface of the VSD of one subunit and the RCK1 domain of another subunit of the BK channel. Their extensive mutagenesis study suggested that the Mg^{2+} binding site was formed between the cytosolic E374 and E399 residues, along with the D99 and N172 located in the membrane spanning domain of the VSD.

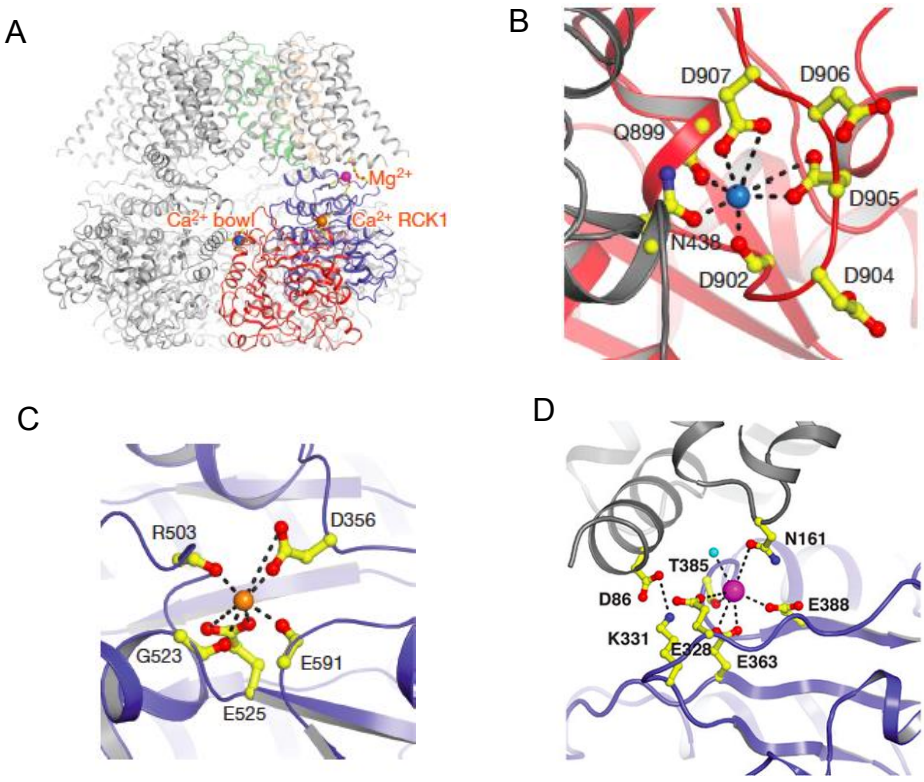

Figure 1.5: Calcium and Magnesium binding sites in the BK cryo-EM structure of *Aplysia californica*. A Ca^{2+} binding site in RCK1 domain (blue) along with the Ca^{2+} bowl (red) in one subunit of the BK tetramer whereas the other subunits are shown in grey. **B** Ribbon structure of BK channel showing Ca^{2+} bowl, RCK2 domain (red) and the neighbouring RCK1 domain (grey). **C** Ca^{2+} binding site in RCK1 domain of the BK channel (blue ribbon). **D** Mg^{2+} binding site in RCK1 domain (blue ribbon) and neighbouring VSD (grey). The side-chains of the atoms (coloured sticks), the water molecule (cyan sphere) and divalent cations (coloured spheres) with coordination bonds (dashed lines) are shown (Adapted from Tao *et al*. 2017).

The *A. californica* BK channel, cryo-EM density published by Tao *et al.* (2017) confirmed the precise location of the Mg^{2+} binding site in BK channels. The Mg^{2+} binding was well co-ordinated with the oxygen atoms of the side-chain carboxylates of E363 (E374 in human BK), E388 (E399 in human BK), the main-chain carbonyl oxygen atoms of T385, the side-chain carboxylate of N161 (N172 in human BK) as well as a water molecule. However, D86 (D99 in human BK) was not directly involved in Mg^{2+} binding and instead, it was suggested that this residue was involved in maintaining charge-charge interactions near the binding site and was therefore, critical for stabilising the Mg^{2+} ion binding in the BK channel (Tao *et al*. 2017; Figure 1.5D).

1.2.5 Pore-gating domain (PGD)

The PGD of each subunit forms the centre of the tetrameric BK channel, which opens and closes to allow selective permeation of K^+ ions. This selection and permeation of K^+ ions occurs through the pore domain (S5-S6) of the channel (Salkoff *et al*. 2006). The PGD of the BK channel is highly conserved across prokaryotic and eukaryotic 2TM and 6TM K^+ channels (Yang *et al*. 2015). In the K^+ channel family, K^+ ion transport occurs through a narrow selectivity filter which connects the larger inner vestibule to the shallow outer vestibule (Doyle *et al*. 1998). In the BK channel, small cations such as Na^+, Tl^+, K^+, NH_4^+, Rb^+, Mg^{2+}, Ca^{2+}, and Sr^{2+} pass through the inner vestibule, of which only NH_4^+, Tl^+, K^+ and Rb^+ pass through the selectivity filter, whereas the other cations act as flickery or fast blockers upon entering the inner vestibule (Brelidze and Magleby, 2005). Across different species, the selectivity filter of K^+ channels contain a unique 'TVGYG' amino acid sequence which is essential for maintaining K^+ ion selectivity (Doyle *et al*. 1998).

1.2.6 K^+ ions permeation through pore-gate domain

The activation of voltage sensors and binding of Ca^{2+} ions leads to the change in structure of the pore domain, which results in opening of the BK channel. These channels have three distinct biophysical features which distinguish them from other K^+ channels. Firstly, amongst the K^+ channels, BK channels show a very large single channel conductance (~100-300 pS). This large conductance is accounted for by a ring of eight negatively charged glutamic acid residues (E321 and E324), located at the base of the S6 helices (Brelidze *et al*. 2003; Nimigean *et al*. 2003) and the aspartic acid residue (D292) on the outer extracellular pore (Haug *et al*. 2004). These negatively charged residues attract K^+ ions, which results in increased local [K^+] and helps enhance K^+ flux through the pore resulting in the large unitary conductance of BK channels (Brelidze *et al*. 2003). Secondly, the inner vestibule of the BK channel is much larger and has a wider cytosolic entrance than most K^+ channels. Previous studies utilised compounds of various sizes and properties to help estimate the size of the central cavity and the cytosolic entrance to BK channels (Flynn and Zagotta, 2001; Li and Aldrich, 2004; Brelidze and Magleby, 2005; Wilkens and Aldrich, 2006; Bruening-Wright *et al*. 2007). The smaller quaternary ammonium (QA) ions, such as

tetrabutylammonium (TBA) and decyltriethylammonium (C_{10}) may have relatively free access to the inner vestibule, independent of the state of the activation gate. These QAs showed faster block and unblock kinetics as compared to their effects on K_V channels, which suggested that BK channels have a larger inner vestibule and a wider cytosolic entrance (Li and Aldrich, 2004). Studies based on the diffusion rate of K^+ ions from the bulk intracellular solution to the central cavity, in the presence of sucrose, showed that the estimated size of the open cytosolic mouth of the BK channel was 16-20 Å, which was two times larger than Shaker K^+ channels (Brelidze and Magleby, 2005).

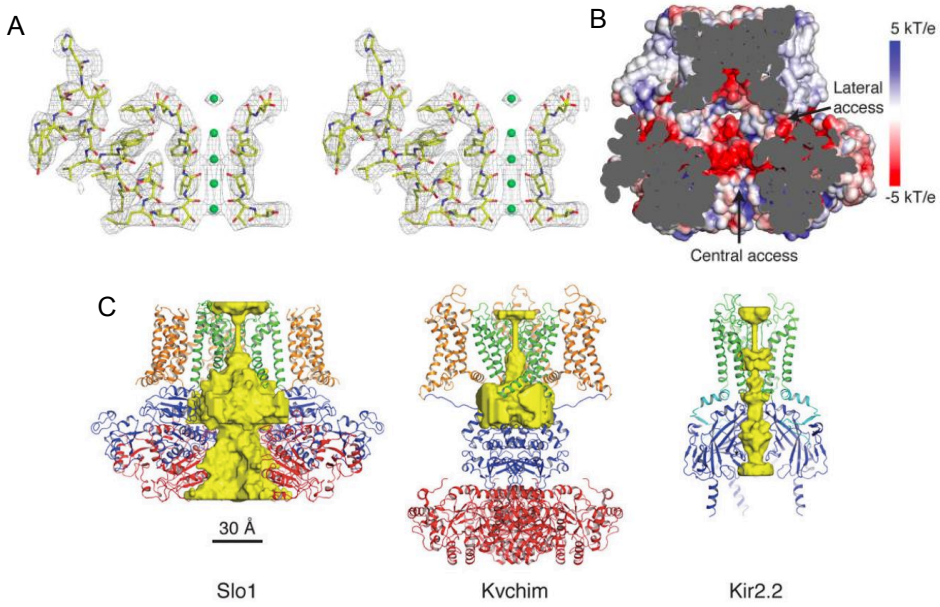

Figure 1.6: Ion Conduction in K^+ channels. A *A. californica* BK channel, cryo-EM density of the selectivity filter (only two subunits) and pore helix (one subunit, sticks coloured according to atom type) in stereo and K^+ ions (green spheres) are shown. **B** Electrostatic surface potential of the *A. californica* BK channel ion conduction pathway indicated by the colour scale. **C** Ribbon diagrams (front subunit excluded) of ion conduction pore in Slo1, Kvchim and Kir2.2 channels (Adapted from Tao *et al*. 2017).

Consistent with the previous findings, the cryo-EM structure by Tao *et al.* (2017) helped to confirm that in the open conformation, the size of the BK channel pore expanded to 30 Å (Figure 1.6C). The cryo-EM density of BK channels also helped confirm that the of the conductive conformation of the selectivity filter and the pore was similar to other K^+ channels (Tao *et al.* 2017; Figure 1.6A). Tao *et al.* (2017) also indicated the electrostatic surface potential of the *A. californica* BK channel ion conduction pathway of K+ ions by colour scale (Figure 1.6B).

The cryo-EM structure also helped to confirm that the pore of the BK channel was positioned beneath the selectivity filter, at the interface of the gating ring and was continuous throughout the gating ring. Therefore, the pore opened into a large, widened funnel on the cytosolic side. In addition, the cryo-EM structure revealed lateral openings between the gating ring and the transmembrane domains which may favour the high conductance of K^+ ions (Tao *et al.* 2017).

A third distinguishing feature of BK channels is that the residues in the S6 segment of the BK channel differ in their orientation compared to K_V channels. A series of cysteine modification and substitution experiments by Geng *et al.* (2011) and Zhou *et al.* (2011) argued that residues A313, A316 and S317 faced the inner pore of the BK channel. In contrast, the analogous residues in Shaker K^+ channels faced away from the aqueous environment (Zhou *et al.* 2011). These results suggested that the movement of the pore-lining helix of S6 in BK channels might differ from other K^+ channels. It was proposed that the BK channel opening involved structural rearrangement of the deep-pore region. In BK channels, the highly conserved glycine-hinge in the middle (Jiang *et al*. 2002b) and the proline-valine-proline (PVP) motif at the C-terminus of S6 helix (Webster *et al*. 2004) were critical for the movement of the activation gate. In addition, multiple pore residues, downstream of the glycine-hinge (L312, A313, M314 and A316) rearranged their side chains during channel gating and provided more flexibility to the S6 helix (Chen *et al*. 2014). Mutations of these residues to charged or polar side-chain substitutions, resulted in constitutively open mutant channels which abolished the voltage sensitivity and Ca^{2+} dependence. This may occur via exposing the hydrophilic side-chain to the aqueous environment of the pore to reduce side-chain solvation energy (Chen *et al*. 2014). The Hite *et al.* (2017) study illustrated that in the cryo-EM structure from the *A. californica,* in the Ca^{2+} bound state, the S6 helices underwent rearrangement such that a bend occurred at G302, close to the selectivity filter, resulting in the wide opening of the pore which had a minimum diameter of 20 Å.

1.2.7 Allosteric mechanism of BK channel opening

BK channels can open with a very low probability (~10^{-6}) in the absence of either voltage sensor activation or Ca^{2+} binding (Horrigan and Aldrich, 1999). However, the activation of the voltage sensors and Ca^{2+} binding enhanced the probability of channel opening markedly (Horrigan *et al.* 1999; Horrigan and Aldrich, 1999). The mechanisms of voltage-dependent activation and calcium binding have been described by various allosteric models (McManus and Magleby, 1991; Cox *et al*. 1997; Horrigan *et al.* 1999; Rothberg and Magleby, 1999; Rothberg and Magleby, 2000; Cui and Aldrich, 2000). However, these early studies failed to rigorously test the predictions of the model. In 2002, Horrigan and Aldrich proposed the HA model (Figure 1.7), explaining the allosteric gating mechanism of BK channels based on single channel and macroscopic current recordings across a wide range of voltages and Ca^{2+} concentrations. As Figure 1.7 suggests, the HA model states that the channel gate undergoes a conformational change from closed (C) to open (O) and this is allosterically coupled to four independent and identical voltage sensors and four Ca^{2+} sensors. The voltage sensors can exist in either the resting (R) or activated (A) state, and Ca^{2+} sensors can exist in unbound Ca^{2+} (X) or bound Ca^{2+} ($X.Ca^{2+}$) state. The conformational changes have equilibrium constants for gate opening (L), voltage sensor activation (J) and Ca^{2+} binding (K). The coupling between domains is depicted by allosteric factors C, D and E and indicates that there is coupling between Ca^{2+} binding and pore opening (C), voltage sensor activation and pore opening (D) as well as Ca^{2+} binding and voltage sensor activation (E), respectively. The data determined that of these three coupling factors, D had the highest value (24) and appeared to be more important wherein the activation of the voltage sensors induced the biggest change in pore opening. This was followed by the coupling between pore opening and Ca^{2+} binding (C) which had a value of ~7. Interestingly, the smallest level of coupling was between the Ca^{2+} binding and voltage sensor activation (E) which had a value of ~2 (Horrigan and Aldrich, 2002).

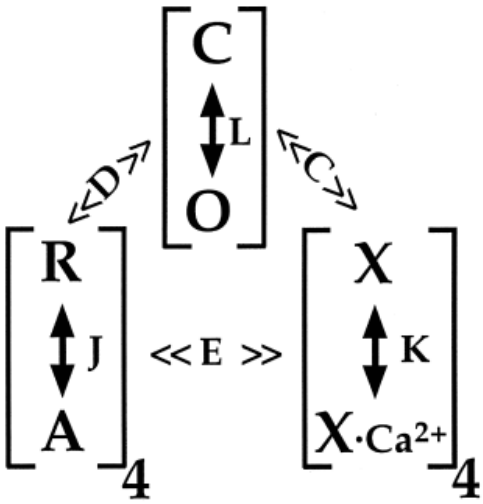

Figure 1.7: Horrigan and Aldrich model. The allosteric model of the BK channel showing possible conformations of the channel gate (C and O), voltage sensors (R and A) and Ca^{2+} sensors (X and X. Ca^{2+}). Each of the conformational state has equilibrium constants L, J and K, respectively. The allosteric coupling amongst the channel is represented by C, D and E (Adapted from Horrigan and Aldrich, 2002).

1.2.8 Coupling between Ca^{2+} sensors and channel opening

Studies based on structural and fluorescence experiments demonstrated that the binding of Ca^{2+} altered the conformational state of the gating ring (Ghatta *et al.* 2006; Yusifov *et al.* 2008; Yusifov *et al.* 2010; Wu *et al.* 2010; Yuan *et al.* 2010; Javaherian *et al.* 2011; Savalli *et al.* 2012; Yuan *et al.* 2012; Miranda *et al*. 2013). The allosteric coupling between the gating ring and the pore gate occurred through a C-linker, which connected the C-terminal to the S6 domain of the BK channel (Niu *et al*. 2004). In addition, the same group also found that reducing the length of the C-linker enhanced channel activity, whereas increasing the linker length decreased the Ca^{2+} sensitivity of the channel (Niu *et al*. 2004). The AC region (A- C) of the RCK1 domain plays a crucial role in connecting the activation gate to the cytosolic domain of the BK channel (Yang *et al.* 2010). In the N-terminal of this region, a mutation of the mouse D369G residue enhanced Ca^{2+} sensitivity and suggested that the co-operativity between the Ca^{2+} binding sites increased as a result of reduced flexibility of the AC region in this mutant. This study proposed that the mD369G mutation enhanced the BK channel activity, possibly via an enhanced allosteric coupling between Ca^{2+} binding sites and the activation gate (Yang *et al.* 2010).

It was demonstrated that the binding of Ca^{2+} to the channel, initiated the rearrangement of the four RCK1 domains resulting in a 10 Å expansion of the BK channel (Yuan *et al.* 2012). Furthermore, with the use of fluorescence resonance energy transfer (FRET) it was demonstrated that the RCK1-RCK2 domains came in close proximity to each other by 40 Å and the C-linker moved outward by 5 Å. This suggested that there was a reversible reduction in the hydrodynamic radius of the gating ring (Miranda *et al*. 2013). Thus, upon Ca^{2+} binding, the expansion of the gating ring generated a mechanical force which pulled the C-linker to open the pore gate of the BK channel (Miranda *et al*. 2013; Latorre *et al.* 2017).

In 2020, Yazdani *et al*. investigated the role of the C-linker with a series of randomly scrambled C-linker mutations (named K0 through to K7) and demonstrated that with a scrambled C-linker sequence, the BK channel activation was altered. The activation $V_{1/2}$ shifted leftwards from 183.4 ± 3.2 mV in WT to 48.7 ± 4.7 mV for the K7 mutant, 89.6 ± 3.5 mV for the K0 mutant, and shifted rightward for K2 mutant (195.5 ± 3.5 mV). This study proposed that when the Y332 residue in the C-linker was in close contact with the membrane interface (in K0 and K7 mutants), it allowed stronger membrane anchoring and stabilised the open state of the channel. This led to a shift in the equilibrium towards the active state of the channel. Therefore, the K0 and K7 mutants showed a leftward shift, whereas the K2 mutant showed a rightward shift in activation $V_{1/2}$ values. Interestingly, the effects mediated by the scrambled C-linker mutants also persisted in the Core-MT constructs where the gating ring was completely absent ($V_{1/2}$ of 235.0 ± 3.1 mV for WT Core-MT and 263.5 ± 4.0 mV for K2 mutant) and hence provided direct evidence that the C-linker played a crucial role in coupling of the gating ring and the pore of BK channels (Yazdani *et al*. 2020).

1.2.9 Coupling between Ca^{2+} sensors and voltage sensors

In 2012, Savalli *et al.* demonstrated a significant leftward shift in conductance and fluorescent-voltage curves upon rapid application of Ca^{2+} to the cytosolic surface of D362A/D367A mutants in the RCK1 domain. Their data provided strong evidence to support the idea of coupling between Ca^{2+} and voltage sensors. They also noted that this coupling was lost when the aspartic acid residues in the Ca^{2+} bowl of the RCK2 domain were neutralised (Savalli *et al.* 2012). In addition, they computed the steady state occupancy of the Ca^{2+} bound

state for RCK1 and RCK2 domains and demonstrated that across a range of membrane potentials, the Ca^{2+} binding in RCK1 was voltage dependent, whereas the Ca^{2+} binding in RCK2 was weaker. It was clear from these experiments that the two high-affinity Ca^{2+} binding sites were not functionally equivalent (Savalli *et al.* 2012).

The Ca^{2+} binding in the RCK1 domain, strongly stabilised the active conformation of the VSD, which was supported by the allosteric coupling factor of 10 (Savalli *et al.* 2012; Latorre *et al.* 2017), whereas the allosteric coupling factor (2.3) between the RCK2 Ca^{2+} sensors and voltage sensors was weaker (Savalli *et al.* 2012; Latorre *et al*. 2017). These differences in coupling of the two Ca^{2+} sensors and voltage sensors may be due to the physical proximity of the RCK1 and the VSD (Savalli *et al.* 2012; Latorre *et al*. 2017).

1.2.10 Coupling between voltage sensors and channel opening

Previous studies have demonstrated that mutations in S6 significantly modified gating of BK channels, which suggested that this helix played an important role in communicating the changes in the VSD to the activation gate (Lippiat *et al.* 2000; Wang *et al.* 2006; Wu *et al.* 2009; Carrasquel-Ursulaez *et al.* 2015).

Horrigan (2012) proposed three hypothetical mechanisms for the interaction between the S4-S5 linker and S6 domain (Figure 1.8). The model depicts the four combinations of states with a voltage sensor and gate from a single subunit. The possibility of a rigid connection between S4-S5/S6 domains which forces the sensor and gate to move as a unit can be ruled out as voltage sensors activate while the channel remains closed. Figure 1.8A illustrates the first proposed mechanism where the S4-S5 linker is always bound with S6. In this case, various S4-S5/S6 regions play a role to move the sensor and gate, if they were coupled via a spring. Figure 1.8B illustrates the second proposed mechanism, in which the S4-S5 linker binds to the open gate only when voltage sensors are in the active state and thus, stabilises the AO state. The last possible mechanism illustrates the S4-S5 linker of the resting voltage sensor might clash sterically with the open gate to destabilise the RO state (Figure 1.8C; Horrigan, 2012).

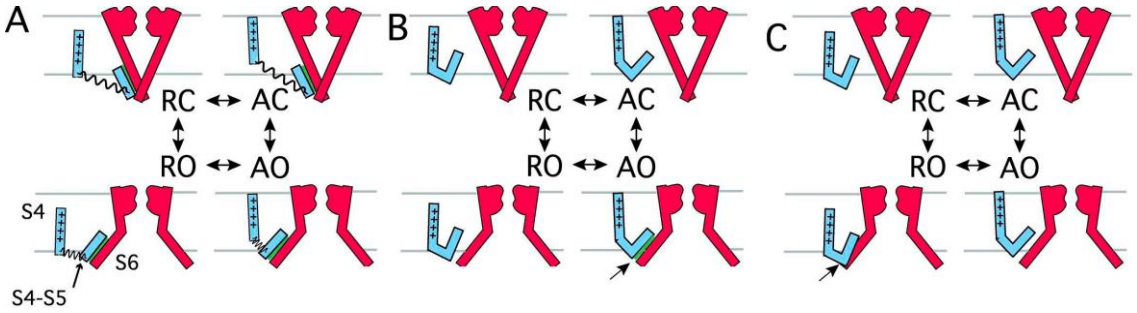

Figure 1.8: Models of coupling between voltage-sensor and channel opening showing the interaction of the S4 S5 linker with the S6 gate in a single subunit. The voltage sensor can be in a resting (R) or activated (A) state, and the gate is closed (C) or open (O). **A** Flexible linkage with S4-S5/S6 interacting in all states. **B** S4-S5/S6 binding stabilizes AO state. **C** Steric hindrance destabilizes the RO state (Adapted from Horrigan, 2012).

Mutations of the human BK F380 residue (corresponding murine BK-F315) to F380I reduced the unitary conductance to ~100 pS, and showed reduced open times compared to WT BK (Lippiat *et al.* 2000). A F380Y mutant also displayed a reduction in single-channel conductance compared to WT BK channels (Wang *et al.* 2006). However, the replacement of F315 and L312 in murine BK with smaller hydrophilic amino acids stabilised the open state of the channel. Their data suggested that the L312 interacted with the F315 of a different subunit, in the closed state (Wu *et al.* 2009). It was proposed that pore opening would break this interaction and disruption of this interaction would stabilise the open state of the BK channel (Wu *et al.* 2009). In support of this hypothesis, when L312 was substituted with polar negative or positively charged residues, it resulted in permanently open channels (Chen *et al.* 2014). The same group also demonstrated that the replacement of A313 or A316 with polar or charged amino acids produced permanently open channels, which suggested that the constitutive channel activity was not restricted to residue 312 (Chen *et al.* 2014). Moreover, the interaction between the F380 and L377 in mouse BK was disrupted by introduction of small hydrophobic amino acids which stabilised the closed state (Wu *et al.* 2009). In 2011, Zhou *et al*. demonstrated that mutation of L312C and F315C mutants, resulted in a significant rightward shift of G(V) curves, which suggested the stabilisation of the closed state.

The substitution of F380 with smaller hydrophobic amino acids such as alanine, leucine or isoleucine hindered channel opening, but did not affect voltage sensing

(Carrasquel-Ursulaez *et al.* 2015). It was demonstrated using the HA model that the F380A mutation weakened the allosteric coupling between the voltage sensor and the calcium binding site along with the coupling between the channel gate and the voltage sensor (Carrasquel-Ursulaez *et al.* 2015). The study by Hite *et al.* (2017) demonstrated that the Ca^{2+} binding induced a series of conformational changes in the gating ring where it resulted in tilting of the RCK1 N-lobes which further led to the opening of the S6 helices through covalent linker interactions and pulled open the S6 helices. The second structural rearrangement caused the displacement of the voltage sensors and S5 helices. This occurred through non-covalent, protein-protein interactions between the RCK1 N-lobes and the voltage sensors (S4–S5 linkers). Therefore, they demonstrated that structural rearrangements between the VSD and the gating ring resulted in opening of the pore of the BK channel (Hite *et al.* 2017). In addition, a study by Zhang *et al.* (2017), demonstrated that the Core-MT channels showed a ~100-fold reduction in the total open probability, compared to WT BK channels. These results indicated that the opening of the gate initiated by the movement of the voltage sensors in the Core-MT constructs was less effective than in WT BK channels. Thus, the removal of the gating ring reduced the coupling between the voltage sensors and the channel opening (Zhang *et al.* 2017).

1.3 BK channel physiology

BK channels are widely expressed across several tissues and cell types in the body including smooth muscle, brain, kidney, thymus, stomach, and small intestine (Butler *et al*. 1993; Garcia-Calvo *et al.* 1994; Pallanck and Ganetzky, 1994). Thus, BK channels play a major role in physiological functions such as muscle contraction (Brayden *et al.* 1992), neurotransmitter release (Robitaille *et al.* 1993), neuronal excitability (Adams *et al*. 1982) and endothelial function (Nilius *et al*. 2001).

The diverse functional roles of BK channels are achieved not only by alternative splicing of the subunit but by interactions with auxiliary subunits, post-translational modifications and altered cellular trafficking and expression levels (Contreras *et al*. 2013; Latorre *et al*. 2017).

In excitable cells, the membrane potential and intracellular calcium dynamics are regulated by BK channels and voltage dependent Ca^{2+} channels (VDCC, Blatz

et al. 1984). The depolarisation of the membrane potential activates VDCC, leading to Ca^{2+} influx and Ca^{2+}-induced Ca^{2+} release from nearby ryanodine receptors. The released Ca^{2+} promotes BK channel activation, which leads to cell hyperpolarisation. In response to this hyperpolarisation, VDCC close and consequently reduce $[Ca^{2+}]_i$ and this mechanism helps control neurotransmitter release, modulate neuronal excitability, and alter smooth muscle tone (Berkefeld *et al.* 2006).

In the Central Nervous System (CNS), BK channels are expressed in dendrites, axon, soma, and synaptic terminals of neurons in different regions of the brain, where they are important in action potential duration, firing frequency and neurotransmitter release (Knaus *et al*. 1996). In neurons, BK channels are expressed at pre- and post-synaptic sites. In postsynaptic sites, they co-localise with PSD95, NMDA receptors and voltage-dependent calcium channels (Ca_v, Sailer *et al.* 2006). During an action potential, membrane depolarisation and increase in intracellular calcium via voltage-dependent calcium channels (Ca_v) activates BK leading to conformational changes and channel opening. This channel activation, shortens the action potential and induces a fast after-hyperpolarization (fAHP) which shuts Ca_v channels (Hu *et al.* 2001; Griguoli *et al.* 2016). Therefore, BK channels regulate calcium influx and neurotransmitter release by decreasing intracellular calcium concentration below the threshold for vesicle fusion (Fakler and Adelman, 2008). Thus, BK channels control neuronal firing frequency and shape the action potential and therefore, act as an 'emergency break' with related hyperexcitability (Knaus *et al*. 1996; Swensen and Bean, 2003; Grunnet and Kaufmann, 2004; Griguoli *et al.* 2016).

In non-excitable cells, BK channels regulate Ca^{2+} entry by voltage independent Ca^{2+} channels such as P2X purinoreceptors and TRP channels (Nilius *et al*. 2001). In these cells, BK channels maintain Ca^{2+} homeostasis and regulate osmoregulation, K^+ secretion, cell migration and cell proliferation (Nilius *et al*. 2001).

1.3.1 BK channel pathophysiology

Given their ubiquitous expression, abnormal expression or function of BK channels can give rise to a range of pathophysiological conditions such as hypertension (Brenner *et al*. 2000b), overactive bladder (Petkov, 2014), mucociliary dysfunction (Manzanares *et al*. 2014) and ataxia (Sausbier *et al.* 2004). The pathological conditions caused due to dysfunction of BK channels are summarised in Table 1.1.

BK channels play an important role in maintenance of smooth muscle arterial tone. In vascular smooth muscle cells, it has been shown that the release of Ca^{2+} via ryanodine receptors on the sarcoplasmic reticulum results in Ca^{2+} sparks, which increase the $[Ca^{2+}]_i$ to micromolar levels (Cheng *et al.* 1993; Nelson *et al.* 1995; Cheng *et al.* 1996; Jaggar *et al.* 2000). The Ca^{2+} from these sparks result in spontaneous transient outward K^+ currents (STOCs) due to the activation of BK 1 channels. Thus, the BK channels serve to hyperpolarise vascular smooth muscle and hence contribute to the modulation of blood pressure (Brenner *et al*. 2000b). The important role played by regulatory 1 subunits was evidenced when they were deleted in genetically modified mice. A number of studies (Bolton and Imaizumi, 1996; Brenner *et al*. 2000b) have demonstrated that reduction in BK 1 subunits results in hypertension. For instance, in primary hypertension patients, there was a reduction of 1 density and STOCs in vascular smooth muscle cells (Yang *et al*. 2013). Interestingly, people with a gain of 1 function mutant (E65K) showed lower chances of moderate and severe diastolic hypertension (Fernandez-Fernandez *et al*. 2004).

In the urinary bladder, BK channels participate in a negative feedback mechanism in smooth muscles, where they help limit contraction amplitude and duration. Moreover, smooth muscles lacking BK channels showed spontaneous activity and enhanced nerve evoked contractions. Consequently, the dysfunction of BK channels in the urinary bladder led to urinary incontinence, overactive bladder (OAB) and detrusor overactivity (Meredith *et al.* 2004; Petkov, 2014).

In the airways, BK channels are abundantly expressed in airway smooth muscle (ASM, Goldklang *et al.* 2013). Goldklang *et al.* (2013) demonstrated that with the use of ovalbumin (OVA) and house dust mite-sensitised mouse models, that the BK channel agonist rottlerin reduced methacholine-induced airway hyperactivity.

In addition, they also found that application of 0.5 M rottlerin to human airway smooth muscle cells resulted in a leftward shift of the activation $V_{1/2}$ by 73.5±13.5 mV and by 71.8±14.6 mV in airway smooth muscle cells isolated from healthy individuals and patients with asthma, respectively. Furthermore, the treatment with rottlerin in the OVA asthmatic mice model illustrated less infiltration of inflammatory cells when compared to PBS treated OVA asthmatic mice (Goldklang *et al.* 2013). These results suggested that activating ASM BK channels in asthma patients would not just relax the bronchioles, but also reduce airway hyperactivity and inflammation.

In 2016, Kis *et al.* demonstrated that the BK channel regulatory 1 subunits were also expressed in airway epithelial cells. They demonstrated that treatment with interferon- and transforming growth factor (TGF)- 1 downregulated 1 and resulted in an overall reduction of BK channel activity, which led to airway surface liquid (ASL) loss, reduced ciliary beat frequency and enhanced reabsorption. This led them to conclude that BK 1 subunits regulated the airway mucociliary homeostasis (Manzanares *et al*. 2014; Manzanares *et al.* 2015; Kis *et al*. 2016).

In the CNS, BK channels are also expressed in Purkinje neurons in the cerebellum, which are crucial for motor co-ordination. This was illustrated in *BK* knockout mice which showed abnormal neural function such as impaired motor co-ordination, ataxia and high frequency hearing loss (Sausbier *et al.* 2004; Salkoff *et al*. 2006). BK channel loss of function and gain of function mutational studies have also been linked to epilepsy. In 2011, N ' G o u demonstrated that BK channels were downregulated in patients with temporal lobe epilepsy (TLE). These patients displayed hyperactivity, seizures and epileptogenesis. However, a gain of function mutation (D434G) in the BK subunit led to increased Ca^{2+} sensitivity with an increased neuronal excitability which resulted in human idiopathic generalised epilepsy (Yang *et al.* 2010). These results suggested that upregulation or down regulation of BK channels can lead to remarkably similar pathophysiological characteristics like seizures and hyperactivity associated with epilepsy.

In a recent study by Buckley *et al.* (2020) it was reported that the K457E mutation on exon 11 of the *KCNMA1* gene was linked to a number of clinical observations associated with movement disorders like chronic ataxia, paroxysmal dyskinesia,

and tremor. The murine K392E mutant (corresponding to human BK-K457E), on an R393D mutant background, has been previously shown to result in a loss of function, as evidenced by a rightward shift in activation $V_{1/2}$ (Hou *et al.* 2013; Liu *et al.* 2014). However, to date, the effects of the single K392E mutant have not been published, although recent unpublished experiments in our lab (Dudem and Hollywood, 2021, unpublished observations) suggest that these mutant channels were unable to open in the presence of 100 nM $[Ca^{2+}]_i$ even when depolarised to +200 mV. Increasing the cytosolic $[Ca^{2+}]_i$ tenfold, only produced small currents even at potentials as positive as +200 mV. In the presence of 10 M $[Ca^{2+}]_i$, a massive rightward (+130 mV) shift in the activation $V_{1/2}$ was observed with this mutant, compared to WT BK channels (Dudem and Hollywood, 2021, unpublished observations).

Table 1.1 BK-related pathologies

Disease	***Tissue affected***	***Subunit***	***Reference***
Hypertension	Vascular smooth muscle	BK 1	Fernandez-Fernandez *et al*. (2004); Yang *et al*. (2013)
Overactive bladder (OAB)	Urinary bladder smooth muscle	BK	Meredith *et al.* (2004); Petkov, (2014).
Asthma	Airway smooth muscle	BK	Goldklang *et al.* (2013)
Mucociliary dysfunction	Airway epithelial cells	BK 1	Manzanares *et al*. (2014); Manzanares *et al.* (2015); Kis *et al*. (2016).
Epilepsy	CNS	BK	N ' G o u e m o (2 0
Chronic ataxia, paroxysmal dyskinesia, and tremor	CNS	BK	Buckley *et al.* (2020)

1.4 BK channel modulators

Given the involvement of BK channels in smooth muscle physiology, it is not surprising that the BK channel has been targeted in a range of drug development programs. BK channel openers have a therapeutic potential in human pathophysiological conditions. There are several openers which either occur naturally or are synthetic in origin and alter the biophysical and pharmacological properties of the BK channels.

For instance, the addition of dehydrosoyasaponin1 (DHS-I) increased the open probability of the BK channels by 80-fold in tracheal smooth muscles (McManus *et al*. 1993). The effects of natural BK channel openers are summarised in Table 1.2. Apart from the natural BK channel openers, numerous synthetic BK channel openers have also been developed. Previously in our lab, a series of anthraquinone analogs called the GoSlo-SR compounds were developed which shifted the voltage-dependence of BK channels leftwards (-100 mV) in bladder smooth muscle cells (Roy *et al*. 2012; Roy *et al.* 2014; Large *et al.* 2015). The effects of other such synthetic BK channel openers are detailed in Table 1.3.

BK channel activity can also be modulated by several blockers as reviewed by Yu *et al.* (2016). For instance, the addition of iberiotoxin (IbTX) extracted from the crude venom of scorpion, blocked BK channels with an IC_{50} in the range of 2 − 1 0 n M (*et al.* 1990). Recently, Vouga *et al.* (2021) reported that the addition of -opioid agonist loperamide (LOP), blocked BK channels with an IC_{50} of 1.4 M. The effects of other such BK channel blockers are detailed in Table 1.4.

Table 1.2 Types of natural BK channel openers

Names	***Effect***	***Reference***
Unsaturated free fatty acids- arachidonic acid palmitoleic, oleic, linoleic, eicosapentaenoic acid (2.5 M each)	Showed an increase in BK channel activity by 3.6±0.86 fold by 1.36±0.19 fold by 1.91±0.86 fold by 2.08±0.44 fold by 4.01±0.14 fold as compared to 0.24±0.05 in 100 nM $[Ca^{2+}]_i$	Denson *et al*. (2000)
Omega-3 docosahexaenoic acid (DHA)	Increased BK channel activity, + 1 together showed a leftward shift in $V_{1/2}$ by 57.3±1.0 mV and in the presence of + 4, showed a leftward shift in $V_{1/2}$ by 66.3±2.3 mV	Hoshi *et al.* (2013a); Hoshi *et al.* (2013b)
17 -estradiol	Increased open probability (P_0) of BK channels from 0.022 to 0.063 upon addition of 4.2 M 17 -estradiol	Valverde *et al*. (1999)
Corticosterone	In the presence of 4, increased BK channel activity by 88.2±28.2% in the presence of 1 M corticosterone	King *et al*. (2006)
Dehydroepiandrosterone (DHEA)	In the presence of 4, increased BK channel activity by 9.6±10.4% in the presence of 1 M DHEA	King *et al*. (2006)
-defensin 2	Activated BK channels in the presence of 1 with a $V_{1/2}$ of 55.9±1.1 mV and reduced blood pressure	Liu *et al*. (2013)
dehydrosoyasaponin1 (DHS-I) (origin herbs)	Increased open probability of BK channels by 80-fold in tracheal smooth muscle	McManus *et al*. (1993)
Terpene and glucoside derivates from roots and leaves of plants and fungi	Treatment of asthma and smooth muscle disorders	Nardi *et al.* (2006)

Table 1.3 Types of synthetic BK channel openers

Names	***Effect***	***Reference***
Tamoxifen	In the presence of 1, activated BK channels with a P_0 of 0.975	Dick *et al.* (2001)
Zonisamide, Chlorozoxazone, Cilastazol	Increased BK channel activity by reducing mean closing time of the channel	Huang *et al*. (2007); Liu *et al*. (2003); Wu *et al.* (2004)
Benzimidazolone derivatives- *NS004*	Activated BK channels by a leftward shift of 40 mV	Olesen *et al.* (1994)
NS1619	Potential therapeutic agent in pulmonary hypertension, erectile dysfunction, bladder instability, shock-induced vascular hyperactivity, migranes, inflammatory pain and cytoprotection and shifted activation $V_{1/2}$ by -40 mV	Ghatta *et al*. (2006); Kiraly *et al*. (2013); Revermann *et al*. (2014); La Fuente *et al.* (2014); Hu *et al.* (2014)
NS11021	Improved BK channel activity in diseases, improved cardiac function post ischemia, erectile dysfunction and decreased contractility of urinary bladder smooth muscle and shifted activation $V_{1/2}$ by -62 mV	Bentzen *et al*. (2007); Bentzen *et al*. (2009); Kun *et al*. (2009); Layne *et al*. (2010)
Anthraquinone analogs- GoSlo-SR	BK channel activators that shifted voltage dependence leftward, -100 mV in bladder smooth muscle cells	Roy *et al*. (2012); Roy *et al.* (2014); Large *et al.* (2015)
DiBAC- dye bis-(1,3-dibutylbarbituric acid) trimethine oxonol	Activated in the presence of 1 and shifted activation $V_{1/2}$ by -30 mV	Morimoto *et al*. (2007)

Table 1.4 Types of BK channel blockers

Names	***Effect***	***Reference***
Charybdotoxin (ChTX)	Blocked BK channels with an IC_{50} of 50 nM	Miller *et al.* (1985)
Iberiotoxin (IbTX)	Blocked BK channels with an IC_{50} in the range of 2 − 1 M n	Galvez *et al*. (1990)
BmTx1, BmTx2	Blocked BK channels with an IC_{50} of 0.6 nM and 0.3 nM, respectively.	Blanc *et al.* (1998); Romi-Lebrun *et al.* (1997)
Lqh 15-1 (Chtx2)	Blocked BK channels with an IC_{50} of 50 nM	Marshall *et al*. (1994)
Slotoxin	Blocked BK channels with an IC_{50} of 1.5 nM	Garcia-Valdes *et al*. (2001)
Kaliotoxin (KTX)	Blocked BK channels with an IC_{50} of 20 nM	Crest *et al*. (1992)
Martentoxin (MarTX, BmTx3B)	Blocked BK channels with an IC_{50} of 78 nM	Tao *et al*. (2014)
BmP09	Blocked BK channels with an IC_{50} of 27 nM	Yao *et al.* (2005)
BmBKTx1 (BmK37)	Blocked BK channels with an IC_{50} of 82 nM for pSlo, 194 nM for dSlo, and had no effect on hSlo	Cai *et al.* (2004)
Natrin	Blocked BK channels with an IC_{50} of 34.4 nM	Wang *et al.* (2005)
Paxilline (PAX)	Blocked BK channels with an IC_{50} of 10.8 nM	Zhou *et al.* (2014)
Loperamide (LOP)	Blocked BK channels with an IC_{50} of 1.4 M	Vouga *et al.* (2021)

1.5 BK channel auxiliary subunits

Although BK channels are ubiquitously expressed throughout the body, their biophysical properties differ significantly depending on where the channels are located. Although these differences can be partially explained by alternative splicing and metabolic regulation, the presence of the various regulatory subunits has the largest effect on the biophysical and pharmacological properties of these channels (Dworetzky *et al.* 1996; Wallner *et al*. 1999; Xia *et al.* 1999; Orio *et al.* 2002; Gessner *et al*. 2005; Latorre *et al.* 2017). To date, two main families of subunits, the and auxiliary subunits have been identified (Solaro and Lingle 1992; Knaus *et al*. 1994b; Herrington *et al*. 1995; Uebele *et al*. 2000; Yan and Aldrich, 2010; Yan and Aldrich, 2012) and have been shown to alter the properties of the pore forming BK subunit.

1.5.1 BK channel subunits

subunits create diversity amongst BK channels by modifying their gating kinetics and pharmacology. So far, four subunits (1-4) have been cloned and characterised and each of them is encoded by a different gene (Orio *et al.* 2002; Latorre *et al*. 2017). Figure 1.9A shows the sequence of each of the domains of the 4 subunits, which consist of two transmembrane domains (TM1 and TM2), an NH_2-terminal, a COOH-terminal, and an extracellular loop, as illustrated in Figure 1.9B. In all subunits, the NH_2 and the COOH termini, along with the inactivation particle for 2 and 3 subunits are located on the intracellular side of the membrane (Orio *et al.* 2002; Latorre *et al*. 2017).

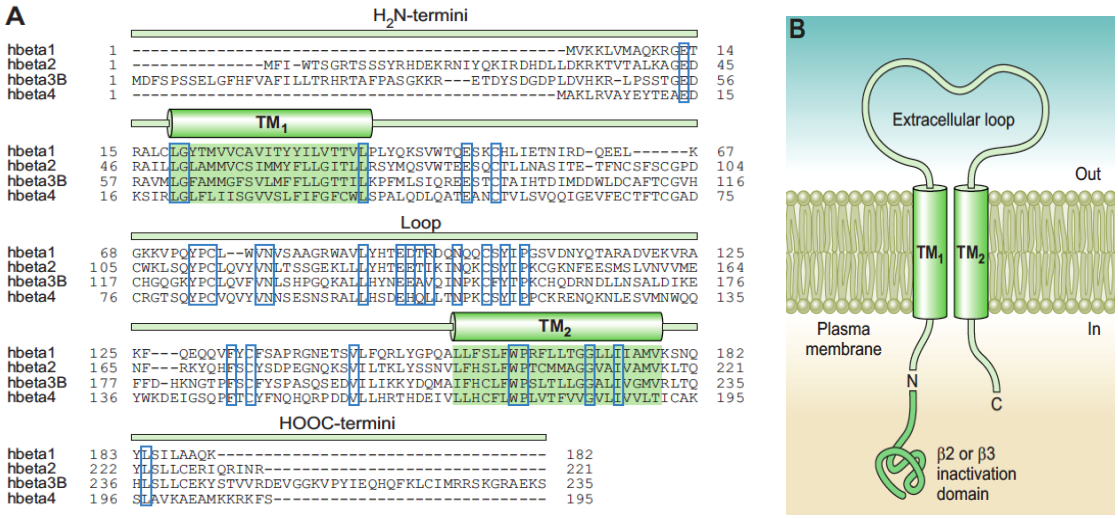

Figure 1.9: Multiple sequence alignment and topology of subunits. A Sequence alignment of all 4 subunits. **B** Schematic shared by all subunits showing the transmembrane domains (TM1 and TM2) linked by an extracellular loop, NH_2 and the COOH termini face the intracellular side along with the inactivation particle for 2 and 3 subunits (Adapted from Latorre *et al*. 2017).

1.5.2 1 subunit

The first BK subunit to be identified was 1, encoded by the *KCNMB1* gene and was cloned from tracheal and aortic smooth muscle (Knaus *et al*. 1994a). 1 subunits are widely expressed in smooth muscle including the bladder, uterus, trachea and blood vessels (Garcia-Calvo *et al.* 1994; Knaus *et al*. 1994a; Knaus *et al*. 1994b). The molecular weight of the subunit was found to be 31 kDa (Garcia-Calvo *et al.* 1994; Knaus *et al*. 1994b). In 1995, McManus *et al.* demonstrated that when and 1 subunits were co-expressed in *Xenopus* oocytes, they increased the apparent Ca^{2+} sensitivity of BK channels. The association of 1 subunits with BK slowed down both the activation and deactivation kinetics of these channels (Dworetzky *et al*. 1996). When BK and 1 subunits were co-expressed, they showed a -70 mV shift in activation $V_{1/2}$ at higher $[Ca^{2+}]_i$ (McManus *et al.* 1995; Wallner *et al.* 1996; Brenner *et al.* 2000b; Latorre *et al.* 2017) compared to BK alone. In addition, the 1 subunit was an absolute requirement for the binding of activators such as 17 -estradiol, tamoxifen and lithocholic acid, since these compounds did not show effects on BK channels alone (Valverde *et al*. 1999; Bukiya *et al.* 2011; Latorre *et al*. 2017).

Together these results suggested that 1 subunits not only modulated BK channel gating but also modified their pharmacology.

1.5.3 2 subunit

The 2 subunit also enhanced the apparent sensitivity of the BK channels to Ca^{2+} and slowed down gating kinetics (Wallner *et al*. 1999; Xia *et al.* 1999) but, unlike 1 caused inactivation of the BK channels. These inactivating BK currents were observed for the first time in chromaffin cells of the adrenal gland, in pancreatic -cell lines and in hippocampal neurons (Solaro and Lingle, 1992; Herrington *et al*. 1995; Hicks and Marrion, 1998; Li *et al*. 1999). The 2 subunits are encoded by the *KCNMB2* gene (Wallner *et al*. 1999). The inactivation of these BK currents was abolished by enzymatic degradation, in a manner similar to that shown in inactivating Shaker K^+ channels (Hoshi *et al*. 1990) and Na^+ channels (Armstrong *et al*. 1973). These experiments suggested that an intracellular particle may be responsible for inactivation (Solaro and Lingle, 1992). Furthermore, in chromaffin cells obtained from 2 knockout mice, the inactivation of BK currents was abolished and showed reduced action potential firing rate (Martinez-Espinosa *et al.* 2014).

The 2 mediated inactivation of the BK channels had five distinct features. Firstly, the time constant of inactivation ($_i$) showed apparent voltage and Ca^{2+} dependence. It was observed that with increases in $[Ca^{2+}]_i$, the $_i$ was faster at more depolarising membrane potentials (Wallner *et al*. 1999; Xia *et al.* 1999). Secondly, inactivating currents in excised patches from cells co-expressing BK 2 subunits, were converted to sustained currents upon trypsin application. The gradual slowing of the time constant of inactivation with trypsin, was consistent with earlier reports which suggested that more than one 2 subunit was associated with the tetrameric BK channel (Wallner *et al*. 1999). Thirdly, in contrast to other potassium channels, the QA ion channel blockers like QX-314 did not alter the rate of inactivation. This suggested that the 2 mediated inactivation involved a different site to that of the cytosolic blockers. Fourthly, BK 2 possessed a different pharmacology to BK channels since they had a reduced sensitivity to charybdotoxin (CTX) and increased sensitivity to DHS-I, compared to BK alone. Lastly, like 1, 2 subunits also shifted the voltage-

dependent activation recorded in 10 M $[Ca^{2+}]_i$ to more negative membrane potentials (Solaro *et al*. 1997; Wallner *et al*. 1999; Xia *et al.* 1999).

1.5.4 Mechanism of 2 inactivation

The inactivation conferred by 2 was similar to the N-type inactivation mediated by the 20 amino acids in the NH_2-terminal of the Shaker K^+ channels (Hoshi *et al.* 1990; Solaro and Lingle 1992). In 1999, Wallner *et al*. illustrated that the 2 mediated inactivation, was due to the inactive present at the N-terminus of the 2 subunit. Subsequent mutagenesis experiments using deletion constructs showed that inactivation was abolished when 2-19 and 2-33 regions of the 2 N-terminus were deleted. Furthermore, Wallner *et al*. (1999) showed that synthetic peptides containing the first 19 or the first 26 amino acids of the 2 subunit, induced similar inactivation in BK channels. Taken together, these data suggested that the N-terminus of the 2 subunit was responsible for the inactivation of the BK current in *Xenopous laevis* oocytes (Wallner *et al*. 1999; Xia *et al*. 1999).

In 2003, Xia *et al*. identified the precise residues in the N-terminus responsible for inactivation. Their mutagenesis study demonstrated that the deletion of three hydrophobic amino acid residues (FIW) located at position 2-4 on the N-terminus or combined point mutations in the N-terminus eliminated inactivation. They also suggested that hydrophobic interactions may occur with residues in the wall of the BK channel's inner cavity (Xia *et al*. 2003). In contrast, deletion of residues 4-36 from the linker region failed to alter inactivation, suggesting that that neither the charge nor the structure of the linker affected inactivation (Xia *et al*. 2003). Their study concluded that a linker containing 12 amino acids and the terminal FIW motif were sufficient to impart inactivation by the 2 subunit (Xia *et al*. 2003).

1.5.5 3 subunit

3 subunits are predominantly expressed in the heart, liver, pancreas, adrenal medulla, adrenal cortex and stomach (Xia *et al*. 2000). This subunit is encoded by the *KCNMB3* gene which generates four different isoforms (3 a-d) as a result of alternative splicing (Uebele *et al*. 2000; Xia *et al*. 2000). Interestingly, 2 and 3 subunits share a 60% sequence similarity. BK 3 co-expression produced

rapid but incomplete inactivation in each of the 3a-c isoforms, but this was absent in the 3d isoform. The time constant of inactivation ($_i$) at +80 mV in presence of 30 M $[Ca^{2+}]_i$ was 45±15 ms for 3a, 60±6 ms for 3c, whereas for 3b the inactivation was much faster with a $_i$ of 1.5±0.2 ms (Brenner *et al*. 2000a; Uebele *et al*. 2000).

The fast inactivating currents generated by 3b subunits of BK channels showed a number of distinctive features. Firstly, like BK channels, the BK 3b were both voltage and Ca^{2+}-dependent, but the activation $V_{1/2}$ were shifted to more negative membrane potentials compared to BK channels. Secondly, although these currents were very rapid to inactivate, they showed incomplete inactivation. Interestingly however, the pharmacological properties of BK 3 subunits were not significantly different to BK alone, as exemplified by the effects of CTX, which blocked BK 3 currents with a similar affinity shown for BK currents. Finally, like 2, 3b inactivation was mediated by the N-terminal since deletion of 21 amino acid residues from N-terminus abolished the inactivation (Xia *et al*. 2000).

1.5.6 4 subunit

4 subunits are abundantly expressed in the brain and are encoded by the *KCNMB4* gene. This subunit plays a crucial role in modulating the excitability of neurons in the CNS (Weiger *et al*. 2000; Gonzalez-Perez and Lingle, 2019). Recently, Tao and MacKinnon (2019) published the detailed cryo-EM structure of the open human BK 3 channel along with the 4 subunit. Figure 1.10 shows the side view of the four 4 subunits (shown in blue) which protruded extracellularly above the BK 3 subunits (shown in red) by almost 40 Å. The human 4 complex in the presence of 10 mM Ca^{2+} had approximate dimensions of 150 Å x 150 Å x 150 Å (Figure 1.10; Tao and MacKinnon, 2019). The quaternary structure also confirmed that the transmembrane helices of the 4 subunits resided between the voltage sensor domains (VSDs) and that each 4 subunit interacted with neighbouring two VSDs simultaneously, which was consistent with disulphide cross-linking data from previous studies (Liu *et al*. 2008; Wu *et al*. 2009; Liu *et al.* 2010; Wu *et al.* 2013; Tao and MacKinnon, 2019). In addition, the

Tao and MacKinnon (2019) study illustrated that the linker between the two transmembrane domains (TM1 and TM2) of each 4 subunit consisted of 120 amino acids and formed a well-ordered structure on the extracellular side of the membrane. Collectively, the four 4 subunits formed a ‘crown’ shaped on top of the BK channel (Figure 1.10; Tao and MacKinnon, 2019).

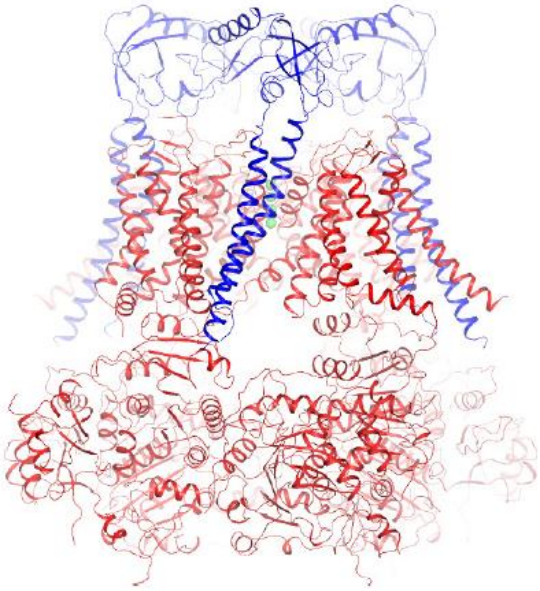

Figure 1.10: Overall cryo-EM structure of the human BK 3channel with 4 subunit.
The side view of human 4 complex, shown parallel to the cell membrane. The coloured ribbon structure represents the BK (red) and the 4 subunits (blue). The green spheres represent the K^+ ions in the selectivity filter (Adapted from Tao and MacKinnon, 2019).

From a biophysical point of view, co-expression of 4 subunits with BK slowed down both the activation and deactivation kinetics of BK channels (Brenner *et al*. 2000a), but their effect on Ca^{2+} sensitivity was more complex. The BK 4 currents recorded in lower $[Ca^{2+}]_i$ (<7 M) activated at more positive membrane potentials compared to BK alone. However, in higher $[Ca^{2+}]_i$, the BK 4 activated more negatively and showed enhanced activity compared to BK alone (Brenner *et al*. 2000a). An important characteristic of the 4 subunit was that in the presence of BK , the channels became resistant to blockers such as CTX and iberiotoxin (IbTx, Gan *et al*. 2008).

1.5.7 BK channel subunits

subunits are known to modulate BK subunit activity primarily by altering their voltage dependence. There are at least four auxiliary subunits and the ones characterised to date (Yan and Aldrich, 2010; Yan and Aldrich, 2012) are encoded by four different genes, namely *LRRC26, LRRC52, LRRC55* and *LRRC38*. The subunits belong to a group of leucine-rich repeat (LRR)-containing membrane proteins as reviewed by Latorre *et al*. (2017).

Prior to their discovery, Gessner *et al*. (2005) observed unusual biophysical properties of the K^+ channel in a prostate cancer cell line (LNCaP). These channels showed BK-like characteristics, however they activated at very negative membrane potentials under Ca^{2+} free conditions, as evidenced by a -100 mV shift in activation $V_{1/2}$ in LNCaP cells. However, Gessner and colleagues were unable to identify the reason for the negative shift in activation $V_{1/2}$ and consequently named these channels as 'BK-like' channels (BK_L, Gessner *et al*. 2005). However, Yan and Aldrich (2010) carried out a proteomic study to determine novel interacting partners which altered gating kinetics of BK channels in LNCaP cells. They identified a 35 kDa LRR-containing protein called LRRC26, which they named 1. The deletion of LRRC26 in LNCaP cells abolished the negative shift in $V_{1/2}$ observed in BK channels in 0 $[Ca^{2+}]_i$. Conversely, BK +LRRC26 co-expression in HEK293 cells shifted half maximal activation of BK channels by ~ -140 mV (Yan and Aldrich, 2010). The leftward shift in $V_{1/2}$ was subsequently shown to be due to the structural elements of the transmembrane domain and the adjacent cluster of positively charged amino acids in the cytosolic tail of the subunits (Li *et al.* 2015).

In 2012, Yan and Aldrich identified three other LRR-containing membrane proteins LRRC52 (2), LRRC55 (3) and LRRC38 (4) which were named according to their ability to promote a leftward shift of the BK channel conductance-voltage (G/V) curve (Figure 1.11B). Thus 2 shifted the $V_{1/2}$ by -100 mV, whereas 3 and 4 shifted it by -50 mV and -20 mV respectively (Yan and Aldrich, 2012).

Not only did each of these subunits modify the biophysical properties of BK channels, but they also showed a rather tissue specific distribution. For example, 1 subunits were highly expressed in prostate and salivary glands and they

showed relatively less expression in colon, small intestine, stomach, testis and arterial smooth muscle (Egland *et al*. 2006; Yan and Aldrich, 2010; Evanson *et al*. 2014). Along with the ability to promote a leftward shift in activation $V_{1/2}$ of BK channels, the 1 subunit also altered the pharmacology of BK channels. For instance, the BK channel activator mallotoxin shifted the activation $V_{1/2}$ by more than -100 mV (Zakharov *et al*. 2005) in the absence of the 1 subunit, but had very little voltage effect in native parotid acinar cells which expressed 1 subunits (Almassy and Begenisich, 2012). In 2017, Guan *et al.* demonstrated that mallotoxin shifted the activation $V_{1/2}$ of BK alone by -72 mV, however when the BK + 1 subunits were co-expressed in HEK293 cells and 2 M mallotoxin was applied, it only shifted the activation $V_{1/2}$ by -9 mV.

The 2 subunits are mainly expressed in skeletal muscles and testis whereas 3 are abundantly expressed in the brain and 4 subunits are highly expressed in adrenal gland, thymus and skeletal muscle (Yan and Aldrich, 2012; Zhang *et al*. 2018).

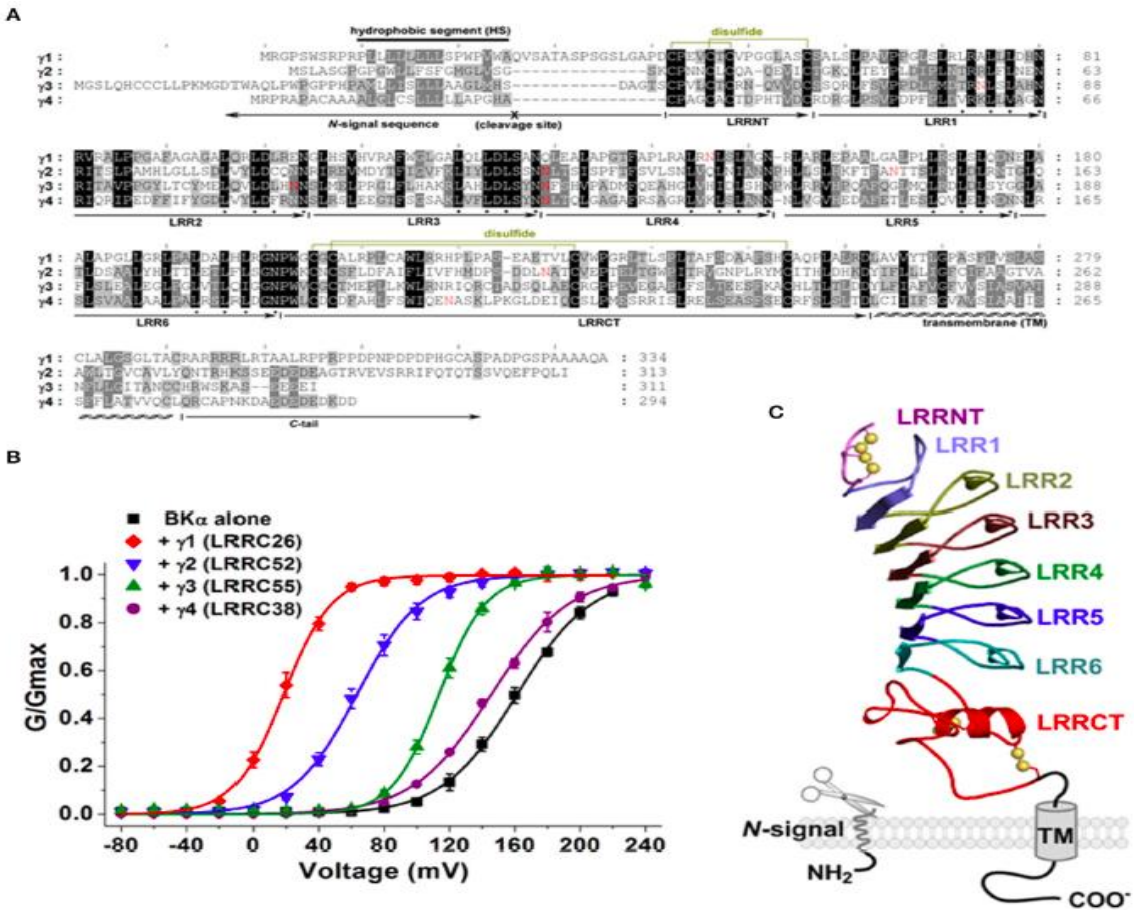

Figure 1.11: Multiple sequence alignment and topology of subunits. A Sequence alignment of 1-4 subunits with highlighted regions for LRR domain, transmembrane domain and cytosolic tail. **B** Effects of 1-4 subunits on voltage-dependent activation of BK channels in absence of $[Ca^{2+}]_i$ in HEK293 cells co-expressed with + 1-4 subunits. **C** Predicted membrane topology of subunit (Adapted from Zhang *et al*. 2014).

The subunits share 30-40% amino acid similarity (Figure 1.11A). The predicted structure of the subunits (Figure 1.11C) consists of a single-spanning transmembrane domain with an extracellular N-terminus, 6 extracellular LRR domains and a shorter C-terminus on the intracellular side. Note that the 1 has multiple proline residues in the C-terminus whereas the other subunits have polyacidic residues at the end of the C-terminus. The LRR motifs have a conserved sequence of LxxLxLxxN flanked by two cysteine-rich domains called LRRNT and LRRCT. These LRR domains are conserved with a high similarity as compared to the non-LRR regions between the subunits (Zhang *et al.* 2014).

The major functional effects of BK channels with specific subunits are summarised in Table 1.5.

Table 1.5 Modulatory effects of BK channel subunits (Adapted from Gonzalez-Perez and Lingle, 2019).

BK channel	[((***alone***	***Inactivation***	***Pharmacology***
-alone	NA	NA	CTX (2-4 nM)
1-containing	-70 mV leftward shift at higher Ca^{2+}	None	CTX (8 nM)
2-containing	-50 mV leftward shift at higher Ca^{2+}	Complete inactivation 20-40 ms	Some CTX and iberiotoxin (IbTx) resistance, CTX (30-60 nM)
3-containing	-30 mV leftward at both 0 and higher Ca^{2+}(mouse)	Human: β-50ams (incomplete) (but incompl ms. Mouse: β (complete), inactivation. β3: no inactivation.	CTX (60-80 nM)
4-containing	+20 mV rightward shift at low Ca^{2+}, but a -25 to -50 mV leftward shift at higher Ca^{2+}	None	Almost complete resistance to IbTx and CTX block
1-containing	-120 mV leftward shift at both 0 and higher Ca^{2+}	None	Mallotoxin resistance
2-containing	-100 mV leftward shift at all Ca^{2+}	None	None
3-containing	-50 mV leftward shift at both 0 and higher Ca^{2+}	None	None
4-containing	-20 mV leftward shift at both 0 and higher Ca^{2+}	None	None

1.6 Leucine rich repeat (LRR)-containing proteins

The subunits described above are members of a much larger family of leucine rich repeat proteins, commonly known as LRR and are conserved across bacteria, viruses, archaea, plants and other eukaryotic species (Matsushima *et al*. 2012). LRR-containing proteins participate in protein-ligand or protein-protein interactions. These repeating units have a highly conserved segment (HCS) at the N-terminal and a variable segment at the C-terminal. The HCS consists of a stretch of 20-30 amino acids which contain LxxLxLxxNxL or LxxLxLxxCxxL,

where: x is any amino acid; with a fixed position of leucine L, or a hydrophobic amino acid like valine, isoleucine or phenylalanine; N is asparagine, threonine, cysteine or serine; and C is cysteine or serine (Ohyanagi and Matsushima, 1997; Kajava, 1998; Kobe and Kajava, 2001).

1.6.1 Structure of LRR-containing proteins

The individual LRRs are arranged in two or more repeats that form the LRR motif of these proteins. The highly conserved part of the LRR domain forms a -strand and a loop, which connects to the C-terminal part of the repeat (Kajava, 1998; Kobe and Kajava, 2001). The first crystal structure of an LRR containing protein was from the ribonuclease inhibitor protein (RI, PDB ID: 2BNH, Figure 1.12B) and illustrated that it formed a single continuous arc or horseshoe shape (Kobe and Deisenhofer, 1993). Figure 1.12A shows the individual LRR from RI protein, which is composed of a right-handed -strand (orange) connected by a loop region (teal) to an -helix motif (red) roughly parallel to the strand (de Wit *et al.* 2011). The significant feature of an LRR domain was the concave side of the arc which was formed by -strand of each repeat and the convex side of the domain consisted of -helices. The LRR domains showed a greater number of -helices on the convex side and therefore a more pronounced curvature, this suggested that varying the length and number of repeats of -helices affected the curvature of the domain (Bella *et al.* 2008; de Wit *et al.* 2011). Figure 1.12B-F show different examples of LRRs of various proteins (de Wit *et al.* 2011). The curved structure consisting of an exposed -sheet and variable -helices in these LRR domains, is thought to increase the number of potential ligand binding sites and thus enhance protein-protein interactions (Kobe and Kajava, 2001).

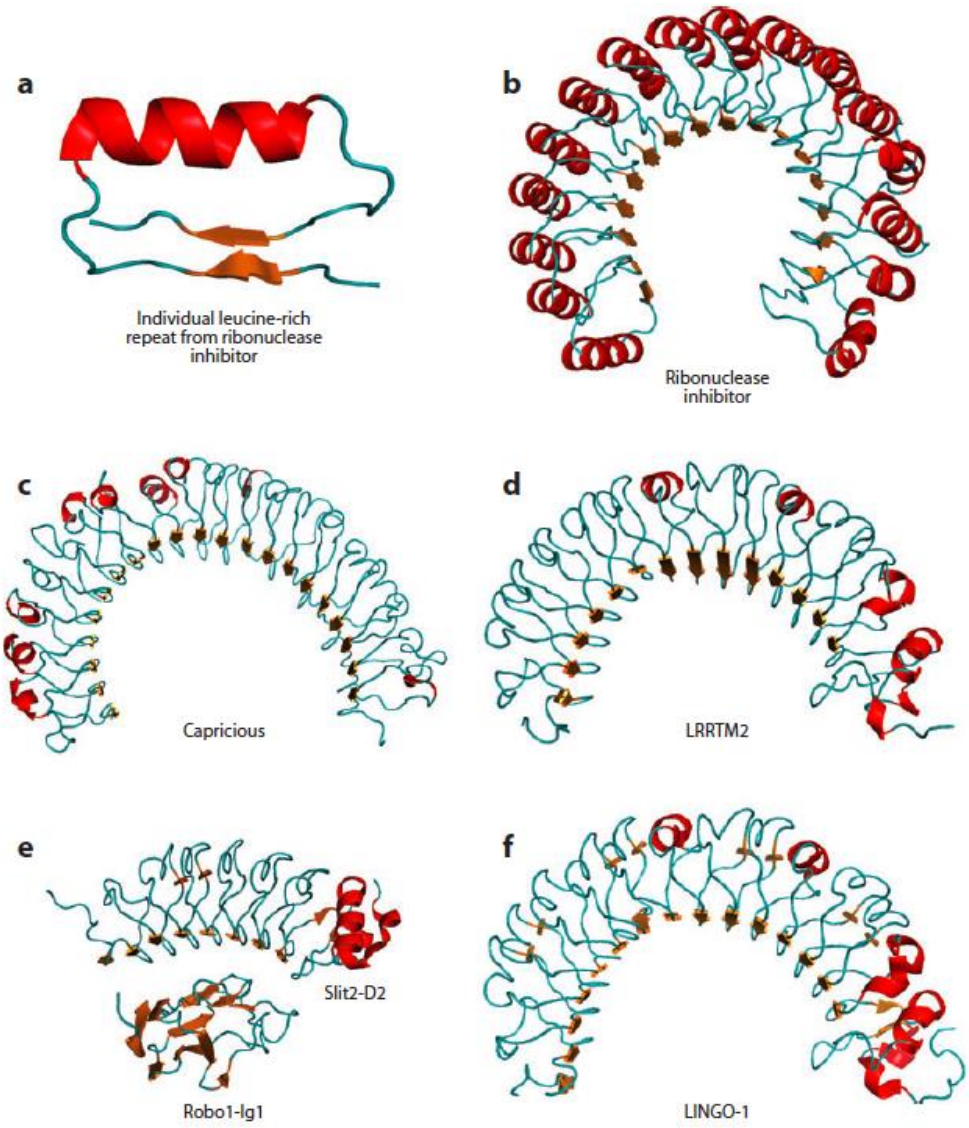

Figure 1.12: Structure of LRR domains in various proteins. A Individual LRR from RI. The -strand (orange) is connected by a loop (teal) to an -helix motif (red). The -strand of the consecutive LRR is also shown. The colour code is identical for all panels. **B** Ribbon diagram of the 3D structure of the porcine RI. **C** Homology model of the ectodomain of Drosophila Capricious. **D** Homology model of the ectodomain of human LRRTM2. **E** 3D structure of the second LRR domain of Slit in complex with the first immunoglobulin-like (Ig) domain of Robo1. **F** 3D structure of the LINGO1 ectodomain (Adapted from de Wit *et al*. 2011).

1.6.2 Classification of LRR proteins

The LRR proteins are classified into intracellular and extracellular LRR proteins, both of which are known to be important for the immune system in plants and innate immune system in mammals (Nurnberger *et al*. 2004). The extracellular class of the LRR-proteins (eLRRs) in vertebrates has expanded to about 140 genes coding for these proteins. In 2007, Dolan *et al*. classified these eLRRs based on domain architecture and clustering into four major categories namely,

1. LRR-Ig/Fn3 proteins consisting of an Immunoglobulin (Ig) or Fibronectin type-3 (FN3) domain and extracellular LRRs,

2. LRR-Tollkin proteins which contained a cytoplasmic Toll/interleukin 1 receptor domain along with extracellular LRRs,

3. LRR-Other proteins consisted of LRRs with other domain repeats, like epidermal growth factor (EGF) or a G-protein-coupled receptor (GPCR) domains and

4. LRR-Only category contained no other identifiable domain apart from LRR (Dolan *et al.* 2007).

1.6.3 Function of eLRRs

The role of a large number of eLRRs still remains to be elucidated. Apart from Toll-like receptors, which are known to be involved in immunity, several of these proteins are involved in neuronal growth and development, synapse formation, myelination, neuronal survival, axon guidance, increased plasticity, and nerve regeneration in nervous system (Long *et al*. 2004; Bando *et al.* 2005; McGee *et al*. 2005; Mi *et al*. 2005; Bermingham *et al*. 2006; de Wit *et al*. 2011). Given their importance in neuronal development, more of these eLRRs are being studied and have been implicated in neurological or psychiatric disorders like Tourette's syndrome, schizophrenia, Alzheimer's disease, autism, and epilepsy (Majercak *et al.* 2006; Kielian, 2009; Okun *et al.* 2009; Sousa *et al.* 2010).

1.6.4 LRRIG proteins

The LRRIG proteins are a family of proteins consisting of both the LRR and Ig domains. The presence of an Ig domain enables the numerous interactions of these proteins with other proteins consisting of an Ig domain or other molecules like antigens and sugars. Thus, the presence of two unique binding (LRR and Ig) domains enhances the wide range of protein-protein interactions (Mandai *et al.* 2009). The LRRIG family comprises of 36 separate proteins, which have been categorised (Homma *et al.* 2009) into several different subclasses consisting of (1) four LINGO (LRR and Ig domain-containing, Nogo Receptor-interacting) proteins, (2) three NGL proteins (netrin-G ligand), (3) five SALM proteins (synaptic adhesion-like molecules), (4) three NLRR proteins (neuronal leucine-rich repeat), (5) three Pal proteins, (6) two ISLR proteins (immunoglobulin superfamily containing leucine-rich repeat), (7) three LRIG (leucine rich repeats and immunoglobulin-like domains proteins), (8) two GPCR, GPR124 and GPR125 (G protein-coupled receptor 124 and G protein-coupled receptor 125), (9) two Adlican (adhesion protein with leucine-rich repeats and Immunoglobulin domains related to perlecan) proteins, (10) two human Peroxidasin-like proteins, (11) three Trk neurotrophin receptors, (12) yet an unnamed protein, AAI11068 and finally (13) three AMIGO proteins (amphoterin-induced gene and ORF).

1.7 LINGO proteins

The LINGO (LRR and Ig domain-containing, Nogo Receptor-interacting) proteins have four subtypes *viz*. LINGO1, LINGO2, LINGO3 and LINGO4. The amino acid sequence of LINGO1 and LINGO2 share 61% similarity, whereas LINGO3 shares 56% similarity with LINGO1 and LINGO4 shares 44% sequence similarity with LINGO1 (Mi *et al*. 2013).

1.7.1 LINGO1 protein

LINGO1 is evolutionarily conserved, where human and mouse orthologs share 99.5% sequence identity. LINGO1 is abundantly expressed in brain and spinal cord and is apparently absent in non-neuronal tissues like heart, lung, kidney, small intestine, pancreas, muscle and liver in rat tissue lysates (Mi *et al*. 2013). Interestingly however, the human protein database suggested that there may be considerable LINGO1 protein expression in the human lung tissue, as well as

abundant expression in the brain (https://www.proteinatlas.org/ENSG00000169783-LINGO1/tissue; Uhlén *et al.* 2015).

1.7.2 Structure of LINGO1

The *LINGO1* gene is located on chromosome number 15 and encodes LINGO1 protein, which consists of 620 amino acids and contains five major structural elements namely: LRR domain, Ig domain, stalk, transmembrane region, and a cytosolic tail (Mi *et al*. 2013; Saha *et al.* 2014).

The crystal structure of the extracellular part of human LINGO1 protein, which was expressed in lectin-resistant CHO cells was resolved by Mosyak *et al*. (2006) at a resolution of 2.7 Å. Their data suggested that the LINGO1 protein formed a stable tetramer and enabled the protein-protein interactions with the Nogo receptor (NgR) complex (Mosyak *et al*. 2006).

The LRR part of LINGO1 monomers fold to structure as illustrated in Figure 1.13. The N-terminal of the LRR motif shares structural similarity with the NgR ectodomain, although there are subtle differences in the arc length (Mosyak *et al*. 2006). In LINGO1 there are 12 LRRs, each consisting of 23-25 residues. Every LRR contains a conserved repeat motif of the following 24 pattern xLxxLxLxxNxLxxLxxxxFxxLx, where x is any amino acid; L are hydrophobic residues, preferably Leu, but also Ile, Val, Met, Phe, or Thr; N are less conserved in nature and mostly include Asn, but also Cys, Asp, Leu, or Trp; F represents Phe or Leu (Mosyak *et al*. 2006). The conserved residues at the indicated positions form the interior of the LRR domain and this is flanked by cysteine-rich regions on either side. The Ig domain contains five-strand -sheets which are tightly curved and twisted (A ,' C, C ,' F, and G) and four flattened and smaller (A, B, D, and E) -sheets. This Ig domain is highly homologous to the structure of the Ig3 domain of the neural cell adhesion molecule (NCAM; Soroka *et al*. 2003). The perpendicular topological arrangement of the LRR and the Ig domain creates a wide, 22 Å deep and 35 Å long, cleft which enables binding of various proteins (Mosyak *et al.* 2006).

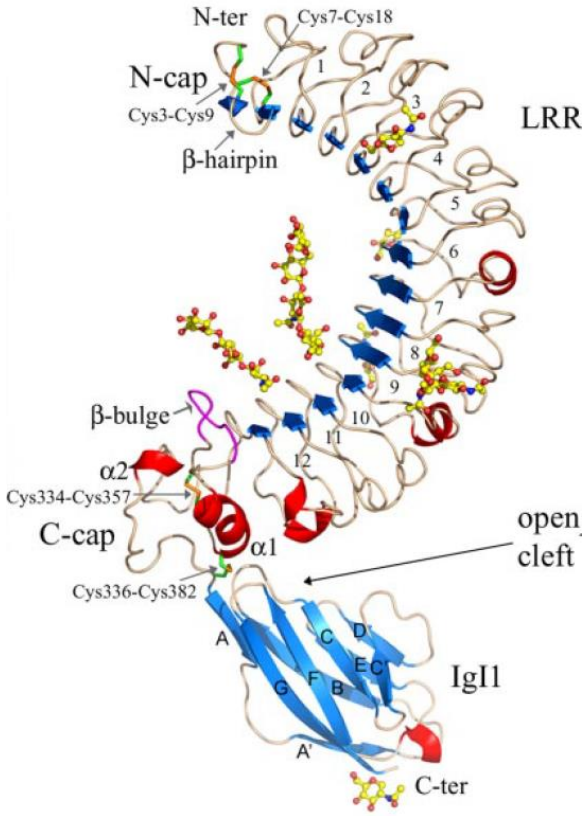

Figure 1.13: Structure of the LINGO1 protein. Side view of the LINGO1 protein showing the architecture according to the secondary structure. Different colours represent the LRR coil (beige), strand (blue), and -helix (red). The LRR coil consist of 12 LRRs (numbered). The disulphide bridges are shown in green and the N-linked carbohydrates are shown in yellow. The Ig domain is shown below on the right-hand side (Adapted from Mosyak *et al*. 2006).

1.7.3 Function of LINGO1

LINGO1 is abundantly expressed in the oligodendrocytes and neurons of the CNS and is thought to be involved in the negative regulation of oligodendrocyte differentiation, neuronal survival, and axonal regeneration (Mi *et al.* 2004; Mi *et al.* 2005; Yin and Hu, 2014). LINGO1 levels are upregulated during CNS injury across species and is also elevated in human CNS disorders like autoimmune encephalomyelitis (Mi *et al*. 2007; Mi *et al*. 2009). However, the mechanisms which lead to upregulation of LINGO1 are still unknown.

Additionally, it has been reported that LINGO1 promotes the lysosomal degradation of -amyloid precursor protein (A PP) and carboxy-terminal fragment (CTF), in the presence of the -secretase inhibitor in cortical neurons (de Laat *et al.* 2015). Interestingly, LINGO1 expression was localised to

intracellular puncta, possibly reflecting expression on intracellular membranous organelles, however, no cell-surface LINGO immunoreactivity was apparent in both mouse cerebellar granule neurons and cardiac myocytes (Meabon *et al.* 2015).

Moreover, LINGO1 binds to growth factor receptors like NgR, TrkB, EGFR and Erb-B2 in the CNS and negatively regulates downstream signalling molecules involved in axonal regeneration, neuronal survival, oligodendrocyte differentiation and myelination (Mi *et al*. 2013). In Multiple Sclerosis (MS), demyelination of neurons leads to inflammation which is chronic and progressive. The use of an anti-LINGO1 antibody increased the number of thinly myelinated axons in demyelinated area, demonstrating that anti-LINGO1-antibody treatment promoted axonal remyelination (Mi *et al*. 2009). This approach has been proposed as a possible treatment method for MS (Mi *et al*. 2009), although Phase II clinical trials have not been successful (https://clinicaltrials.gov/ct2/show/NCT03222973). Despite this setback, LINGO1 continues to be targeted in drug development programmes and Li-81, an antagonist of LINGO1, has been shown to promote myelination of neurons in patients with MS (Pepinsky *et al*. 2014). This study provided the crystal structure of extracellular LINGO1 bound to the Li-81 antibody and demonstrated that it attached to the convex surface of the LINGO1-Li81-Fab complex. Pepinsky *et al*. (2014) demonstrated that this inhibited the tetramerisation of LINGO1, presumably inhibiting it and promoting myelination of neurons.

In 2004, Mi *et al.* uncovered the physical interaction of LINGO1 with the NgR1 receptor complex by probing protein interactions in cell-binding assays. LINGO1 is a part of NgR1 complex which is involved in Rho activation and axon degeneration. Upon binding of inhibitory molecules like myelin-associated glycoprotein (MAG), Oligodendrocyte-myelin glycoprotein (OMgp) and NogoA, the NgR1 receptor forms a complex with LINGO1 and P75/Troy, activates RhoA and blocks neurite outgrowth (Mi *et al.* 2004). In 2006, Ji *et al.* demonstrated that mouse models of spinal cord injury which showed complete hind limb paralysis, when treated with continuous intrathecal infusion of LINGO1-Fc reduced both, axon retraction and RhoA activation and therefore, improved hind limb function. This data supported the idea that blocking LINGO1 promoted axonal regeneration and recovery following spinal cord injury.

LINGO1 is negatively associated with axonal regeneration, neuronal survival, oligodendrocyte differentiation and myelination and has also been shown to be upregulated in patients with Parkinson (PD, Delay *et al.* 2014; Seiler and Widme, 2015). In 2007, Inoue *et al.* demonstrated that inhibition of endogenous LINGO1 using genetic (*LINGO1* knock out mice) or pharmacological (anti-LINGO1 antibody and LINGO1-Fc protein) approaches resulted in restoring the regenerative properties of dopaminergic neurons in a PD model. Other studies have demonstrated that LINGO1 was upregulated in the cerebellar cortex and cerebellar white matter of patients who suffered from Essential Tremor (ET) for more than twenty years (Delay *et al.* 2014). LINGO1 has also been implicated in other neurodegenerative diseases like glaucoma and the use of anti-LINGO1 antibody reduced retinal ganglion cell loss in rat hypertension models (Fu *et al*. 2008).

In 2010, Vilariño-Güell *et al.* performed genome sequencing from a cohort of patients with ET and PD and identified novel variants of LINGO1 (chromosome 15; S4C, V107M, A277T, R423R, G537A, and D610D) and LINGO2 (chromosome 9; D135D, P217P, and V565V). In addition, other single nucleotide polymorphisms (rs7033345 and rs10812774) of LINGO2 have been implicated in movement disorders like ET and PD, which suggested that LINGO2 may have a role in neurological function (Wu *et al.* 2011). LINGO2 was implicated in autism spectrum disorders which suggested that it may be a part of novel autism risk genes (Matsunami *et al.* 2013). Previous studies have shown that LINGO2 is predominantly expressed in the CNS (Haines *et al*. 2008; Homma *et al.* 2009). Interestingly, a recent study demonstrated that LINGO2 co-immunoprecipitated and showed co-localisation with Trefoil factor 3 (TFF3) in intestinal epithelial cells (Ji *et al*. 2019). It has also been demonstrated by Hansel *et al*. (2015) that the single nucleotide polymorphisms (rs10491678, rs683471, rs10813121 and rs640850) of LINGO2 have been implicated in Chronic Obstructive Pulmonary Disease (COPD).

In 2008, Haines *et al.* demonstrated via whole mount *in situ* hybridisation, that LINGO3 was expressed in the CNS during early embryogenesis in mouse. In a recent study it was demonstrated that LINGO3 was expressed in human and mouse mucosal epithelia near Trefoil factor 2 (TFF2) secretion sites (Zullo *et al.* 2018). Furthermore, the expression of LINGO4, similar to the other LINGO

subtypes, was restricted to the CNS during early mouse embryogenesis (Haines *et al.* 2008). The role and function of LINGO4 remains to be elucidated.

A recent study published by our lab demonstrates the effects of LINGO1 on BK channels. When LINGO1 protein was co-expressed with BK in HEK cells, these currents showed a rapid and complete inactivation of the BK channels (Dudem *et al.* 2020).

To further investigate how the LINGO1 protein caused inactivation, deletion constructs of the C-terminal tail of the LINGO1 protein were designed (Δ 6 960-620, Δ 6 1632 0 , -620-6) and co-expressed with BK in HEK293 cells. Interestingly, all of the deletion constructs when co-expressed with BK in HEK293 cells abolished inactivation (Dudem *et al.* 2020). The use of these deletion constructs helped us identify that the last eight residues of the LINGO1 C-terminus were responsible for inactivating BK channels (Dudem *et al.* 2020).

1.8 Aim of the study

According to the literature presented previously, it is clear that the pharmacological and the physiological properties of the BK channels can be modulated by auxiliary and subunits. Interestingly, some LRRIG family members appear to have similar features to those of subunits, yet until this study, the effect of the LINGO proteins on the BK channels had not been examined.

This thesis will focus on investigating the interacting partners between BK and LINGO1 proteins. In order to achieve this, we examined the following:

1) the effect of the LINGO tail peptides on BK channels.
2) the contribution of LINGO1 tail residues on BK channel inactivation.
3) elucidated the role of net positive charge and positively charged residues in LINGO1 tail peptide-mediated inactivation of BK channels.

1.9 Methodology: principles of patch-clamp recording

The major technique utilised in this thesis is voltage clamp patch-clamping. The following sections detail the principles and overview of patch-clamp recording.

1.9.1 Electrophysiology

The voltage clamp technique was invente
Marmont and further revised by Hodgkin and Huxley in 1952. In 1976, Neher and Sakmann developed the patch clamp technique. There are two main configurations of the patch clamp technique which are current clamp and voltage clamp. In this study, the voltage clamp technique has been utilised, whereby the voltage difference across the cell membrane was controlled in order to measure the flow of ionic currents.

A glass pipette filled with an appropriate physiological solution was inserted on a chlorided silver electrode. A similar electrode was also used in the bath to act as an earth electrode. In order to record currents from a single cell, the first step is the formation of a gigaseal. This was achieved by applying a suction to the pipette in order to form a high resistance seal (>10 G) between the pipette tip and the cell membrane. The formation of a high resistance seal isolated the membrane patch from the external solution and enabled recording of ionic current and also reduced background noise.

The electrode in the pipette was connected to the negative input (-) of the amplifier and voltage set by the experimenter, known as command potential (V_{com}) was connected to the positive input (+) of the amplifier. A feedback resistor between the output and the negative input helped to compare the voltages between the pipette (V_p) and V_{com}. Whenever a difference between V_p and V_{com} occurred, a compensatory current was injected into the cell through the feedback loop to ensure $V_p=V_{com}$. The compensatory current was recorded which represented the ionic flux across the membrane and helped to understand membrane conductance.

During the recording, the bath was continuously perfused with Hanks solution which was heated via a glass heat exchanger to maintain the bath temperature between 35-37 C. A gravity-fed perfusion drug delivery system was used to apply various drugs to the cells or excised patches. The drug delivery system consisted of a series of 20 ml syringes which were elevated with respect to the position of

the bath. The tubing from these reservoirs was sealed into a 1 ml syringe with silicone to prevent backflow of the fluid. A glass pipette with a diameter of ~200-300 m was attached to the end of a 1 ml syringe and placed at a distance of approximately 100 m from the cell, to allow the application of a drug or a solution to the cell being patched (Figure 1.14).

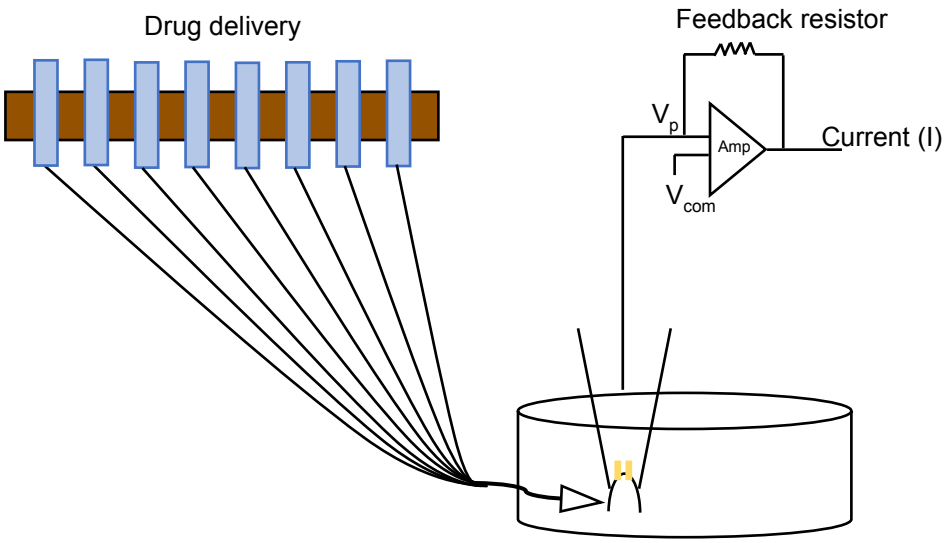

Figure 1.14: Diagrammatic representation of inside-out patch clamp setup. An electrolyte solution was filled in a glass pipette and a tight seal was formed with the cell membrane. The current flowing through the cell was recorded by a silver electrode which was connected to an amplifier. The intracellular environment was altered with the gravity-fed drug delivery system.

There are five main patch clamp configurations namely:
i) Cell-attached configuration, ii) Whole-cell configuration, iii) Inside-out configuration, iv) Outside-out configuration and v) Perforated-cell configuration. A diagrammatic representation of each configuration is shown in Figure 1.15.

1.9.1.1 Cell-attached configuration

In this configuration, a gigaseal was formed between the pipette and the cell membrane by application of suction, while ensuring that the cell membrane remained intact. This configuration is used to study either single or a small number of ion channels present in the membrane surrounded by the pipette. This configuration helps to minimise alterations to the structure and the intracellular milieu of the cell.

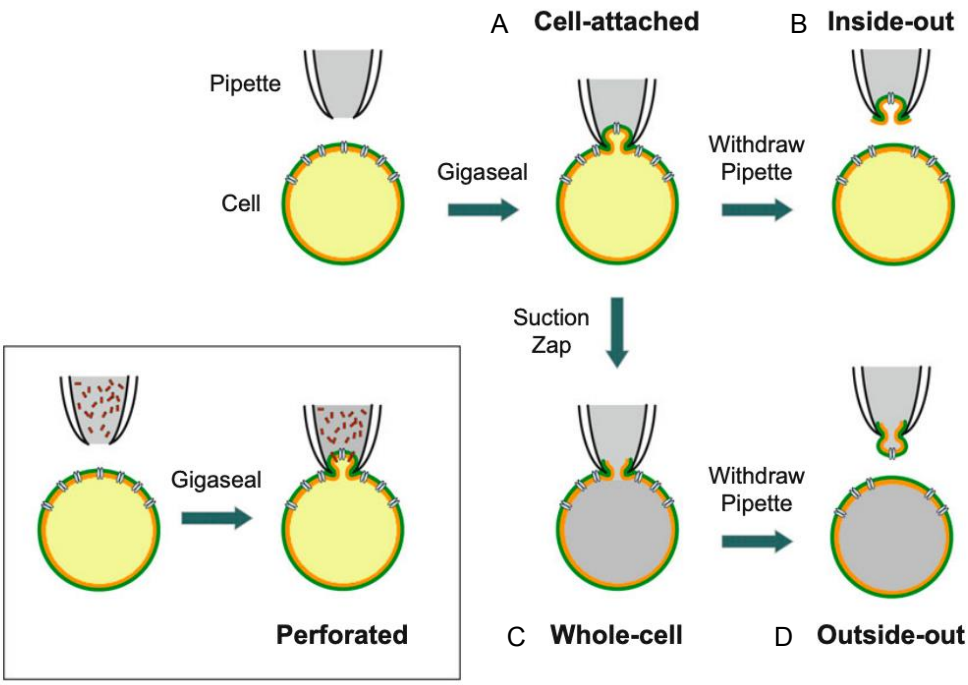

Figure 1.15: Diagrammatic representation of patch clamp configurations. The first step for all patch clamp procedures is to obtain a gigaseal. After formation of a gigaseal the following configurations can be achieved. **A** Cell-attached configuration. **B** Inside-out configuration. **C** Whole-cell configuration. **D** Outside-out configuration. Inset shows perforated-cell configuration (Adapted from Chen, 2017).

1.9.1.2 Whole-cell configuration

In the whole-cell configuration, after a gigaseal was formed, strong suction was applied to rupture the cell membrane enabling the pipette to have direct contact with the cytoplasmic contents of the cell. The patch can be ruptured by either the application of negative pressure or through application of a high voltage zap to the cell membrane via the pipette. Once electrical continuity is achieved between the cell and pipette, ionic currents across the entire cell membrane can be recorded.

1.9.1.3 Inside-out configuration

This configuration was used to investigate the effect of LINGO peptides on WT BK , BK mutants and co-expression studies of BK :LINGO1. In this configuration, after formation of a gigaseal, the pipette was rapidly pulled away from the cell, such that a patch of membrane was excised from the cell and then

the inside of the cell was facing the bath solution (Hamill *et al*. 1981). This configuration of the patch clamp technique is advantageous to study 1) single channel currents from a patch of membrane rather than from the entire cell, 2) the effect of different $[Ca^{2+}]_i$ on a given patch of membrane during the same experiment, 3) the alteration of intracellular environment of the cell membrane by the use of the gravity-fed drug delivery system during the same experiment.

1.9.1.4 Outside-out configuration

In the outside-out configuration, after formation of a gigaseal, strong suction was applied to rip a hole in the cell membrane. The pipette was pulled away so that the two ends of the ruptured cell membrane can meet and join together to form a vesicle. In this configuration, the cytosolic side of the membrane was in direct contact with the contents of the pipette.

1.9.1.5 Perforated-cell configuration

After the formation of the gigaseal, pore-forming agents such as the antibiotic amphotericin were used to perforate the cell membrane and thus, develop electrical continuity between the pipette and the cell. This technique allowed the permeation of small ions across the membrane whilst excluding larger ions. Consequently, this configuration reduced current rundown by preventing the dialysis of second messengers and minimised disruption to the interior of the cell.

2. Materials and Methods

2.1 Mouse dissection and micro dissection

Adult male and female C57BL/6 mice aged between 6-14 weeks were euthanised by intraperitoneal application of pentobarbital. The process of euthanasia was approved by the Dundalk Institute of Technology Animal Care and Use Committee and complied with EU directive 2010/63/EU.

The trachea and lungs were removed and placed in a Petri dish with a sylgard base, containing calcium-free Hanks solution (for composition refer to Section 2.13). After performing fine dissection under the microscope, the primary bronchi were obtained.

2.2 RNA extraction

For bronchus tissue: The bronchi from two WT mice of the same age and sex were dissected as described above and tissue obtained was pooled as a single RNA sample. The dissected tissue was stored in 200 l RNA later (Sigma). The bronchial tissue was flash frozen in liquid nitrogen and then pulverised using a chilled (-80 C) mortar and pestle. The pulverised tissue was immediately transferred into an RNase-free Eppendorf tube (1.5 ml) and homogenised in 500 l TRIzol (Invitrogen). The mixture was then incubated at room temperature (RT) for 5 minutes before trituration using 18-Gauge and 21-Gauge needles to break down the tissue sample further. RNA from the brain tissue was extracted using a similar protocol but the pulverisation step was omitted. Next, 200 l of chloroform (Sigma) was added and the samples were vortexed for 15 seconds followed by incubation at RT for 3 minutes. Samples were then centrifuged at 16,000 g at 4 C for 15 minutes. The upper aqueous phase was transferred to a sterile Eppendorf tube. RNA was precipitated by adding 500 l of isopropanol (Sigma) per ml of TRIzol. Samples were vortexed again and incubated at RT for 10 minutes before being centrifuged at 16,000 g for 10 minutes at 4 C and the supernatant was decanted and the remaining pellet was washed with 75% ethanol (Sigma). Samples were vortexed and centrifuged at 16,000 g for 5 minutes at 4 C. Supernatant was removed prior to air drying the pellet for 5 minutes. This was resuspended in 30 l of Nuclease Free Water (NFW) by passing the pellet

through a pipette tip. Sample purity and concentration was quantified using a NanoDrop 2000 spectrophotometer (Thermo Scientific) and was stored at -80 C until further use.

2.3 Reverse Transcriptase Polymerase Chain Reaction (RT-PCR)

2.3.1 DNase Treatment

For the synthesis of complimentary DNA (cDNA), RNA samples were first treated with DNase 1 (Invitrogen) to eliminate genomic DNA contamination. DNase 1 (1 l) was added to each RNA sample (1 g / 10 l) and incubated for 15 min at RT. The reaction was terminated by addition of EDTA (25 mM; 1 l) to the sample and then heated at 65 C for 10 minutes. Upon completion of DNase treatment, the RNA sample was ready to be used for reverse transcription.

2.3.2 Synthesis of cDNA

The double-stranded DNA synthesised from single stranded RNA catalysed by reverse transcriptase enzyme is called complimentary DNA (cDNA). RNA isolated from brain and primary bronchus tissues was synthesised into cDNA using SuperScript^{TM}II RNase-H Reverse Transcriptase (Invitrogen). To reverse transcribe 5-10 l / 1-5 g of total RNA, random hexamers (200 g/ l) were used. The reverse transcription reaction was carried out in a TECHNE TC-512 thermal cycler. For the first step of the reaction, a mixture containing total RNA, random hexamers and deoxyribonucleotide triphosphates (dNTPs) was heated for 5 minutes at 65 C. This was followed by a quick chill on ice and the addition of First-Strand cDNA synthesis buffer (Invitrogen), 0.1 M dithiothreitol (DTT) and RNaseOUT^{TM} Recombinant Ribonuclease Inhibitor (5000 units). The mixture was then vortexed and incubated at 25 C for 2 minutes. SuperScript^{TM}II Reverse Transcriptase (200 units) was added to the mixture and incubated at 25 C for 2 minutes. A step for the initial activation of the Superscript was achieved at 42 C for 50 minutes and this was then reversed by an inactivation step at 70 C for 15 minutes. The synthesised cDNA was stored at -20 C.

2.3.3 Reverse Transcriptase-PCR (RT-PCR)

The Polymerase Chain Reaction (PCR) involves three major steps (denaturation, annealing and elongation) performed at specific temperatures. It requires components such as thermostable DNA polymerase, a buffer solution containing magnesium ions and dNTPs. In this study, to check the presence of genes of interest in brain and primary bronchi, the PCR technique was used. For the RT-PCR experiments, a commercially available PCR Mastermix-AmpliTaq Gold™ (Fisher Scientific), containing all the necessary components was used. The PCR reaction also required three more components: the cDNA template, the forward and finally the reverse primers (10 M). The volume of each component used for a single PCR reaction is detailed in Table 2.1.

Table 2.1 PCR reagents

Contents	***Volume (l)***
AmpliTaq Gold mixture (x2)	12.5
Nuclease Free Water	8.5
Forward primer	1
Reverse primer	1
Synthesised cDNA	2
Total volume	25

A TECHNE TC-512 thermal cycler was used to carry out RT-PCR reactions. These reactions had an initial denaturation step at 95 C, followed by pre-programmed thermal protocol for 40 cycles. Table 2.2 details the temperature and duration of each step. The PCR products were stored at -20 C until further use.

Table 2.2 Steps used in PCR amplification

Step	*Temperature (C)*	*Time (minutes)*	*Number of cycles*
Initial denaturation	95	5	1
Denaturation Annealing Extension	95 60 72	0.5 0.5 0.5	40
Final Extension	72	1	1

2.3.4 Custom Primer Design

To design custom primers for each gene of interest, the following procedure was used. An mRNA sequence of a given gene was identified using Nucleotide database on NCBI (https://www.ncbi.nlm.nih.gov/nucleotide/). A RefSeq sequence of the gene was used and its GenBank reference number was noted and the Primer BLAST tool of NCBI was used (https://www.ncbi.nlm.nih.gov/tools/primer-blast/). The following parameters were used to design primers: primer length range between 18-24 bp, amplicon size between 100-300 bp, to ensure that the same primer pairs could be used in both RT-PCR and quantitative real-time PCR (Q-PCR). Oligo Calc: Oligonucleotide Properties Calculator was used to ensure the minimal occurrence of hairpin loops, palindromes and primer-primer interaction within gene specific primers (http://biotools.nubic.northwestern.edu/OligoCalc.html). The required primers were synthesised by Bio-Sciences Limited (Dublin, Ireland) and were stored at -20 C until further use. The sequence of each primer used in this study is listed in Table 2.3.

Table 2.3 Primer sequences

Primer name	***- / / /***	***Genbank ID***	***Expected Amplicon Size (bp)***
Mouse LINGO1 F Mouse LINGO1 R	ATGCTGGCAGGGGGTATGA GTCTTGATGCGGTTTTTGCCC	NM_181074.5	236
Mouse LINGO2 F Mouse LINGO2 R	ATGCTTCACACGGCTATACCA TCGTCTTCTGTGGCAGCTAAC	NM_175516	141
Mouse LINGO3 F Mouse LINGO3 R	CTGGACCTGAGCGAGAACAA CGGGAGATGAACACCAGGTC	NM_001013758.2	110
Mouse LINGO4 F Mouse LINGO4 R	AGGCGACTGGACACTATTCC TCAGGGTGAGTAGACTTTGTAGG	NM_177250	196

2.3.5 Agarose Gel Electrophoresis

Nucleic acid gel electrophoresis was used to separate DNA fragments according to their size on an agarose gel. The movement of negatively charged DNA occurs through the porous matrix of the agarose gel based on amplicon size, wherein the smaller DNA amplicons move faster as compared to the larger molecules. In this study, a 2% agarose gel was used. The gel was prepared using 2.4 g of Ultra-Pure Agarose powder (Invitrogen) in 120 ml of 1X Tris Acetate-EDTA buffer (TAE, Sigma). This was heated to the boiling point in a microwave oven and then allowed to cool to temperatures between 50-55 C, before the addition of 8 l of SYBR Safe DNA gel stain (Invitrogen), which was included to allow the visualisation of DNA during UV illumination. The gel mixture was poured into an electrophoresis casting tray and a comb was inserted to obtain the desired number of wells. The gel was left to solidify for 30 minutes, prior to insertion in an electrophoresis chamber (Scie-Plas, UK) filled with 1X TAE buffer. The comb was removed and the chamber was connected to a power supply. 10 l of RT-PCR product was mixed with 2 l of 6X DNA loading buffer (Thermo Fisher Scientific) and subsequently added into the wells. To help indicate relative amplicon size, a mixture containing 2 l of 100 bp DNA Ladder (Thermo Fisher Scientific), 2 l of 6X DNA loading buffer and 2 l of 1X TAE buffer was loaded onto the gel. Gel electrophoresis was carried out at 80 V for 60 minutes. To visualise the DNA bands under UV exposure (312 nm), the gel was transferred to an INGENIUS gel

documentation system (Syngene Bio Imaging) and a digital image of the gel was collected and stored electronically.

2.4 BK and LINGO1 plasmid constructs

The BK subunit was isolated from rabbit urethral smooth muscle tissue and cloned into the pcDNA TOPO 3.3 vector (Life technologies). The cloned BK transcript corresponds to the ZERO variant of mouse BK and to variant 2 (NM_002247.3) of human BK .

The untagged human LINGO1 (NM_032808.6) clone was purchased from ORIGENE technologies (Catalogue number: SC111475) which was supplied in pCMV6-Entry vector.

2.5 Preparation of Competent Cells

Competent cells were prepared using calcium chloride method (Inoue *et al*. 1990). A stab from the bacterial glycerol stock of *E.coli* DH5 was streaked on a LB agar plate and incubated at 37 C. On the following day, a single colony was inoculated into 10 ml of LB broth and grown overnight at 37 C in a shaker incubator. This culture was further sub-cultured (0.1-0.5% inoculum density) into 250 ml of LB broth and the culture was grown in a shaker incubator until it reached 0.6 optical density (OD). After the desired OD was achieved, the culture was chilled on ice for 30 minutes and then the culture was centrifuged at 5000 rpm for 5 minutes. The bacterial pellet was then resuspended in chilled 0.1 M $MgCl_2$ and incubated on ice for 15 minutes. This mixture was then centrifuged for 5 minutes at 5000 rpm. Finally, cells were resuspended in 2 ml of ice cold 0.1 M $CaCl_2$ with 20% glycerol and 50 l aliquots were stored at -80 C.

2.6 Site-directed Mutagenesis

The site-directed mutagenesis technique was used to incorporate one or more base-pair specific mutations in the desired gene and primers with the specific alterations to the respective DNA template were synthesised.

In this study, the mutant constructs for BK were synthesised using Phusion hot start II DNA polymerase method (Chester *et al*. 1993; Frey *et al*. 1995). Figure 2.1 shows the outline of the steps carried out for insertion of the desired mutation.

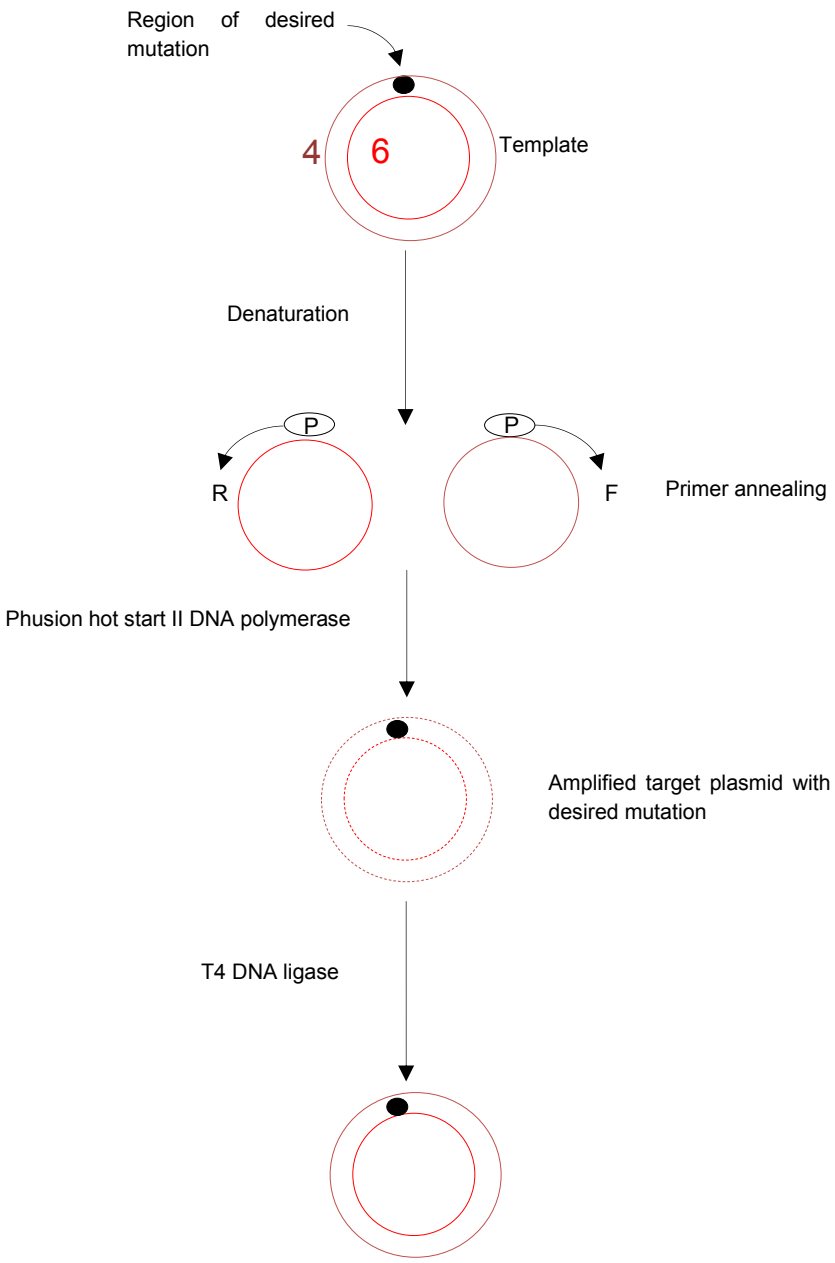

Figure 2.1: Schematic representation of site-directed mutagenesis using the Phusion hot start II DNA polymerase method. The forward primer (F) was designed on the sense strand of the template DNA whereas the reverse primer (R) was designed on the anti-sense strand. The incorporated mutation in the double stranded DNA is indicated by ●.The thick lines show the target amplified plasmid with the desired mutation.

The main steps of the process are as follows: 1) PCR amplification of template DNA, 2) Dpn1 treatment and 3) Ligation of PCR product.

2.6.1 PCR amplification of the template DNA

The rabbit BK pcDNA 3.3 construct was used as a DNA template. To ensure the mutation was incorporated in the circular plasmid, a pair of primers were designed against the template DNA. These primers were phosphorylated on their D (using T(4 Polynucleotide kinase (PNK).

The phosphorylation of the forward and reverse primers was carried out separately using the following reaction components for a total volume of 50 l:

Nuclease Free water 41 l

Primer (100 mM) 3 l

T4 DNA Ligase buffer (Thermo Fisher Scientific) 5 l

T4 PNK (PNK, 10 U/ l, Thermo Fisher Scientific) 1 l

This reaction mixture was incubated at 37 C for 30 minutes followed by 65 C for 10 minutes and cooled down to 4 C.

The above reaction mixture now contained the phosphorylated primers which were used to set up a PCR reaction of 50 l.

The components of the PCR reaction are described below:

Template DNA (50 ng / l) 1 l

10 mM dNTPs 1 l

Forward primer 4 l

Reverse primer 4 l

GC buffer (Thermo Scientific) 10 l

Phusion DNA polymerase (2 U/ l, Thermo Scientific) 0.5 l

Nuclease Free Water 28 l

DMSO (Thermo Scientific) 1.5 l

The plasmid DNA was amplified using a TECHNE TC-512 thermal cycler and the experimental conditions used are detailed in Table 2.4.

Table 2.4 Thermal cycler conditions for template DNA amplification

Step	***Temperature (C)***	***Time***	***Number of cycles***
Initial denaturation	98	30 seconds	1
Denaturation Annealing Extension	98 65-72 72	30 seconds 30 seconds 3-5 minutes	25
Final Extension	72	10 minutes	1

The amplified PCR products were analysed using agarose gel electrophoresis with appropriate template controls.

2.6.2 Dpn1 Treatment

The reaction mixture from Section 2.6.1 contains the two different strands of DNA, one is methylated dsDNA template and the other is hemi-methylated dsDNA (a hybrid of mutant strand and template sense strand) which have high transformation efficiency. To cleave the methylated DNA, 1 l of 10X CutSmart™ Buffer (New England Biolabs), 1 l of Dpn1 (20 U / l, New England Biolabs) along with 8 l of PCR product with a total volume of 10 l were incubated at 37 C for 1 hour.

2.6.3 Ligation of PCR product

The Dpn1 treated PCR product was circularised using T4 DNA ligase (5 U / l, Thermo Fisher Scientific). This ligase catalyses the phosphodiester bond (((D (DNA. This enzyme repairs single strand nicks in the duplex DNA and joins the DNA fragments with either cohesive or blunt ends.

To achieve ligation, the following components were mixed with DNA (10-20 ng, 5 l) to a total volume of 20 l.

10X T4 DNA Ligase Buffer (Thermo Scientific) 2 l

T4 DNA Ligase (5 U / l, Thermo Scientific) 1 l

Nuclease Free Water 12 l

The reaction was carried out at RT for 1 hour and a total of 5 l of the ligation reaction product was used for transformation of *E.coli* DH5 .

2.7 Transformation

E.coli DH5 competent cells were prepared as detailed in Section 2.5 and used for transformation. 50 l of competent cells were incubated with the desired DNA construct on ice for 30 minutes. The chemical method of transformation (Mandel *et al*. 1970; Hanahan, 1983) facilitated the attachment of DNA to the bacterial cell membrane. This was followed by heat shock of cells for 30 seconds at 42 C, in a circulating hot water bath which created pores in the bacterial membrane and allowed the entry of DNA into the cell. Cells were then incubated on ice for 2 minutes. Next, 200 l of enriched SOC media (Invitrogen) was added to the cells, which were allowed to grow at 37 C in a shaker incubator. The cells were then plated on an LB agar plate with antibiotic resistance used as a marker for identifying transformed colonies.

The plasmids were isolated from transformed colonies using the Isolate II Plasmid Mini Kit (Bioline) and all mutations were verified by sequencing.

2.8 Cell culture

HEK293 cells were cultured in 50% W (g + 50%([Minimal Essential Medium (DMEM, MEM, Gibco) media consisting of 10% Fetal Bovine Serum (FBS, Gibco) and 1% antibiotics (penicillin and streptomycin, 10,000 U / ml, Gibco). The cells were maintained at 37 C with 5% CO_2 in a 95% humidifying incubator. Sub-culturing was done using 0.05% Trypsin-EDTA (Gibco).

2.9 Lipofectamine mediated Transfection

Wild type (WT) BK along with WT LINGO1 or WT BK by itself or mutant BK alone constructs were co-transfected with enhanced Green Fluorescent Protein (eGFP) plasmids into HEK293 cells using lipofectamine mediated transfections. The day before transfection, cells were plated in 35 mm dishes at approximately 30% confluence. As an example, the transfection of WT BK for 2 dishes was carried out as follows, in an Eppendorf tube the cDNA for BK (100 ng) and eGFP (150 ng) was diluted in 200 l serum free media (D 9 . (W (g Medium + 50% Minimal Essential Medium (DMEM, MEM, Gibco)). In another tube 1.5 l lipofectamine reagent (Invitrogen) was diluted in 200 l serum free

media. These two solutions were then mixed together and further incubated for 15 minutes at RT. Prior to transfection, the dishes containing HEK cells were incubated with serum and antibiotic free media. Then, 200 l of the transfection mixture was added drop by drop, into each dish containing HEK cells and then incubated at 37 C for 4 hours. The transfection was stopped by removing the media and replacing it with fresh growth media.

2.10 Patch Clamp Recording

For electrophysiological recordings in inside-out configuration, HEK293 cells were maintained at 35-37 C and perfused with Hanks solution (see composition in Section 2.13) after 24 hours of transfection. The patch pipettes for inside-out recordings were pulled from thick borosilicate glass (1.5 mm O.D. x 0.86 mm I.D.). All pipettes were fabricated using Sutter P-97 micropipette puller and were fire polished using a Narashige microforge. The pipettes had a resistance of 3-5 Mv when filled with pipette solution (140 mM K^+, 100 nM Ca^{2+}).

The currents were amplified with an Axopatch 1D amplifier (Molecular Devices) and digitised using a Digidata 1440A converter (Molecular Devices). Any residual 50 Hz electrical noise was electronically subtracted using a HumBug (Quest Scientific), inserted between the amplifier and the digitiser. Capacitance and leak currents were subtracted either with the P/4 protocol or by manual leak subtraction. The series resistance was compensated electronically by ~50%. The Clampex and Clampfit programmes from pCLAMP 10 software were utilised for stimulus generation, data acquisition and data analysis. The data was acquired at 10 kHz, filtered at 2 kHz and stored on a PC for offline analysis.

2.10.1 Current, voltage and resistance

The movement of charged ions such as Na^+, Ca^{2+}, K^+ and Cl^- across the cell membrane determine the electrical activity of the cell. The flow of ions across the cell membrane is current (I, measured in amperes) and the movement of these ions is determined by the driving force. Voltage (V, measured in mV) is the energy required to move these ions across the cell membrane. The cell membrane is selectively permeable and therefore, ions move across the cell membrane via ions channels, which are embedded in the cell membrane.

In order to study the relationship between current, voltage and resistance (R, measured in ohms v) i ((to patch-clamping studies. It has the following formula:

$$V=IR$$

Rearranging this equation yields,

$$I=V/R$$

From the equation, it is clear that voltage is directly proportional to current, whereas resistance is inversely proportional to current. This is explained in Figure 2.2, when a brief voltage pulse of 5 mV was applied repeatedly, it resulted in a current of approximately 1.4 nA (Figure 2.2A). When the pipette touched the cell surface, the resistance increased and this caused a decrease in current, as shown in Figure 2.2B. The application of negative pressure resulted in the formation of a tight seal between the glass pipette and the cell membrane as evidenced by practical abolition of ionic current across the membrane (Figure 2.2C). At this stage, a high resistance gigaseal was formed and the resistance of

((((((i

$$R=V/I$$

$$R= (5 \times 10^{-3}) V / (1.4 \times 10^{-9}) A$$

$$= 3.57 Mv$$

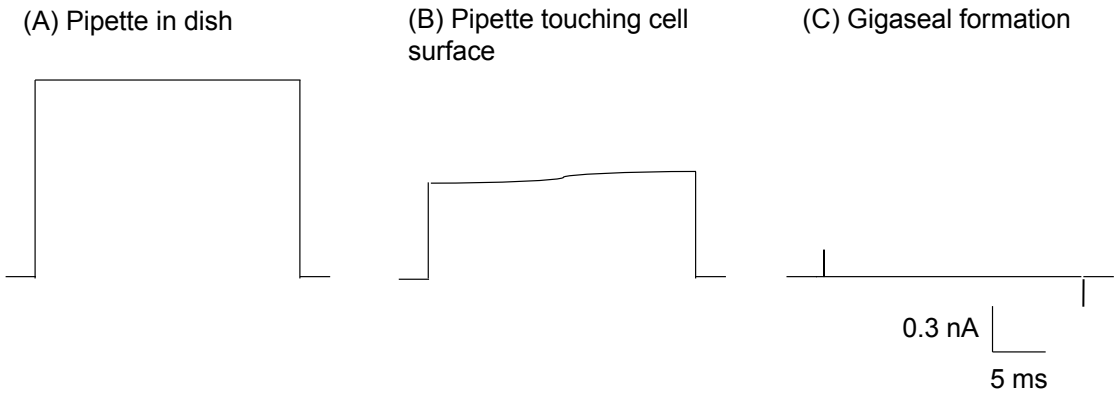

Figure 2.2: Diagrammatic representation of gigaseal formation. A Voltage pulse of 5 mV was applied for 25 ms which kept the current of 1.4 nA flowing through the patch pipette immersed in the bath solution. **B** When the tip of the pipette touched the HEK cell, the current reduced approximately by half, due to increase in resistance. **C** A gigaseal was formed by the application of negative pressure (suction) during which little to no current flowed through the pipette.

2.10.2 Leak subtraction

A current recorded from a patch of membrane containing ion channels usually consists of three components:

(i) Leakage current: A passive current flowing through the membrane resistance and membrane capacitance. This current is generally linear with voltage.

(ii) Non-linear gating current: Arises due to movement of gating charges across the electric field.

(iii) Non-linear ionic current: A current which is indicative of the opening of ion channels as a result of voltage changes.

In electrophysiological experiments, it is important to separate the ionic current from the passive linear components and this is done through leak subtraction. There are two approaches that can be used to subtract the leakage currents. The first method is a lengthy protocol that involves recording currents in the presence and absence of selective ion channel blockers. Since these blockers would only abolish the actual ionic current and not the leak currents, the two traces can be subtracted to yield the ionic current without any contaminating leakage current. The second method used is called P/N subtraction, where P represents the test pulse and N is the number of sub-sweeps that each have a magnitude of $1/N^{th}$ of the test pulse (Liu *et al.* 2000). An example of this protocol used in HEK cells, is illustrated in Figure 2.3. In this experiment, the chosen protocol was designed to record currents evoked from a step to +20 mV, from a holding potential of -60 mV. In this experiment, 4 sub-sweeps were applied at $1/4^{th}$ of the amplitude of the test pulse (i.e. 80/4 = 20 mV). Prior to applying the sub-sweeps, the cell was held at -100 mV before the 5 ms long steps to -80 mV were applied. These more negative potentials were used in an attempt to ensure that no ionic currents were activated by the P/4 sub-sweeps. After completion of the sub-sweeps, the holding potential was returned to -60 mV and the main depolarising step was conducted. The averaged sub-sweep currents which should consist of only leakage and capacitative currents were then scaled and subtracted from the recorded currents to produce the non-linear ionic current, without any contaminant leakage or capacitative currents.

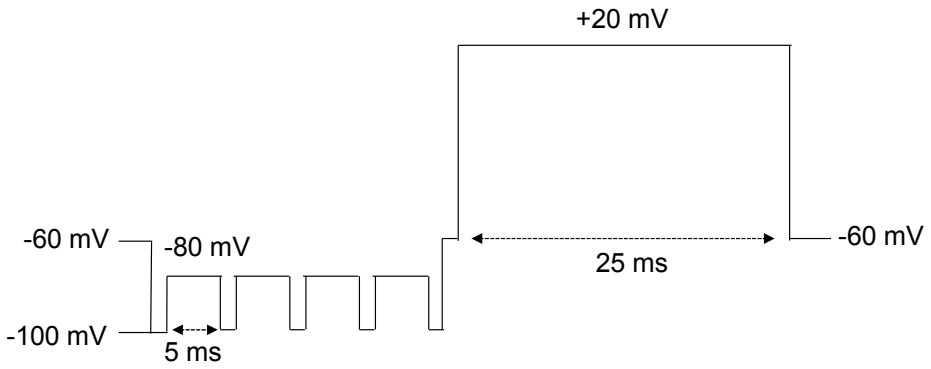

Figure 2.3: Diagrammatic representation of P/4 protocol. The figure shows 4 leak voltage pulses having 1/4th the magnitude of the test pulse. The four leak voltage pulses precede the main test pulse. A depolarising step to +20 mV was applied from the holding potential of -60 mV. The current from the four depolarising sub-sweeps was summed, scaled and subtracted from the final current trace to separate the non-linear ionic current.

2.10.3 Membrane Capacitance

The cell membrane is capable of storing electrical charge (Q) at a given potential and this property is termed as capacitance (C). The amount of stored charge is calculated by the following formula:

$$Q = C.V$$

The capacitance of the membrane depends upon the physical dimensions of the cell membrane. For instance in a larger cell, the amount of charge stored will also be greater, hence the capacitance is directly proportional to membrane surface area (A). Although capacitance is inversely proportional to the thickness of the membrane, since the electromagnetic field strength which is responsible for attracting ions on either side of the membrane reduces with distance (d). Finally, the material separating the two conductors (the intracellular and the extracellular space) also affects the electromagnetic field. The variable for dielectric constant $_r$ defines the properties of the membrane pertaining to capacitance. Most living cells have similar membrane thickness and dielectric constants.

$$C = A\ _r/d$$

The electrical charges present across the intracellular and the extracellular membrane can move towards or away from the membrane inducing a current flow through the capacitor. This current is called the capacitive current (I_c), which flows only when the voltage across the membrane changes with respect to time.

The equation for capacitive current (I_c), can be derived from the capacitive equation as shown below.

$$Q = C.V$$

Dividing both sides of the equation by time yields,

$$Q / t = C. V / t$$

By introducing differential terms on both sides of the equation gives,

$$dQ / dt = C. (dV/dt)$$

Since capacitive current,

$$I_c = dQ / dt$$

$$I_c = C. (dV/dt)$$

From the above equation, the capacitive current is proportional to the magnitude of change in voltage. Capacitive transients were removed using the capacitance compensation circuitry on the amplifier.

2.10.4 Series resistance

Series resistance (R_s) is equivalent to the sum of the pipette resistance (R_p) and the access resistance (R_a) in an experiment. The series resistance gives rise to a voltage drop across the membrane between the command voltage and the actual voltage at which the membrane is clamped. This error can be significant when recording currents, particularly if they have large amplitudes (Armstrong and Gilly, 1992).

In the inside-out configuration, the series resistance equals pipette resistance since there is no access resistance. The resultant voltage error can be calculated by V=IR when the pipette resistance is known. For example, the mean amplitude of BK (currents in 10 M $[Ca^{2+}]_i$ was 8053±879 pA (n=7) at +200 mV and the calculated pipette resistance was ~4 Mv . The calculated voltage error from the above formula would be ~32 mV. It was possible to routinely compensate ~50% of the series resistance, using the series resistance compensation circuitry on the amplifier and in this example, would result in a voltage error of ~16 mV. Attempts to increase the degree of series resistance compensation with the Molecular Devices = W((and breakdown of the ((seals. Therefore, to help further minimise voltage errors, pipette resistances were

no greater than 5 Mv and patches that showed currents greater than 10 nA at +160 mV in 100 nM $[Ca^{2+}]_i$ bath solution were discarded.

2.10.5 Liquid Junction Potential

Liquid junction potentials arise due to differences in the mobility of ions at the interface of the two electrolyte solutions with different ionic concentrations. A potential difference is created as a result of some ions crossing the concentration gradient more rapidly than the other ions (Neher, 1992). This can arise in patch clamp experiments where the pipette and bath solutions can have very different ionic compositions. The liquid junction potentials typically range between 2-12 mV for routinely used solutions in electrophysiological experiments (Neher, 1992). However, in the majority of the experiments presented here the pipette and bath solutions were identical. In our experiments the measured liquid junction potential was low (<2 mV) and was not corrected for.

2.11 Data Analysis

In case of concentration effect curves, the IC_{50} value for the LINGO peptides was determined by fitting the data with the Hill-Langmuir equation of the form:

$$\frac{}{1} \quad \frac{}{}$$

where I is the current recorded in the presence of the drug, $I_{control}$ is the current in the absence of the drug, IC_{50} is the half-maximal effective concentration and [Drug] is the concentration of drug applied.

2.12 Statistical analysis

All experimental data sets were obtained from a minimum of 5 cells and the size of each respective data set was ((7 (o (experiments were represented as the mean ± standard error of mean (SEM). GraphPad Prism software was used to compare all electrophysiological data. Statistical differences for the comparison between LINGO peptides were assessed using two-tailed S -t(st, two-tailed S((t-test, Mann-Whitney test, ordinary one-way ANOVA for multiple comparisons

with Bonferroni tests, as appropriate. A p value <0.05 was considered significant and represented with *, whereas p<0.01, p<0.001 and p<0.0001 were represented with **, *** and **** respectively.

2.13 Solutions

The compounds used in each solution are listed below. All salt concentrations are given in millimolar (mM).

2.13.1 Calcium-free Hanks:

NaCl (125), KCl (5.36), glucose (10.0), sucrose (2.9), $NaHCO_3$ (15.5), KH_2PO_4 (0.44), Na_2HPO_4 (0.33), HEPES (10.0). The solution pH was adjusted to 7.4 with 3 M NaOH.

2.13.2 Hanks solution:

NaCl (140), KCl (5.36), glucose (10), sucrose (2.9), $NaHCO_3$ (4.17), KH_2PO_4 (0.44), Na_2HPO_4 (0.33), $MgCl_2.6H_2O$ (1.8), $CaCl_2.2H_2O$ (1.8), $MgSO_4.7H_2O$ (0.4), HEPES (10). Solution pH was adjusted to 7.4 with 3 M NaOH.

2.13.3 Recording solutions for inside-out configuration:

100 nM Ca^{2+} solution (single-channel bath and pipette solution):
KCl (140), glucose (10), HEPES (10), EGTA (1)
146.2 l of 1 M $CaCl_2$ added for 500 ml of 100 nM Ca^{2+}solution.
pH adjusted to 7.2 with 1 M KOH.

1 M Ca^{2+} and 10 M Ca^{2+} solution (single-channel bath solution):
KCl (140), glucose (10), HEPES (10), H-EDTA (1).
114.7 l of 1 M $CaCl_2$ added for 300 ml of 1 M Ca^{2+} solution.
174.1 l of 1 M $CaCl_2$ added for 200 ml of 10 M Ca^{2+} solution.
pH adjusted to 7.2 with 1 M KOH.

The required calcium concentration was calculated for desired Free (Ca^{2+}) with Schoenmakers Chelator software (https://www.ru.nl/animal/research/chelator/) and the free calcium concentration was measured using a calcium electrode as

per Schoenmakers *et al.* (1992). Patch pipettes were filled with 100 nM Ca^{2+} solution. All the recording solutions were made up with Milli-Q water.

2.14 Peptides

The LINGO synthetic tail peptides used in this study were custom made and purified by the Peptide Synthesis Laboratory in the Royal College of Surgeons in Ireland, Dublin, Ireland and by Dr. Nicholas Mullins at Dundalk Institute of Technology, Dundalk, Ireland. The peptides were unprotected at both the N and C termini unless otherwise stated in the text. The modifications at both the N and C termini resulted in three different subtypes of peptides used in this study namely, amino free acid (NH_2 at N-terminus and OH at C-terminus), acylated free acid (Ac at N-terminus and OH at C-terminus) and acylated amide (Ac at N-terminus and NH_2 at C-terminus) peptides. Table 2.5 summarises the nomenclature for the peptides used in this study.

Table 2.5 Name and structure of LINGO peptides

Peptide Name	*Peptide Sequence*	*N-terminus*	*C-terminus*
LINGO1-tail peptide	RKFNMKMI	NH_2	OH
LINGO2-tail peptide	RRFNMKMI	NH_2	OH
LINGO4-tail peptide	GNRVTAKLF	NH_2	OH
Acylated free acid LINGO1	RKFNMKMI	Ac	OH
Acylated amide LINGO1	RKFNMKMI	Ac	NH_2
Scrambled LINGO1	MFKNKIRM	NH_2	OH
RKFNMAMI	RKFNMAMI	NH_2	OH
RKFNMQMI	RKFNMQMI	NH_2	OH
AAFNMKMI	AAFNMKMI	NH_2	OH
AAFNMAMI	AAFNMAMI	Ac	NH_2
RAFNMKMI	RAFNMKMI	Ac	NH_2
AKFNMKMI	AKFNMKMI	Ac	NH_2
RKFNMAAA	RKFNMAAA	Ac	NH_2
RAFNMAMI	RAFNMAMI	Ac	NH_2
RKAAAKMI	RKAAAKMI	Ac	NH_2
AKFNMAMI	AKFNMAMI	Ac	NH_2
SSADAPRKFNMKMI	SSADAPRKFNMKMI	Ac	NH_2
FNMKMI	FNMKMI	Ac	NH_2
RKANMKMI	RKANMKMI	Ac	NH_2
RKFNMAMI	RKFNMAMI	Ac	OH
MKMI	MKMI	Ac	OH
RKFNAKMI	RKFNAKMI	Ac	OH
RKFAMKMI	RKFAMKMI	Ac	OH
RKANMKMI	RKANMKMI	Ac	OH
RKFNMKAI	RKFNMKAI	Ac	OH

3. Effect of LINGO tail peptides on BK channels

3.1 Introduction

Previous studies have demonstrated that LINGO subtypes are predominantly expressed in the central nervous system (Haines *et al*. 2008; Mi *et al.* 2013). LINGO1 is expressed in the brain and spinal cord but is apparently absent in the non-neuronal tissues (Mi *et al.* 2013). LINGO1 is involved in axonal regeneration, neuronal survival, oligodendrocyte differentiation and myelination (Mi *et al*. 2013). It is also known to be associated with neurological disorders including MS, PD, ET and spinal cord injury (Mi *et al*. 2013; Seiler and Widme, 2015). The single nucleotide polymorphisms of LINGO2 are implicated in PD (Wu *et al.* 2011), ET (Vilariño-Güell *et al.* 2010) and COPD (Hansel *et al*. 2015). Recent studies have demonstrated that LINGO2 is present in intestinal epithelial cells (Ji *et al*. 2019) and LINGO3 is present in mucosal epithelium (Zullo *et al.* 2018). Interestingly, recent publicly available data has suggested that considerable amount of LINGO1 protein is found in the human lung and is abundantly expressed in the brain (https://www.proteinatlas.org/ENSG00000169783-LINGO1/tissue; Uhlén *et al.* 2015).

LINGO1 belongs to the LRRIG family of proteins and shares structural similarities with BK subunits (Mosyak *et al*. 2006; de Wit *et al*. 2011). Figure 3.1A shows a cartoon of the LINGO1 protein, which consists of 12 LRR domains, an Ig1 domain, a stalk, a single transmembrane domain and a 37 amino acid long, intracellular C-terminus. Figure 3.1B shows the predicted regions overlaid upon the protein sequence of LINGO1, namely N-cap (magenta), LRRC (black), C-cap (orange), Ig1 domain (aqua), stalk (fuschia), transmembrane domain (green) and C-terminus (purple, yellow, blue and red).

The physiological and pharmacological properties of BK channels are known to be modulated by both and subunits (Gonzalez-Perez and Lingle, 2019), as detailed in Sections 1.5.3, 1.5.5, 1.5.7 and summarised in Table 1.5.

When LINGO1 protein was co-expressed with BK , these currents showed a rapid and complete inactivation of the BK channels (Dudem *et al.* 2020). A typical example of this effect is shown in Figure 3.2, where families of currents were recorded from excised patches in varying calcium concentrations, from cells

expressing BK alone (Figure 3.2A) and cells co-expressing BK :LINGO1 (Figure 3.2B). For electrophysiological recordings, excised patches were held at -60 mV and currents were elicited from -100 mV to +200 mV in 20 mV steps for 50 ms, before patches were repolarised back to -80 mV to evoke tail currents. Figure 3.2A shows representative traces of large and sustained outward BK currents recorded in different $[Ca^{2+}]_i$ (100 nM, 1 M and 10 M) which show increased current amplitude with increased calcium concentrations. However, as observed in Figure 3.2B, BK :LINGO1 currents exhibited rapid and nearly complete inactivation in 100 nM $[Ca^{2+}]_i$. It was also observed that these patches often exhibited smaller currents and their tail currents deactivated more slowly than BK only currents. In presence of higher $[Ca^{2+}]_i$ (1 M and 10 M), the current amplitude reduced drastically in BK :LINGO1 patches, compared to BK containing patches. These results suggest that currents recorded from cells co-expressing BK :LINGO1 were sensitive to both voltage and $[Ca^{2+}]_i$. However, in contrast to BK , BK :LINGO1 currents appeared to be inhibited in response to elevated $[Ca^{2+}]_i$ as shown previously by Dudem *et al.* (2020).

To further investigate how the LINGO1 protein caused inactivation, deletion constructs were designed and co-expressed with BK . The use of deletion constructs of LINGO1 helped us identify that the last eight residues of the LINGO1 C-terminus were responsible for inactivating BK channels (Dudem *et al.* 2020).

In the present chapter, the transcriptional expression profile of LINGO subtypes in murine tissues was examined and the effect of synthetic LINGO amino free acid (NH_2 at N-terminus and OH at C-terminus) tail peptides were assessed on HEK293 cells transiently transfected with BK .

A.

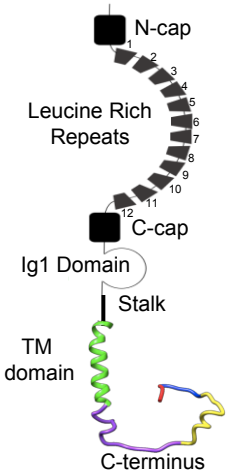

B.

```
1   MQVSKRMLAG GVRSMPSPLL ACWQPILLLV LGSVLSGSAT GCPPRCECSA
                N-cap
51  QDRAVLCHRK RFVAVPEGIP TETRLLDLGK NRIKTLNQDE FASFPHLEEL
101 ELNENIVSAV EPGAFNNLFN LRTLGLRSNR LKLIPLGVFT GLSNLTKLDI
151 SENKIVILLD YMFQDLYNLK SLEVGDNDLV YISHRAFSGL NSLEQLTLEK
                                                          LRRC
201 CNLTSIPTEA LSHLHGLIVL RLRHLNINAI RDYSFKRLYR LKVLEISHWP
251 YLDTMTPNCL YGLNLTSLSI THCNLTAVPY LAVRHLVYLR FLNLSYNPIS
301 TIEGSMLHEL LRLQEIQLVG GQLAVVEPYA FRGLNYLRVL NVSGNQLTTL
                                C-cap
351 EESVFHSVGN LETLILDSNP LACDCRLLWV FRRRWRLNFN RQQPTCATPE
401 FVQGKEFKDF PDVLLPNYFT CRRARIRDRK AQQVFVDEGH TVQFVCRADG
                                Ig1 domain
451 DPPPAILWLS PRKHLVSAKS NGRLTVFPDG TLEVRYAQVQ DNGTYLCIAA
                    Stalk
501 NAGGNDSMPA HLHVRSYSPD WPHQPNKTFA FISNQPGEGE ANSTRATVPF
        Transmembrane domain                C-terminus
551 PFDIKTLIIA TTMGFISFLG VVLFCLVLLF LWSRGKGNTK HNIEIEYVPR

601 KSDAGISSAD APRKFNMKMI
```

Figure 3.1: Schematic representation and protein sequence of LINGO1. A Structural representation of the LINGO1 protein. The LINGO1 protein has 5 domains. They are LRR domain (comprising 12 LRR repeats as well as N-cap and C-cap), Ig1 domain, stalk, transmembrane domain and C-terminus. The intracellular C-terminus has no particular secondary structure. **B** The predicted regions are shown in the protein sequence of LINGO1. The extracellular side of LINGO1 protein has N-cap, LRRC, C-cap, Ig1 domain and stalk. The transmembrane domain is coloured in green and cytosolic C-terminus (584-620) residues are shown in different colours (Adapted from Dudem, 2019).

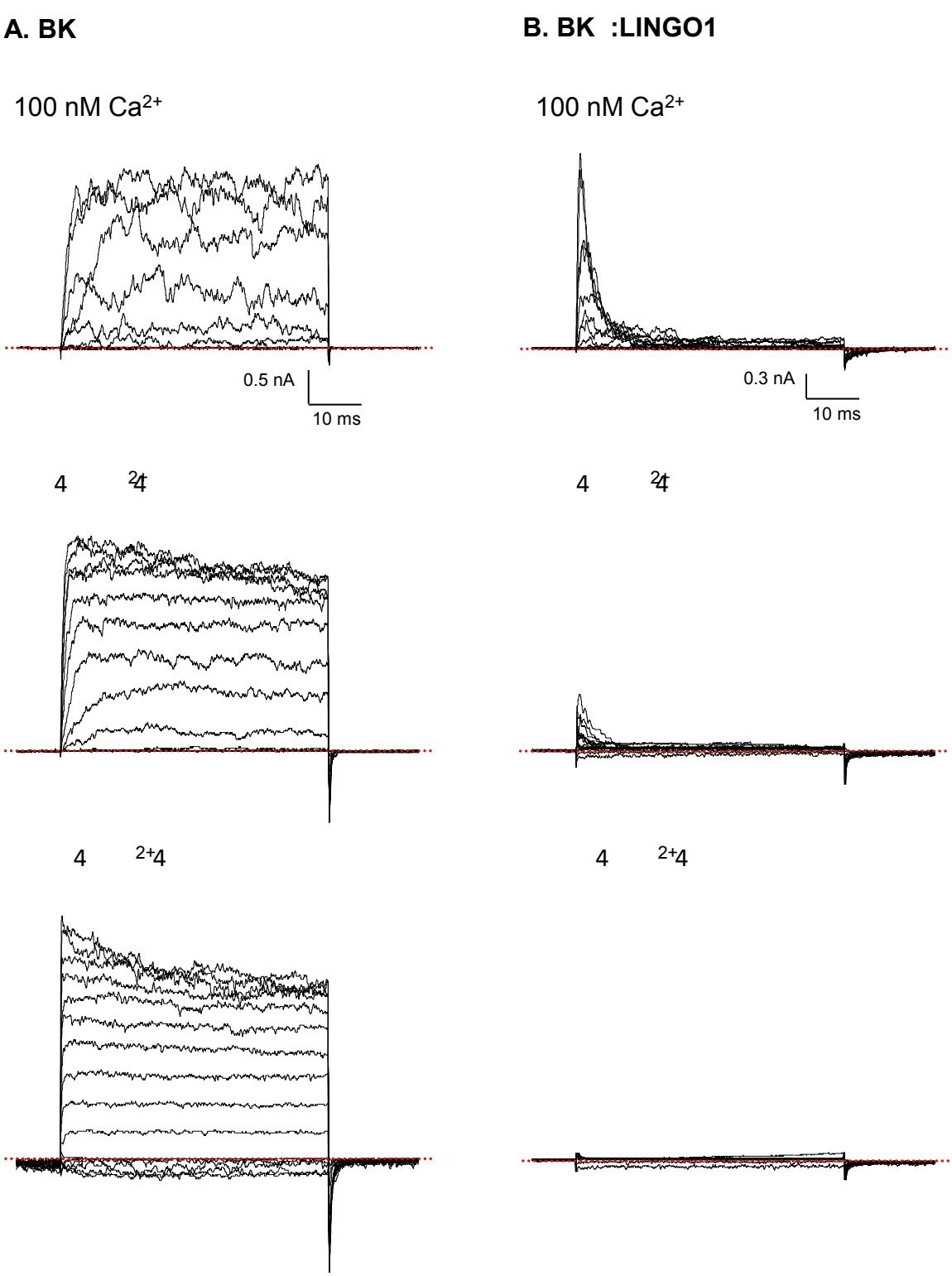

Figure 3.2: Voltage and Ca^{2+}-dependent activation of currents resulting from BK alone and BK :LINGO1 co-expression studies.
A Macroscopic currents from inside-out patches expressing BK alone in 100 nM, 1 and 10 $[Ca^{2+}]_i$. Patches were held at -60 mV and currents were elicited from -100 mV to +200 mV in 20 mV increments, tail currents were evoked by stepping back to -80 mV. **B** Representative current traces show BK :LINGO1 co-expression with the same conditions in panel A. The co-expression of BK :LINGO1 resulted in the inactivation of BK currents (Adapted from Dudem, 2019).

3.2 Results

3.2.1 Transcriptional expression of LINGO genes in murine tissues

To examine the transcriptional expression of *LINGO1-4* in the murine airway, primers were designed against these genes and RT-PCR was carried out. Details of the primers used can be found in Table 2.3. Figure 3.3A shows a typical gel which illustrated that *LINGO1*, *LINGO2*, *LINGO3* and *LINGO4* were expressed at the transcriptional level, in both murine bronchi and in brain tissue which was used as a positive control (N=3). After converting the visual image of agarose gel into semi-quantified data using Image J, Figure 3.3B confirmed the differential expression of *LINGO1-4* transcripts among murine brain and bronchus cDNA samples. Interestingly, the transcript levels of *LINGO1* were higher in the bronchus tissue compared to the brain tissue. However, the transcript levels of *LINGO2-4* in bronchus tissue were significantly lower than the levels in brain tissue. The relative expression was calculated as the expression ratio of *LINGO1-4* genes in murine brain (control) and bronchus (test) tissue samples ($p<0.0001$, one-way ANOVA). These experiments will require further experimental confirmation with real time-PCR and immunocytochemistry.

A. Murine tissues

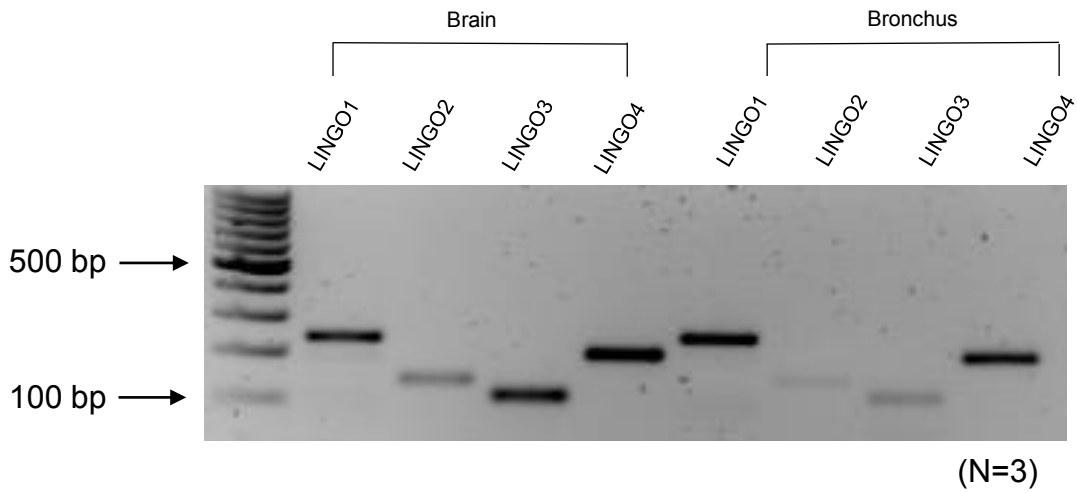

B. Transcript expression analysis using semi-quantitative RT-PCR for *LINGO1-4*

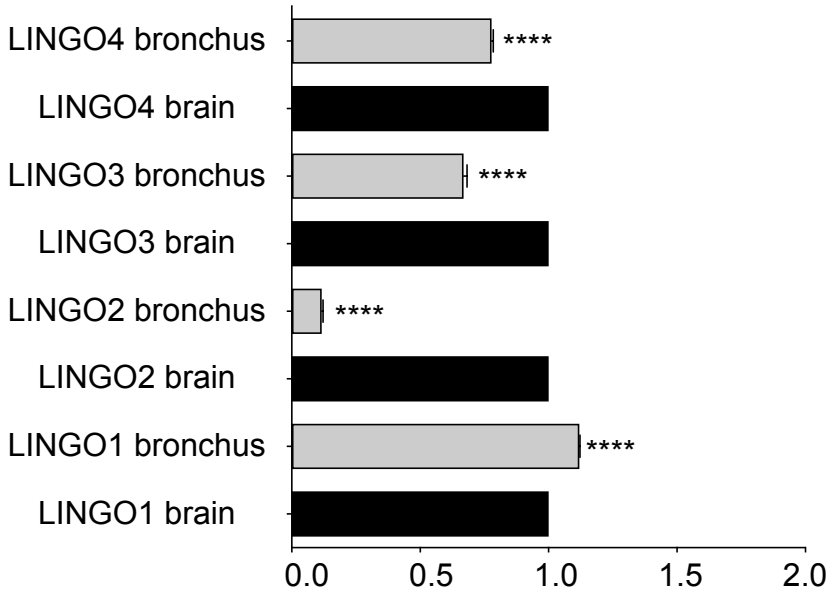

C. Multiple sequence alignment of LINGO TM and tail domains

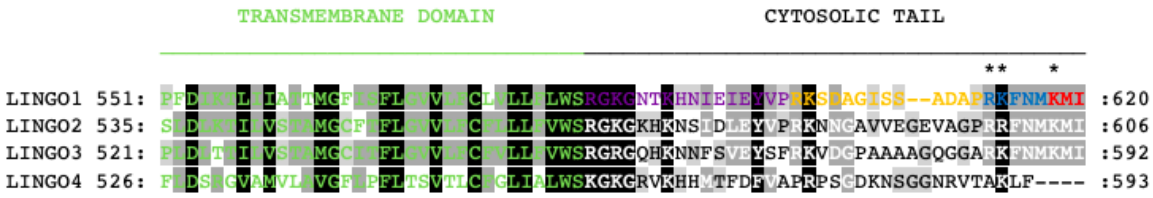

Figure 3.3: Transcriptional expression profile of LINGO1-4 in murine tissues and their protein sequence.
A Image of agarose gel illustrates a transcriptional expression of *LINGO1-4* occurs in brain and in peripheral tissues such as mouse bronchus (N=3). Amplicons were separated on 2% agarose gel by gel electrophoresis. **B** Transcript expression analysis using semi-quantitative RT-PCR for *LINGO1-4*. Relative expression was calculated as the expression ratio of LINGO 1-4 genes in murine brain (control) and bronchus (test) tissue samples (one-way ANOVA, **** p<0.0001). **C** Sequences of terminal amino acid residues of LINGO1, 2, 3 and 4 proteins. The transmembrane domain (TM) is represented in green and black bars represent the intracellular tail for each protein. The coloured residues in the cytosolic tail correspond to the homology model shown in Figure 3.1. The asterisks above the sequences represent the 3 positively charged residues present in LINGO1-4.

3.2.2 Terminal 8 amino acid (NH_2-RKFNMKMI-OH) synthetic tail peptide of LINGO1 inactivated BK channels

As seen from Figure 3.2, the co-expression of LINGO1 and BK resulted in inactivating BK channels. To examine how LINGO1 mediated this effect on BK channels, subsequent deletion constructs were designed for the protein and it was found that the last 8 residues in the protein bring about the inactivation of the BK channel (Dudem *et al.* 2020). To test if the last 8 LINGO1 amino acid residues alone could mimic inactivation, a synthetic, amino free acid (NH_2-RKFNMKMI-OH) tail peptide, equivalent to the C-terminus of LINGO1 was applied to the cytosolic surface of excised patches expressing BK alone. In these experiments, the patches were held at -60 mV and currents were elicited by stepping to +160 mV for 100 ms in 1 M $[Ca^{2+}]_i$ before stepping down to -80 mV to evoke tail currents. As Figure 3.4A suggests, the LINGO1 tail peptide (300 nM to 100 M), when applied to the cytosolic surface of the patches, induced concentration-dependent inactivation and reduced current amplitude. Figure 3.4B shows summary data fitted with the Hill-Langmuir equation. The IC_{50} was 8±3 M (n=7) when measured in the first 5 ms of the depolarisation (white circles) and 308±60 nM (n=7) when measured in the last 5 ms of the depolarisation (black circles). These values were significantly different from each other ($p<0.05$, paired t-test). As seen from Figure 3.4A, LINGO1 synthetic tail peptide inactivated BK channels rapidly. The rate of inactivation of BK currents in each concentration of the peptide was assessed by fitting the decay phase with a single exponential and the summary data for this is shown in Figure 3.4C. This data suggests the rate of inactivation increased with the concentration of LINGO1. Figures 3.5A and B show families of BK currents in 1 M $[Ca^{2+}]_i$ before and during the application of a single concentration of 10 M LINGO1 tail peptide, to examine how the effect of LINGO1 tail peptide altered BK currents at different voltages. During the application of the tail peptide, the amplitude of the currents measured in the last 5 ms of each voltage step reduced rapidly and was summarised in Figure 3.5C before (white circles) and during peptide application (black circles). As Figure 3.5B suggests, the currents inactivated more rapidly at positive potentials. The inactivation at different voltages was quantified by fitting the decay phase of each current with a single exponential. The time constants of inactivation ( ) were

plotted in Figure 3.5D and demonstrated that inactivation showed an apparent voltage-dependence. These results suggest that the last 8 amino acids of the LINGO1 C-terminus mimicked the inactivation of the BK channels observed when LINGO1 was co-expressed with BK , as shown in Figure 3.2B.

A. LINGO1 *(NH_2-RKFNMKMI-OH)*

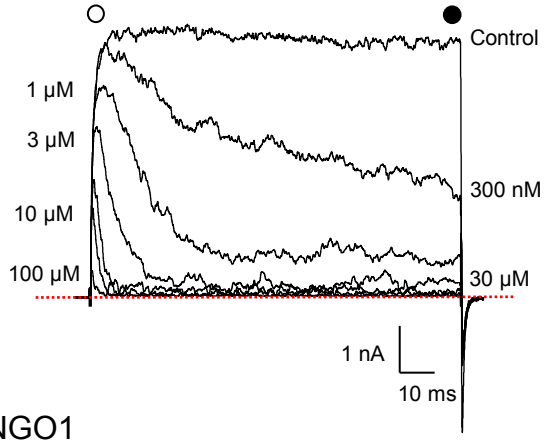

B. Summary of LINGO1

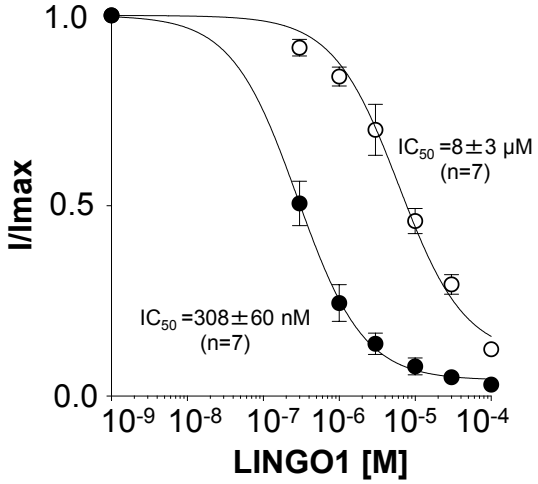

C. Summary of LINGO1 $_{inact}$

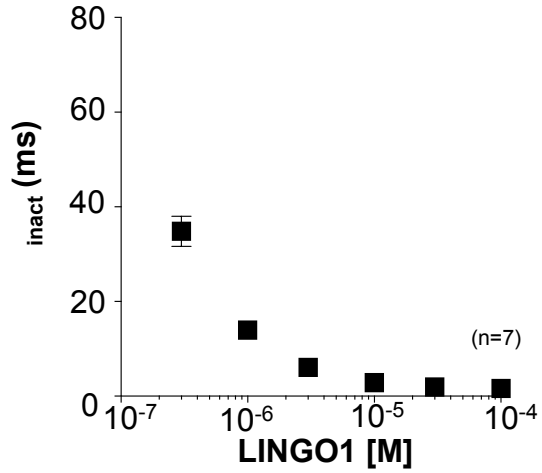

Figure 3.4: Concentration-dependent effect of LINGO1 tail peptide on WT BK .
A Representative concentration-dependent effect of LINGO1 synthetic tail peptide on HEK cells expressing WT BK . Currents were evoked by a step from -60 mV to +160 mV in the presence of 300 nM, 1, 3, 10, 30, 100 M of LINGO1 tail peptide. **B** Summary concentration effect curve for the effect of LINGO1 on BK currents (n=7). Data were fitted with the Hill-Langmuir equation. **C** The rate of inactivation of BK currents was assessed by fitting the decay phase with a single exponential. The rate of inactivation increased with the concentration of LINGO1 tail peptide (n=7).

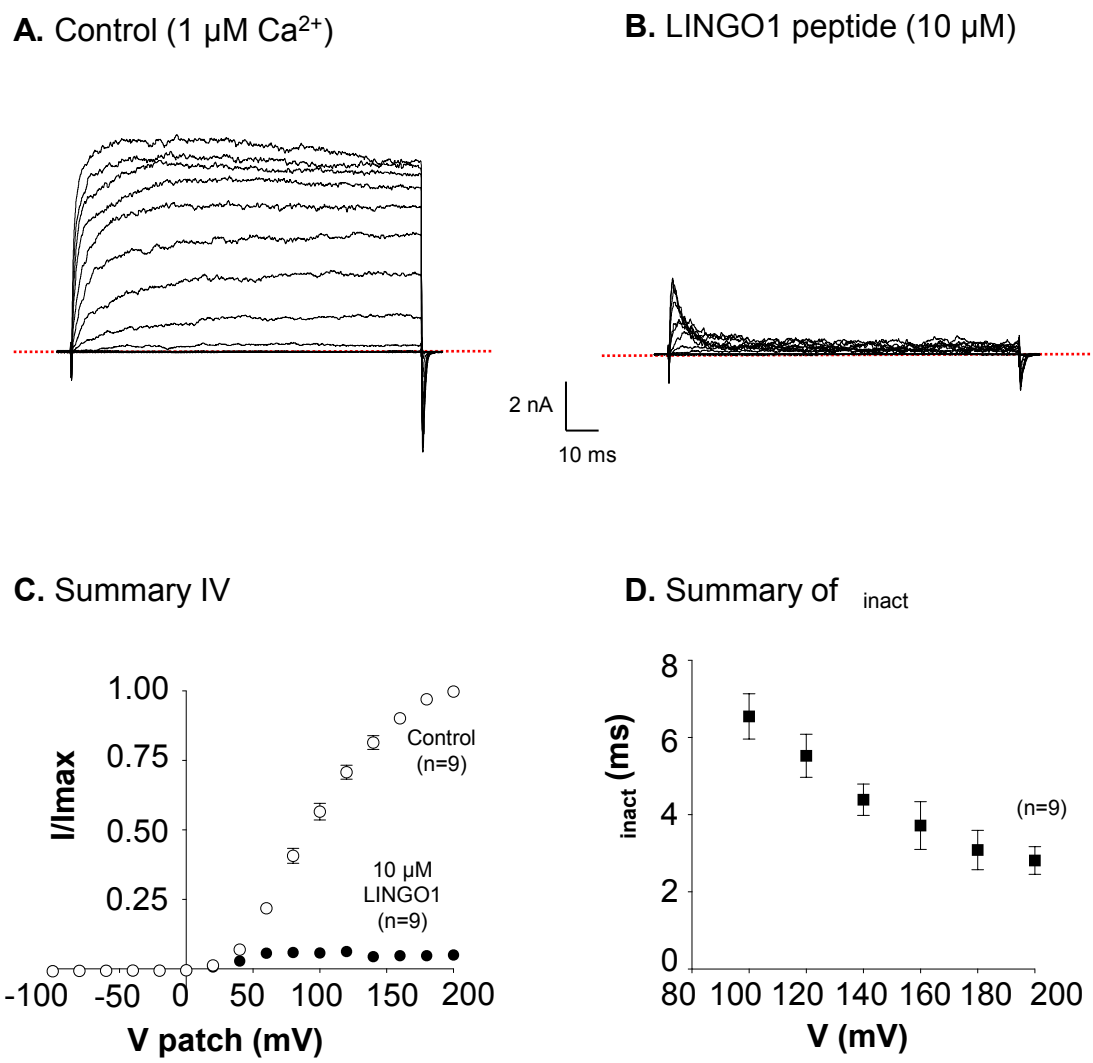

Figure 3.5: Voltage-dependence of LINGO1 tail peptide on BK .
A & **B** Macroscopic currents from inside-out patches expressing BK alone, show typical records in control (1 μM $[Ca^{2+}]_i$) and after application of 10 μM LINGO1 tail peptide. Patches were held at -60 mV and stepped from -100 mV to +200 mV in 20 mV increments and stepped back down to -80 mV to generate tail currents. **C** Summary of I/Imax measured in the last 5 ms of the pulse (n=9). **D** The rate of inactivation of BK currents was assessed by fitting the decay phase with a single exponential. The currents showed an apparent voltage-dependence at more positive potentials (n=9).

3.2.3 Terminal 8 amino acid (NH_2-RRFNMKMI-OH) synthetic tail peptide of LINGO2 inactivated BK channels

We next wanted to investigate if the tails of the other LINGO proteins could also induce inactivation. Therefore, we synthesised an 8 amino acid long synthetic, amino free acid, tail peptide, identical to the C-terminus of LINGO2 (NH_2-RRFNMKMI-OH) and applied it to the cytosolic surface of excised patches of cells expressing BK alone. The same protocol as used in Figure 3.4A was utilised in these experiments. As Figure 3.6A suggests, the LINGO2 synthetic peptide (100 nM to 30 M) also induced inactivation in a concentration-dependent manner and showed a reduction in current amplitude at the beginning, but particularly at the end of the depolarising pulse. The summary data quantifying the degree of block by the peptide at the beginning and end of each pulse is shown in Figure 3.6B and was fitted with the Hill-Langmuir equation to yield an IC_{50} value of 8±3 M (first 5 ms, white circles, n=7) and 321±81 nM (last 5 ms, black circles, n=7). These values were significantly different from each other ($p<0.05$, paired t-test). Interestingly, when we compared the IC_{50} values for the last 5 ms of LINGO1 and LINGO2 tail peptides, they were not significantly different to each other (ns, unpaired t-test). Like LINGO1, the LINGO2 peptide inactivated the BK channels more rapidly at higher concentrations, as summarised in Figure 3.6C. For instance, the rate of inactivation with 10 M LINGO1 tail peptide was similar to the rate of inactivation with 10 M LINGO2 tail peptide (3±0.4 ms with 10 M LINGO1 peptide and 4±1 ms with 10 M LINGO2 peptide, ns, unpaired t-test). To test the apparent voltage-dependence of the peptide's effect on BK currents, we next applied 10 M LINGO2 tail peptide after producing a family of currents from -100 to +200 mV in 1 M $[Ca^{2+}]_i$ (Figure 3.7A). This peptide, as expected, reduced current amplitude and caused almost complete inactivation (Figure 3.7B). To summarise this effect, we measured current amplitude in the last 5 ms of the depolarising pulses and plotted this in Figure 3.7C in the absence (white circles) and presence of (black circles) of the LINGO2 tail peptide. It is apparent from this graph that LINGO2 effectively blocked the BK currents at potentials positive to +40 mV. For example, at +200 mV, the amount of sustained current present at the end of the pulse was 3±1% (n=6) for LINGO2 tail peptide which was not significantly different to 5±1% (n=9)

observed with LINGO1 tail peptide (ns, Mann-Whitney test). Figure 3.7D shows a summary of the of inactivation, measured at different voltages and suggests that the LINGO2 peptide also showed an apparent voltage-dependent inactivation. For instance, at +200 mV, the of inactivation of LINGO1 and LINGO2 tail peptides were not significantly different from each other (ns, unpaired t-test). Taken together these results suggest that last 8 amino acids of the LINGO2 C-terminus were also sufficient to confer inactivation of BK channels.

A. LINGO2 *(NH_2-RRFNMKMI-OH)*

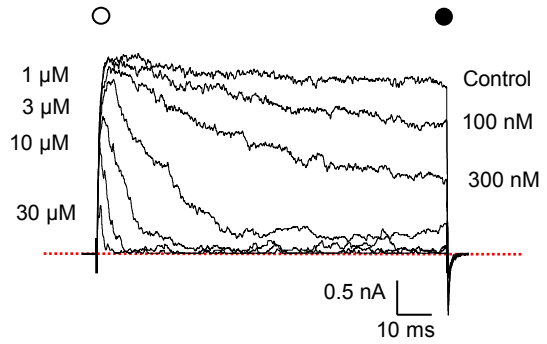

B. Summary of LINGO2

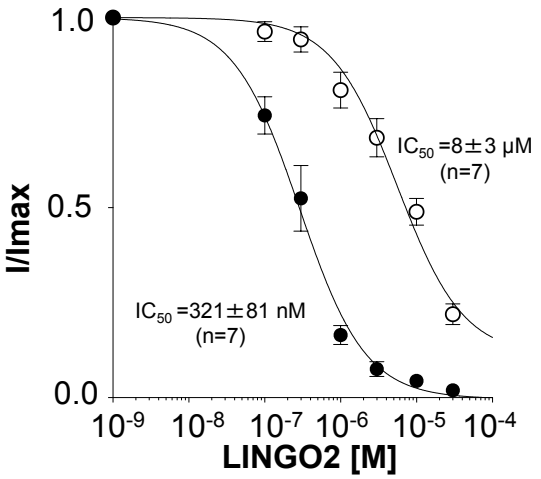

C. Summary of LINGO2 $_{inact}$

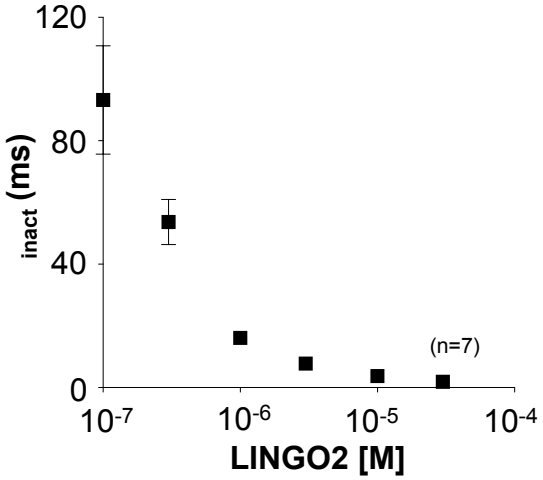

Figure 3.6: Concentration-dependent effect of LINGO2 tail peptide on WT BK .
A Representative concentration-dependent effect of LINGO2 synthetic tail peptide on HEK cells expressing WT BK . Currents were evoked by a step from -60 mV to +160 mV in the presence of 100 nM, 300 nM, 1, 3, 10, 30 M of LINGO2 tail peptide. **B** Summary concentration effect curve for the effect of LINGO2 on BK currents (n=7). Data were fitted with the Hill-Langmuir equation. **C** The rate of inactivation of BK currents was assessed by fitting the decay phase with a single exponential. The rate of inactivation increased with the concentration of LINGO2 tail peptide (n=7).

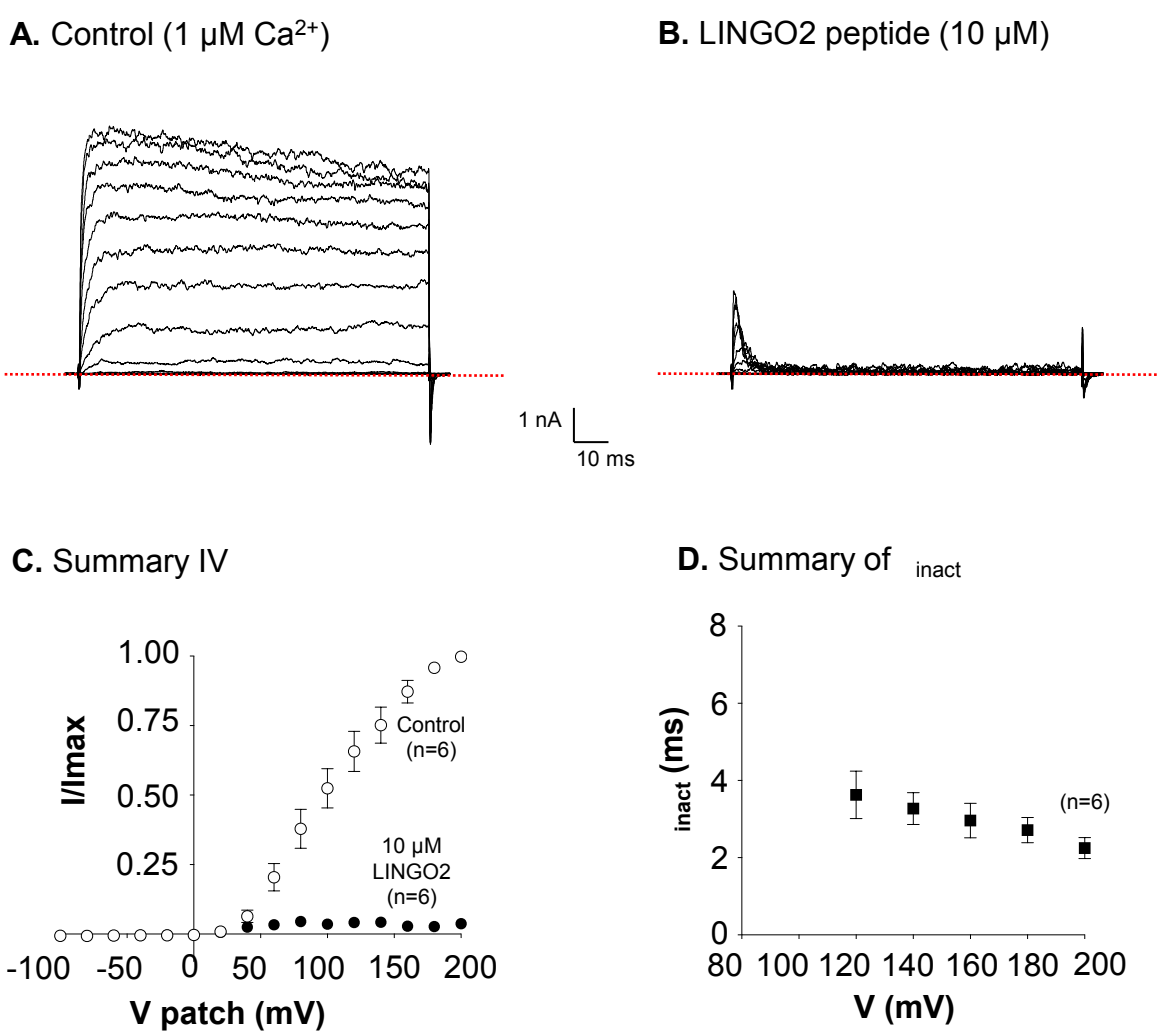

Figure 3.7: Voltage-dependence of LINGO2 synthetic tail peptide on BK .
A & **B** Macroscopic currents from inside-out patches expressing BK alone, show typical records in control (1 μM $[Ca^{2+}]_i$) and after application of 10 μM LINGO2 tail peptide. Patches were held at -60 mV and stepped from -100 mV to +200 mV in 20 mV increments and stepped back down to -80 mV to generate tail currents. **C** Summary of I/Imax measured in the last 5 ms of the pulse (n=6). **D** The rate of inactivation of BK currents was assessed by fitting the decay phase with a single exponential. The currents showed an apparent voltage dependence at more positive potentials (n=6).

3.2.4 Terminal 9 amino acid (NH_2-GNRVTAKLF-OH) synthetic tail peptide of LINGO4 does not inactivate BK channels

As demonstrated in Sections 3.2.2 and 3.2.3, both LINGO1 and LINGO2 tail peptides reduced current amplitude and induced inactivation of BK channels. Given that the terminal 8 amino acids of LINGO3 protein are identical to LINGO1 (Figure 3.3C), it is clear that it would also induce inactivation. However, LINGO4 has a shorter sequence compared to LINGO1 and LINGO2 subtypes. Next, we went on to examine the effect of LINGO4 tail peptide on BK channels. In order to do so, a synthetic amino free acid, (NH_2-GNRVTAKLF-OH) tail peptide identical to the last 9 amino acid residues of the C-terminus of LINGO4 was synthesised. It was necessary to include the 9th amino acid residue because peptides terminating in asparagine (N, the 8th residue, from the right of the C-terminus in LINGO4) were difficult to synthesise, due to a variety of side chain reactions that could occur at the asparagine residue. This peptide was applied to the cytosolic surface of excised patches expressing BK alone. As described previously, excised patches were held at -60 mV and currents were elicited by stepping to +160 mV for 100 ms in 1 M $[Ca^{2+}]_i$ before stepping down to -80 mV to evoke tail currents. Figure 3.8A shows that the LINGO4 synthetic peptide (300 nM to 100 M) when applied to the cytosolic surface of the patches, reduced current amplitude but did not induce rapid inactivation. The summary data was fitted to the Hill-Langmuir equation (Figure 3.8B) and the IC_{50} value for currents recorded in the first 5 ms (white circles, n=6) was 26±9 M compared to 19±3 M in the last 5 ms (black circles, n=6). These values were not significantly different to each other (ns, paired t-test). However, the IC_{50} value determined in the last 5 ms was significantly higher than LINGO1 tail peptide ($p<0.0001$, unpaired t-test). Figures 3.9A and B show families of BK currents in the absence and presence of 10 M LINGO4 tail peptide, which as expected, reduced BK current amplitude. As observed in Figure 3.9B the peptide blocked the current at more positive potentials. Figure 3.9C shows a summary of the effect in the last 5 ms of the depolarising pulse, before (white circles) and during the application (black circles) of the peptide. As shown in the black symbols, the current amplitude during the application of the peptide was reduced by ~40% at potentials positive to +80 mV. Together these results demonstrated that the terminal 9 residues of LINGO4 tail

peptide reduced current amplitude but, unlike the LINGO1 and 2 tail peptides, did not induce inactivation of the BK channels.

A. LINGO4 *(NH_2-GNRVTAKLF-OH)*

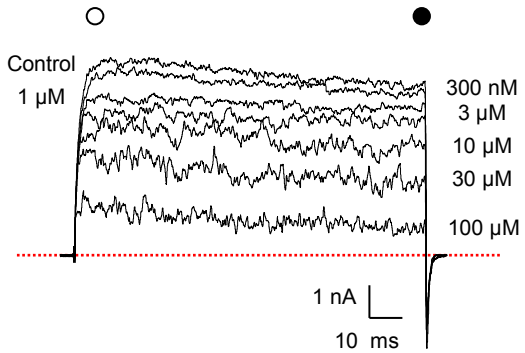

B. Summary of LINGO4

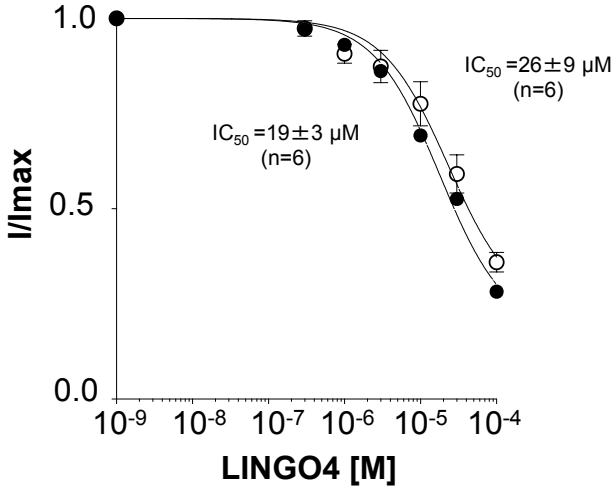

Figure 3.8: Concentration-dependent effect of LINGO4 tail peptide on WT BK .
A Representative concentration-dependent effect of LINGO4 synthetic tail peptide on HEK cells expressing WT BK . Currents were evoked by a step from -60 mV to +160 mV in the presence of 300 nM, 1, 3, 10, 30, 100 M of LINGO4 tail peptide. **B** Summary concentration effect curve for the effect of LINGO4 on BK currents (n=6). Data were fitted with the Hill-Langmuir equation. LINGO4 did not inactivate BK currents.

A. Control (1 μM Ca^{2+})

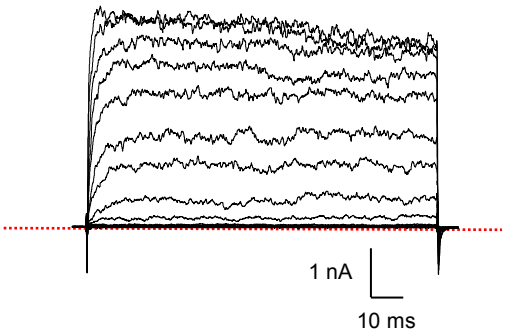

B. LINGO4 peptide (10 μM)

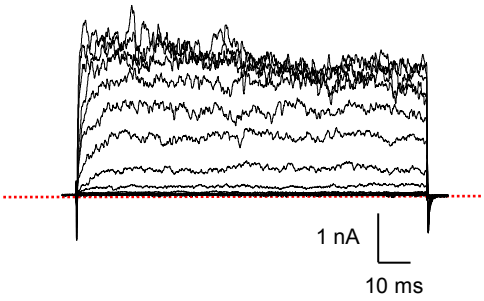

C. Summary IV

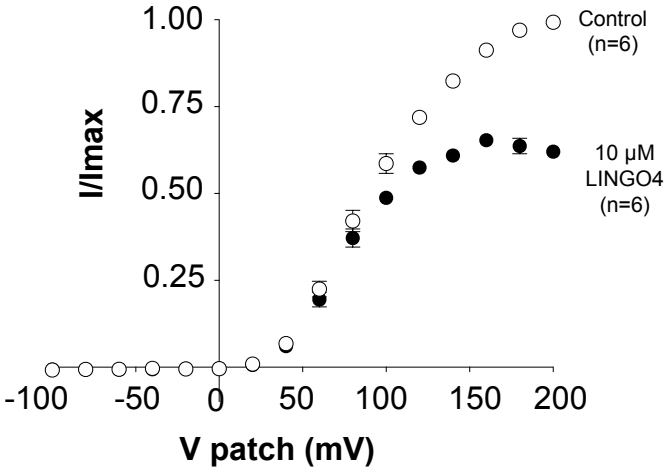

Figure 3.9: Voltage-dependence of LINGO4 synthetic tail peptide on BK .
A & **B** Macroscopic currents from inside-out patches expressing BK alone, show typical records in control (1 μM $[Ca^{2+}]_i$) and after application of 10 μM LINGO4 tail peptide. Patches were held at -60 mV and stepped from -100 mV to +200 mV in 20 mV increments and stepped back down to -80 mV to generate tail currents. **C** Summary of I/Imax measured in the last 5 ms of the pulse (n=6).

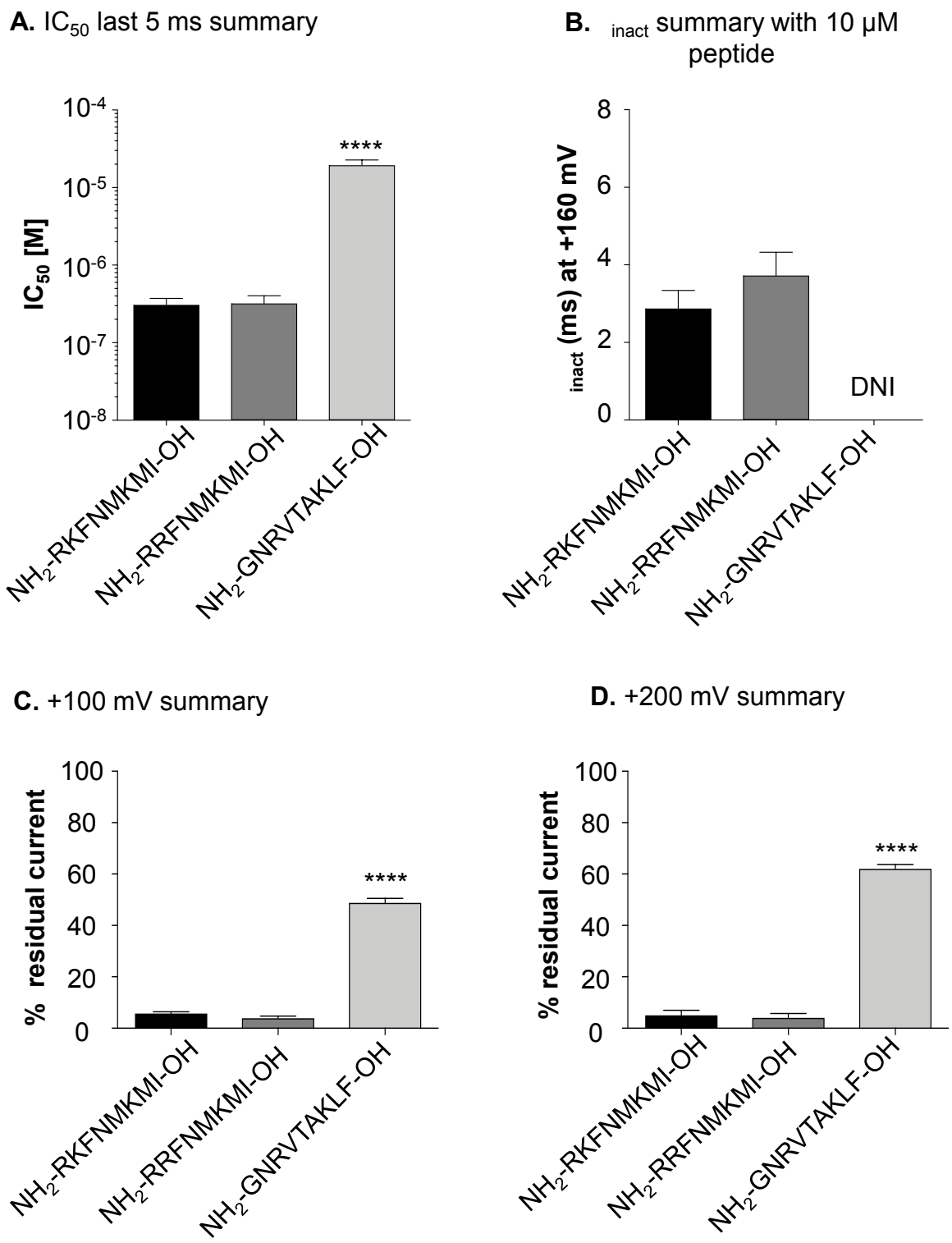

Figure 3.10: Comparison of the effect of LINGO tail peptides on BK .
A Effect of LINGO tail peptides in the last 5 ms of the depolarising pulse, which shows similar IC_{50} values for LINGO1 and LINGO2 but higher value for LINGO4 (one-way ANOVA, **** p<0.0001). **B** Mean inactivation time constant ($_{inact}$) of currents at +160 mV in the presence of 10 µM LINGO1 and LINGO2 tail peptides. **C** Percentage of residual current measured in the last 5 ms at +100 mV and **D** at +200 mV in the presence of LINGO1, LINGO2 and LINGO4 tail peptides (one-way ANOVA, **** p<0.0001).

3.3 Discussion

In the present study, we demonstrated the following:

1. Transcriptional expression of all four LINGO subtypes in murine airway and brain.
2. Synthetic tail peptides of LINGO1 and LINGO2 inactivated BK channels.
3. Synthetic tail peptide of LINGO4 blocked but did not inactivate BK channels.

Previously it has been shown that in rat tissue lysates, LINGO1 is abundantly expressed in the brain and spinal cord and is apparently absent in non-neuronal tissues (Mi *et al.* 2013). LINGO1 is also known to be evolutionarily conserved across species since human and mouse orthologs share 99.5% sequence identity (Mi *et al.* 2013). Although the expression of LINGO subtypes in different organs remains unknown, we demonstrated using RT-PCR experiments that *LINGO1-4* can be detected at the transcriptional level in murine brain and bronchus tissues (Figure 3.3A). Figure 3.3B confirmed the differential expression of *LINGO1-4* transcripts among murine brain and bronchus cDNA samples. These experiments will require further experimental confirmation with real time-PCR and immunocytochemistry. Moreover, recent publicly available data suggests that LINGO1 protein is also found in the human lung and is abundantly expressed in the brain (https://www.proteinatlas.org/ENSG00000169783-LINGO1/tissue; Uhlén *et al.* 2015). This suggests that LINGO proteins may be expressed under normal conditions in the murine brain and bronchus, although this will require further experimental confirmation using immunocytochemistry.

When LINGO proteins were compared using the multiple sequence alignment tool ClustalW2, it was clear that the number of amino acids in these subtypes varied, LINGO1-(620 a.a), LINGO2-(606 a.a), LINGO3-(592 a.a) and LINGO4-(593 a.a). It was also observed that LINGO1 and 2 shared 61% sequence similarity, LINGO1 and 3 shared 56% sequence similarity, whereas LINGO1 and LINGO4 shared only 44% sequence similarity (Mi *et al.* 2013). Also, the C-terminus of LINGO1-3 proteins have a common KMI motif which was clearly absent in LINGO4 protein (Figure 3.3C). As mentioned previously in Section 1.6, the BK subunits and LINGO proteins belong to a much larger family of leucine

rich repeat proteins. In our recently published paper (Dudem *et al.* 2020), we have illustrated the differences between the BK subunits and LINGO proteins, both of which contained extracellular LRRs however, BK subunits had 6 LRRC domains whereas, LINGO proteins had 12 LRRC domains. In addition, the LINGO proteins contained an Ig domain which was absent in the BK subunits. Interestingly, the BK subunits and LINGO1 protein shared <20% sequence similarity. Furthermore, when the multiple-sequence alignment of the transmembrane regions and portion of the intracellular tails from various LRR proteins was used to construct a phylogenetic tree, it suggested that all the LINGO (1-4) subtypes were evolutionarily close to BK subunits (Dudem *et al.* 2020).

Recently in our lab, we demonstrated that LINGO1 when co-expressed with BK channels showed three major characteristics: (i) rapid and complete inactivation of BK currents, (ii) the activation $V_{1/2}$ showed a -60 mV shift as compared to BK alone and (iii) the inactivation showed an apparent calcium and voltage-dependence (Dudem *et al.* 2020).

For the first time, we assessed the effects of synthetic tail peptides of LINGO proteins on BK channels and found that the LINGO1 tail peptide (NH_2-RKFNMKMI-OH) mimicked the inactivation of the full-length LINGO1 protein when co-expressed with BK channels. The application of the LINGO1 tail peptide reduced current amplitude and induced inactivation of BK currents with an IC_{50} of 308 nM (Figure 3.10A). The rate of inactivation when assessed with a single exponential, increased with increase in concentration of the peptide. With a concentration of 10 M LINGO1, at +160 mV, the time constant of inactivation was ~3 ms (Figure 3.10B). During the application of 10 M LINGO1, there was almost complete inactivation of BK currents as evidenced by the absence of sustained current at depolarisations positive to +100 mV (Figure 3.10C & D).

We next examined the effect of LINGO2 tail peptide (NH_2-RRFNMKMI-OH) on the BK currents. LINGO2 tail peptide inactivated BK channels with an IC_{50} value similar to LINGO1 tail peptide (Figure 3.10A). There was no significant difference between the time constant of inactivation with the effect of 10 M LINGO2 and 10 M LINGO1 at +160 mV (ns, unpaired t-test; Figure 3.10B), suggesting that

they had similar affinities for the BK channel. During the application of 10 M LINGO2 tail peptide, there was almost complete inactivation and the absence of sustained current at depolarisations positive to +100 mV, as observed with LINGO1 (Figure 3.10C and D). LINGO1 and LINGO2 tail peptides showed similar features in inactivating BK currents, which may be accounted for by the 61% sequence similarity and the common KMI motif between the two proteins. Furthermore, there was only a single amino acid residue difference in the last eight amino acids between LINGO1 and LINGO2 proteins (Mi *et al*. 2013, Figure 3.3C).

Since LINGO1 and LINGO3 share 56% sequence similarity and the sequence of the last eight amino acid residues for both the proteins is identical (RKFNMKMI) (Mi *et al*. 2013, Figure 3.3C), it indicates that LINGO3 protein may also inactivate BK channels, but this will require experimental confirmation.

We then assessed the effect of LINGO4 tail peptide on BK channels. This tail peptide consisted of nine amino acid (NH_2-GNRVTAKLF-OH) residues. Interestingly, the LINGO4 tail peptide did not induce inactivation of the BK channels but only reduced current amplitude. This effect could be accounted for by the absence of the KMI motif which is present in the other three LINGO subtypes (Mi *et al*. 2013, Figure 3.3C). The IC_{50} value with this peptide was significantly higher than LINGO1 and LINGO2 tail peptides (Figure 3.10A). In addition, the effect of 10 M LINGO4 tail peptide showed no inactivation even at potentials positive to +100 mV (Figure 3.9B). Moreover, the amount of sustained current at the end of the depolarisation pulse was significantly higher compared to LINGO1 and LINGO2 tail peptides (Figure 3.10C and D). For example, at +200 mV the residual current at the end of the depolarising pulse was 62±1% (n=6) in the presence of the LINGO4 tail peptide compared to 5±1% (n=9) with LINGO1 tail peptide ($p<0.001$, Mann-Whitney test), perhaps suggesting that block by the LINGO4 tail peptide was more unstable compared to the other LINGO tail peptides.

Previous studies by Murrell-Lagnado and Aldrich (1993a, 1993b) demonstrated that the rate of block of the ShB peptide on ShB**r** 6-46 channels increased with increase in net positive charge within the C-terminus of the peptide, suggesting

that the peptide valence played an important role in inactivation of the ShB**r** 6-46 channels. The terminal 8 residues in the C-terminus of LINGO proteins (Figure 3.3C), show that LINGO1 and LINGO2 proteins have three positively charged residues, whereas LINGO4 has two positively charged residues. The difference between the number of positively charged residues, which help in determining the net positive charge of the LINGO peptide may play a role in mediating inactivation of BK channels.

Collectively these results demonstrated that amongst the amino free acid synthetic tail peptides used, LINGO1 and LINGO2 tail peptides inactivated the BK channels, whereas LINGO4 tail peptide did not. The LINGO1 tail peptide mimicked the inactivation features observed when the full-length LINGO1 protein was co-expressed with BK channels (Dudem *et al.* 2020).

4. The effect of acylated amide LINGO1 tail peptide modifications on inactivation of BK channels

4.1 Introduction

As seen in Chapter 3, the amino free acid tail peptide versions of LINGO1 and LINGO2, rapidly inactivated BK channels but LINGO4 did not. The net charges of the LINGO tail peptides are due to the presence of charged amino acid residues. In the LINGO1 peptide for example, with the amino acid sequence NH_2^+-RKFNMKMI-COO^-, there are three positively charged amino acid residues (R, K and K) and the charges at N and C termini neutralise each other thus, resulting in a net charge of +3. Similarly, LINGO2 (NH_2-RRFNMKMI-OH) and LINGO3 (NH_2-RKFNMKMI-OH) peptides have a net charge of +3, whereas LINGO4 peptide (NH_2-GNRVTAKLF-OH) has a net charge of +2.

The LINGO1 tail peptide utilised in Chapter 3 had an NH_2-terminal and a COOH-terminal. However, in the native full-length LINGO1 protein, the terminal residues RKFNMKMI would have no charge at the beginning of R613 residue but have a negatively charged C-terminus at the end of I620 residue. We further wished to investigate the importance of net charge attributed by the positively charged residues in the LINGO1 peptide-mediated inactivation of BK channels.

Previous studies by Murrell-Lagnado and Aldrich (1993a; 1993b) have utilised acylated amidated peptides and investigated the role of net charge in the ShB peptide-mediated inactivation of ShB 6-46 channels. A similar approach was also utilised by Li and Aldrich (2006) who investigated the inactivation of BK channels mediated by the enhanced ball peptide.

With this in mind, we next synthesised a series of acylated amide LINGO1 peptides to eliminate charged atoms at both N and C termini and then assessed the effects of changing different residues in these peptides to examine their impact on BK channel inactivation.

4.2 Results

4.2.1 Acylation and Amidation of LINGO1 synthetic tail peptide does not affect its inactivating effect on BK channels

We first neutralised the charged ends of the LINGO1 tail peptide by acylating the N-terminus and amidating the C-terminus, before we assessed the effects of this peptide (Ac-RKFNMKMI-NH_2) on BK channels. This peptide had a net charge of +3 and we expected that it would have similar effects to the amino free acid version of LINGO1 peptide (NH_2-RKFNMKMI-OH), shown in the previous chapter (see Figure 3.4A). To test this, the previously described protocol was used. Thus, patches were held at -60 mV and currents were elicited by stepping to +160 mV for 100 ms in 1 M $[Ca^{2+}]_i$ before stepping down to -80 mV to evoke tail currents. Figure 4.1A shows a typical experiment in which Ac-RKFNMKMI-NH_2 (300 nM to 100 M), when applied to the cytosolic surface of the patches, induced inactivation in a concentration-dependent manner and as a result, reduced current amplitude. Figure 4.1B shows summary data fitted with the Hill-Langmuir equation. Note that the grey dashed line represents the fit to the data obtained with the NH_2-RKFNMKMI-OH peptide as per Figure 3.4B. The IC_{50} was 5±1 M (n=6), when measured from currents during the first 5 ms (white circles) and 228±30 nM (n=6) when measured in the last 5 ms (black circles) of the depolarising step (Figure 4.1B). These values were significantly different from each other and indicated that this peptide caused a time dependent inactivation of BK currents ($p<0.01$, paired t-test). However, when the IC_{50} value determined from current amplitudes in the last 5 ms were compared with that obtained with the amino free acid version of the peptide, there was no significant difference (ns, unpaired t-test). The rate of inactivation of the inactivating BK currents was next assessed by fitting the decay phase of the currents with a single exponential, and the results are shown in Figure 4.1C. Like the NH_2-RKFNMKMI-OH peptide, shown in grey symbols in Figure 4.1C, the rate of inactivation increased with the concentration of Ac-RKFNMKMI-NH_2 and both peptides showed practically identical time constants of inactivation, as exemplified with 10 M of each peptide, where there was no significant difference between them (ns, unpaired t-test). Figures 4.2A and B show families of BK currents in 1 M $[Ca^{2+}]_i$ evoked

from patches in the absence and presence of 10 M of the Ac-RKFNMKMI-NH_2 peptide, respectively. These effects were, as expected, similar to those observed with the amino free acid version of LINGO1 peptide (see Figure 3.5) and consequently, the vast majority of the current was inactivated at the end of the pulse as shown in Figure 4.2B and summarised, for 7 patches, in Figure 4.2C. When the time constant of inactivation ( )for currents at each voltage was plotted for the same 7 experiments shown in Figure 4.2D, it was clear that the currents inactivated more rapidly at positive potentials. For instance, at +200 mV, the rate of inactivation for the Ac-RKFNMKMI-NH_2 peptide was significantly faster than NH_2-RKFNMKMI-OH peptide ($p<0.01$, unpaired t-test).

A. Ac-*RKFNMKMI*-NH_2

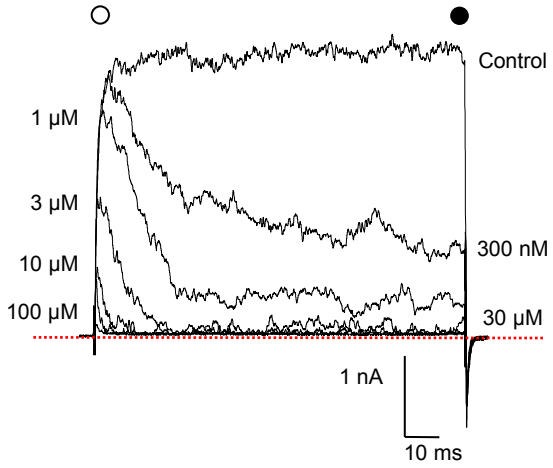

B. Summary of Ac-*RKFNMKMI*-NH_2

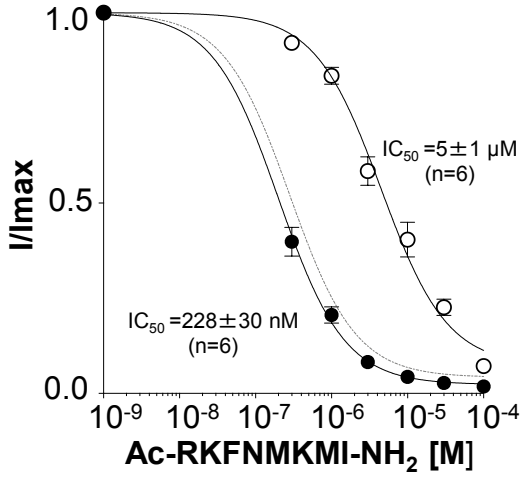

C. Summary of Ac-*RKFNMKMI*-NH_2 $_{inact}$

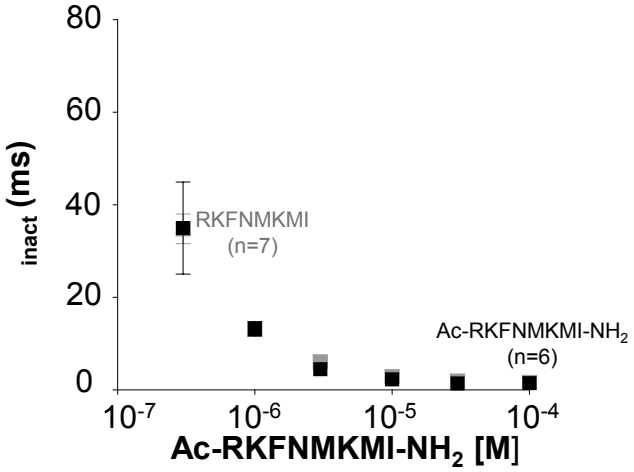

Figure 4.1: Concentration-dependent effect of Ac-RKFNMKMI-NH_2 synthetic peptide on WT BK .

A Representative concentration-dependent effect of Ac-RKFNMKMI-NH_2 synthetic peptide on HEK cells expressing WT BK . Currents were evoked by a step from -60 mV to +160 mV in the presence of 300 nM, 1, 3, 10, 30, 100 µM of Ac-RKFNMKMI-NH_2 peptide. **B** Summary concentration effect curve for the effect of Ac-RKFNMKMI-NH_2 on BK currents (n=6). Data were fitted with the Hill-Langmuir equation (grey trace LINGO1 tail peptide). **C** The rate of inactivation of BK currents was assessed by fitting the decay phase with a single exponential (grey trace LINGO1 tail peptide). The rate of inactivation increased with the concentration of Ac-RKFNMKMI-NH_2 synthetic peptide (n=6).

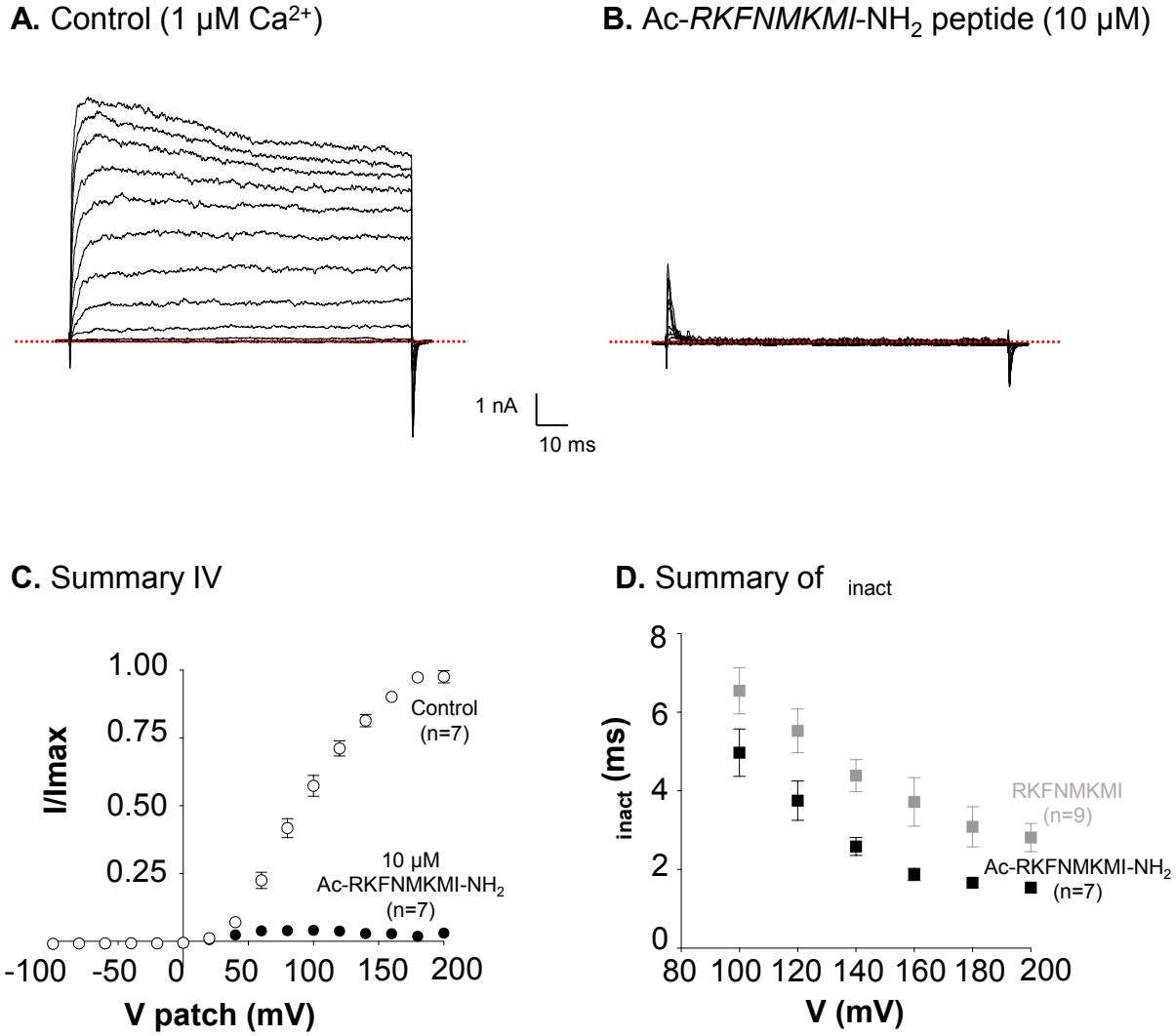

Figure 4.2: Voltage-dependence of Ac-RKFNMKMI-NH_2 synthetic peptide on BK .
A & **B** Macroscopic currents from inside-out patches expressing BK alone, show typical records in control (1 μM $[Ca^{2+}]_i$) and after application of 10 μM Ac-RKFNMKMI-NH_2 peptide. Patches were held at -60 mV and stepped from -100 mV to +200 mV in 20 mV increments and stepped back down to -80 mV to generate tail currents. **C** Summary of I/Imax measured in the last 5 ms of the pulse (n=7). **D** The rate of inactivation of BK currents was assessed by fitting the decay phase with a single exponential (grey trace LINGO1 tail peptide). The currents showed an apparent voltage-dependence at more positive potentials (n=7).

4.2.2 Acylation and Amidation of 14 amino acids of LINGO1 synthetic tail peptide does not affect its inactivating effect on BK currents

The results of the previous experiments suggested that the last 8 amino acids of the LINGO1 C-terminal were sufficient to confer inactivation of BK channels. However, we further wished to investigate if increasing the length of the peptide while maintaining a net charge of +3, affected the efficacy of the LINGO1 tail peptide to inactivate BK channels. Therefore, we synthesised the acylated amide (Ac-SSADAPRKFNMKMI-NH_2) peptide containing the terminal 14 amino acids from the C-terminal of the LINGO1 protein and applied it to excised patches of HEK cells overexpressing BK bathed in 1 M $[Ca^{2+}]_i$. Figure 4.3A shows application of the Ac-SSADAPRKFNMKMI-NH_2 peptide induced inactivation and reduction of current amplitude in a concentration-dependent manner (300 nM to 100 M). Figure 4.3B summarises 7 similar experiments in which the IC_{50} obtained from the first 5 ms was 6±1 M (n=7) and last 5 ms was 700±80 nM (n=7). These values were not significantly different from each other (ns, paired t-test). The IC_{50} value for the last 5 ms with the Ac-SSADAPRKFNMKMI-NH_2 peptide was ~3-fold higher compared to that of Ac-RKFNMKMI-NH_2 peptide ($p<0.001$, unpaired t-test). The rate of inactivation of BK currents was again assessed by fitting the decay phase with a single exponential as shown in Figure 4.3C. The rate of inactivation with 1 M of the peptide was slower compared to 1 M of the Ac-RKFNMKMI-NH_2 peptide ($p<0.01$, unpaired t-test). However, with 100 M concentration of the peptides, there was no significant difference between the rates of inactivation observed with the two peptides (ns, unpaired t-test). Figure 4.4B shows that 10 M of the peptide induced rapid and almost complete inactivation of BK currents. Figure 4.4C summarises 9 similar experiments in which the amount of residual current at +200 mV showed no significant difference when compared to that of Ac-RKFNMKMI-NH_2 peptide (ns, Mann-Whitney test). The inactivation of currents with 10 M of Ac-SSADAPRKFNMKMI-NH_2 peptide was apparent at potentials positive to +40 mV. The rate of inactivation of these currents was slower at all potentials measured from +100 to +200 mV, compared to Ac-RKFNMKMI-NH_2 peptide shown in grey in Figure 4.4D ($p<0.05$, one-way ANOVA).

A. Ac-*SSADAPRKFNMKMI*-NH_2

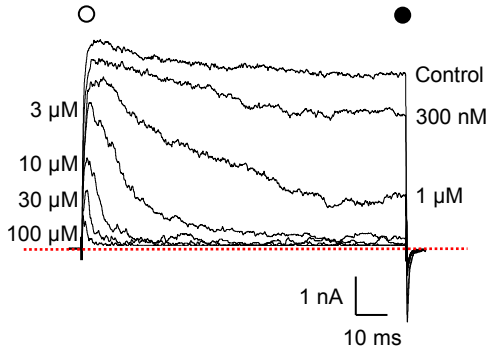

B. Summary of Ac-*SSADAPRKFNMKMI*-NH_2

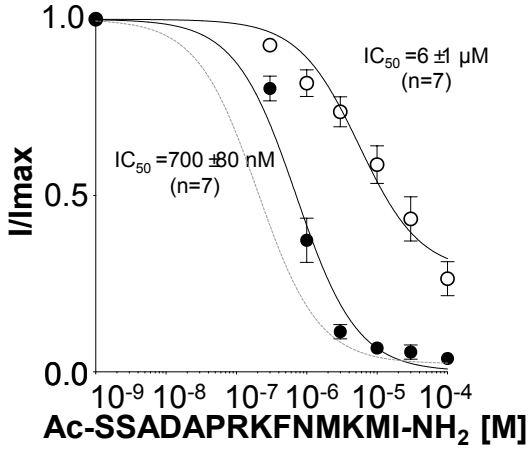

C. Summary of Ac-*SSADAPRKFNMKMI*-NH_2 $_{inact}$

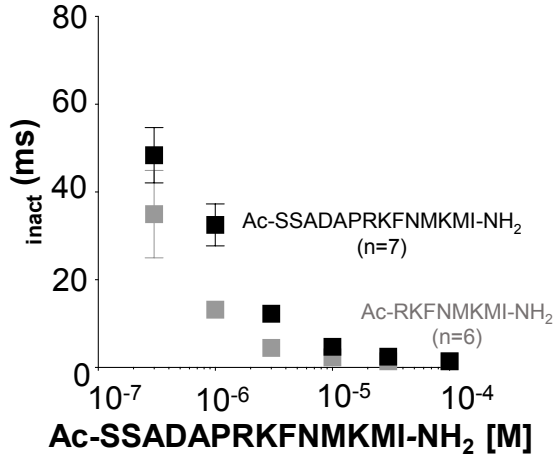

Figure 4.3: Concentration-dependent effect of Ac-SSADAPRKFNMKMI-NH_2 synthetic peptide on WT BK .
A Representative concentration-dependent effect of Ac-SSADAPRKFNMKMI-NH_2 synthetic peptide on HEK cells expressing WT BK . Currents were evoked by a step from -60 mV to +160 mV in the presence of 300 nM, 1, 3, 10, 30, 100 µM of Ac-SSADAPRKFNMKMI-NH_2 peptide. **B** Summary concentration effect curve for the effect of Ac-SSADAPRKFNMKMI-NH_2 on BK currents (n=7). Data were fitted with the Hill-Langmuir equation (grey trace Ac-RKFNMKMI-NH_2 peptide). **C** The rate of inactivation of BK currents was assessed by fitting the decay phase with a single exponential (grey trace Ac-RKFNMKMI-NH_2 peptide). The rate of inactivation increased with the concentration of Ac-SSADAPRKFNMKMI-NH_2 peptide (n=7).

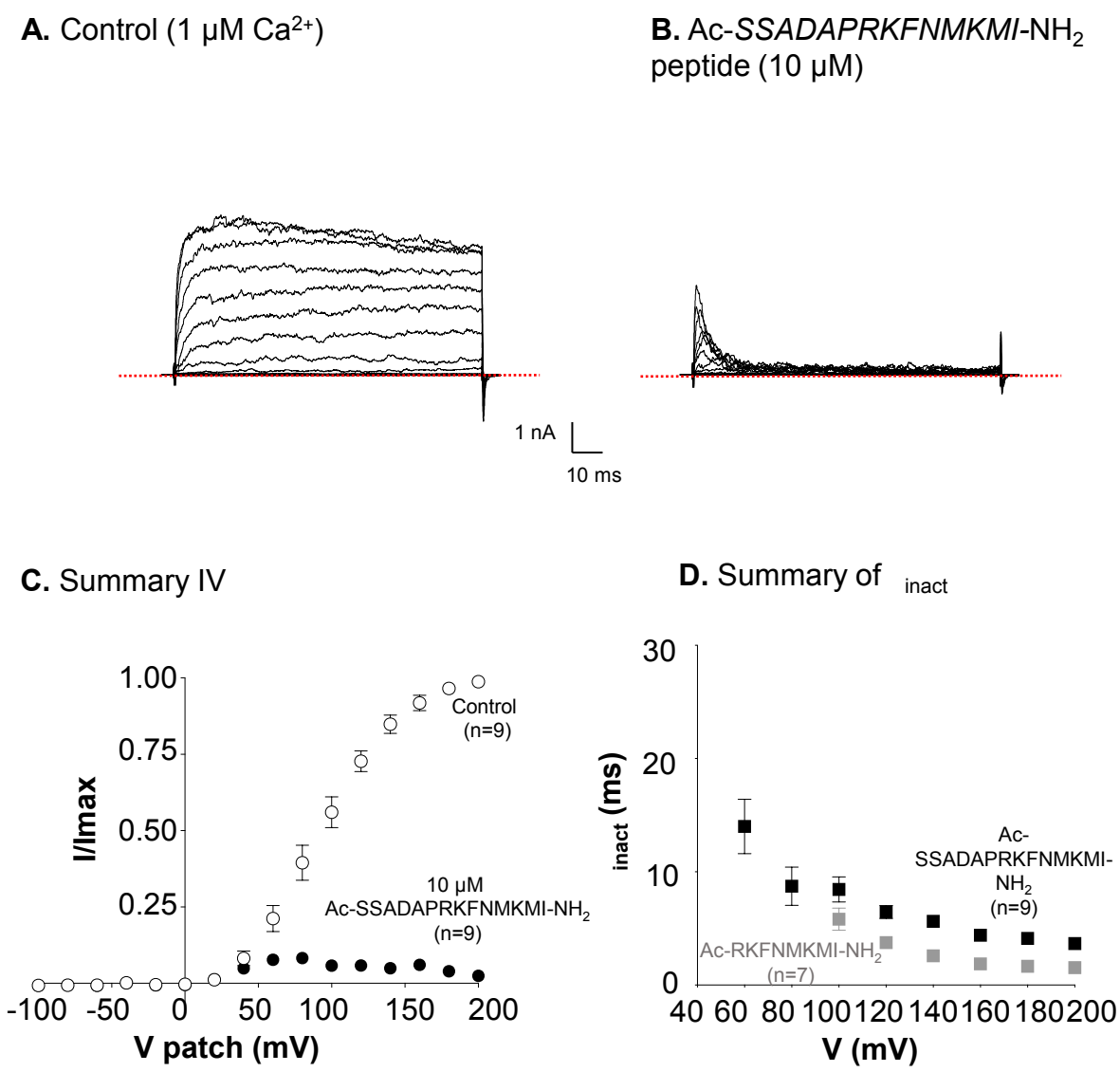

Figure 4.4: Voltage-dependence of Ac-SSADAPRKFNMKMI-NH_2 peptide on WT BK .
A & **B** Macroscopic currents from inside-out patches expressing BK alone, show typical records in control (1 μM $[Ca^{2+}]_i$) and after application of 10 μM Ac-SSADAPRKFNMKMI-NH_2 peptide. Patches were held at -60 mV and stepped from -100 mV to +200 mV in 20 mV increments and stepped back down to -80 mV to generate tail currents. **C** Summary of I/Imax measured in the last 5 ms of the pulse (n=9). **D** The rate of inactivation of BK currents was assessed by fitting the decay phase with a single exponential (grey trace Ac-RKFNMKMI-NH_2 peptide). The currents showed an apparent voltage-dependence at more positive potentials (n=9).

4.2.3 Neutralising a positively charged residue (R613) in LINGO1 synthetic tail peptide does not affect its inactivating effect on BK channels

The above data confirmed that the last 8 residues of the LINGO1 protein were sufficient to mimic the inactivation of BK currents like the full-length LINGO1. Therefore, we returned to using 8 residue long peptides to investigate the contribution of the positively charged residues in the LINGO1 tail to mediate BK current inactivation. To test this, we first synthesised a peptide where the first positively charged residue, R613, was neutralised to alanine (Ac-**A**KFNMKMI-NH_2), reducing its net charge to +2. As Figure 4.5A shows, application of Ac-**A**KFNMKMI-NH_2 reduced current amplitude and induced inactivation of BK currents in a concentration-dependent manner. The IC_{50} value obtained for the first 5 ms was 10±2 M (n=5) and the last 5 ms was 2±1 M (n=5) and these values were significantly different ($p<0.05$, paired t-test). The IC_{50} value obtained for the last 5 ms was 8-fold higher than that of the Ac-RKFNMKMI-NH_2 peptide, as illustrated with the grey dotted line in Figure 4.5B ($p<0.0001$, unpaired t-test). As Figure 4.5C suggests, the rate of inactivation of these currents with 10 M of the peptide was similar to that observed with 10 M of Ac-RKFNMKMI-NH_2 peptide (ns, unpaired t-test). Figures 4.6A and B show families of BK currents recorded in 1 M $[Ca^{2+}]_i$ before and during the application of 10 M Ac-**A**KFNMKMI-NH_2 synthetic peptide, respectively and suggests that this peptide was less effective than the Ac-RKFNMKMI-NH_2 peptide at inducing complete inactivation. For example, in the summary data shown in Figure 4.6C, the Ac-**A**KFNMKMI-NH_2 peptide reduced peak currents (last 5 ms) recorded at +200 mV to 11±1% (n=6) which was significantly higher than 3±1% (n=7) observed at the end of the pulse in the presence of the Ac-RKFNMKMI-NH_2 peptide ($p<0.01$, Mann-Whitney test). The inactivation induced by 10 M Ac-**A**KFNMKMI-NH_2 peptide was more apparent at potentials positive to +100 mV (Figure 4.6B) and the rate of inactivation of these currents at +200 mV was significantly slower to that observed with the Ac-RKFNMKMI-NH_2 peptide, as illustrated in grey in Figure 4.6D ($p<0.001$, unpaired t-test). These data suggest that neutralising the positively charged arginine at 613 reduced the efficacy of LINGO1 tail peptide to inactivate BK channels.

A. Ac-*AKFNMKMI*-NH_2

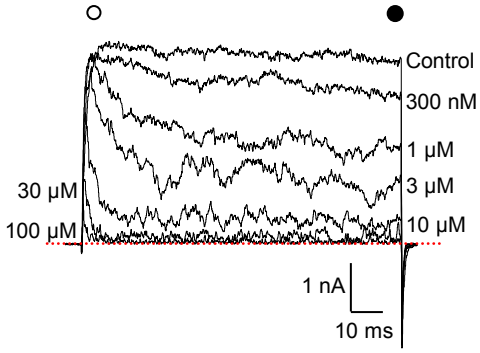

B. Summary of Ac-*AKFNMKMI*-NH_2

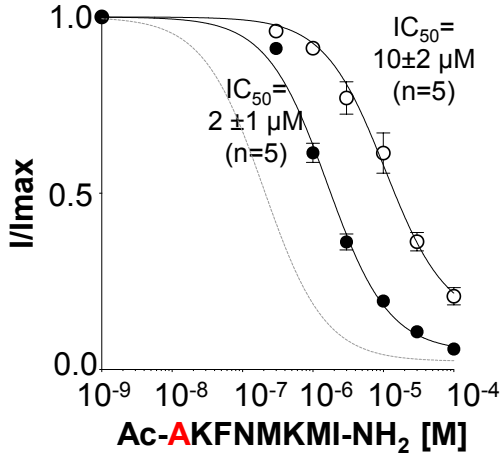

C. Summary of Ac-*AKFNMKMI*-NH_2 inact

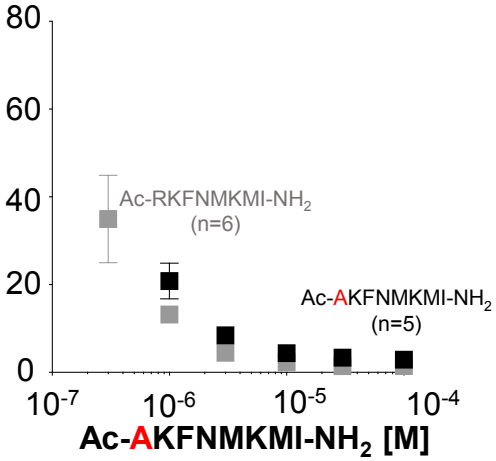

Figure 4.5: Concentration-dependent effect of Ac-AKFNMKMI-NH_2 peptide on WT BK .
A Representative concentration-dependent effect of Ac-AKFNMKMI-NH_2 synthetic peptide on HEK cells expressing WT BK . Currents were evoked by a step from -60 mV to +160 mV in the presence of 300 nM, 1, 3, 10, 30, 100 µM of Ac-AKFNMKMI-NH_2 peptide. **B** Summary concentration effect curve for the effect of Ac-AKFNMKMI-NH_2 on BK currents (n=5). Data were fitted with the Hill-Langmuir equation (grey trace Ac-RKFNMKMI-NH_2 peptide). **C** The rate of inactivation of BK currents was assessed by fitting the decay phase with a single exponential (grey trace Ac-RKFNMKMI-NH_2 peptide). The rate of inactivation increased with the concentration of Ac-AKFNMKMI-NH_2 peptide (n=5).

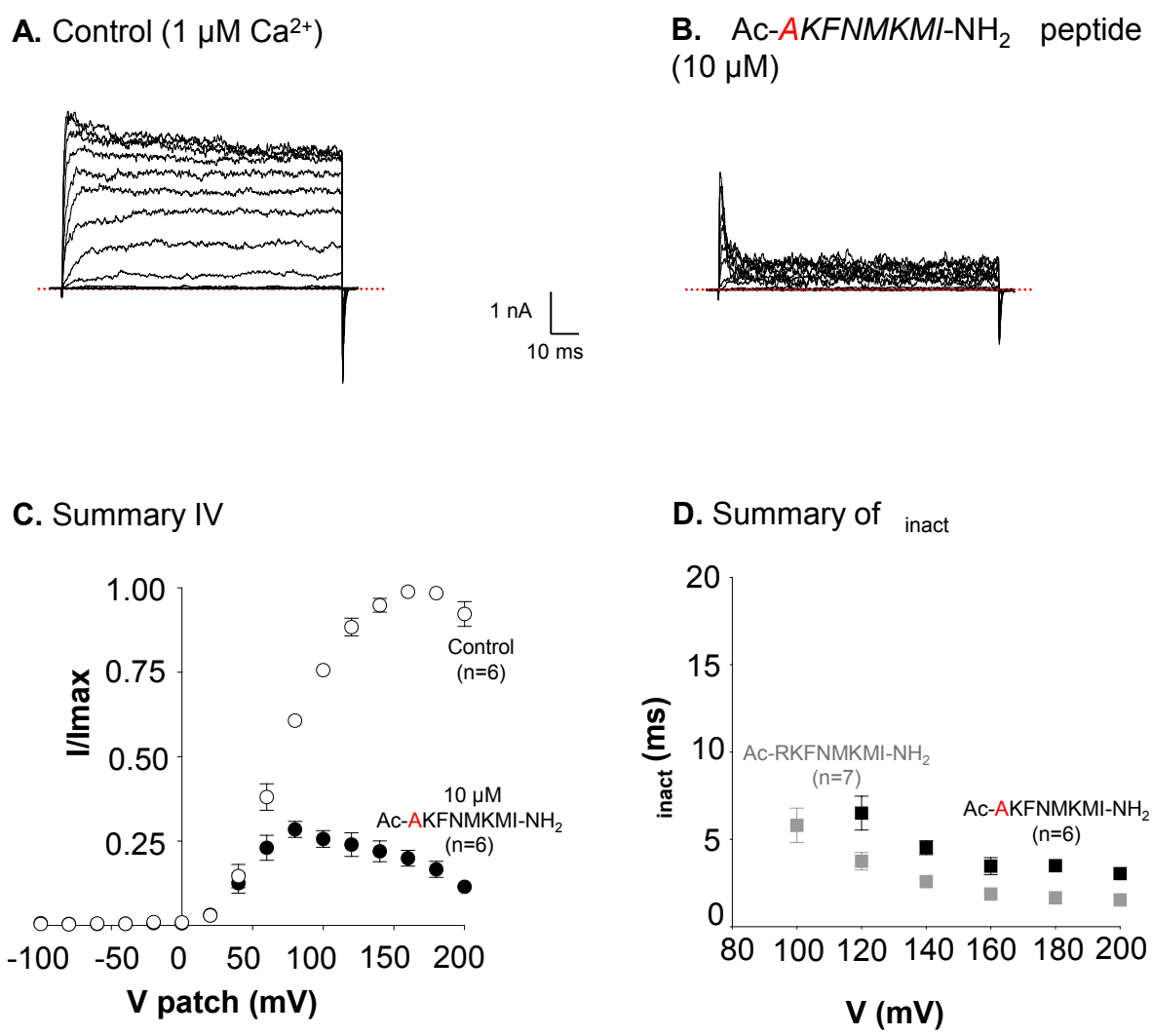

Figure 4.6: Voltage-dependence of Ac-AKFNMKMI-NH_2 peptide on WT BK .
A & **B** Macroscopic currents from inside-out patches expressing BK alone, show typical records in control (1 μM $[Ca^{2+}]_i$) and after application of 10 μM Ac-AKFNMKMI-NH_2 peptide. Patches were held at -60 mV and stepped from -100 mV to +200 mV in 20 mV increments and stepped back down to -80 mV to generate tail currents. **C** Summary of I/Imax measured in the last 5 ms of the pulse (n=6). **D** The rate of inactivation of BK currents was assessed by fitting the decay phase with a single exponential (grey trace Ac-RKFNMKMI-NH_2 peptide). The currents showed an apparent voltage-dependence at more positive potentials (n=6).

4.2.4 Neutralising a positively charged residue (K614) in LINGO1 synthetic tail peptide does not affect its inactivating effect on BK channels

We next examined the effects of neutralising the positively charged lysine residue at 614 with alanine, by synthesising the Ac-R**A**FNMKMI-NH_2 peptide (net charge of +2) and assessing its effects on HEK cells expressing BK alone. This peptide (Figure 4.7A) produced qualitatively similar effects to those observed with the Ac-**A**KFNMKMI-NH_2 peptide in Figure 4.5, as they both inactivated BK channels. In 7 similar experiments, the IC_{50} from the first 5 ms was 2±0.8 M (n=7) and the last 5 ms was 1±0.1 M (n=7, ns, paired t-test). The IC_{50} value for the last 5 ms was 4-fold higher than that obtained with the Ac-RKFNMKMI-NH_2 peptide ($p<0.0001$, unpaired t-test), but was not significantly different to that recorded with the Ac-**A**KFNMKMI-NH_2 peptide (ns, unpaired t-test). The rate of inactivation of the currents with 10 M of the peptide was like that observed with the Ac-RKFNMKMI-NH_2 peptide (grey trace, Figure 4.7C, ns, unpaired t-test). When 10 M of Ac-R**A**FNMKMI-NH_2 peptide was reapplied and subjected to an IV protocol (Figure 4.8B) this peptide appeared to be less able to induce complete inactivation, as evidenced by the sustained current in the last few ms of the depolarisations. This is apparent in Figure 4.8C, where the sustained current at +200 mV in the last 5 ms with Ac-R**A**FNMKMI-NH_2 peptide was 16±3% (n=7), which was significantly greater than that recorded in the presence of the Ac-RKFNMKMI-NH_2 peptide (3±1%, $p<0.01$, Mann-Whitney test). However, when compared to the Ac-**A**KFNMKMI-NH_2 peptide, the amount of sustained current with the Ac-R**A**FNMKMI-NH_2 peptide was not statistically different (ns, unpaired t-test). The apparent voltage-dependence of inactivation by Ac-R**A**FNMKMI-NH_2 peptide was observed at potentials positive to +100 mV (Figure 4.8D) and the rate of inactivation of these currents at +200 mV was practically identical to that observed with the Ac-**A**KFNMKMI-NH_2 (ns, unpaired t-test) but was significantly slower than the Ac-RKFNMKMI-NH_2 peptide ($p<0.001$, unpaired t-test). These data suggest that neutralising the positively charged lysine at 614 also reduced the efficacy of LINGO1 tail peptide to inactivate BK channels.

A. Ac-*RAFNMKMI*-NH_2

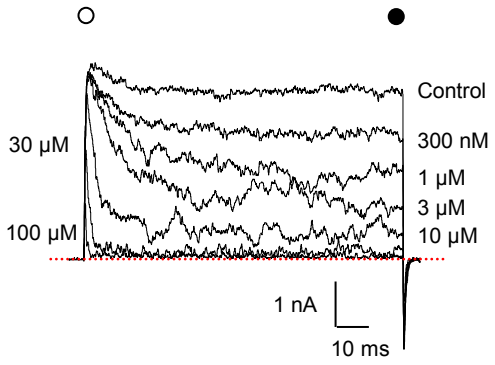

B. Summary of Ac-*RAFNMKMI*-NH_2

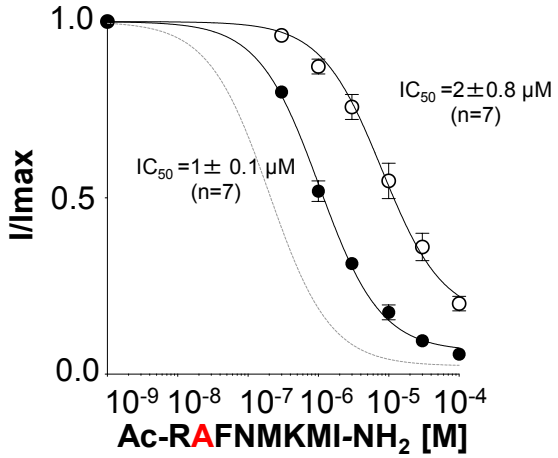

C. Summary of Ac-*RAFNMKMI*-NH_2 inact

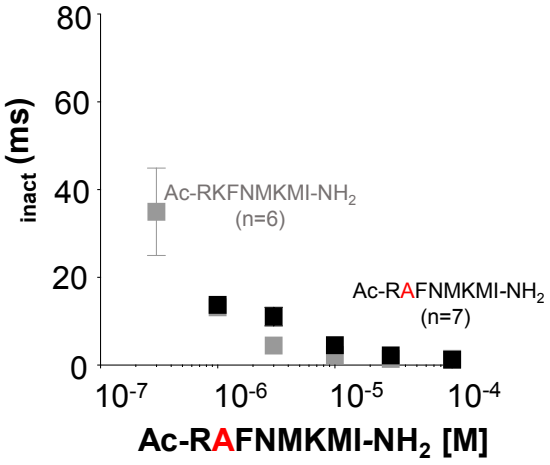

Figure 4.7: Concentration-dependent effect of Ac-RAFNMKMI-NH_2 peptide on WT BK .
A Representative concentration-dependent effect of Ac-RAFNMKMI-NH_2 synthetic peptide on HEK cells expressing WT BK . Currents were evoked by a step from -60 mV to +160 mV in the presence of 300 nM, 1, 3, 10, 30, 100 µM of Ac-RAFNMKMI-NH_2 peptide. **B** Summary concentration effect curve for the effect of Ac-RAFNMKMI-NH_2 on BK currents (n=7). Data were fitted with the Hill-Langmuir equation (grey trace Ac-RKFNMKMI-NH_2 peptide). **C** The rate of inactivation of BK currents was assessed by fitting the decay phase with a single exponential (grey trace Ac-RKFNMKMI-NH_2 peptide). The rate of inactivation increased with the concentration of Ac-RAFNMKMI-NH_2 tail peptide (n=7).

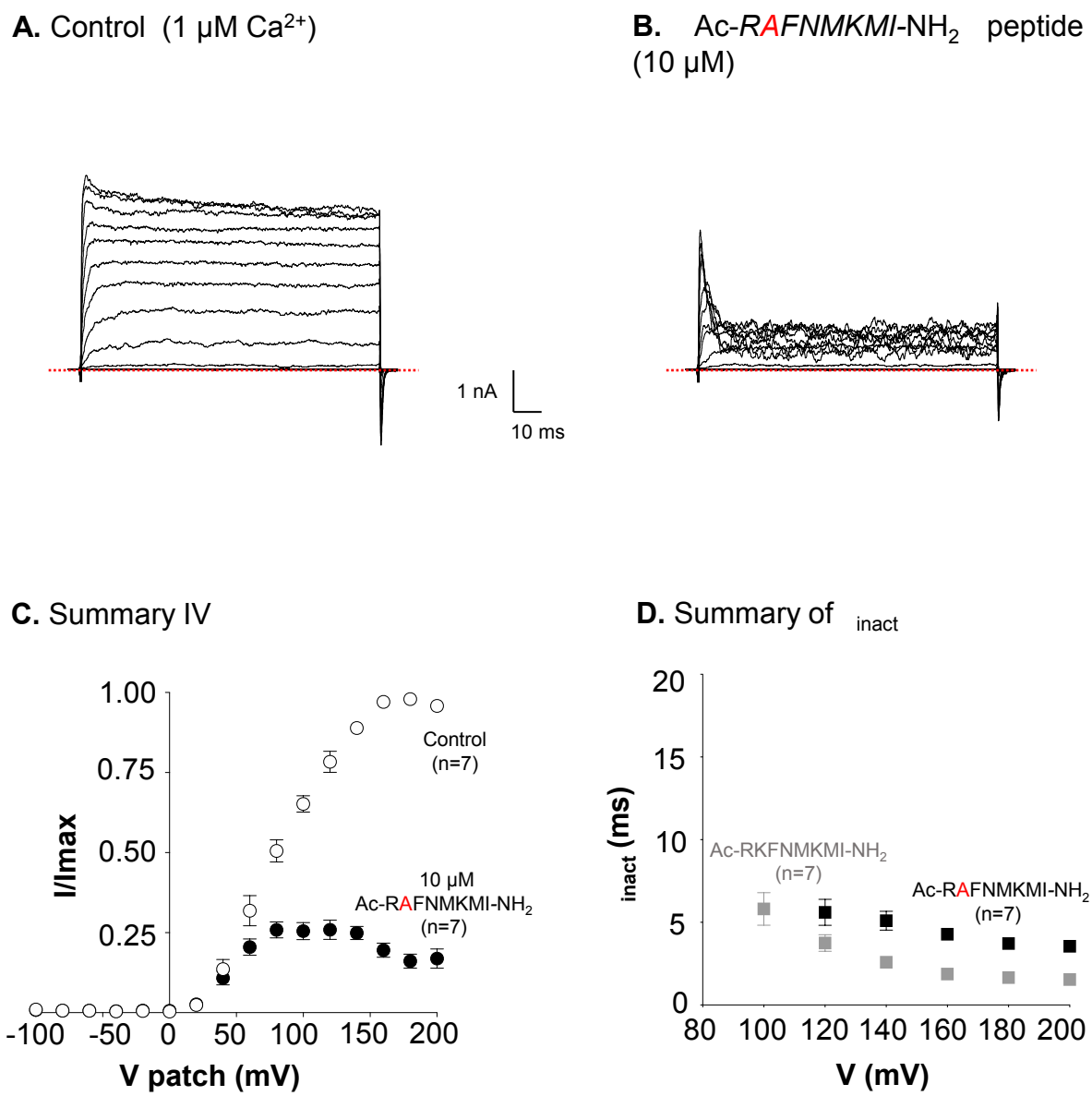

Figure 4.8: Voltage-dependence of Ac-RAFNMKMI-NH_2 peptide on WT BK .
A & **B** Macroscopic currents from inside-out patches expressing BK alone, show typical records in control (1 μM $[Ca^{2+}]_i$) and after application of 10 μM Ac-RAFNMKMI-NH_2 peptide. Patches were held at -60 mV and stepped from -100 mV to +200 mV in 20 mV increments and stepped back down to -80 mV to generate tail currents. **C** Summary of I/Imax measured in the last 5 ms of the pulse (n=7). **D** The rate of inactivation of BK currents was assessed by fitting the decay phase with a single exponential (grey trace Ac-RKFNMKMI-NH_2 peptide). The currents showed an apparent voltage-dependence at more positive potentials (n=7).

4.2.5 Deletion of the two positively charged residues (R613 and K614) in LINGO1 synthetic tail peptide does not affect its inactivating effect on BK channels

We next eliminated the arginine at 613 and lysine at 614 by synthesising a 6-residue peptide, Ac-FNMKMI-NH_2, which had a net charge of +1. As seen in Figure 4.9A, this peptide reduced current amplitude and appeared to induce inactivation of BK currents at higher concentrations. Figure 4.9B shows the summary of IC_{50} values obtained from the first 5 ms was 7±2 M (n=6) and the last 5 ms was 5±1 M (n=6) which were not significantly different (ns, paired t-test). The IC_{50} for the last 5 ms was 21-fold higher than that recorded with the Ac-RKFNMKMI-NH_2 peptide ($p<0.0001$, unpaired t-test). Clear time-dependent inactivation of the currents was reliably recorded with 10 and 30 M of the Ac-FNMKMI-NH_2 peptide. However, 100 M of the peptide only reduced current amplitude without causing clear inactivation as observed in Figure 4.9A. The rate of inactivation with 10 and 30 M of Ac-FNMKMI-NH_2 peptide was significantly slower than observed with 10 and 30 M of the Ac-RKFNMKMI-NH_2 peptide ($p<0.001$, one-way ANOVA). When a family of currents was recorded in 1 M $[Ca^{2+}]_i$ (Figure 4.10A) before and during the application of 10 M Ac-FNMKMI-NH_2 (Figure 4.10B), the peptide was less effective at blocking BK currents, as summarised in Figure 4.10C. For instance, at +200 mV, the amount of sustained current present in the last 5 ms of the pulse was 34±3% (n=7, $p<0.001$, Mann-Whitney test compared to Ac-RKFNMKMI-NH_2). Time-dependent inactivation of the currents was only observed at potentials positive to +140 mV with this peptide (Figure 4.10D) and was significantly slower at all potentials measured ($p<0.0001$, one-way ANOVA, compared to Ac-RKFNMKMI-NH_2). These results illustrate that despite the deletion of the two positively charged residues (R613 and K614) the peptide still induced inactivation of BK channels, albeit with a reduced efficacy.

A. Ac-*FNMKMI*-NH_2

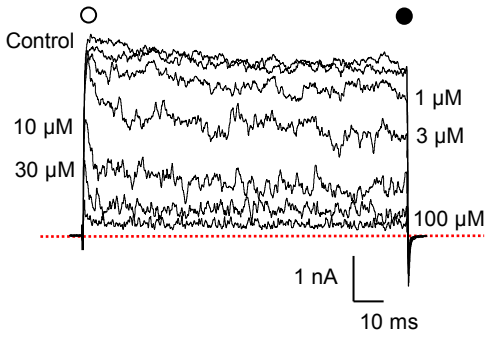

B. Summary of Ac-*FNMKMI*-NH_2

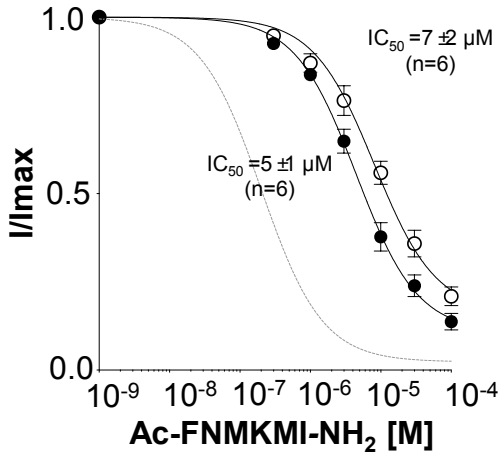

C. Summary of Ac-*FNMKMI*-NH_2 $_{inact}$

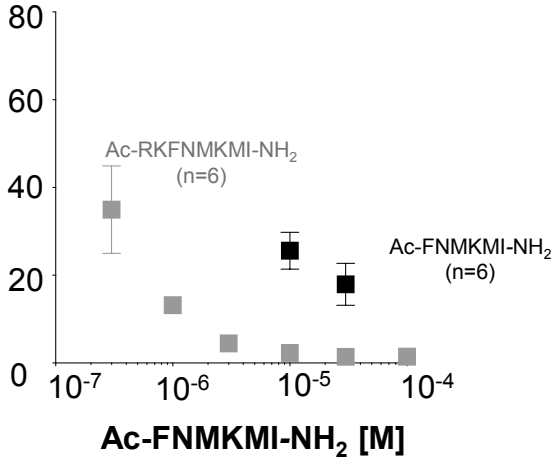

Figure 4.9: Concentration-dependent effect of Ac-FNMKMI-NH_2 peptide on WT BK .
A Representative concentration-dependent effect of Ac-FNMKMI-NH_2 synthetic peptide on HEK cells expressing WT BK . Currents were evoked by a step from -60 mV to +160 mV in the presence of 300 nM, 1, 3, 10, 30, 100 μM of Ac-FNMKMI-NH_2 peptide. **B** Summary concentration effect curve for the effect of Ac-FNMKMI-NH_2 on BK currents (n=6). Data were fitted with the Hill-Langmuir equation (grey trace Ac-RKFNMKMI-NH_2 peptide). **C** The rate of inactivation of BK currents was assessed by fitting the decay phase with a single exponential (grey trace Ac-RKFNMKMI-NH_2 peptide). The rate of inactivation increased with the concentration of Ac-FNMKMI-NH_2 tail peptide (n=6).

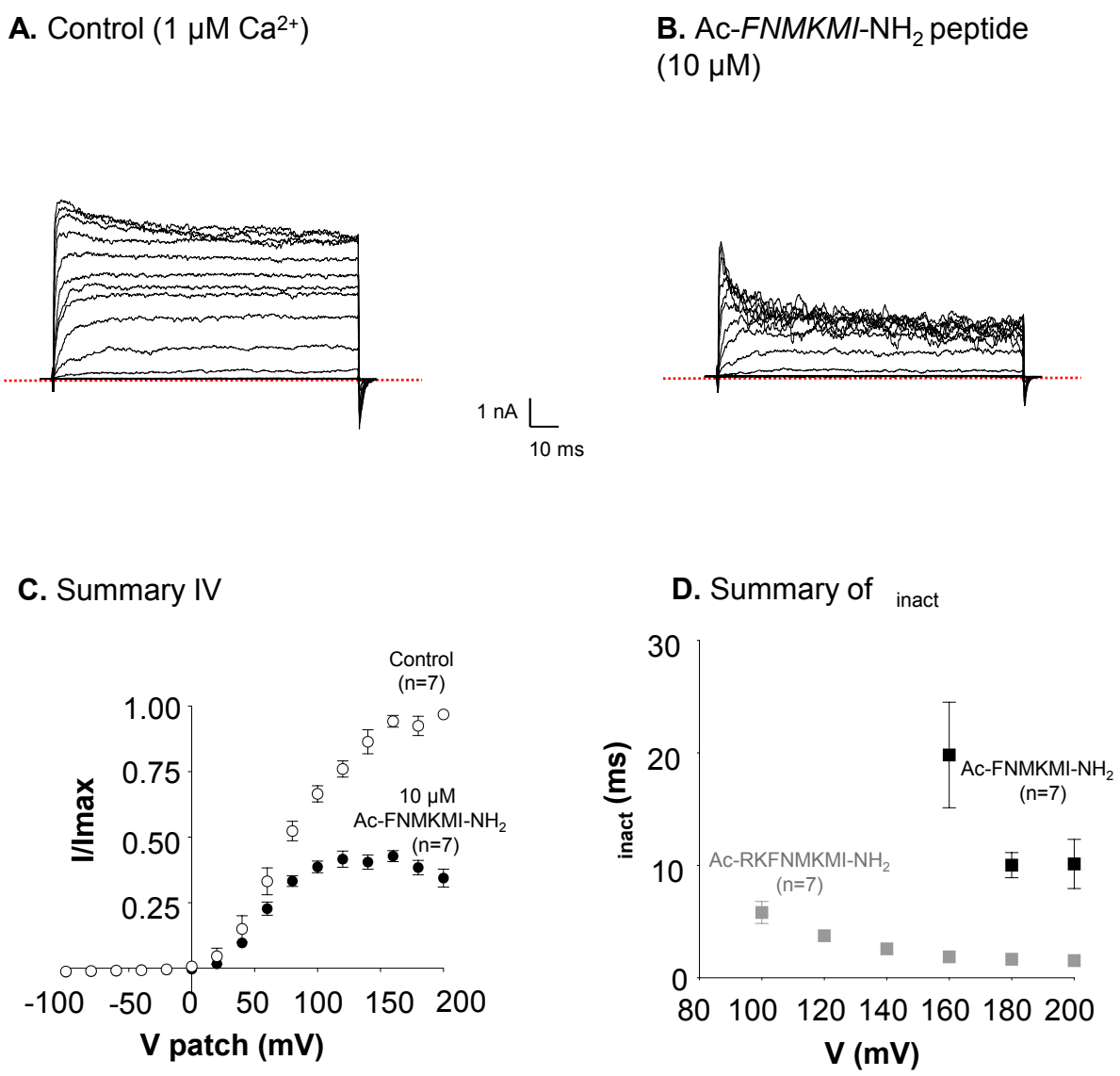

Figure 4.10: Voltage-dependence of Ac-FNMKMI-NH_2 peptide on WT BK .
A & **B** Macroscopic currents from inside-out patches expressing BK alone, show typical records in control (1 μM $[Ca^{2+}]_i$) and after application of 10 μM Ac-FNMKMI-NH_2 peptide. Patches were held at -60 mV and stepped from -100 mV to +200 mV in 20 mV increments and stepped back down to -80 mV to generate tail currents. **C** Summary of I/Imax measured in the last 5 ms of the pulse (n=7). **D** The rate of inactivation of BK currents was assessed by fitting the decay phase with a single exponential (grey trace Ac-RKFNMKMI-NH_2 peptide). The currents showed an apparent voltage-dependence at more positive potentials (n=7).

4.2.6 Neutralising two positively charged residues (R613 and K618) in LINGO1 synthetic tail peptide abolished inactivation of BK currents

We also examined the effect of charge neutralisation on the 8-residue peptide, by synthesising an Ac-**A**KFNM**A**MI-NH_2 peptide. As shown in Figure 4.11A, this peptide was ineffective at inducing inactivation of BK channels, compared to any of the peptides described above. Although it clearly reduced current amplitude in a concentration-dependent manner (300 nM to 100 M), Ac-**A**KFNM**A**MI-NH_2 failed to induce rapid inactivation. As shown in Figure 4.11B, the IC_{50} from the first 5 ms was 47±12 M (n=6) and from the last 5 ms was 41±6 M (n=6). Although these values were not significantly different to each other (ns, paired t-test), the IC_{50} value for the last 5 ms was significantly higher than that recorded with the Ac-RKFNMKMI-NH_2 peptide and all of the charge reduction peptides ($p<0.0001$, one-way ANOVA). The reduced efficacy of the Ac-**A**KFNM**A**MI-NH_2 peptide is illustrated in Figure 4.12B, where 10 M of it failed to inactivate BK currents but did produce a weak block at positive potentials. This effect is summarised in Figure 4.12C, where the peptide produced very little block of currents at potentials negative to +100 mV. Even at +200 mV, 86±2% (n=6) of the current remained, compared to only 3±1% (n=7) with the Ac-RKFNMKMI-NH_2 peptide ($p<0.01$, Mann-Whitney test). These data suggest that either the position of the positively charged residues (R613 and K618) in LINGO1 tail peptide play an important role in inactivating BK channels, or the net positive charge of the LINGO1 tail peptide is the important determinant for binding and inactivation of BK channels.

A. Ac-*AKFNMAMI*-NH_2

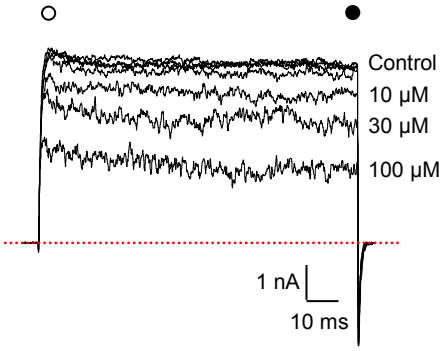

B. Summary of Ac-*AKFNMAMI*-NH_2

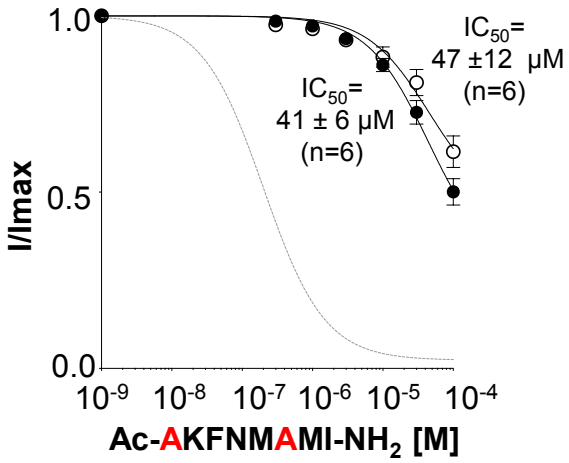

Figure 4.11: Concentration-dependent effect of Ac-AKFNMAMI-NH_2 peptide on WT BK .
A Representative concentration-dependent effect of Ac-AKFNMAMI-NH_2 synthetic peptide on HEK cells expressing WT BK . Currents were evoked by a step from -60 mV to +160 mV in the presence of 300 nM, 1, 3, 10, 30, 100 µM of Ac-AKFNMAMI-NH_2 peptide. **B** Summary concentration effect curve for the effect of Ac-AKFNMAMI-NH_2 on BK currents (n=6). Data were fitted with the Hill-Langmuir equation (grey trace Ac-RKFNMKMI-NH_2 peptide).

A. Control (1 μM Ca^{2+})

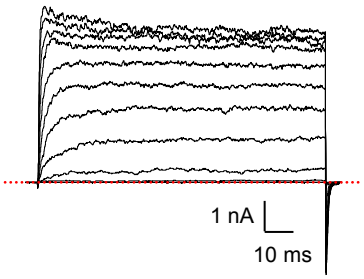

B. Ac-*AKFNMAMI*-NH_2 peptide (10 μM)

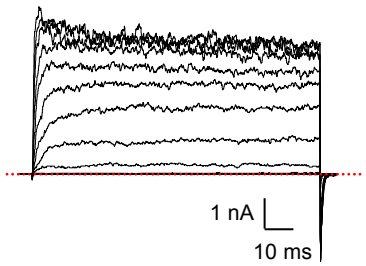

C. Summary IV

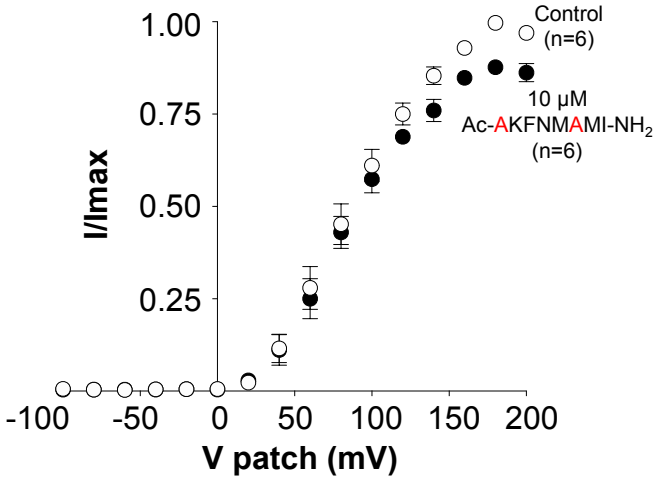

Figure 4.12: Voltage-dependence of Ac-AKFNMAMI-NH_2 peptide on WT BK .
A & **B** Macroscopic currents from inside-out patches expressing BK alone, show typical records in control (1 μM $[Ca^{2+}]_i$) and after application of 10 μM Ac-AKFNMAMI-NH_2 peptide. Patches were held at -60 mV and stepped from -100 mV to +200 mV in 20 mV increments and stepped back down to -80 mV to generate tail currents. **C** Summary of I/Imax measured in the last 5 ms of the pulse (n=6).

4.2.7 Neutralising two positively charged residues (K614 and K618) in LINGO1 synthetic tail peptide abolished inactivation of BK currents

We further investigated if the position of the positive charges or the net positive charge played a greater role in LINGO1-mediated inactivation of BK currents. To test these possibilities, we next substituted the two positively charged lysine residues at 614 and 618 with alanine by synthesising the Ac-R**A**FNM**A**MI-NH_2 peptide. Its effects were qualitatively similar to the Ac-**A**KFNM**A**MI-NH_2 peptide since it reduced BK current amplitude in a concentration-dependent manner (300 nM to 100 M) and failed to induce inactivation (Figure 4.13A). Figure 4.13B shows the data fitted with the Hill-Langmuir equation. The IC_{50} value obtained from the first 5 ms was greater than 100 M (152±22 M, n=6) and from the last 5 ms was 92±10 M (n=6, $p<0.05$, paired t-test). These values were significantly higher than that of Ac-RKFNMKMI-NH_2 peptide (grey dashed line, Figure 4.13B, $p<0.0001$, unpaired t-test). Furthermore, when compared with the Ac-**A**KFNM**A**MI-NH_2 peptide, the IC_{50} values were also significantly higher ($p<0.01$, unpaired t-test). Figure 4.14B shows currents recorded across a range of voltages up to +200 mV in the presence of 10 M Ac-R**A**FNM**A**MI-NH_2 peptide and it is clear that this peptide induced very little block of BK currents. This effect was summarised in Figure 4.14C where even at +200 mV, 85±1% (n=6) of the current remained when measured in the last 5 ms of the pulse, which was not significantly different to that observed with the other +1 charged peptide (Ac-**A**KFNM**A**MI-NH_2 peptide, ns, Mann-Whitney test). These results suggest that either the positively charged lysine residues at 614 and 618 in the LINGO1 tail play an important role in the inactivation of BK channels or alternatively, the net positive charge along with the position of the positively charged residues in the LINGO1 tail peptide are important for binding and inactivation of BK channels.

A. Ac-*RAFNMAMI*-NH_2

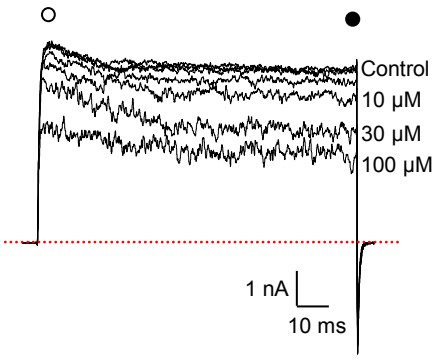

B. Summary of Ac-*RAFNMAMI*-NH_2

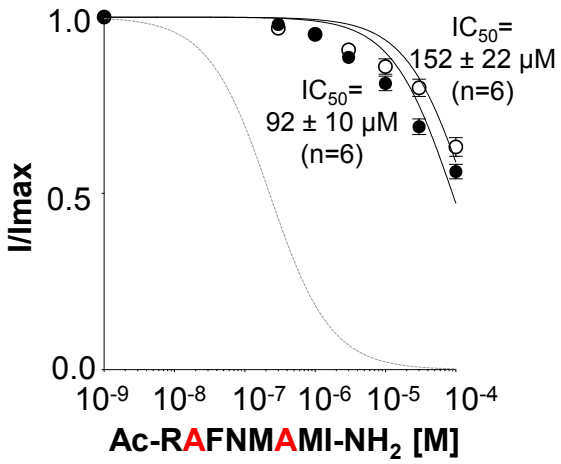

Figure 4.13: Concentration-dependent effect of Ac-RAFNMAMI-NH_2 peptide on WT BK .
A Representative concentration-dependent effect of Ac-RAFNMAMI-NH_2 synthetic peptide on HEK cells expressing WT BK . Currents were evoked by a step from -60 mV to +160 mV in the presence of 300 nM, 1, 3, 10, 30, 100 µM of Ac-RAFNMAMI-NH_2 peptide. **B** Summary concentration effect curve for the effect of Ac-RAFNMAMI-NH_2 on BK currents (n=6). Data were fitted with the Hill-Langmuir equation (grey trace Ac-RKFNMKMI-NH_2 peptide).

A. Control (1 μM Ca^{2+})

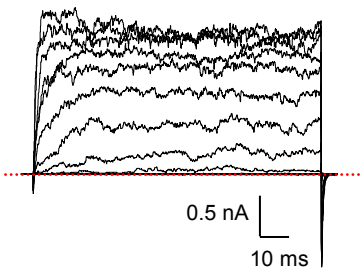

B. Ac-*RAFNMAMI*-NH_2 peptide (10 μM)

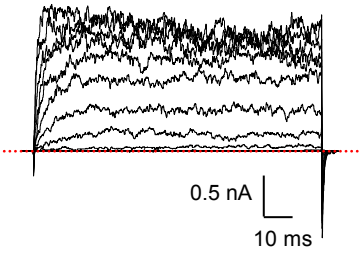

C. Summary IV

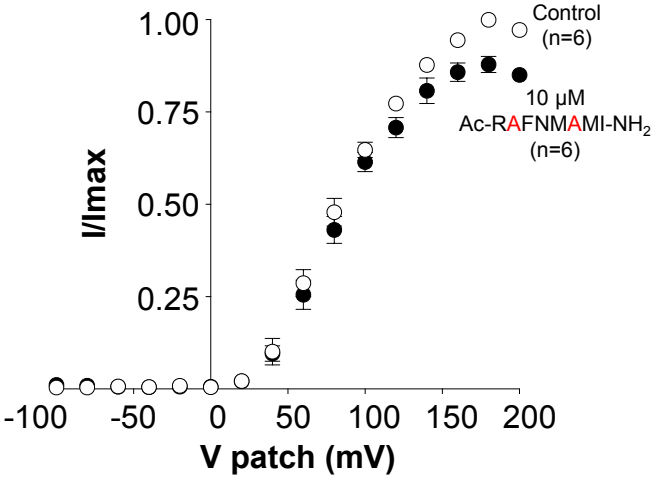

Figure 4.14: Voltage-dependence of Ac-RAFNMAMI-NH_2 peptide on WT BK .
A & **B** Macroscopic currents from inside-out patches expressing BK alone, show typical records in control (1 μM $[Ca^{2+}]_i$) and after application of 10 μM Ac-RAFNMAMI-NH_2 peptide. Patches were held at -60 mV and stepped from -100 mV to +200 mV in 20 mV increments and stepped back down to -80 mV to generate tail currents. **C** Summary of I/Imax measured in the last 5 ms of the pulse (n=6).

4.2.8 Neutralising all three positively charged residues (R613, K614 and K618) in LINGO1 synthetic tail peptide has a minor effect on BK channels

We further neutralised all the three positive charges (R613, K614 and K618) to generate the Ac-**AA**FNM**A**MI-NH_2 peptide and this, not only failed to induce inactivation, but also failed to block the BK currents, except at high concentrations. For instance, with 100 M Ac-**AA**FNM**A**MI-NH_2 peptide, only ~20% of the current was blocked as seen in Figure 4.15A. Thus, we were unable to determine the IC_{50} values of the Ac-**AA**FNM**A**MI-NH_2 peptide, but it was clear that it was well in excess of 100 M. When we carried out IV protocols in the absence and presence of 10 M Ac-**AA**FNM**A**MI-NH_2, it became clear that this peptide failed to significantly block the BK currents (Figure 4.16B). As the summary data presented in Figure 4.16C suggests, 89±3% (n=6) of the current remained at +200 mV at the end of the depolarisation pulse. These results indicate that positive charges in the LINGO1 tail peptide play an important role in the inactivation of BK channels.

A. Ac-*AAFNMAMI*-NH_2

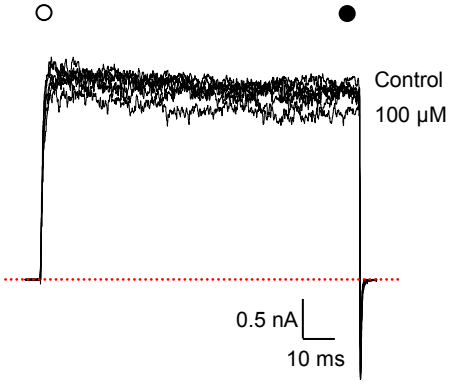

B. Summary of Ac-*AAFNMAMI*-NH_2

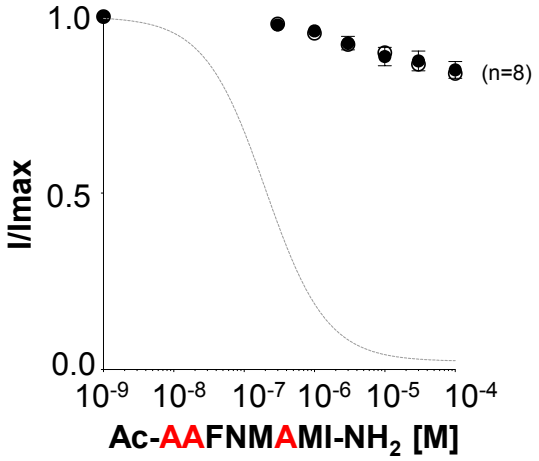

Figure 4.15: Concentration-dependent effect of Ac-AAFNMAMI-NH_2 peptide on WT BK .
A Representative concentration-dependent effect of Ac-AAFNMAMI-NH_2 synthetic peptide on HEK cells expressing WT BK . Currents were evoked by a step from -60 mV to +160 mV in the presence of 300 nM, 1, 3, 10, 30, 100 µM of Ac-AAFNMAMI-NH_2 peptide. **B** Summary concentration effect curve for the effect of Ac-AAFNMAMI-NH_2 on BK currents (n=8). Data were fitted with the Hill-Langmuir equation (grey trace Ac-RKFNMKMI-NH_2 peptide).

A. Control (1 μM Ca^{2+})

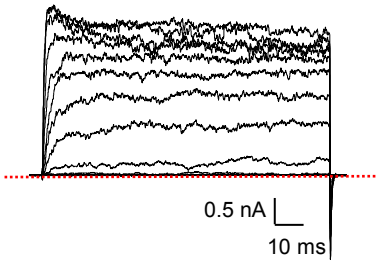

B. Ac-*AAFNMAMI*-NH_2 peptide (10 μM)

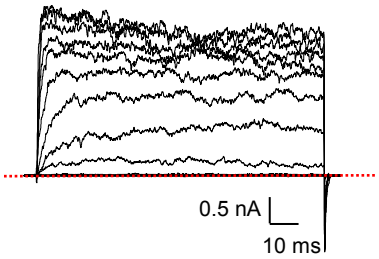

C. Summary IV

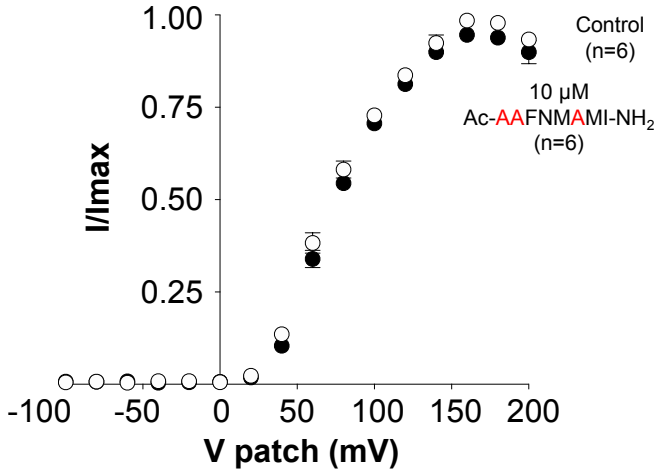

Figure 4.16: Voltage-dependence of Ac-AAFNMAMI-NH_2 peptide on WT BK .
A & **B** Macroscopic currents from inside-out patches expressing BK alone, show typical records in control (1 μM $[Ca^{2+}]_i$) and after application of 10 μM Ac-AAFNMAMI-NH_2 peptide. Patches were held at -60 mV and stepped from -100 mV to +200 mV in 20 mV increments and stepped back down to -80 mV to generate tail currents. **C** Summary of I/Imax measured in the last 5 ms of the pulse (n=6).

4.2.9 Substituting the terminal three residues (K618, M619 and I620) in LINGO1 synthetic tail peptide with alanine abolished inactivation of BK currents

In our next modification we substituted the terminal three residues K618, M619 and I620 with alanine residues to generate an Ac-RKFNM**AAA**-NH_2 peptide with a net charge of +2. Interestingly, it also failed to induce inactivation but did reduce BK current amplitude in a concentration-dependent manner (300 nM to 100 M, Figure 4.17A). These effects were qualitatively similar to those obtained with the Ac-R**A**FNM**A**MI-NH_2 peptide (Figure 4.13A). The IC_{50} values obtained with the Ac-RKFNM**AAA**-NH_2 peptide from the first 5 ms was 32±19 M (n=6) and from the last 5 ms was 21±4 M (n=6, ns, paired t-test). The IC_{50} was 92-fold higher than that of Ac-RKFNMKMI-NH_2 peptide ($p<0.001$, unpaired t-test) shown as grey dashed line in Figure 4.17B. Interestingly, the IC_{50} values observed in the last 5 ms for Ac-RKFNM**AAA**-NH_2 peptide and the Ac-R**A**FNM**A**MI-NH_2 peptide (net charge of +1) were also significantly different ($p<0.0001$, unpaired t-test). In addition, when the IC_{50} for the last 5 ms was compared with the Ac-**A**KFNMKMI-NH_2 and Ac-R**A**FNMKMI-NH_2 peptides, it was significantly higher ($p<0.0001$, one-way ANOVA), suggesting that the replacement of the KMI motif with alanines, reduced the efficacy of the peptide even more than substituting two positively charged residues simultaneously. Figure 4.18B shows the effect of 10 M of Ac-RKFNM**AAA**-NH_2 peptide across a range of voltages up to +200 mV, where the peptide induced reduction of BK current amplitude. At +200 mV, 69±3% (n=5, Figure 4.18C) sustained current remained at the end of the pulse. Moreover, when compared with the peptides that had a net charge of +2 (Ac-**A**KFNMKMI-NH_2 and Ac-R**A**FNMKMI-NH_2), the Ac-RKFNM**AAA**-NH_2 peptide left a significantly higher amount of residual current at the end of the depolarisation ($p<0.0001$, one-way ANOVA). These results suggest that the positively charged lysine residue (at 618) along with the hydrophobic methionine (at 619) and isoleucine (at 620) residues in the LINGO1 tail peptide play important roles in the inactivation of BK channels.

A. Ac-*RKFNMAAA*-NH_2

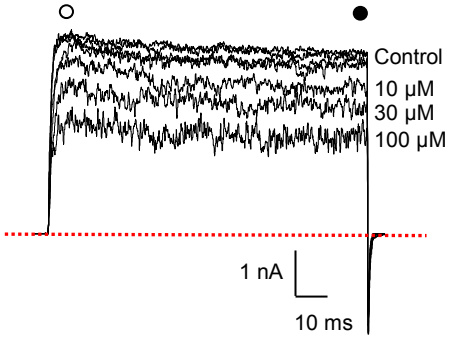

B. Summary of Ac-*RKFNMAAA*-NH_2

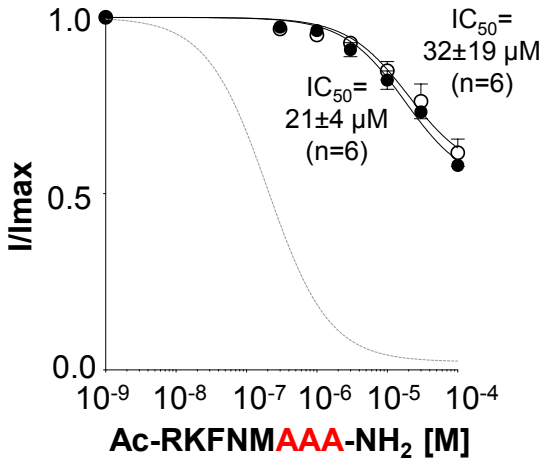

Figure 4.17: Concentration-dependent effect of Ac-RKFNMAAA-NH_2 peptide on WT BK .
A Representative concentration-dependent effect of Ac-RKFNMAAA-NH_2 synthetic peptide on HEK cells expressing WT BK . Currents were evoked by a step from -60 mV to +160 mV in the presence of 300 nM, 1, 3, 10, 30, 100 µM of Ac-RKFNMAAA-NH_2 peptide. **B** Summary concentration effect curve for the effect of Ac-RKFNMAAA-NH_2 on BK currents (n=6). Data were fitted with the Hill-Langmuir equation (grey trace Ac-RKFNMKMI-NH_2 peptide).

A. Control (1 μM Ca^{2+})

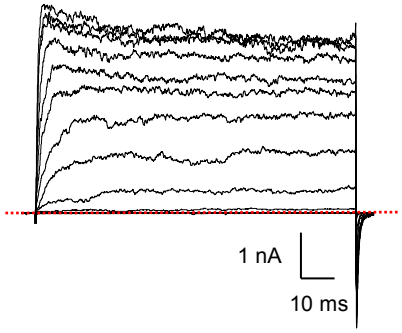

B. Ac-*RKFNMAAA*-NH_2 peptide (10 μM)

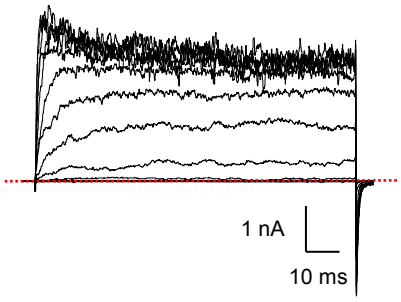

C. Summary IV

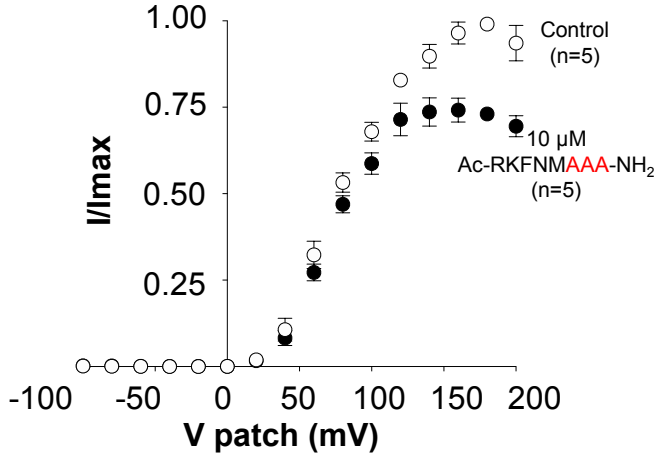

Figure 4.18: Voltage-dependence of Ac-RKFNMAAA-NH_2 peptide on WT BK .
A & **B** Macroscopic currents from inside-out patches expressing BK alone, show typical records in control (1 μM $[Ca^{2+}]_i$) and after application of 10 μM Ac-RKFNMAAA-NH_2 peptide. Patches were held at -60 mV and stepped from -100 mV to +200 mV in 20 mV increments and stepped back down to -80 mV to generate tail currents. **C** Summary of I/Imax measured in the last 5 ms of the pulse (n=5).

4.2.10 Substituting the aromatic amino acid (F615) with alanine in LINGO1 synthetic tail peptide does not affect its inactivating effect on BK channels

Having established that the positively charged residues in the LINGO1 tail peptide played a role in inactivation, we further investigated the role of other uncharged residues in the LINGO1 tail peptide-mediated inactivation of BK channels. We first replaced the aromatic phenylalanine with alanine, to generate Ac-RK**A**NMKMI-NH_2 peptide. As Figure 4.19A shows, this 'full peptide' reduced current amplitude and induced inactivation in a concentration-dependent manner (300 nM to 100 M). Figure 4.19B shows a summary of IC_{50} values obtained from the first 5 ms was 4±1 M (n=10) and last 5 ms was 1±0.2 M (n=10) which were significantly different from each other ($p<0.05$, paired t-test). The IC_{50} value obtained from the last 5 ms was 4-fold higher than that of the Ac-RKFNMKMI-NH_2 peptide shown in grey ($p<0.01$, unpaired t-test). The rate of inactivation of these currents was assessed by fitting the decay phase with a single exponential (Figure 4.19C) and the rate of inactivation of the Ac-RK**A**NMKMI-NH_2 peptide was similar to that of Ac-RKFNMKMI-NH_2 peptide (ns, one-way ANOVA). Figures 4.20A and B show families of BK currents in 1 M $[Ca^{2+}]_i$ before and during the application of 10 M Ac-RK**A**NMKMI-NH_2 peptide. The Ac-RK**A**NMKMI-NH_2 peptide was slightly less effective than the Ac-RKFNMKMI-NH_2 peptide, and the currents appeared noisy (Figure 4.20B). These effects were reflected in the summary data shown in Figure 4.20C, where the Ac-RK**A**NMKMI-NH_2 peptide reduced peak currents (last 5 ms) recorded at +200 mV to 12±2% which was significantly higher than 3±1% with the Ac-RKFNMKMI-NH_2 peptide ($p<0.01$, Mann-Whitney test). The inactivation of the currents with 10 M of Ac-RK**A**NMKMI-NH_2 peptide was more apparent at potentials positive to +100 mV (Figure 4.20D), but was significantly slower at potentials measured from +120 to +200 mV than Ac-RKFNMKMI-NH_2 peptide ($p<0.01$, one-way ANOVA). These data suggest that replacement of the phenylalanine at 615, despite maintaining a net charge of +3, moderately reduced the efficacy of LINGO1 tail peptide to inactivate BK channels.

A. Ac-*RKANMKMI*-NH_2

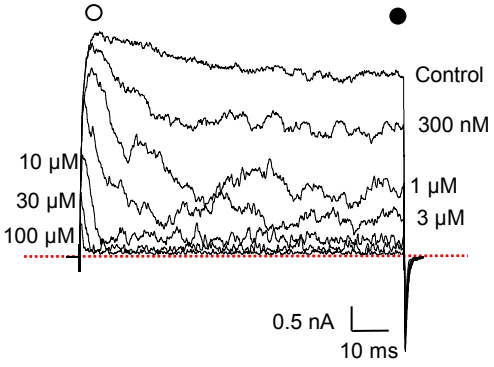

B. Summary of Ac-*RKANMKMI*-NH_2

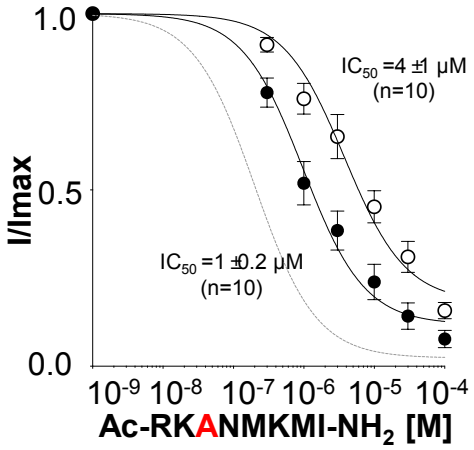

C. Summary of Ac-*RKANMKMI*-NH_2 inact

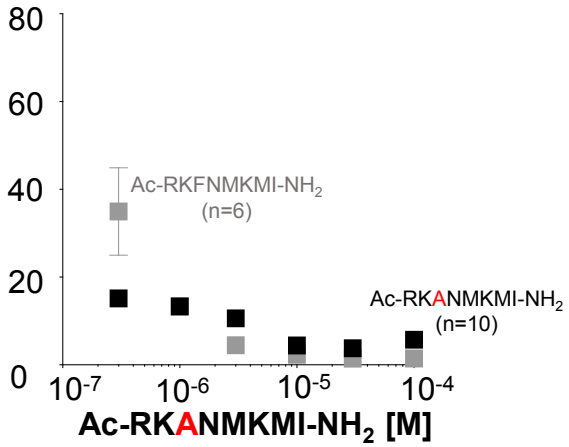

Figure 4.19: Concentration-dependent effect of Ac-RKANMKMI-NH_2 peptide on WT BK .
A Representative concentration-dependent effect of Ac-RKANMKMI-NH_2 synthetic peptide on HEK cells expressing WT BK . Currents were evoked by a step from -60 mV to +160 mV in the presence of 300 nM, 1, 3, 10, 30, 100 µM of Ac-RKANMKMI-NH_2 peptide. **B** Summary concentration effect curve for the effect of Ac-RKANMKMI-NH_2 on BK currents (n=10). Data were fitted with the Hill-Langmuir equation (grey trace Ac-RKFNMKMI-NH_2 peptide). **C** The rate of inactivation of BK currents was assessed by fitting the decay phase with a single exponential (grey trace Ac-RKFNMKMI-NH_2 peptide). The rate of inactivation increased with the concentration of Ac-RKANMKMI-NH_2 tail peptide (n=10).

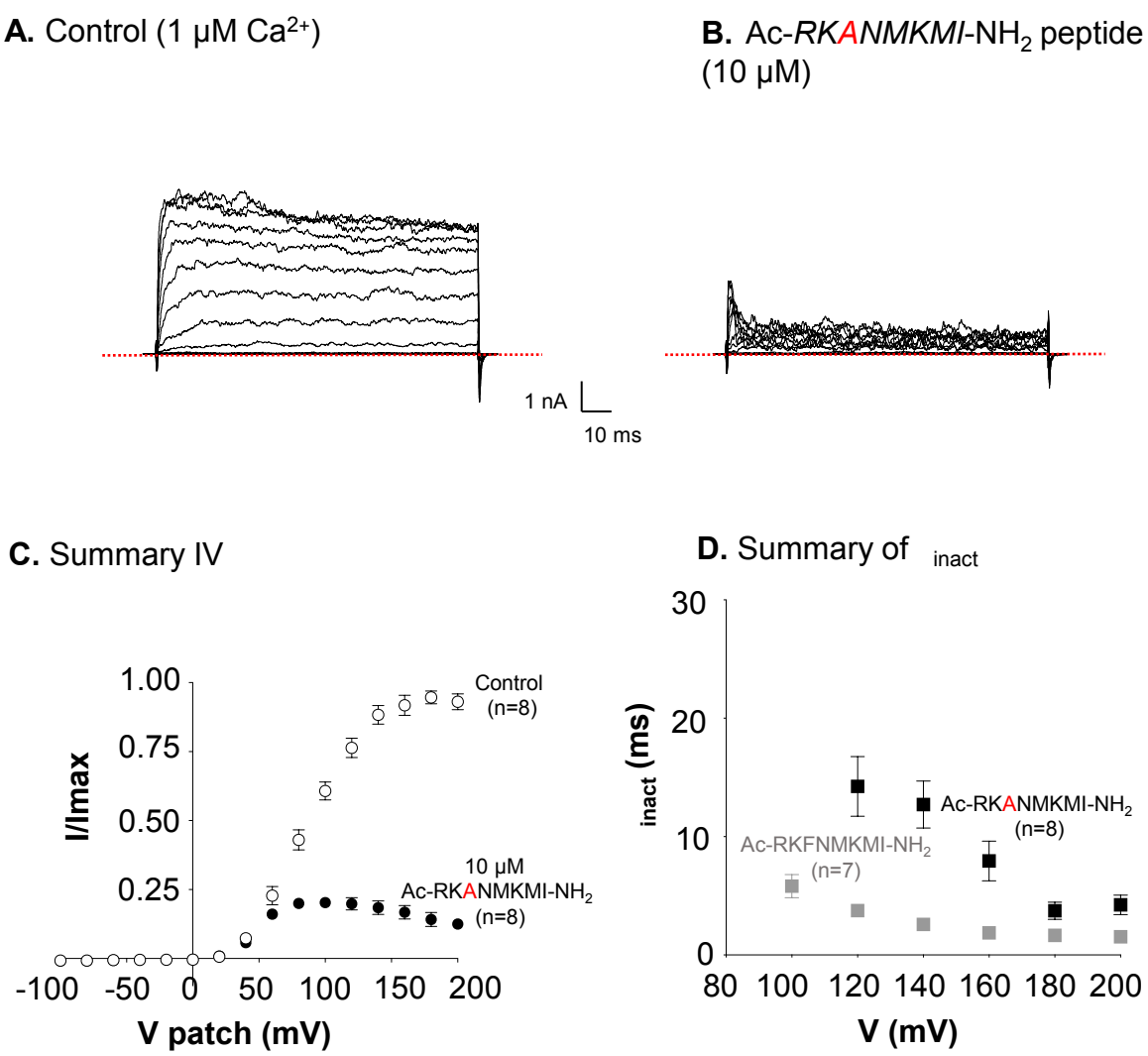

Figure 4.20: Voltage-dependence of Ac-RKANMKMI-NH_2 peptide on WT BK .
A & **B** Macroscopic currents from inside-out patches expressing BK alone, show typical records in control (1 μM $[Ca^{2+}]_i$) and after application of 10 μM Ac-RKANMKMI-NH_2 peptide. Patches were held at -60 mV and stepped from -100 mV to +200 mV in 20 mV increments and stepped back down to -80 mV to generate tail currents. **C** Summary of I/Imax measured in the last 5 ms of the pulse (n=8). **D** The rate of inactivation of BK currents was assessed by fitting the decay phase with a single exponential (grey trace Ac-RKFNMKMI-NH_2 peptide). The currents showed an apparent voltage-dependence at more positive potentials (n=8).

4.2.11 Substituting the residues at F615, N616 and M617 with alanine in LINGO1 synthetic tail peptide does not affect its inactivating effect on BK channels

To further investigate the role of the uncharged residues in the LINGO1 tail peptide-mediated inactivation of BK channels we substituted the phenylalanine at 615, asparagine at 616 and methionine at 617 with alanine residues and generated the Ac-RK**AAA**KMI-NH_2 peptide, which retained its net charge of +3. This peptide reduced BK current amplitude and induced some inactivation of currents as shown in Figure 4.21A. As Figure 4.21B shows the IC_{50} values obtained from the first 5 ms was 7±1 M (n=8), compared to 3±0.3 M (n=8) from the last 5 ms ($p<0.05$, paired t-test). The IC_{50} value obtained from the last 5 ms was 13-fold higher than that of the 'control' Ac-RKFNMKMI-NH_2 peptide shown as a dashed line in Figure 4.21B ($p<0.0001$, unpaired t-test). The currents recorded in the presence of this peptide appeared noisy and inactivated especially with higher concentrations of the peptide. As Figure 4.21C suggests, the rate of inactivation with 10 and 30 M of Ac-RK**AAA**KMI-NH_2 peptide was significantly slower than that observed with Ac-RKFNMKMI-NH_2 ($p<0.0001$, one-way ANOVA). However, 100 M of the Ac-RK**AAA**KMI-NH_2 peptide only reduced the current amplitude as seen in Figure 4.21C. With 10 M of Ac-RK**AAA**KMI-NH_2 (Figure 4.22B), it was clear that the ability of the peptide to block BK channels was reduced, as summarised in Figure 4.22C. For example, at +200 mV, the Ac-RK**AAA**KMI-NH_2 peptide reduced current amplitude to 36±4% (n=9) which was significantly higher than 3±1% (n=7) with the Ac-RKFNMKMI-NH_2 peptide ($p<0.001$, Mann-Whitney test). The rate of inactivation increased with depolarisation, albeit only at potentials positive to +140 mV (Figure 4.22D). However, the time constants of inactivation from +140 to +200 mV were significantly slower than that observed with the Ac-RKFNMKMI-NH_2 peptide ($p<0.0001$, one-way ANOVA). These results suggest that the substitution of phenylalanine at 615, asparagine at 616 and methionine at 617 with alanine residues, despite maintaining a net charge of +3, also reduced the efficacy of LINGO1 tail peptide to inactivate BK channels.

A. Ac-*RKAAAKMI*-NH_2

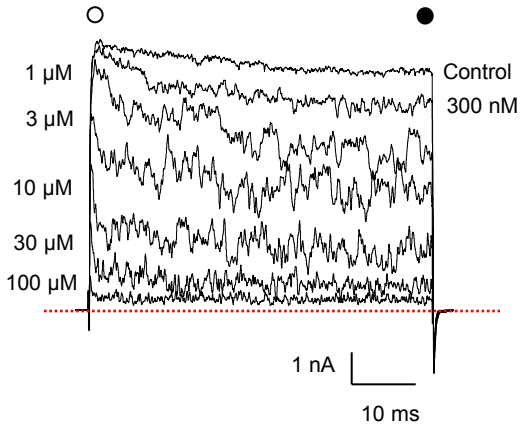

B. Summary of Ac-*RKAAAKMI*-NH_2

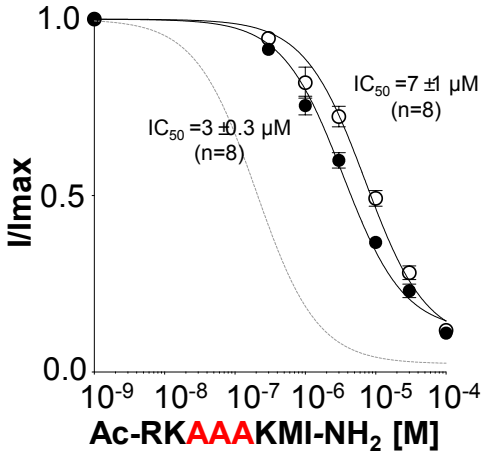

C. Summary of Ac-*RKAAAKMI*-NH_2 $_{inact}$

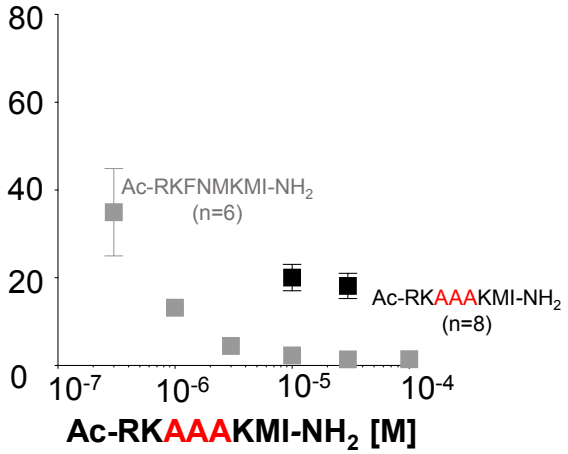

Figure 4.21: Concentration-dependent effect of Ac-RKAAAKMI-NH_2 peptide on WT BK .
A Representative concentration-dependent effect of Ac-RKAAAKMI-NH_2 synthetic peptide on HEK cells expressing WT BK . Currents were evoked by a step from -60 mV to +160 mV in the presence of 300 nM, 1, 3, 10, 30, 100 µM of Ac-RKAAAKMI-NH_2 peptide. **B** Summary concentration effect curve for the effect of Ac-RKAAAKMI-NH_2 on BK currents (n=8). Data were fitted with the Hill-Langmuir equation (grey trace Ac-RKFNMKMI-NH_2 peptide). **C** The rate of inactivation of BK currents was assessed by fitting the decay phase with a single exponential (grey trace Ac-RKFNMKMI-NH_2 peptide). The rate of inactivation increased with the concentration of Ac-RKAAAKMI-NH_2 tail peptide (n=8).

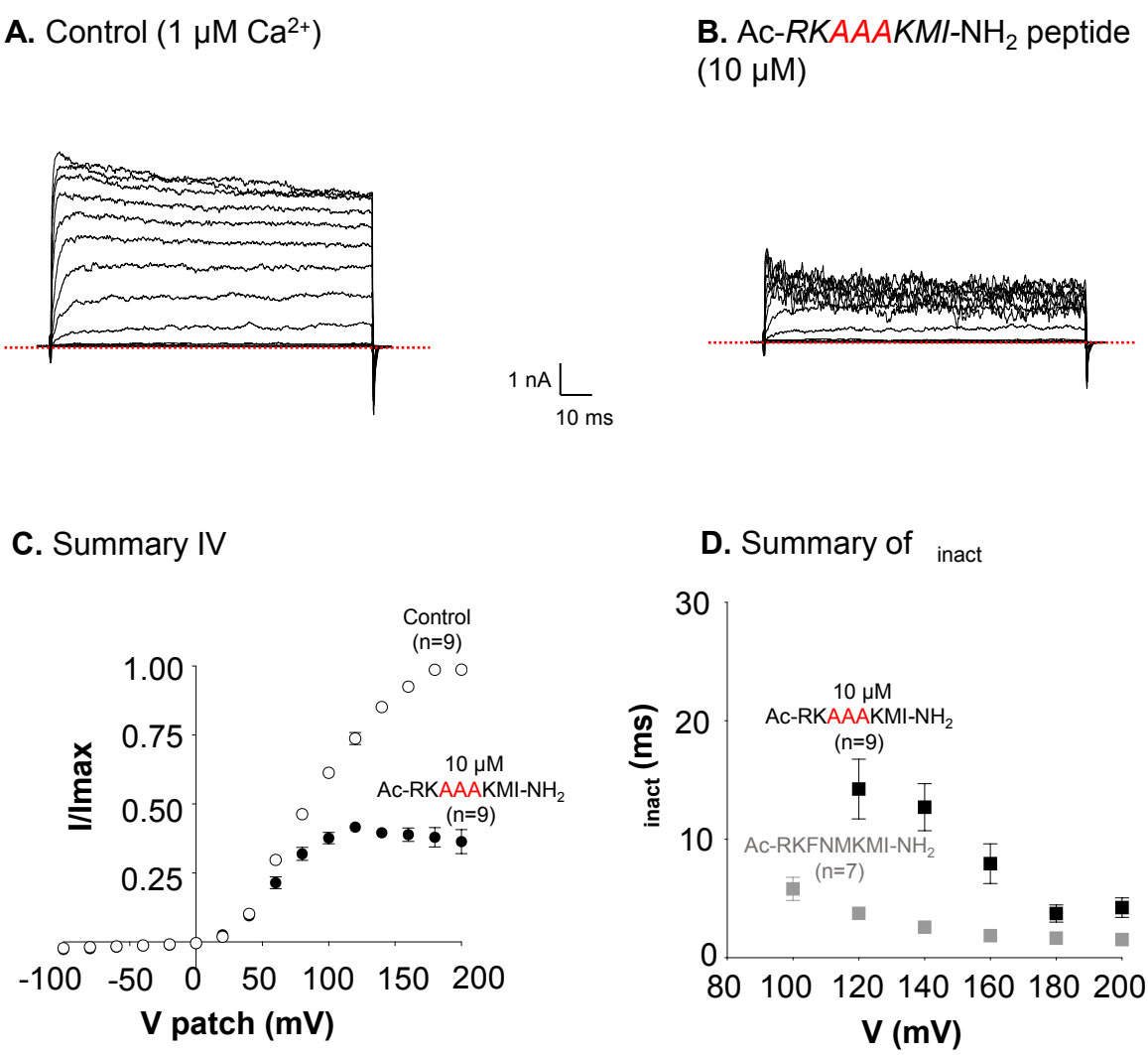

Figure 4.22: Voltage-dependence of Ac-RKAAAKMI-NH_2 peptide on WT BK .
A & **B** Macroscopic currents from inside-out patches expressing BK alone, show typical records in control (1 μM $[Ca^{2+}]_i$) and after application of 10 μM Ac-RKAAAKMI-NH_2 peptide. Patches were held at -60 mV and stepped from -100 mV to +200 mV in 20 mV increments and stepped back down to -80 mV to generate tail currents. **C** Summary of I/Imax measured in the last 5 ms of the pulse (n=9). **D** The rate of inactivation of BK currents was assessed by fitting the decay phase with a single exponential (grey trace Ac-RKFNMKMI-NH_2 peptide). The currents showed an apparent voltage-dependence at more positive potentials (n=9).

Table 4.1 The effect of acylated amide modifications of LINGO1 peptide on BK channels

Peptide (Ac-Am)	Net charge	Inactivation	IC_{50} (last 5 ms)	Residual current at +200 mV (last 5 ms)
NH_2-RKFNMKMI-OH	+3		308±60 nM	5±1%
Ac-RKFNMKMI-NH_2	+3		228±30 nM	3±0.1%
Ac-SSADAPRKFNMKMI-NH_2	+3		700±80 nM	2±0.2%
Ac-AKFNMKMI-NH_2	+2		2±1 μM	11±1%
Ac-RAFNMKMI-NH_2	+2		1±0.1 μM	16±3%
Ac-FNMKMI-NH_2	+1		5±1 μM	34±3%
Ac-AKFNMAMI-NH_2	+1		41±6 μM	86±2%
Ac-RAFNMAMI-NH_2	+1		92±10 μM	85±1%
Ac-AAFNMAMI-NH_2	0		ND	89±3%
Ac-RKFNMAAA-NH_2	+2		21±4 μM	69±3%
Ac-RKANMKMI-NH_2	+3		1±0.2 μM	12±2%
Ac-RKAAAKMI-NH_2	+3		3±0.3 μM	36±4%

A. IC_{50} last 5 ms summary

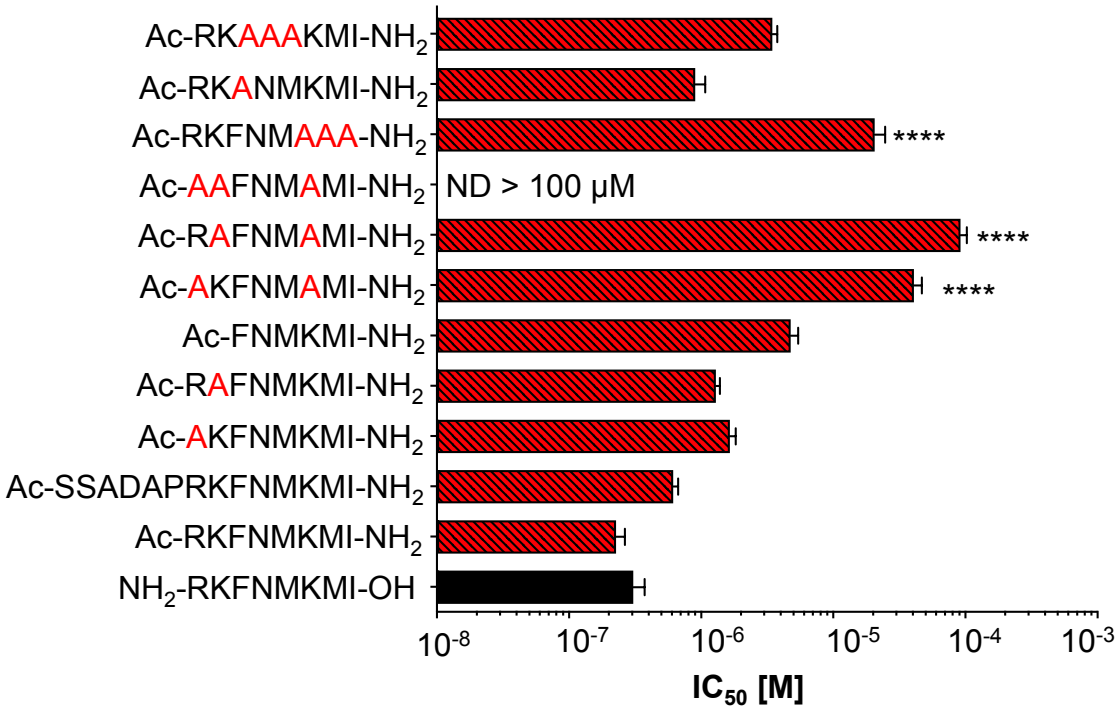

B. $_{inact}$ summary with 10 µM peptide

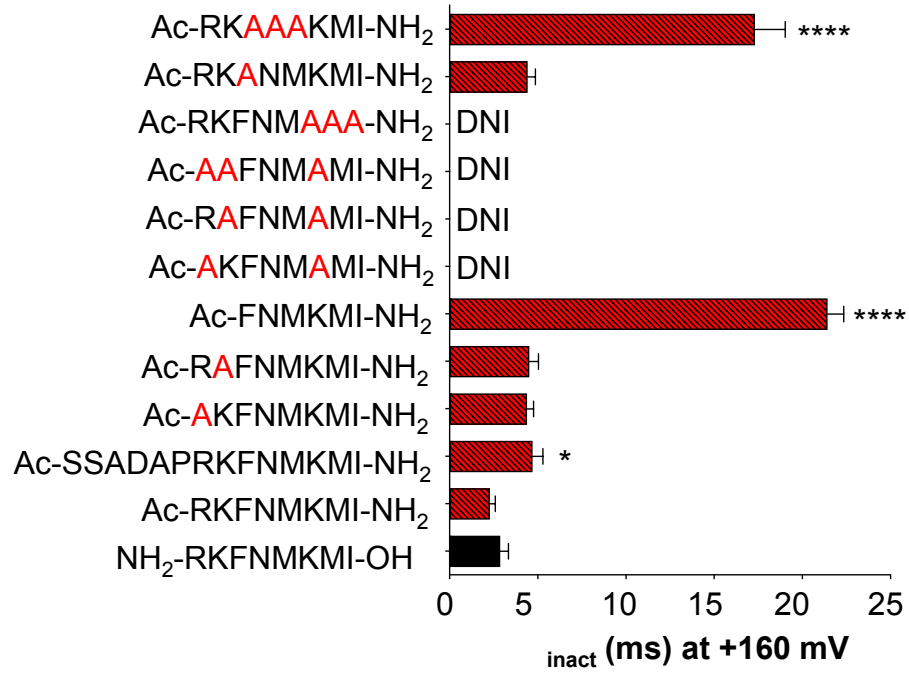

Figure 4.23: Comparison between variants of LINGO1 tail peptide on BK .
A Effect of LINGO tail peptides in the last 5 ms of the depolarising pulse, which shows IC_{50} values for LINGO1 and the variants of LINGO1 tail peptide (one-way ANOVA, **** $p<0.0001$). **B** Mean inactivation time constant ($_{inact}$) of currents in the presence of 10 µM of LINGO1 and variants of LINGO1 tail peptide (one-way ANOVA, * $p<0.05$,**** $p<0.0001$).

A. +100 mV summary

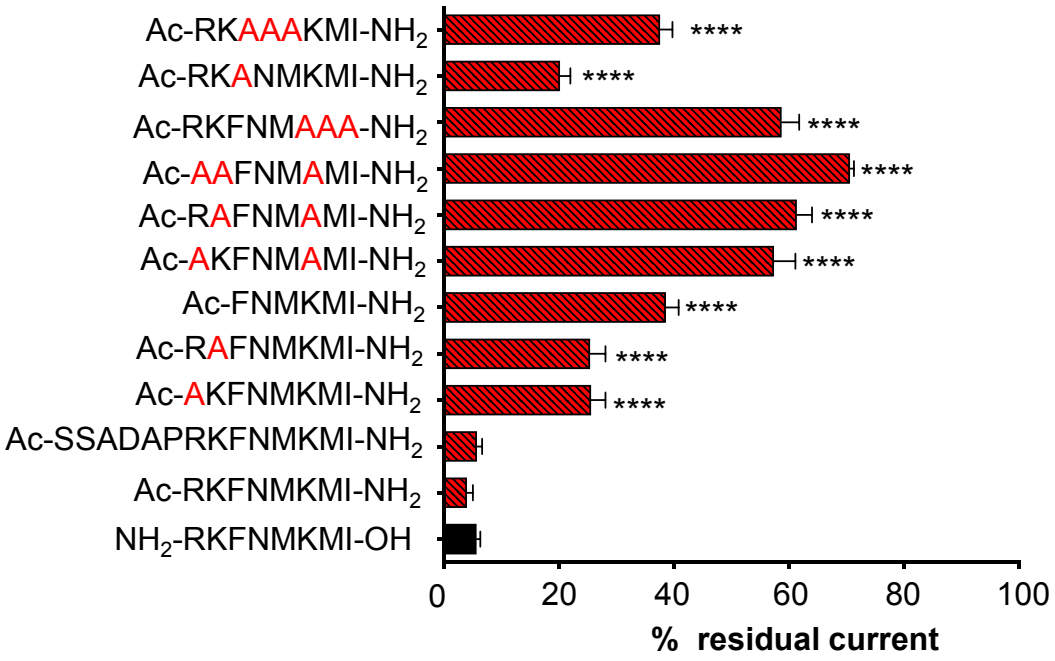

B. +200 mV summary

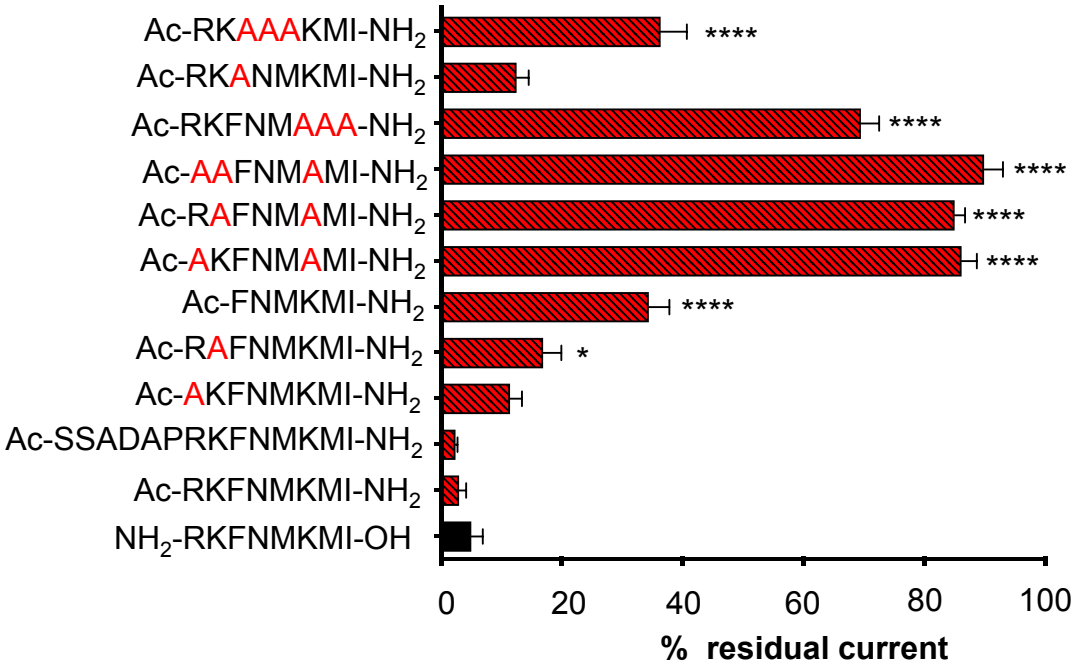

Figure 4.24: Comparison between variants of LINGO1 tail peptide on BK .
A Percentage of residual current measured in the last 5 ms at +100 mV and **B** at +200 mV in the presence of LINGO1 and variants of LINGO1 tail peptide (one-way ANOVA, * $p<0.05$, **** $p<0.0001$).

A. Summary of $_{inact}$ at +100 mV

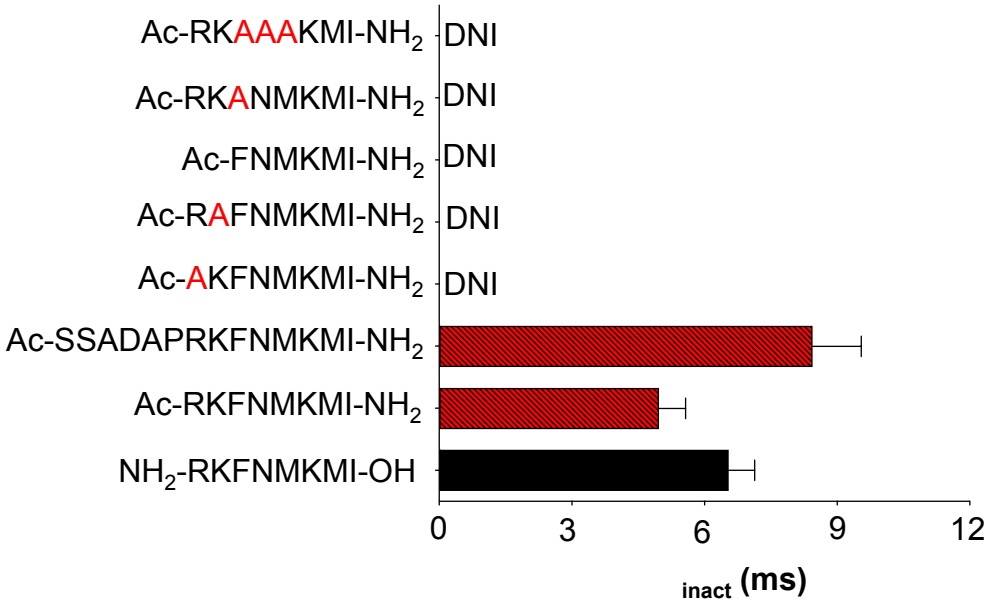

B. Summary of $_{inact}$ at +200 mV

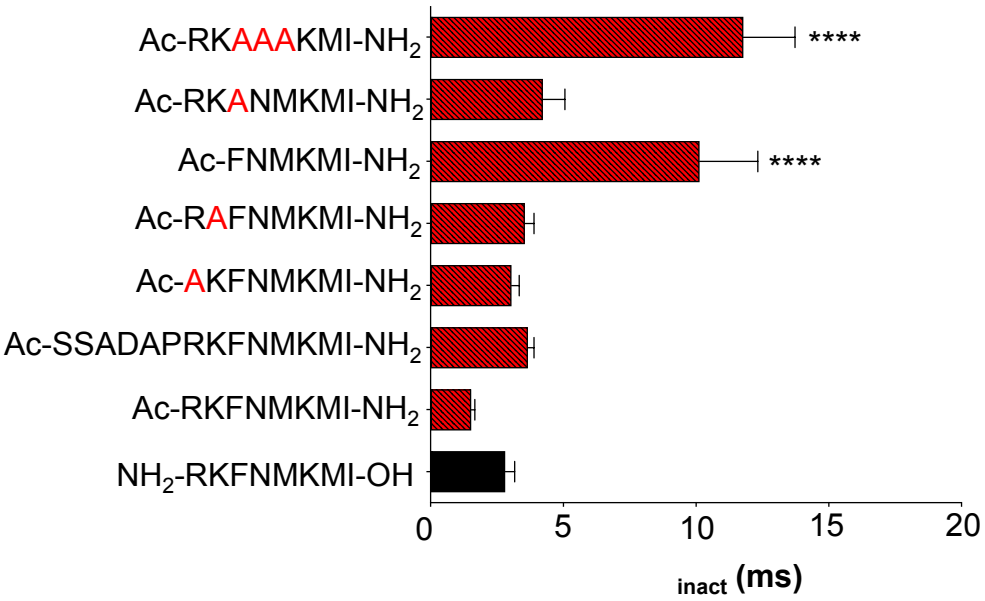

Figure 4.25: Comparison between variants of LINGO1 tail peptide on BK .
The rate of inactivation of BK currents was assessed by fitting the decay phase with a single exponential, the inactivation time constant ($_{inact}$) of currents **A** at +100 mV and **B** at +200 mV in the presence of 10 μM of LINGO1 and variants of LINGO1 tail peptide (one-way ANOVA, **** p<0.0001).

4.3 Discussion

In the present chapter we demonstrated the following results:

1. The net positive charge of LINGO1 tail peptide affected its ability to bind and inactivate BK channels.
2. The positively charged residues in LINGO1 tail peptide play an important role in inactivating BK channels.
3. The position of the positively charged residues in LINGO1 tail peptide may play a role in peptide binding and inactivation of BK channels.

In the previous chapter we demonstrated that LINGO1 and LINGO2 amino free acid tail peptides inactivated BK channels, although LINGO4 tail peptide did not. This led us to investigate the contribution of different residues in the LINGO1-mediated inactivation of BK channels. Since this tail peptide has a net positive charge of +3, in the amino free acid form (NH_2^+-RKFNMKMI-COO^-), we first examined if this charge was an important determinant inactivate BK currents. In order to achieve this, we acylated the N-terminus and amidated the C-terminus of the LINGO1 peptide to remove any charge from the N and C termini and also generated variants of the LINGO1 peptide. The effects of these acylated amide modifications of the LINGO1 peptide on inactivation of BK channels are summarised in Table 4.1.

We first eliminated charges from the N and C termini by acylating the N-terminus and amidating the C-terminus of the LINGO1 peptide. As expected, the acylated amidated peptide induced inactivation of BK currents and its effects were practically indistinguishable from the effects of the amino free acid version of the LINGO1 tail peptide, as evidenced by the comparable IC_{50} values (Figure 4.23A), the similar time constants of inactivation (Figure 4.23B), the amount of residual current that remained in the presence of 10 M Ac-RKFNMKMI-NH_2 (Figures 4.24A and B) and the apparent voltage-dependence of inactivation (Figures 4.25A and B).

In the second modification, we investigated if increasing the number of the amino acids to 14 while maintaining a net charge of +3, altered the efficacy of the Ac-SSADAPRKFNMKMI-NH_2 peptide to inactivate BK channels. Although this

peptide induced inactivation of BK currents, it was slightly less potent compared to the 8 amino acids long LINGO1 peptide, as evidenced by the rightward shift in IC_{50} values (Figure 4.23A). The time constant of inactivation was also slower than that of the 8 amino acids long LINGO1 tail peptide, perhaps suggesting that the forward rate constant (Murrell-Lagnado and Aldrich, 1993a; 1993b) of the block by the peptide decreased with this modification (Figure 4.23B). Nevertheless, application of 10 M of Ac-SSADAPRKFNMKMI-NH_2 peptide induced rapid and complete inactivation of BK currents at positive potentials (+100 mV and +200 mV: Figures 4.24 A and B). The time constant of inactivation showed apparent voltage-dependence similar to that of the 8 amino acids long LINGO1 peptide (Figures 4.25 A and B), suggesting that elongation of the peptide only slightly altered the efficacy to inactivate BK channels. Our results are consistent with previous studies which demonstrated that increasing the number of amino acids in the variants of the ShB peptide altered the efficacy of the peptides to inactivate ShB 6-46 channels (Zagotta *et al.* 1990; Murrell-Lagnado and Aldrich 1993a).

Previous studies have investigated the role of positively charged amino acid residues via substitutions and deletions in the NH_2-terminus of the ShB peptide and demonstrated that altering the charged residues slowed the rate of inactivation of the ShB 6-46 channels (Hoshi *et al.* 1990). Furthermore, when the net charge within the NH_2-terminus of the ShB peptide was altered, it produced qualitatively smaller effects on the rate of block of the ShB 6-46 channels. This suggested that the structural features of the peptide played a role in determining the binding and unbinding rates of the peptide to the channel (Zagotta *et al*. 1990; Murrell-Lagnado and Aldrich, 1993a; 1993b).

We also investigated if the number of charged residues or their position in the peptide played a role in mediating inactivation of BK channels. There are three positively charged residues (R613, K614 and K618) in the LINGO1 tail peptide and when we neutralised R613 and K614 individually, by substitution with alanine, we found that both peptides had similar effects to each other. These results are confirmed by the IC_{50} values which showed a rightward shift (Figure 4.23A) compared to the control, acylated amidated LINGO1 tail peptide (Figure 4.23B), suggesting that their affinity for the BK channel was altered. Interestingly,

in the presence of 10 M of either Ac-**A**KFNMKMI-NH_2 or Ac-R**A**FNMKMI-NH_2, the sustained current at +100 mV (last 5 ms) was significantly higher than with the control Ac-RKFNMKMI-NH_2 peptide (Figure 4.24A), suggesting that the stability of the peptide binding was reduced, perhaps as a consequence of an increase in the rate of unbinding, as previously demonstrated by Murrell-Lagnado and Aldrich (1993a; 1993b) with ShB peptide variants. In addition, both of these peptides showed a rather weak apparent voltage-dependence of binding and only showed inactivation at very positive potentials (Figure 4.25B). These results suggest that a reduction of net charge by 1 reduced the efficacy of these peptides.

We next reduced the net charge of the LINGO1 peptide by 2, by either deletion of R613 and K614 or by neutralising two positively charged residues with alanine. Higher concentrations of the Ac-FNMKMI-NH_2 peptide (10 and 30 M) were required to inactivate BK channels and the time constant of inactivation was significantly slower compared to the Ac-RKFNMKMI-NH_2 peptide (Figure 4.23B), suggesting that the rate of the block (Murrell-Lagnado and Aldrich, 1993a; 1993b) decreased. This effect alone could contribute to the significant rightward shift in the IC_{50} values (Figure 4.23A). However, an increase in the amount of sustained current at positive potentials at the end of the depolarisation pulse (Figures 4.24A and B) indicated that the binding of this peptide was more unstable, presumably as a result of the increased rate. This could also contribute to the higher IC_{50} observed with this peptide.

Interestingly, with both the Ac-**A**KFNM**A**MI-NH_2 and Ac-R**A**FNM**A**MI-NH_2 peptides, we observed that i) the inactivation was abolished (Figures 4.11A and 4.13A), ii) there was a significant rightward shift in IC_{50} values (Figure 4.23A), iii) the amount of sustained current at the end of the pulse was significantly higher compared to control (Figures 4.24A and B), which suggests that the binding efficiency of these peptides may be markedly reduced. These results support the idea that the presence of a positive charge at residue 618 is crucial to mediate inactivation of the BK channels and that the presence of positive charges at positions 613 and 614 play a role in maintaining the stability of the block by the LINGO1 tail peptide. The above data indicated that the position and the positive charge at 618 residue is crucial to mediate inactivation of BK channels. If we were to investigate the effects of the Ac-RKFNM**A**MI-NH_2 peptide, we would expect

that this peptide would block the channels but may not induce inactivation. This possibility is investigated in Chapter 5 of this thesis, with an amino free acid modified peptide (NH_2-RKFNM**A**MI-OH) which has an effective net charge of +2 similar to that of the Ac-RKFNM**A**MI-NH_2 peptide.

Previous studies conducted by Murrell-Lagnado and Aldrich (1993a; 1993b) investigated the role of positively charged residues in the ShB peptide mediated inactivation of the ShB 6-46 channels and suggested that charged residues participated in long-range electrostatic interactions and enhanced the diffusion rates of the peptide towards its binding site. The pore of the BK channel is lined with a ring of eight negatively charged glutamic acid (E321 and E324) residues located at the base of the S6 helices (Brelidze *et al.* 2003; Nimigean *et al.* 2003). Li and Aldrich (2006) demonstrated that the electrostatic and hydrophobic interactions of the enhanced ball peptide (EBP) with the negatively charged (E321 and E324) residues in the pore of the BK channels are critical for binding of the ball peptide. These negatively charged (E321 and E324) residues in the BK channel pore may play an important role in attracting the positively charged residues in the LINGO1 tail peptide and thereby stabilise binding of the LINGO1 peptide in the pore of the BK channel. This possibility is tested in Chapter 6 of this thesis.

In our next modification, we neutralised all three charges by synthesising the Ac-**AA**FNM**A**MI-NH_2 peptide and noted that it not only failed to induce inactivation, but barely reduced BK current amplitude, even when 100 M of the peptide was applied to the cytosolic surface of patches. It is clear from Figures 4.24A and B, that the amount of sustained current at the end of the pulse was significantly higher at potentials positive to +100 mV compared to the control peptide. These results suggest that the positively charged residues in the LINGO1 tail peptide play a critical role in LINGO1 binding, perhaps by interacting electrostatically with the negatively charged E321 and E324 residues in the BK channel pore.

After examining the role of positively charged residues in the LINGO1 tail, we next investigated the role of the terminal KMI motif, which is located distally in LINGO1-3 proteins but is absent in LINGO4 (Figure 3.3B). We replaced this motif with alanine residues (Ac-RKFNM**AAA**-NH_2) and interestingly noted that, even

though this peptide had a net charge of +2, it failed to induce inactivation of BK currents and showed a significantly higher IC_{50} (Figure 4.23A) compared to the control peptide. The sustained current at the end of the pulse was also significantly greater than that observed with the control peptide (Figures 4.24A and B). These data suggest that the terminal three residues in LINGO1 are essential for inactivation and are in agreement with the results of Dudem *et al*. (2020) who demonstrated that deletion of these three residues in the full-length LINGO1 protein (618-620) practically abolished inactivation. In addition, my results suggest that the position of the positively charged K618 and the hydrophobic residues M619 and I620 may play a role in mediating the electrostatic and hydrophobic interactions of the LINGO1 tail peptide binding in the BK channel pore, respectively.

In our final set of modifications, we attempted to investigate the role of other uncharged residues at F615, N616 and M617. Both peptides, (Ac-RK**A**NMKMI-NH_2 and Ac-RK**AAA**KMI-NH_2) had a net charge of +3 and although they were able to induce BK inactivation, higher concentrations were required to achieve this. The time constant of inactivation with 10 M of either peptide was significantly slower compared to the control peptide (Figure 4.23B) suggesting that the forward rate (Murrell-Lagnado and Aldrich, 1993a; 1993b) of the block was reduced. The amount of sustained current at more positive potentials was also significantly higher with the Ac-RK**A**NMKMI-NH_2 and the Ac-RK**AAA**KMI-NH_2 peptides (Figures 4.24A and B), suggesting that the ‘off-rate’ also increased. Either of these effects could account for the significant rightward shift in IC_{50} values (Figure 4.23A) observed with both of these peptides. These results suggest that the replacement of the bulky phenylalanine at 615 alone or the simultaneous substitution of all three uncharged F615, N616 and M617 residues, with the retention of the positive charge at residue 618, reduced binding and potency of the LINGO1 peptide.

Interestingly, the effect of neutralising the positive charges at R613, K614 residues (Ac-**A**KFNMKMI-NH_2 or Ac-R**A**FNMKMI-NH_2) and substitution of F615 with alanine residue (Ac-RK**A**NMKMI-NH_2) had similar effects on the inactivation of BK channels (Figures 4.23, 4.24, 4.25 and Table 4.1). This effect may possibly

be due to the retention of the positive charge at K618, which further supports the idea that the positive charge at residue 618 is crucial to mediate inactivation of the BK channels. Moreover, the positive charges at positions R613 and K614 may play a role in electrostatic interactions along with the F615 which may be involved in hydrophobic interactions of the LINGO1 tail peptide binding in the BK channel pore.

Collectively these results indicate that the positively charged residues R613, K614 and K618 along with the other uncharged residues in the LINGO1 tail peptide may be critical for the binding of the peptide in the BK channel pore and thereby induce inactivation of BK channels.

5. Assessing the role of individual residues in acylated free acid modifications of LINGO1 tail peptide

5.1 Introduction

In the previous chapters we investigated the effect of the amino free acid (NH_2 at N-terminus and OH at C-terminus) and acylated amide (Ac at N-terminus and NH_2 at C-terminus) modifications of LINGO1 tail peptide on BK channels. However, in the native full-length LINGO1 protein the amino terminus of the R613 residue would be uncharged and there would be a negatively charged C-terminus (COO^-) at the end of the protein sequence. Therefore, to replicate these conditions, we synthesised additional peptides with an uncharged, acylated (Ac) N-terminus and a negatively charged C-terminus (COO^-/OH). Thus, with this modification the net charge of the LINGO1 peptide reduced to +2, due to the presence of the negative charge at the C-terminus (Ac-RKFNMKMI-OH) and the three positively charged residues (R, K, K) in the peptide.

Previous studies have demonstrated that in the variants of the ShB peptide where the net charge increased from +2 to +6, there was an increase in association rate constants and affinity of the peptide for the ShB Δ6-46 channels (Murrell-Lagnado and Aldrich, 1993a). This variant of the ShB peptide was further referred to as the enhanced ball peptide (EBP) which also exhibited a higher affinity for BK channels than the ShB peptide from which it was derived (Li and Aldrich 2006).

In this chapter we have utilised acylated free acid and amino free acid modifications of the LINGO1 synthetic tail peptides to examine 1) the effects of substituting the charged residues with uncharged residues and 2) the effects of scrambling the amino acid sequence of the LINGO1 peptide, in an attempt to determine the contribution of individual residues in the LINGO1 tail peptide-mediated inactivation of BK channels.

5.2 Results

5.2.1 Modified order of amino acid residues in LINGO1 synthetic tail peptide does not affect its inactivating effect on BK channels

As previously demonstrated in Figure 3.5, the ‘WT’ (NH_2-RKFNMKMI-OH) peptide mimicked the main features of inactivation observed with when full-length LINGO1 was co-expressed with BK . In addition, as seen in Chapter 4, reducing the net charge of the LINGO1 peptides reduced their ability to bind to BK channels, as evidenced by Figures 4.23, 4.24 and 4.25. We were also interested to examine if the order of positively charged residues contributed to the inactivating effect of the peptide on BK channels. Consequently, we synthesised a scrambled LINGO1 peptide (NH_2-MFKNKIRM-OH), which had a net charge of +3 and assessed its effects on HEK cells expressing BK . In these experiments, patches were held at -60 mV and currents were elicited by stepping to +160 mV in 1 M $[Ca^{2+}]_i$ before stepping down to -80 mV to evoke tail currents. As Figure 5.1A shows, application of scrambled LINGO1 decreased current amplitude, but rapid inactivation was only apparent at higher concentrations (>3 M) of the peptide. Slow inactivation was sometimes noticed with lower concentrations of this peptide, but the relatively short duration of the depolarising pulse used did not allow us to accurately fit the data with an exponential. As seen from Figure 5.1B, the IC_{50} values obtained for currents measured in the first 5 ms of the depolarisation was 12±3 M (n=6) and the last 5 ms was 3±1 M (n=6), which were significantly different ($p<0.05$, paired t-test). The IC_{50} value for the last 5 ms was 10-fold higher than that of the WT LINGO1 tail peptide ($p<0.01$, unpaired t-test). Inactivation of the BK currents was assessed by fitting the decay phase of the currents (at concentrations >3 M) with a single exponential, as shown in Figure 5.1C. The time constant of inactivation with 10 M of the scrambled peptide was similar to 10 M of the WT peptide (ns, unpaired t-test). Figures 5.2A and B show families of BK currents in 1 M $[Ca^{2+}]_i$ before and after the application of 10 M scrambled LINGO1 peptide, respectively. It is clear from this trace that the scrambled peptide was less effective than the NH_2-RKFNMKMI-OH peptide and that inactivation was only detectable at potentials positive to +120 mV (Figure 5.2D). This is reflected in the summary data shown in Figure

5.2C, where the scrambled peptide reduced peak currents recorded at +200 mV to 15±2% as compared to 5±1% with the WT LINGO1 peptide. Although the residual current at this voltage was greater than WT LINGO1 peptide, it was not statistically significant (ns, Mann-Whitney test). The apparent voltage-dependence of inactivation was observed at potentials positive to +120 mV (Figure 5.2D) and the time constant of inactivation of these currents was practically identical to that observed with WT LINGO1 peptide (ns, one-way ANOVA). These data suggest that altering the position of the positively charged residues in the LINGO1 peptide reduced its efficacy, but did not abolish its ability to inactivate BK channels.

A. LINGO1 scrambled peptide *(*NH_2*-MFKNKIRM-*OH*)*

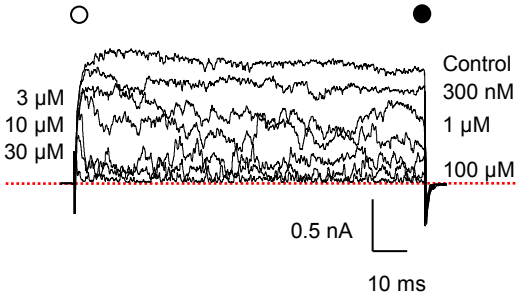

B. Summary of NH_2-*MFKNKIRM*-OH

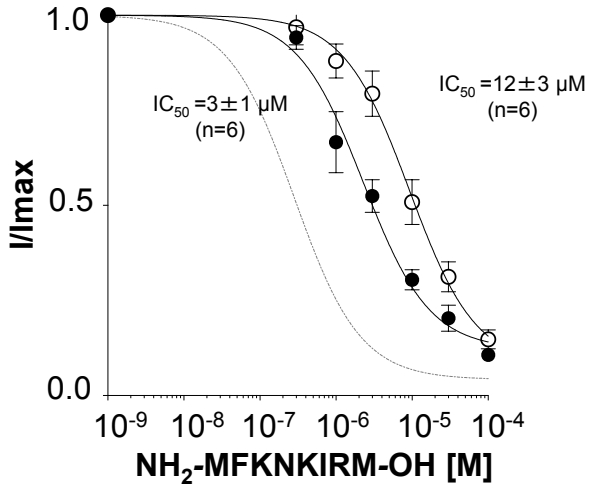

C. Summary of NH_2-*MFKNKIRM*-OH $_{inact}$

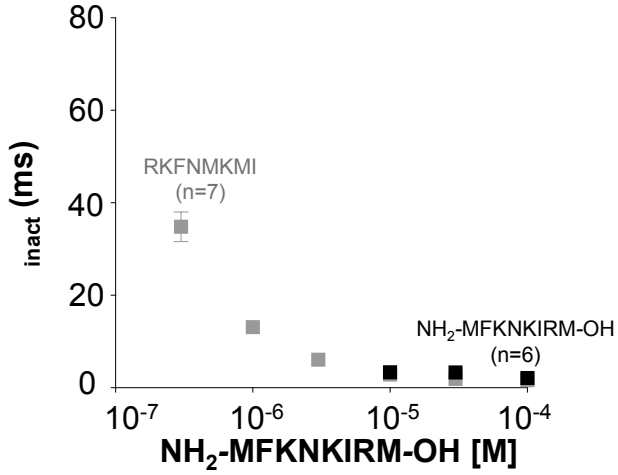

Figure 5.1: Concentration-dependent effect of NH_2-MFKNKIRM-OH synthetic peptide on WT BK . A Representative concentration-dependent effect of NH_2-MFKNKIRM-OH synthetic peptide on HEK cells expressing WT BK . Currents were evoked by a step from -60 mV to +160 mV in the presence of 300 nM, 1, 3, 10, 30, 100 µM of NH_2-MFKNKIRM-OH peptide. **B** Summary concentration effect curve for the effect of NH_2-MFKNKIRM-OH on BK currents (n=6). Data were fitted with the Hill-Langmuir equation (grey trace LINGO1 tail peptide). **C** The rate of inactivation of BK currents was assessed by fitting the decay phase with a single exponential (grey trace LINGO1 tail peptide). The rate of inactivation increased with the concentration of NH_2-MFKNKIRM-OH peptide (n=6).

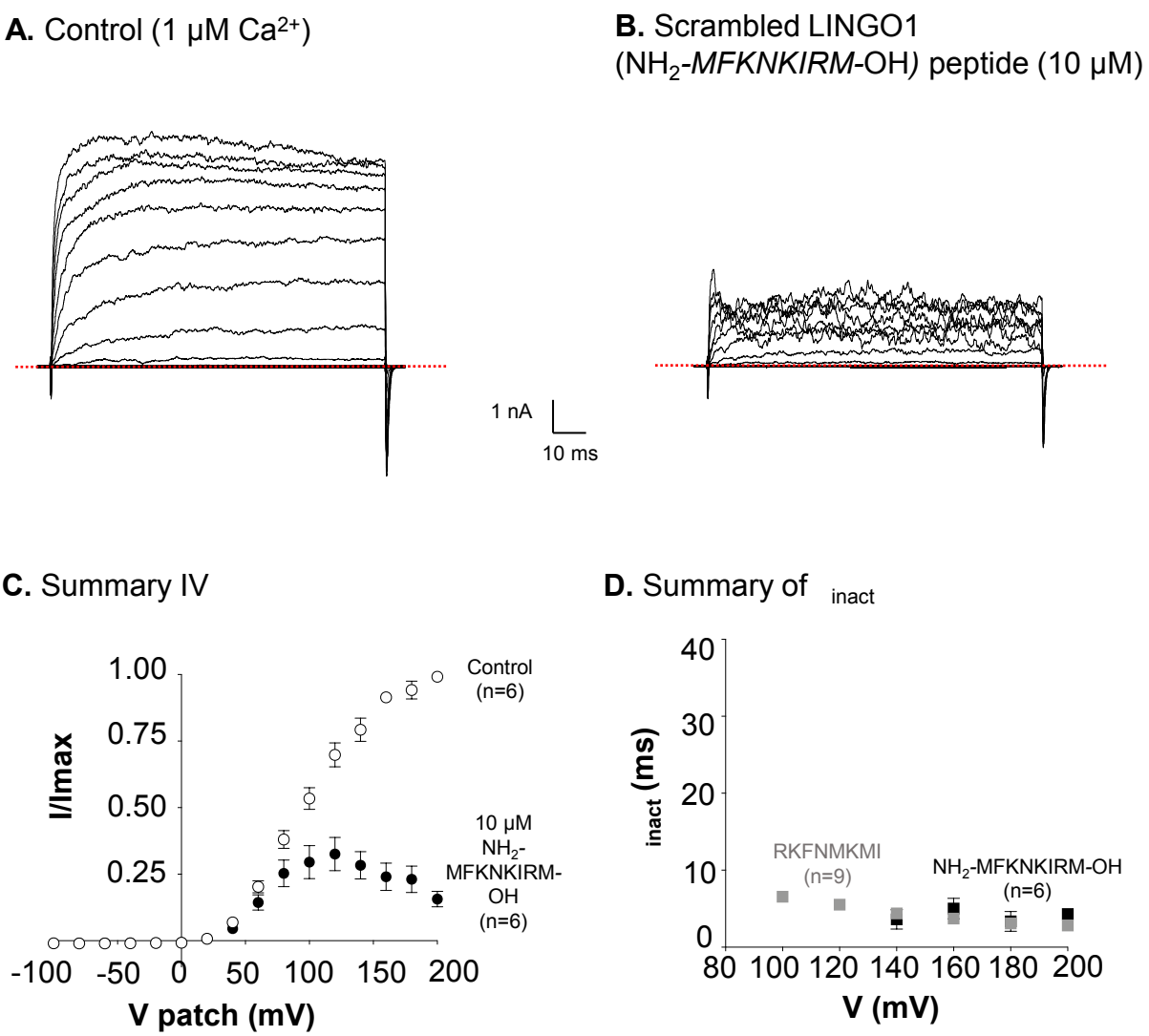

Figure 5.2: Voltage-dependence of NH_2-MFKNKIRM-OH synthetic peptide on BK . A & **B** Macroscopic currents from inside-out patches expressing BK alone, show typical records in control (1 μM $[Ca^{2+}]_i$) and after application of 10 μM NH_2-MFKNKIRM-OH peptide. Patches were held at -60 mV and stepped from -100 mV to +200 mV in 20 mV increments and stepped back down to -80 mV to generate tail currents. **C** Summary of I/Imax measured in the last 5 ms of the pulse (n=6). **D** The rate of inactivation of BK currents was assessed by fitting the decay phase with a single exponential (grey trace LINGO1 tail peptide). The currents showed an apparent voltage-dependence at more positive potentials (n=6).

5.2.2 Neutralising a positively charged residue (K618) in LINGO1 synthetic tail peptide abolished inactivation of BK currents

The data from the previous Chapter (Sections 4.2.6 - 4.2.8) suggested that both the net charge and the position of positive charges in the LINGO1 tail peptide played important roles in LINGO1-mediated inactivation of BK channels. To examine this further, we reduced the charge of the LINGO1 tail peptide by replacing each of the 3 positively charged residues- arginine at 613, lysine residues at 614 and 618, with alanine. Firstly, we replaced K618 with alanine to generate a peptide of the following sequence NH_2-RKFNM**A**MI-OH (net charge +2) and assessed its effects on HEK cells expressing BK alone. As Figure 5.3A shows, application of NH_2-RKFNM**A**MI-OH peptide reduced current amplitude in a concentration-dependent manner (100 nM to 30 M), but failed to induce inactivation (Figure 5.3A). In addition, the currents in the presence of the peptide became increasingly noisy as the peptide concentration applied, was increased, suggesting that this peptide blocked and unblocked rapidly. When the data were fitted with the Hill-Langmuir equation (Figure 5.3B), the IC_{50} obtained from currents measured in the first 5 ms was 38±7 M (n=6) and from the last 5 ms was 32±4 M (n=6). These values were not significantly different to each other (ns, paired t-test), but were much higher than that recorded with the LINGO1 'WT' peptide (p<0.0001, unpaired t-test). Figure 5.4B shows the effects of the same peptide (10 M) across a range of voltages, up to +200 mV. Again it is clear that NH_2-RKFNM**A**MI-OH peptide was less effective at blocking BK channels compared to the WT peptide (Figure 3.5B). Furthermore, as Figure 5.4C suggests, this peptide produced very little block of currents at potentials negative to +100 mV. Even at +200 mV, 56±3% of the current remained, compared to 5±1% of the current with the WT peptide (p<0.001, Mann-Whitney test), perhaps suggesting that the 'efficacy' (Furukawa and Furukawa, 1990; Purrell-Lagnado and Aldrich, 1993a; 1993b) for this peptide was much higher than 'WT'. These data indicate that the LINGO1 peptide the neutralisation of K618 alone had very significant effects and suggests that this residue plays a central role in inactivation, compared to the other positively charged residues in the LINGO1 tail.

A. NH_2-*RKFNMAMI*-OH

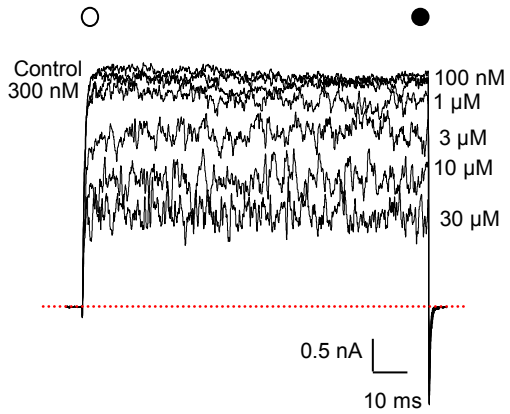

B. Summary of NH_2-*RKFNMAMI*-OH

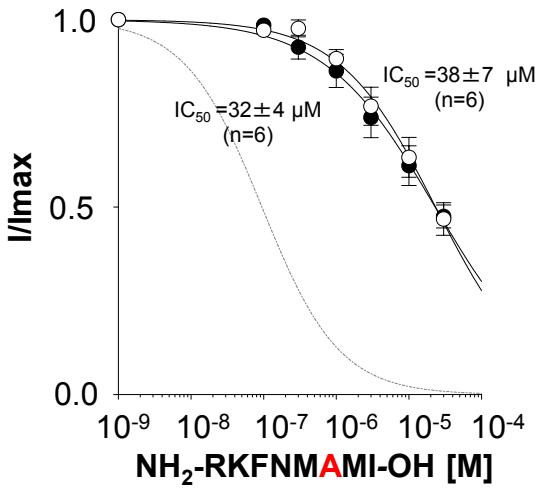

Figure 5.3: Concentration-dependent effect of NH_2-RKFNMAMI-OH on WT BK .
A Representative concentration-dependent effect of NH_2-RKFNMAMI-OH synthetic peptide on HEK cells expressing WT BK . Currents were evoked by a step from -60 mV to +160 mV in the presence of 100, 300 nM, 1, 3, 10, 30 µM of NH_2-RKFNMAMI-OH peptide. **B** Summary concentration effect curve for the effect of NH_2-RKFNMAMI-OH on BK currents (n=6). Data were fitted with the Hill-Langmuir equation (grey trace LINGO1 tail peptide).

A. Control (1 μM Ca^{2+})

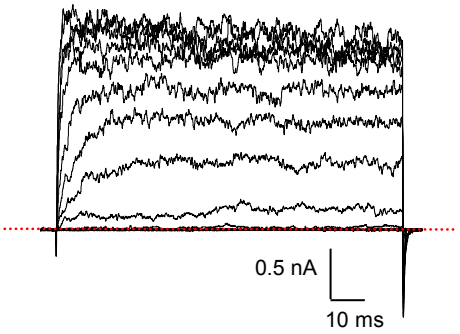

B. NH_2-*RKFNMAMI*-OH peptide (10 μM)

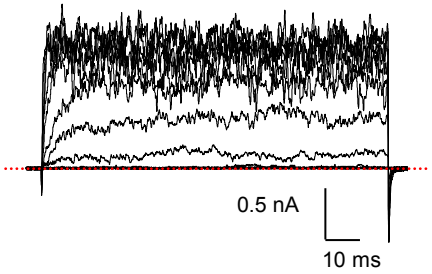

C. Summary IV

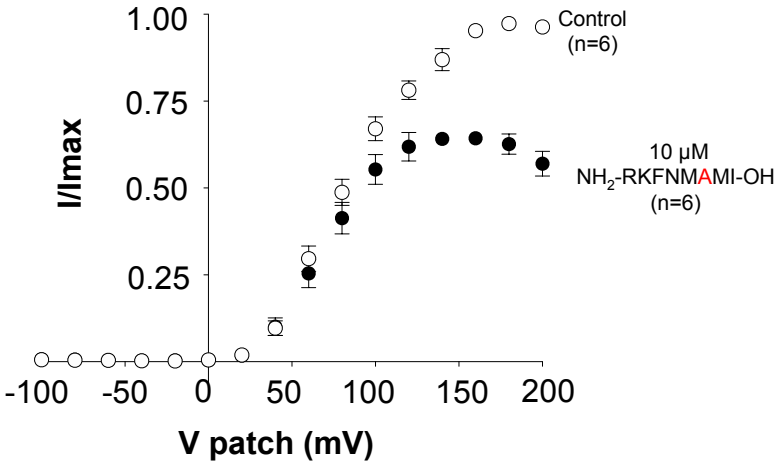

Figure 5.4: Voltage-dependence of NH_2-RKFNMAMI-OH synthetic peptide on BK . A & **B** Macroscopic currents from inside-out patches expressing BK alone, show typical records in control (1 μM $[Ca^{2+}]_i$) and after application of 10 μM NH_2-RKFNMAMI-OH peptide. Patches were held at -60 mV and stepped from -100 mV to +200 mV in 20 mV increments and stepped back down to -80 mV to generate tail currents. **C** Summary of I/Imax measured in the last 5 ms of the pulse (n=6).

5.2.3 Replacing a positively charged amino acid (K618) with a polar amino acid residue in LINGO1 synthetic tail peptide abolished inactivation of BK currents

We next examined the effect of replacing K618 with the hydrophilic, polar amino acid glutamine (Q), rather than the hydrophobic non-polar A618. The resultant NH_2-RKFNM**Q**MI-OH peptide also had a net charge of +2 and produced qualitatively similar results to those observed with NH_2-RKFNM**A**MI-OH in Figure 5.3. Thus, the time-dependent and voltage-dependent inactivation appeared to be reduced (Figure 5.5A) compared to the WT peptide. Thus, when 10 M of NH_2-RKFNM**Q**MI-OH was applied (Figure 5.6B) and a full IV relationship determined, the peptide only blocked currents at potentials positive to +100 mV and a residual current of 64±4% remained at +200 mV, compared to 5±1% of the current with the WT peptide (Figure 5.6C; $p<0.0001$, Mann-Whitney test). In addition, the IC_{50} was 57±9 M (n=7) in the first 5 ms and 28±6 M (n=7) in the last 5 ms, these values were significantly different ($p<0.05$, paired t-test). However, the IC_{50} recorded for the last 5 ms was significantly higher than that observed with the LINGO1 peptide (Figure 5.5B; $p<0.001$, unpaired t-test) and the currents were noisier in higher concentrations of the peptide.

A. NH_2-*RKFNMQMI*-OH

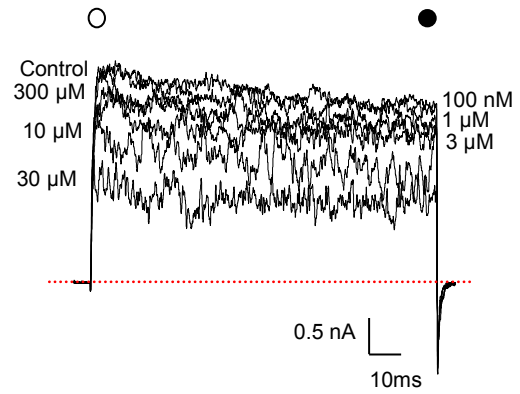

B. Summary of NH_2-*RKFNMQMI*-OH

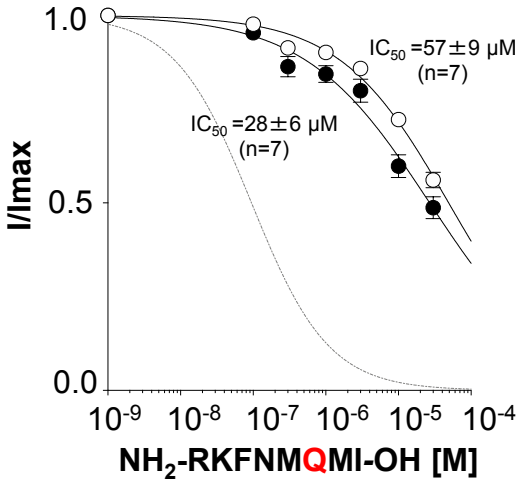

Figure 5.5: Concentration-dependent effect of NH_2-RKFNMQMI-OH on WT BK .
A Representative concentration-dependent effect of NH_2-RKFNMQMI-OH synthetic peptide on HEK cells expressing WT BK . Currents were evoked by a step from -60 mV to +160 mV in the presence of 100, 300 nM, 1, 3, 10, 30 µM of NH_2-RKFNMQMI-OH peptide. **B** Summary concentration effect curve for the effect of NH_2-RKFNMQMI-OH on BK currents (n=7). Data were fitted with the Hill-Langmuir equation (grey trace LINGO1 tail peptide).

A. Control (1 μM Ca^{2+})

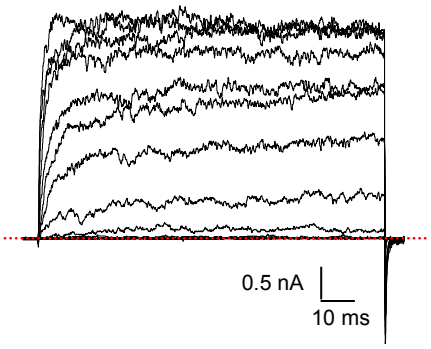

B. NH_2-*RKFNMQMI*-OH peptide (10 μM)

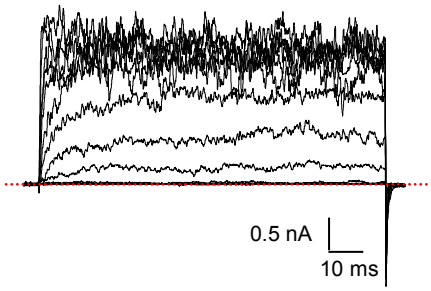

C. Summary IV

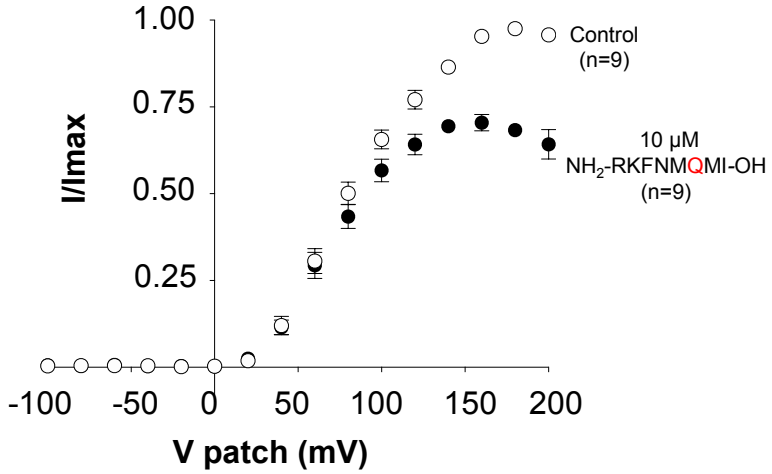

Figure 5.6: Voltage-dependence of NH_2-RKFNMQMI-OH synthetic peptide on BK . A & **B** Macroscopic currents from inside-out patches expressing BK alone, show typical records in control (1 μM $[Ca^{2+}]_i$) and after application of 10 μM NH_2-RKFNMQMI-OH peptide. Patches were held at -60 mV and stepped from -100 mV to +200 mV in 20 mV increments and stepped back down to -80 mV to generate tail currents. **C** Summary of I/Imax measured in the last 5 ms of the pulse (n=9).

5.2.4 Neutralising two positively charged residues (R613 and K614) in LINGO1 synthetic tail peptide does not affect its inactivating effect on BK channels

We next replaced the arginine at 613 and lysine at 614 with alanine residues to form the NH_2-**AA**FNMKMI-OH peptide with a net charge of +1. As shown in Figure 5.7A, this peptide caused a concentration-dependent (300 nM to 100 M) decrease in current amplitude and interestingly, inactivation was obvious at higher concentrations, in contrast to the peptides containing A618 or Q618, described above. When these data were fitted with the Hill-Langmuir equation as shown in Figure 5.7B, the IC_{50} values measured from currents in the first 5 ms was 59±8 M (n=7) and from the last 5 ms was 17±3 M (n=7), which were significantly different ($p<0.001$, paired t-test). In addition, the IC_{50} recorded for the last 5 ms was 56-fold higher than WT LINGO1 peptide ($p<0.0001$, unpaired t-test). The inactivating currents were fitted with a single exponential and summarised in Figure 5.7C, demonstrating that the rate of inactivation increased with increased peptide concentrations. However, the time constant of inactivation with 10 M of NH_2-**AA**FNMKMI-OH peptide (9±1 ms) was significantly slower than 10 M of WT peptide (3±1 ms, $p<0.0001$, unpaired t-test). Figures 5.8A and B show families of BK currents in 1 M $[Ca^{2+}]_i$, elicited from patches in the absence and presence of 10 M of the NH_2-**AA**FNMKMI-OH peptide. In presence of the peptide the currents inactivated and also induced block of BK currents. For example, at +200 mV, 41±5% of sustained current remained in the last 5 ms (Figure 5.8C). This was significantly higher than the WT peptide ($p<0.001$, Mann-Whitney test) and suggests that the peptide association with the BK channel may be rather unstable. Figure 5.8D shows a summary of the apparent voltage-dependence of inactivation and illustrates that the peptide only inactivated currents at potentials positive to +120 mV. However, the time constant of inactivation observed at +200 mV was significantly slower compared to WT LINGO1 peptide ($p<0.01$, unpaired t-test), perhaps suggesting that the voltage-dependence of binding was reduced by the neutralisation of these two charges.

A. NH_2-*AA*FNMKMI-OH

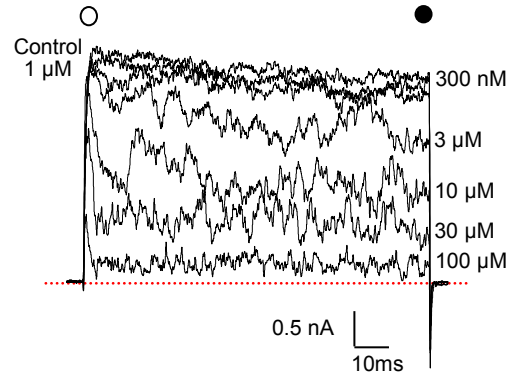

B. Summary of NH_2-*AA*FNMKMI-OH

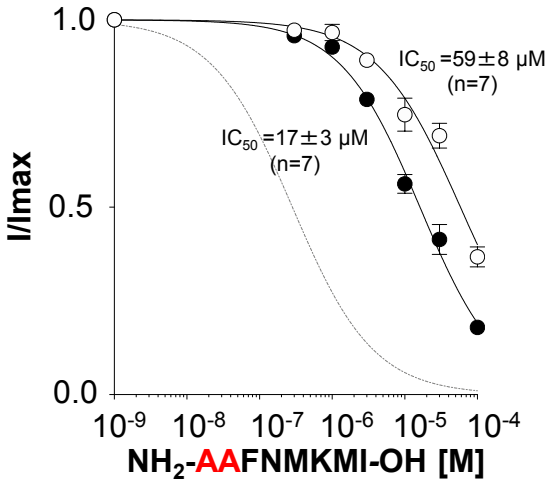

C. Summary of NH_2-*AA*FNMKMI-OH $_{inact}$

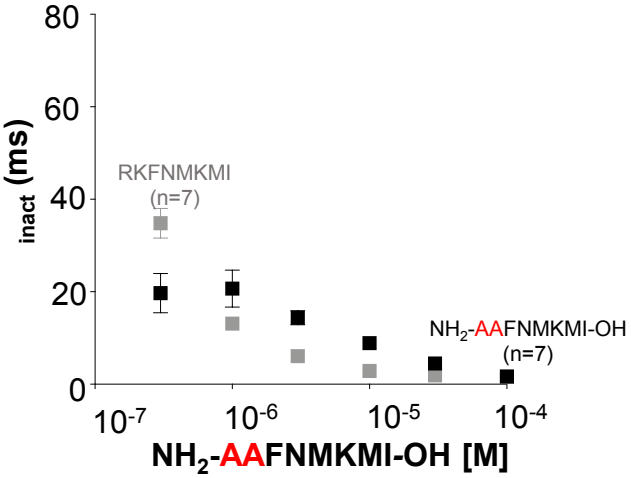

Figure 5.7: Concentration-dependent effect of NH_2-AAFNMKMI-OH on WT BK .
A Representative concentration-dependent effect of NH_2-AAFNMKMI-OH synthetic peptide on HEK cells expressing WT BK . Currents were evoked by a step from -60 mV to +160 mV in the presence of 300 nM, 1, 3, 10, 30, 100 µM of NH_2-AAFNMKMI-OH peptide. **B** Summary concentration effect curve for the effect of NH_2-AAFNMKMI-OH on BK currents (n=7). Data were fitted with the Hill-Langmuir equation (grey trace LINGO1 tail peptide). **C** The rate of inactivation of BK currents was assessed by fitting the decay phase with a single exponential (grey trace LINGO1 tail peptide). The rate of inactivation increased with the concentration of NH_2-AAFNMKMI-OH peptide (n=7).

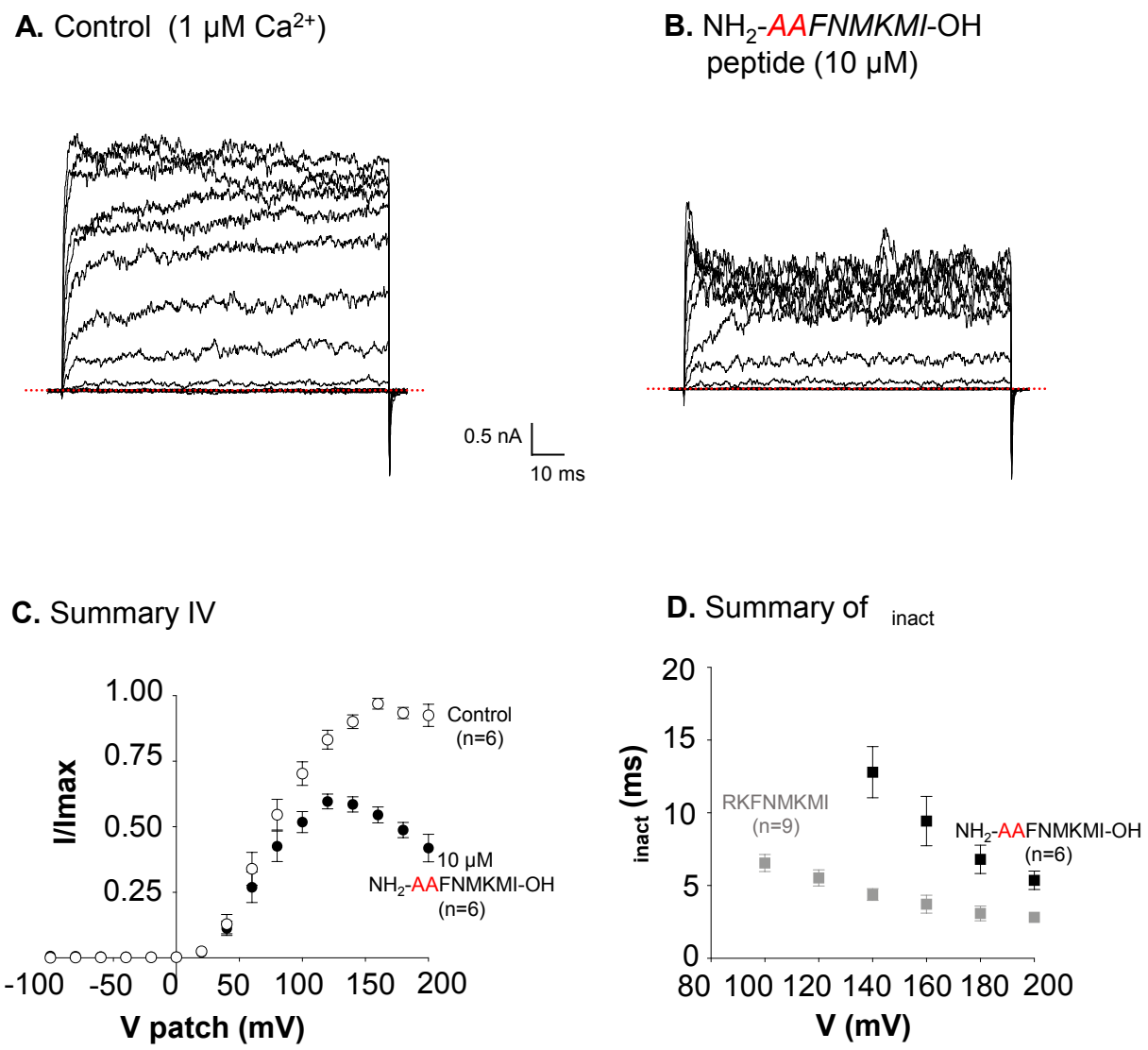

Figure 5.8: Voltage-dependence of NH_2-AAFNMKMI-OH synthetic peptide on BK .
A & **B** Macroscopic currents from inside-out patches expressing BK alone, show typical records in control (1 µM $[Ca^{2+}]_i$) and after application of 10 µM NH_2-AAFNMKMI-OH peptide. Patches were held at -60 mV and stepped from -100 mV to +200 mV in 20 mV increments and stepped back down to -80 mV to generate tail currents. **C** Summary of I/Imax measured in the last 5 ms of the pulse (n=6). **D** The rate of inactivation of BK currents was assessed by fitting the decay phase with a single exponential (grey trace LINGO1 peptide). The currents showed an apparent voltage-dependence at more positive potentials (n=6).

5.2.5 Acylation of LINGO1 synthetic tail peptide at N-terminus does not affect its inactivating effect on BK channels

In Sections 5.2.1 through to 5.2.4 we utilised peptides with NH_2 and COOH termini. However, as described previously for full-length LINGO1, the NH_2 on residue R613 would be uncharged and its sidechain would have a charge of +1. Consequently, we acylated the N-terminus (uncharged) to produce an Ac-RKFNMKMI-OH peptide with a net charge of +2. As Figure 5.9A suggests, the Ac-RKFNMKMI-OH synthetic peptide (100 nM to 30 M), when applied to the cytosolic surface of the patches expressing BK , induced inactivation in a concentration-dependent manner. Figure 5.9B shows summary data fitted with the Hill-Langmuir equation (grey dashed line WT LINGO1 peptide). The IC_{50} was 14±3 M (n=5) when measured from the first 5 ms and 3±1 M (n=5) from the last 5 ms. These values were significantly different from each other and indicated that this peptide caused a time-dependent inactivation of BK currents ($p<0.05$, paired t-test). However, when the IC_{50} obtained for the last 5 ms was compared with the WT LINGO1 tail peptide, it was significantly higher ($p<0.001$, unpaired t-test). As seen from Figure 5.9A, Ac-RKFNMKMI-OH peptide still clearly inactivated BK channels. The rate of inactivation of BK currents was assessed by fitting the decay phase of the currents with a single exponential as shown in Figure 5.9C. This data suggests that the rate of inactivation increased with the concentration of Ac-RKFNMKMI-OH peptide. The time constant of inactivation with 10 M Ac-RKFNMKMI-OH peptide was similar to the time constant of inactivation with 10 M of WT LINGO1 peptide (ns, unpaired t-test). Figures 5.10A and B show a family of BK currents in 1 M $[Ca^{2+}]_i$ before and after the application of 10 M Ac-RKFNMKMI-OH peptide. During the application of the peptide, the amplitude of the currents was reduced, but the proportion of current remaining at the end of the pulse was greater compared to that observed with the WT LINGO1 peptide. This was reflected in the summary data shown in Figure 5.10C where at +200 mV the remaining current in the last 5 ms was significantly higher (16±1%) in the presence of Ac-RKFNMKMI-OH peptide compared to (5±1%) LINGO1 peptide ($p<0.01$, Mann-Whitney test), perhaps suggesting that the ‘off-rate ’of the reaction increased. The binding of this peptide still showed apparent voltage-dependence as reflected in Figure 5.10D, where the rate of

inactivation appeared slightly slower at +100 mV, but this was not significantly different to the rate of inactivation observed with the WT peptide (ns, unpaired t-test). These results suggest that, although Ac-LINGO1 peptide resulted in inactivation of BK currents, it had a reduced efficacy than the amino free acid version of the LINGO1 peptide.

A. Ac-*RKFNMKMI*-OH

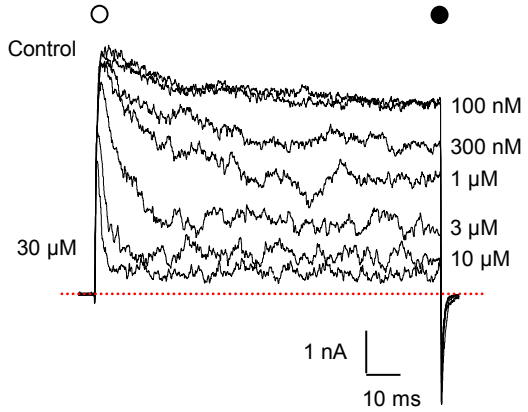

B. Summary of Ac-*RKFNMKMI*-OH

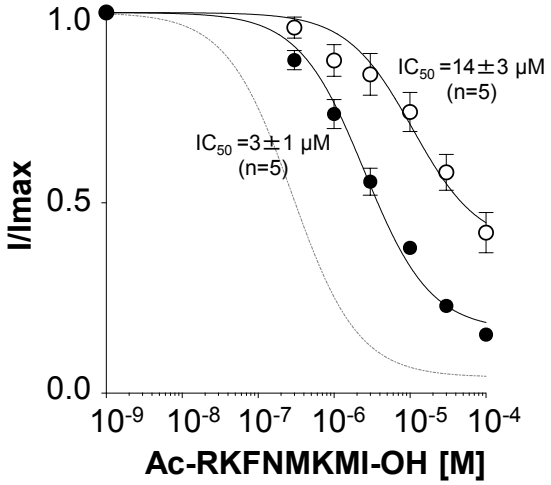

C. Summary of Ac-*RKFNMKMI*-OH $_{inact}$

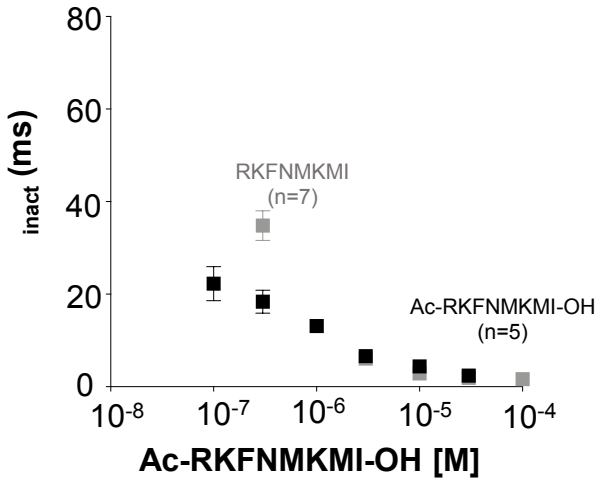

Figure 5.9: Concentration-dependent effect of Ac-RKFNMKMI-OH synthetic peptide on WT BK . A Representative concentration-dependent effect of Ac-RKFNMKMI-OH synthetic peptide on HEK cells expressing WT BK . Currents were evoked by a step from -60 mV to +160 mV in the presence of 100, 300 nM, 1, 3, 10, 30 µM of Ac-RKFNMKMI-OH peptide. **B** Summary concentration effect curve for the effect Ac-RKFNMKMI-OH on BK currents (n=5). Data were fitted with the Hill-Langmuir equation (grey trace LINGO1 tail peptide). **C** The rate of inactivation of BK currents was assessed by fitting the decay phase with a single exponential (grey trace LINGO1 tail peptide). The rate of inactivation increased with the concentration of Ac-RKFNMKMI-OH synthetic peptide (n=5).

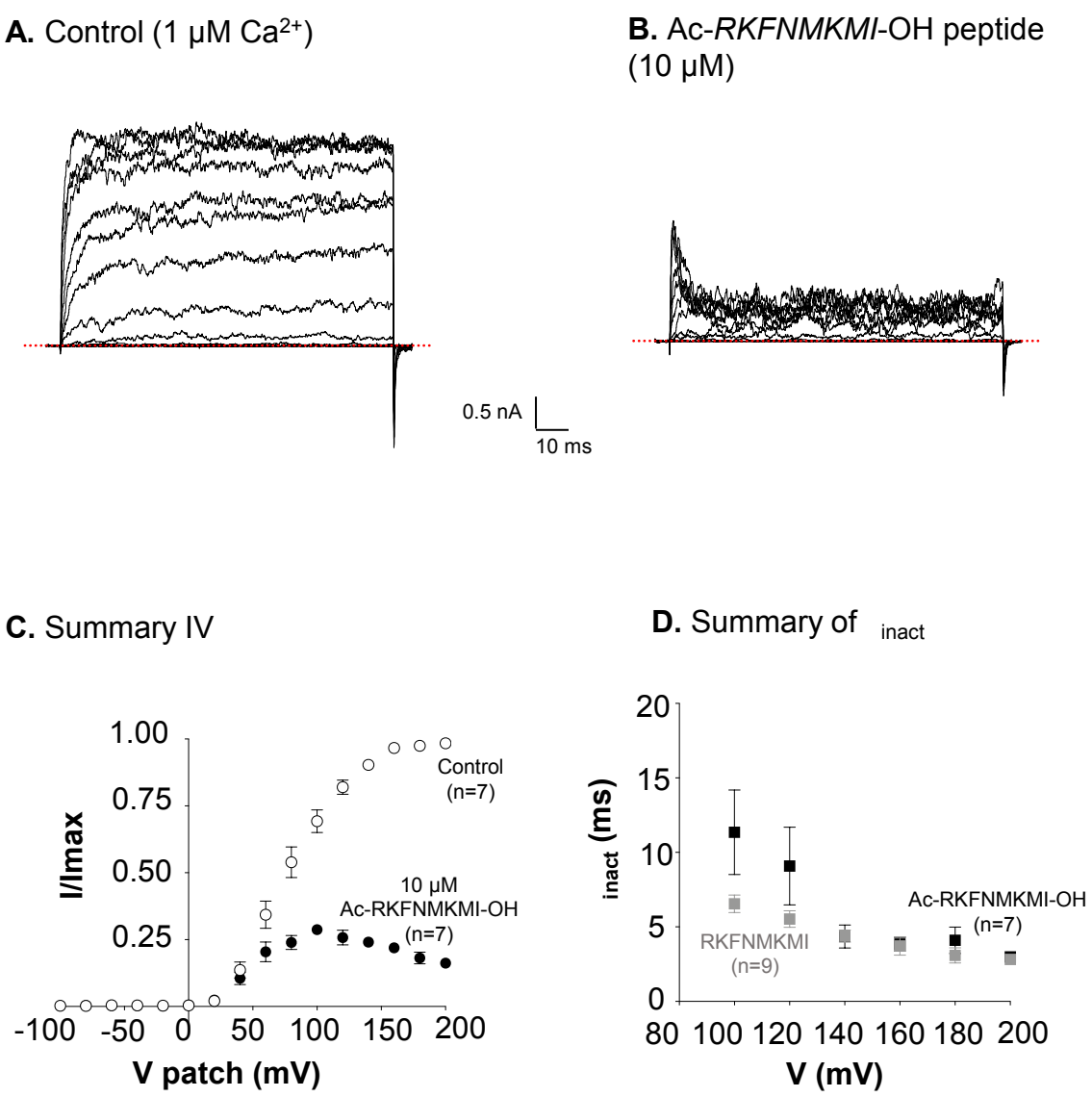

Figure 5.10: Voltage-dependence of Ac-RKFNMKMI-OH synthetic peptide on BK .
A & **B** Macroscopic currents from inside-out patches expressing BK alone, show typical records in control (1 μM $[Ca^{2+}]_i$) and after application of 10 μM Ac-RKFNMKMI-OH peptide. Patches were held at -60 mV and stepped from -100 mV to +200 mV in 20 mV increments and stepped back down to -80 mV to generate tail currents. **C** Summary of I/Imax measured in the last 5 ms of the pulse (n=7). **D** The rate of inactivation of BK currents was assessed by fitting the decay phase with a single exponential (grey trace LINGO1 tail peptide). The currents showed an apparent voltage-dependence at more positive potentials (n=7).

5.2.6 Substitution of methionine (M619) with an alanine residue in LINGO1 synthetic tail peptide abolished inactivation of BK currents

We further investigated the role of individual residues in the LINGO1 peptide by substituting these residues with alanine while maintaining an acylated N-terminus and synthesised the following Ac-RKFNMK**A**I-OH peptide which retained a net charge of +2. Interestingly, even though this peptide contained all of the charged residues in the correct locations, it failed to induce rapid inactivation of BK currents, but did cause a concentration dependent blockade of them (Figure 5.11A). Although there was some evidence of a slow inactivation with higher concentrations of this peptide, it was not possible to obtain reliable exponential fits to these currents. The IC_{50} values obtained from currents in the first and last 5 ms of the pulse were not significantly different (9±0.7 M vs 9±1 M, n=6, ns, paired t-test) but was significantly greater than the Ac-RKFNMKMI-OH peptide ($p<0.001$, unpaired t-test) shown as grey dotted line in Figure 5.11B. When 10 M of Ac-RKFNMK**A**I-OH peptide was applied and a full IV relationship determined, it was apparent that this peptide induced partial block of BK currents (Figure 5.12B), but only at potentials positive to +100 mV. For instance, at +200 mV, 61±2% (n=10) of the sustained current remained at the end of the pulse, which was significantly higher than that observed with the Ac-RKFNMKMI-OH peptide ($p<0.001$, Mann-Whitney test). These results suggest that the methionine residue at 619 also plays a central role in LINGO1 tail peptide-mediated inactivation of BK channels.

A. Ac-*RKFNMKAI*-OH

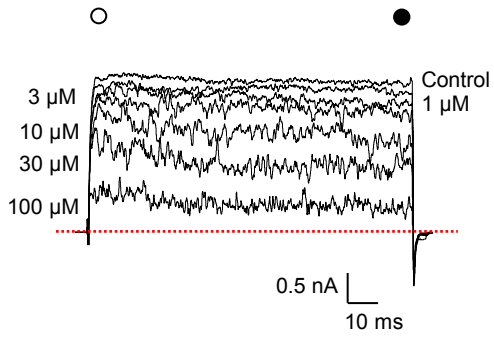

B. Summary of Ac-*RKFNMKAI*-OH

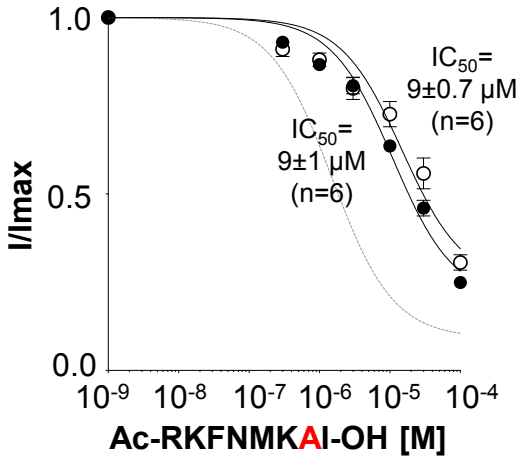

Figure 5.11: Concentration-dependent effect of Ac-RKFNMKAI-OH peptide on WT BK .
A Representative concentration-dependent effect of Ac-RKFNMKAI-OH synthetic peptide on HEK cells expressing WT BK . Currents were evoked by a step from -60 mV to +160 mV in the presence of 300 nM, 1, 3, 10, 30, 100 µM of Ac-RKFNMKAI-OH peptide. **B** Summary concentration effect curve for the effect of Ac-RKFNMKAI-OH on BK currents (n=6). Data were fitted with the Hill-Langmuir equation (grey trace Ac-RKFNMKMI-OH peptide).

A. Control (1 μM Ca^{2+})

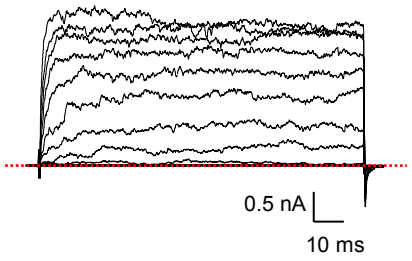

B. Ac-*RKFNMKAI*-OH peptide (10 μM)

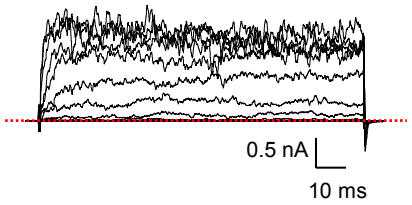

C. Summary IV

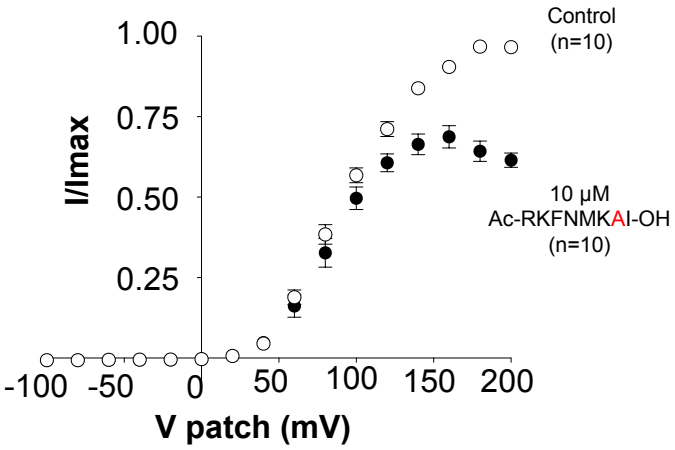

Figure 5.12: Voltage-dependence of Ac-RKFNMKAI-OH peptide on WT BK .
A & **B** Macroscopic currents from inside-out patches expressing BK alone, show typical records in control (1 μM $[Ca^{2+}]_i$) and after application of 10 μM Ac-RKFNMKAI-OH peptide. Patches were held at -60 mV and stepped from -100 mV to +200 mV in 20 mV increments and stepped back down to -80 mV to generate tail currents. **C** Summary of I/Imax measured in the last 5 ms of the pulse (n=10).

5.2.7 Neutralising the positively charged lysine (K618) with an alanine residue in LINGO1 synthetic tail peptide abolished inactivation of BK currents

We next neutralised the positive charge at K618 with an alanine residue to generate the Ac-RKFNM**A**MI-OH peptide, which had a net charge of +1. The effects of the Ac-RKFNM**A**MI-OH peptide were similar to the NH_2-RKFNM**A**MI-OH peptide and resulted in a concentration-dependent reduction (300 nM to 100 M) in current amplitude, even though inactivation was absent (Figure 5.13A). The IC_{50} values obtained from the first 5 ms was in the excess of 100 M (109±10, n=7) and from the last 5 ms was 94±9 M (n=7) were not significantly different to each other (ns, paired t-test) and were significantly different to the effects of the NH_2-RKFNM**A**MI-OH peptide ($p<0.001$, unpaired t-test). In addition, the IC_{50} from the last 5 ms was significantly higher than that observed with the Ac-RKFNMKMI-OH peptide ($p<0.0001$, unpaired t-test), shown as the grey line in Figure 5.13B. Figure 5.14 illustrates the rather weak apparent voltage-dependence of the Ac-RKFNM**A**MI-OH peptide up to +200 mV. The summary in Figure 5.14C demonstrated that at +200 mV, 75±3% (n=6) of residual current remained and this was significantly higher compared to that observed with either the NH_2-RKFNM**A**MI-OH ($p<0.01$, Mann-Whitney test) or the Ac-RKFNMKMI-OH peptides ($p<0.01$, Mann-Whitney test). This data confirms that the lysine at residue 618 in LINGO1 tail peptide plays an important role in inactivation of BK channels.

A. Ac-*RKFNMAMI*-OH

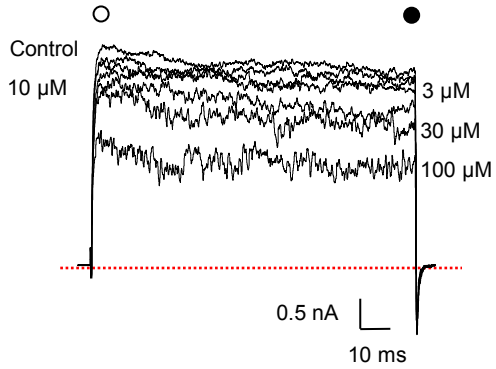

B. Summary of Ac-*RKFNMAMI*-OH

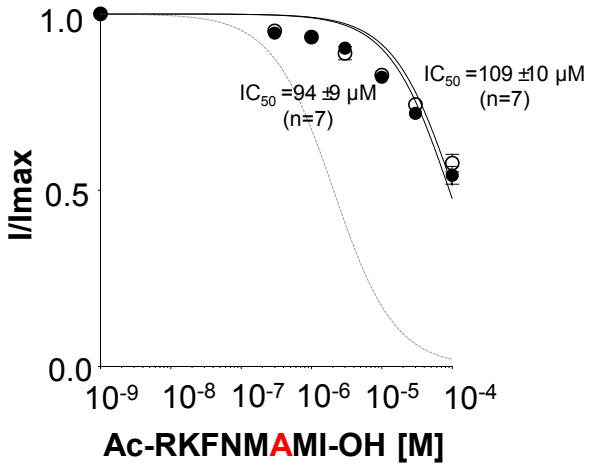

Figure 5.13: Concentration-dependent effect of Ac-RKFNMAMI-OH peptide on WT BK .
A Representative concentration-dependent effect of Ac-RKFNMAMI-OH synthetic peptide on HEK cells expressing WT BK . Currents were evoked by a step from -60 mV to +160 mV in the presence of 300 nM, 1, 3, 10, 30, 100 µM of Ac-RKFNMAMI-OH peptide. **B** Summary concentration effect curve for the effect of Ac-RKFNMAMI-OH on BK currents (n=7). Data were fitted with the Hill-Langmuir equation (grey trace Ac-RKFNMKMI-OH peptide).

A. Control (1 μM Ca^{2+})

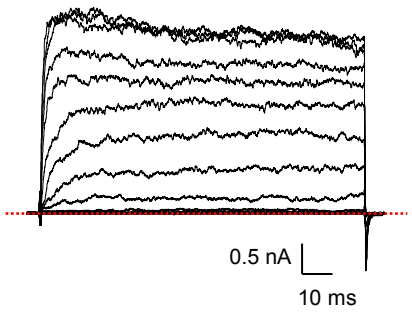

B. Ac-*RKFNMAMI*-OH peptide (10 μM)

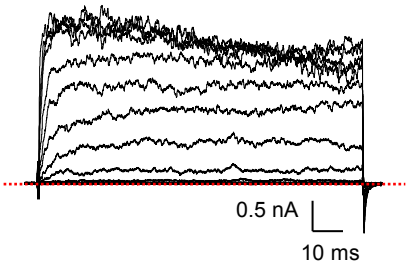

C. Summary IV

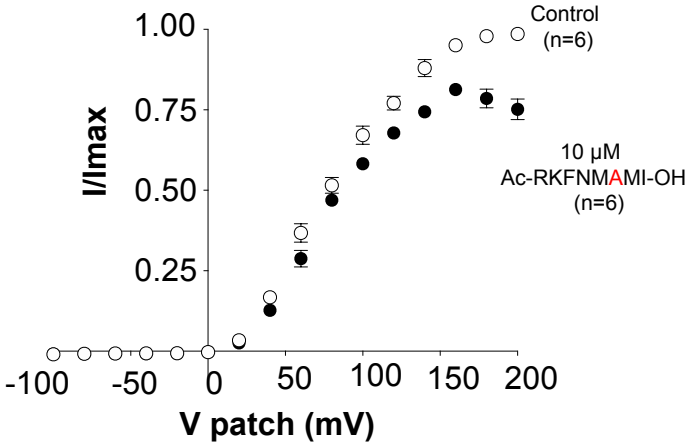

Figure 5.14: Voltage-dependence of Ac-RKFNMAMI-OH peptide on WT BK .
A & **B** Macroscopic currents from inside-out patches expressing BK alone, show typical records in control (1 μM $[Ca^{2+}]_i$) and after application of 10 μM Ac-RKFNMAMI-OH peptide. Patches were held at -60 mV and stepped from -100 mV to +200 mV in 20 mV increments and stepped back down to -80 mV to generate tail currents. **C** Summary of I/Imax measured in the last 5 ms of the pulse (n=6).

5.2.8 Substitution of methionine (M617) with an alanine residue in LINGO1 synthetic tail peptide abolished inactivation of BK currents

We also examined if replacement of M617 with alanine (Ac-RKFN**A**KMI-OH) altered the inactivation properties of the peptide. As Figure 5.15A suggests, this peptide reduced current amplitude in a concentration-dependent manner (300 nM to 30 M), but also failed to induce significant time-dependent inactivation of BK currents. Thus, the IC_{50} values measured in the first and last 5 ms were very similar (13±7 M vs 10±4 M, n=5, ns, paired t-test) and were less efficacious compared to the Ac-RKFNMKMI-OH peptide (ns, unpaired t-test), as illustrated by the grey dashed line in Figure 5.15B. The apparent voltage-dependence of block with Ac-RKFN**A**KMI-OH peptide was also affected, as shown in Figure 5.16B and Figure 5.16C where, even at +200 mV, only ~33% (n=7) of the sustained current was blocked with 10 M of this peptide. These results suggest that the methionine at M617 in LINGO1 tail peptide also plays an important role in inactivating BK channels.

A. Ac-*RKFNAKMI*-OH

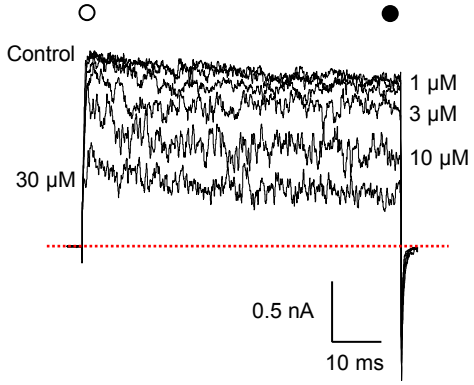

B. Summary of Ac-*RKFNAKMI*-OH

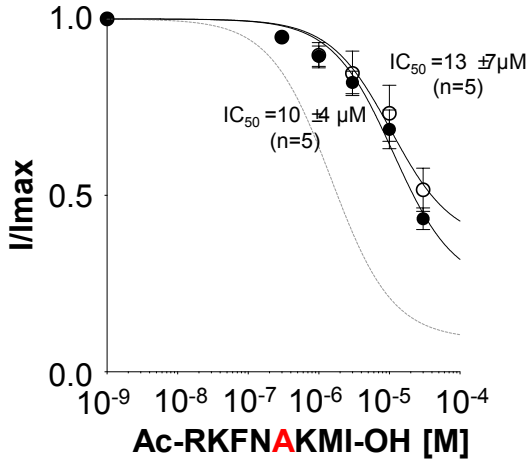

Figure 5.15: Concentration-dependent effect of Ac-RKFNAKMI-OH peptide on WT BK .
A Representative concentration-dependent effect of Ac-RKFNAKMI-OH synthetic peptide on HEK cells expressing WT BK . Currents were evoked by a step from -60 mV to +160 mV in the presence of 300 nM, 1, 3, 10, 30 µM of Ac-RKFNAKMI-OH peptide. **B** Summary concentration effect curve for the effect of Ac-RKFNAKMI-OH on BK currents (n=5). Data were fitted with the Hill-Langmuir equation (grey trace Ac-RKFNMKMI-OH peptide).

A. Control (1 μM Ca^{2+})

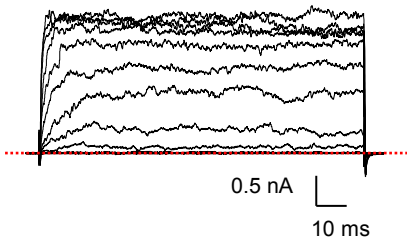

B. Ac-*RKFNAKMI*-OH peptide (10 μM)

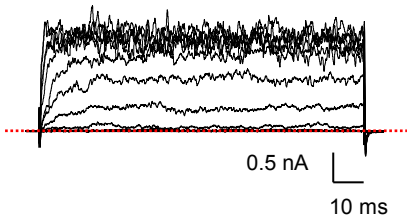

C. Summary IV

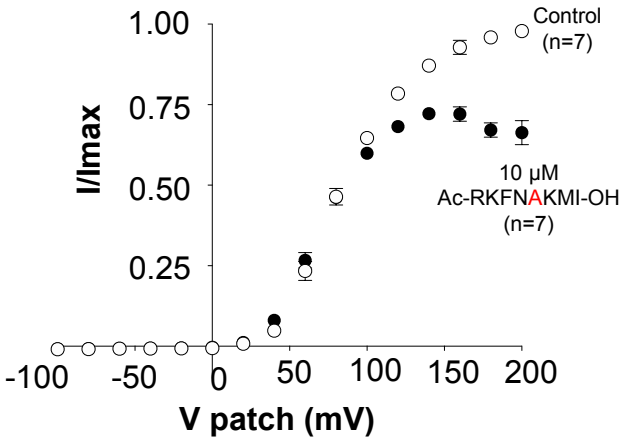

Figure 5.16: Voltage-dependence of Ac-RKFNAKMI-OH peptide on WT BK .
A & **B** Macroscopic currents from inside-out patches expressing BK alone, show typical records in control (1 μM $[Ca^{2+}]_i$) and after application of 10 μM Ac-RKFNAKMI-OH peptide. Patches were held at -60 mV and stepped from -100 mV to +200 mV in 20 mV increments and stepped back down to -80 mV to generate tail currents. **C** Summary of I/Imax measured in the last 5 ms of the pulse (n=7).

5.2.9 Substitution of asparagine (N616) with an alanine residue in LINGO1 synthetic tail peptide does not affect its inactivating effect on BK channels

The results presented so far suggest that alanine substitution of M617, K618 or M619 in the C-terminus of the tail peptide dramatically altered the affinity of the peptide and practically abolished inactivation. We therefore examined if this "critical" region extended proximally to N616 by substituting the asparagine at this position with an alanine residue (Ac-RKF**A**MKMI-OH). Interestingly however, although the affinity of this peptide was reduced compared to the Ac-RKFNMKMI-OH peptide, it did induce inactivation (Figure 5.17A) and the the IC_{50} was 7±1 M and 1±0.1 M (n=9, p<0.01, paired t-test) when determined from the first and last 5 ms of the depolarising pulse, respectively. Interestingly, the affinity of the Ac-RKF**A**MKMI-OH peptide only ~3 fold less than Ac-RKFNMKMI-OH (p<0.01, unpaired t-test) shown as grey dashed line in Figure 5.17B. This suggests that alterations to residues at this position were better tolerated than those closer to the C-terminus. We noted a significant slowing of inactivation with 1 and 3 M of the peptide as compared to Ac-RKFNMKMI-OH peptide (p<0.001, one-way ANOVA, Figure 5.17C), suggesting that replacement of asparagine here with alanine may alter the 'on-rate' of the reaction. In contrast, the amount of sustained current at the end of the depolarising pulse at +200 mV was similar to that observed with the Ac-RKFNMKMI-OH peptide (Figure 5.18, 16±2%, n=9, ns, Mann-Whitney test), suggesting that the 'off-rate' may not have been altered. As seen in Figure 5.18D, the apparent voltage-dependence of inactivating currents was observed at potentials positive to +120 mV, although the time constant of inactivation from +140 to +200 mV was significantly slower compared to the Ac-RKFNMKMI-OH peptide (p<0.01, one-way ANOVA).

A. Ac-*RKFAMKMI*-OH

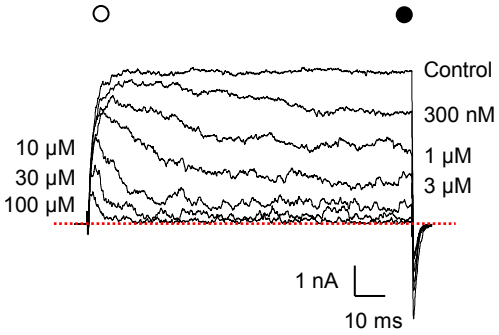

B. Summary of Ac-*RKFAMKMI*-OH

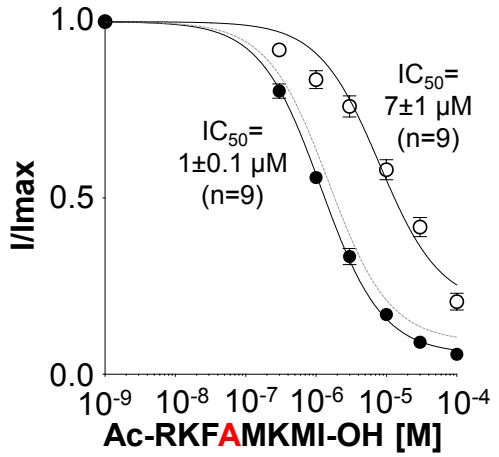

C. Summary of Ac-*RKFAMKMI*-OH $_{inact}$

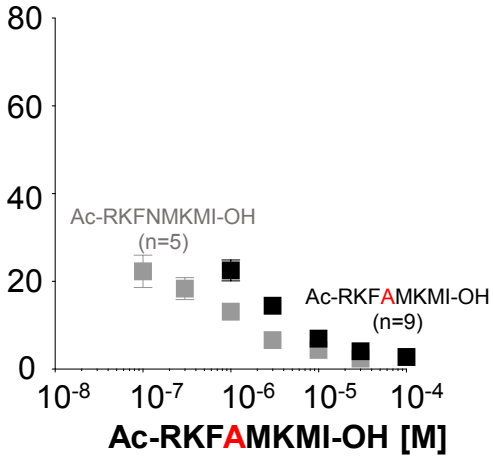

Figure 5.17: Concentration-dependent effect of Ac-RKFAMKMI-OH peptide on WT BK .
A Representative concentration-dependent effect of Ac-RKFAMKMI-OH synthetic peptide on HEK cells expressing WT BK . Currents were evoked by a step from -60 mV to +160 mV in the presence of 300 nM, 1, 3, 10, 30, 100 μM of Ac-RKFAMKMI-OH peptide. **B** Summary concentration effect curve for the effect of Ac-RKFAMKMI-OH on BK currents (n=9). Data were fitted with the Hill-Langmuir equation (grey trace Ac-RKFNMKMI-OH peptide). **C** The rate of inactivation of BK currents was assessed by fitting the decay phase with a single exponential (grey trace Ac-RKFNMKMI-OH peptide). The rate of inactivation increased with the concentration of Ac-RKFAMKMI-OH peptide (n=9).

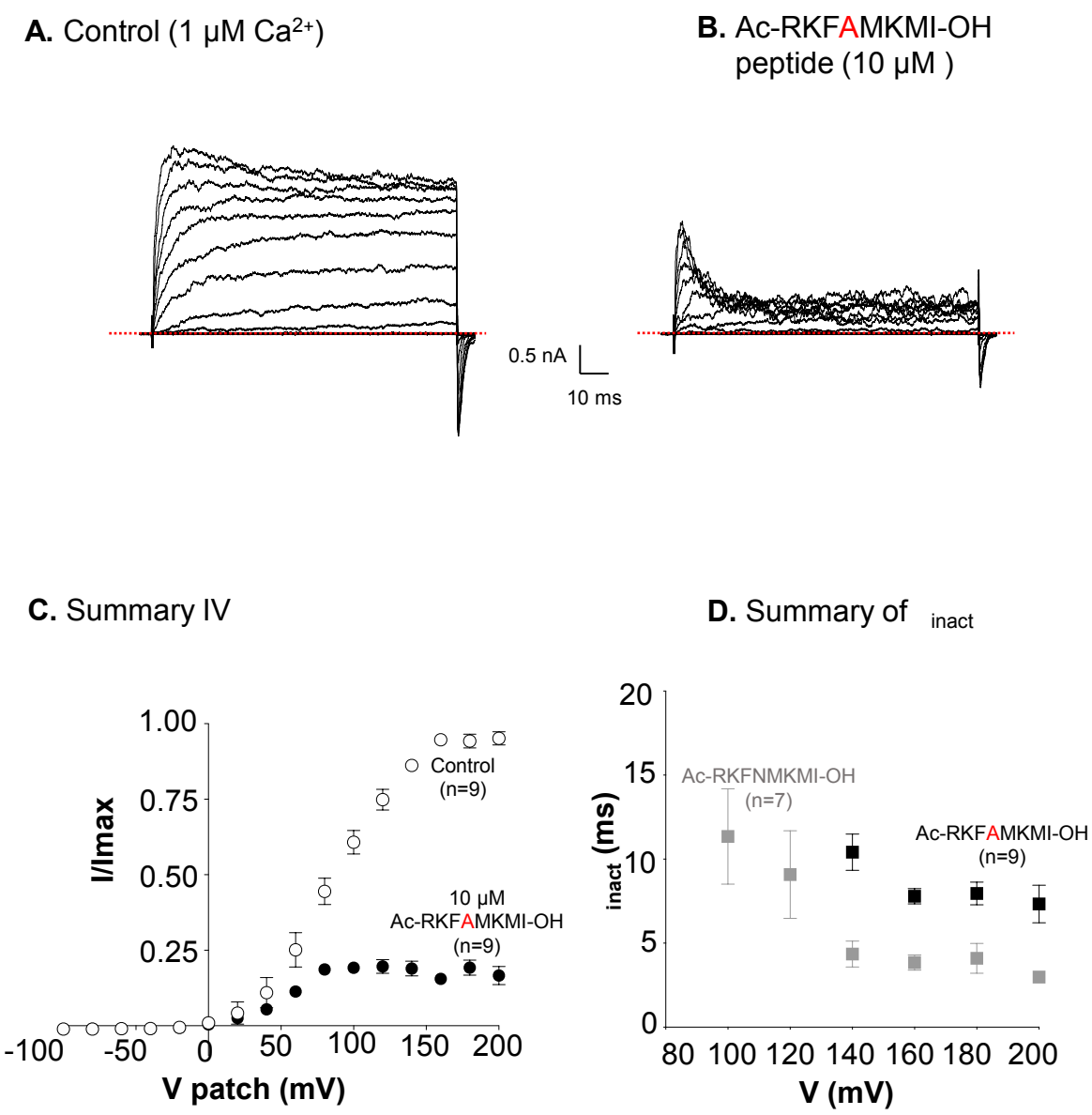

Figure 5.18: Voltage-dependence of Ac-RKFAMKMI-OH peptide on WT BK .
A & **B** Macroscopic currents from inside-out patches expressing BK alone, show typical records in control (1 μM $[Ca^{2+}]_i$) and after application of 10 μM Ac-RKFAMKMI-OH peptide. Patches were held at -60 mV and stepped from -100 mV to +200 mV in 20 mV increments and stepped back down to -80 mV to generate tail currents. **C** Summary of I/Imax measured in the last 5 ms of the pulse (n=9). **D** The rate of inactivation of BK currents was assessed by fitting the decay phase with a single exponential (grey trace Ac-RKFNMKMI-OH peptide). The currents showed an apparent voltage-dependence at more positive potentials (n=9).

5.2.10 Substitution of the aromatic amino acid (F615) with an alanine residue in LINGO1 synthetic tail peptide abolished inactivation of BK currents

We then replaced the phenylalanine at 615 with an alanine residue to generate the Ac-RK**A**NMKMI-OH peptide. Interestingly, although this peptide retained a charge of +2, it failed to inactivate currents, but did cause a concentration-dependent (300 nM to 100 M) reduction in their amplitude (Figure 5.19A). The data for 7 such similar experiments is summarised in Figure 5.19B where the obtained IC_{50} values determined from the first and last 5 ms of the depolarisation were identical (10±0.5 M vs 10±1 M, ns, paired t-test). However, when compared to the Ac-RKFNMKMI-OH peptide, the IC_{50} value was significantly higher ($p<0.001$, unpaired t-test). With the application of 10 M of Ac-RK**A**NMKMI-OH peptide (Figure 5.20B) the apparent voltage-dependence of the block was also affected, and block was evident only at potentials > +100 mV. As shown in the summary data in Figure 5.20C, at +200 mV, 60±2% (n=10) of the current remained which was significantly higher than that observed with the Ac-RKFNMKMI-OH peptide ($p<0.001$, Mann-Whitney test). These results suggest that the phenylalanine at 615 in the LINGO1 tail peptide also plays an important role in inactivating BK currents.

A. Ac-*RKANMKMI*-OH

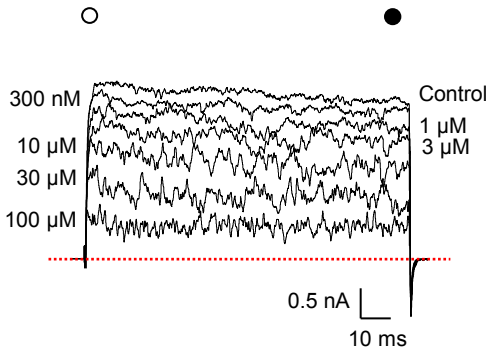

B. Summary of Ac-*RKANMKMI*-OH

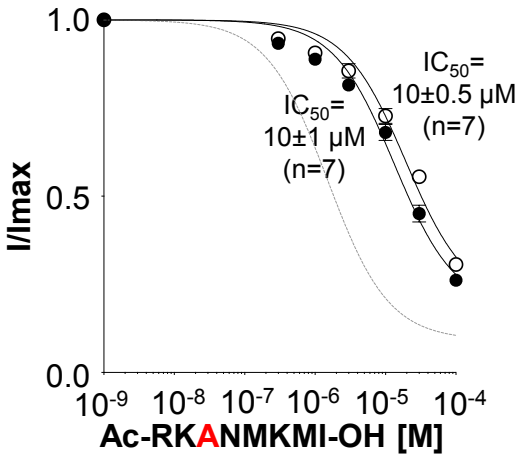

Figure 5.19: Concentration-dependent effect of Ac-RKANMKMI-OH peptide on WT BK .
A Representative concentration-dependent effect of Ac-RKANMKMI-OH synthetic peptide on HEK cells expressing WT BK . Currents were evoked by a step from -60 mV to +160 mV in the presence of 300 nM, 1, 3, 10, 30, 100 µM of Ac-RKANMKMI-OH peptide. **B** Summary concentration effect curve for the effect of Ac-RKANMKMI-OH on BK currents (n=7). Data were fitted with the Hill-Langmuir equation (grey trace Ac-RKFNMKMI-OH peptide).

A. Control (1 μM Ca^{2+})

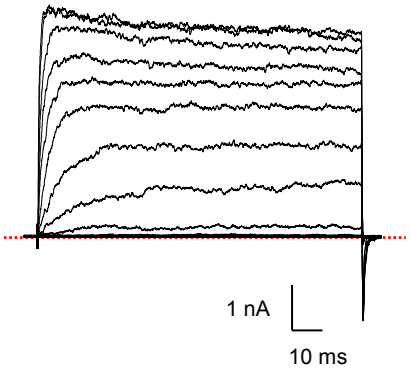

B. Ac-*RKANMKMI*-OH peptide (10 μM)

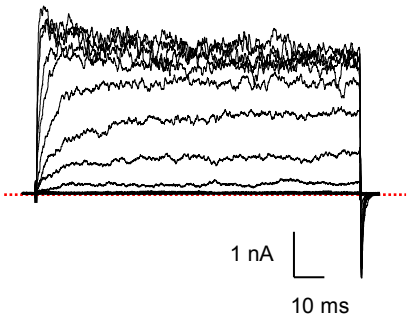

C. Summary IV

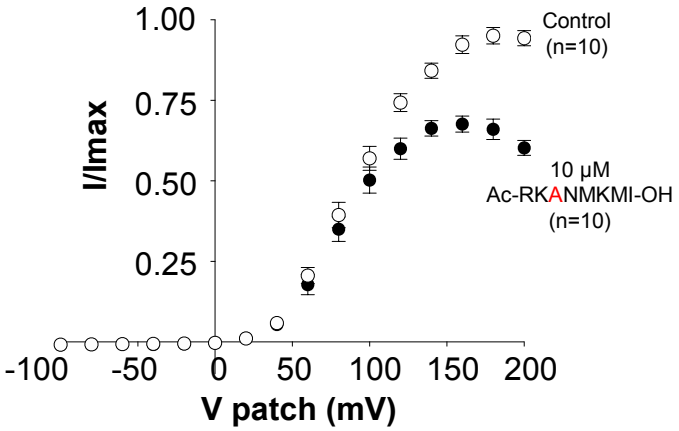

Figure 5.20: Voltage-dependence of Ac-RKANMKMI-OH peptide on WT BK .
A & **B** Macroscopic currents from inside-out patches expressing BK alone, show typical records in control (1 μM $[Ca^{2+}]_i$) and after application of 10 μM Ac-RKANMKMI-OH peptide. Patches were held at -60 mV and stepped from -100 mV to +200 mV in 20 mV increments and stepped back down to -80 mV to generate tail currents. **C** Summary of I/Imax measured in the last 5 ms of the pulse (n=10).

5.2.11 The terminal four residues of LINGO1 tail peptide (M617, K618, M619 and I620) has a minor effect on BK channels

Having established that the MKMI residues appear to be essential for inactivation and binding, we next wanted to establish if a peptide with just these residues could mimic the effects of LINGO1 protein on inactivation. We synthesised Ac-MKMI-OH peptide, which had a net charge of 0, and found that this peptide not only failed to induce inactivation, but barely inhibited BK currents. For example, in Figure 5.21A, 100 M of Ac-MKMI-OH peptide blocked only ~25% of BK current and therefore we were unable to determine the IC_{50} values with this peptide. When a family of currents were recorded during the application of 10 M of Ac-MKMI-OH peptide (Figure 5.22B) only a modest block of BK currents was observed at +200 mV, where 83±2% (n=6) of the current remained. Thus, these data suggest that a 4-residue peptide, identical to that of the C-terminus of the LINGO1 tail is insufficient to mimic the effects of the full-length protein on inactivation of BK channels.

A. Ac-*MKMI*-OH

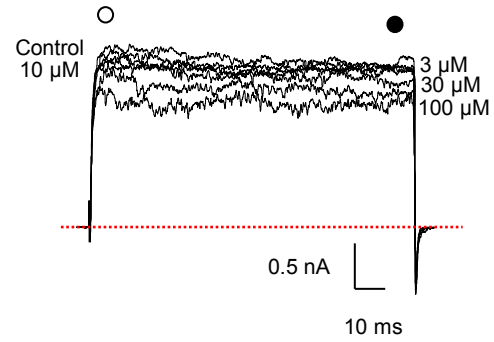

B. Summary of Ac-*MKMI*-OH

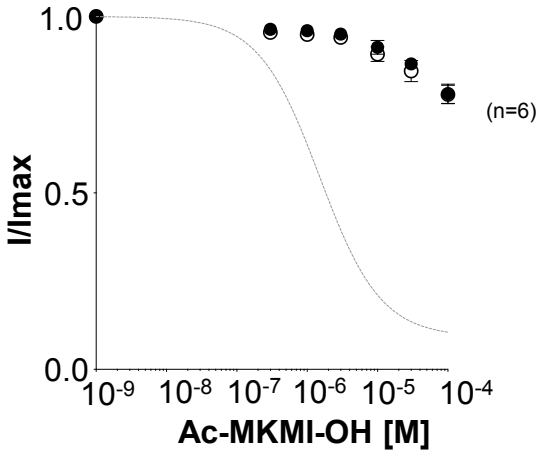

Figure 5.21: Concentration-dependent effect of Ac-MKMI-OH peptide on WT BK .
A Representative concentration-dependent effect of Ac-MKMI-OH synthetic peptide on HEK cells expressing WT BK . Currents were evoked by a step from -60 mV to +160 mV in the presence of 300 nM, 1, 3, 10, 30, 100 µM of Ac-MKMI-OH peptide. **B** Summary concentration effect curve for the effect of Ac-MKMI-OH on BK currents (n=6). Data were fitted with the Hill-Langmuir equation (grey trace Ac-RKFNMKMI-OH peptide).

A. Control (1 μM Ca^{2+})

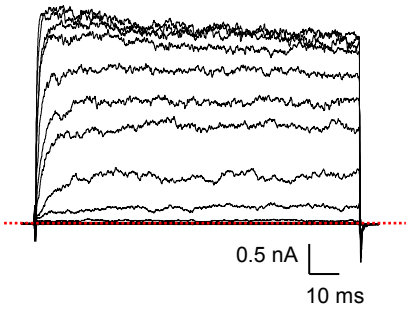

B. Ac-*MKMI*-OH peptide (10 μM)

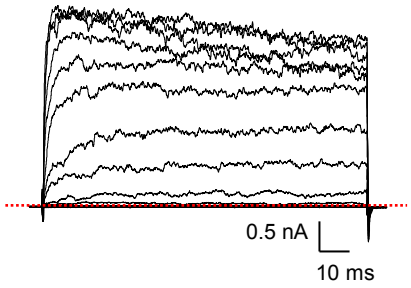

C. Summary IV

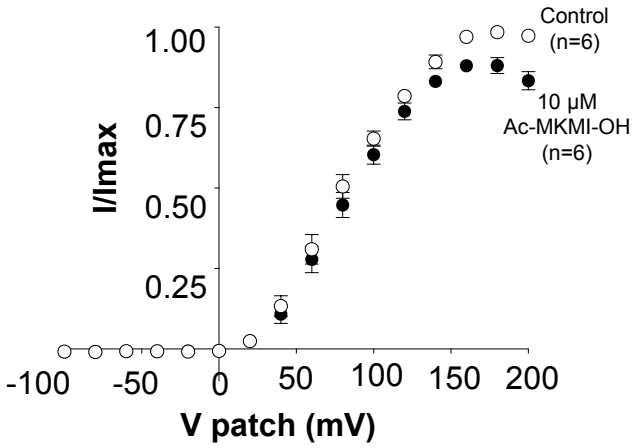

Figure 5.22: Voltage-dependence of Ac-MKMI-OH peptide on WT BK .
A & **B** Macroscopic currents from inside-out patches expressing BK alone, show typical records in control (1 μM $[Ca^{2+}]_i$) and after application of 10 μM Ac-MKMI-OH peptide. Patches were held at -60 mV and stepped from -100 mV to +200 mV in 20 mV increments and stepped back down to -80 mV to generate tail currents. **C** Summary of I/Imax measured in the last 5 ms of the pulse (n=6).

Table 5.1 The effect of acylated free acid modifications of LINGO1 peptides on BK channels

Peptide (Ac-OH)	Net charge	Inactivation	IC_{50} (last 5 ms)	Residual current at +200 mV (last 5 ms)
NH_2-RKFNMKMI-OH	+3		308±60 nM	5±1%
NH_2-MFKNKIRM-OH	+3		3±1 μM	15±2%
NH_2-RKFNMAMI-OH	+2		32±4 μM	56±3%
NH_2-RKFNMQMI-OH	+2		28±6 μM	64±4%
NH_2-AAFNMKMI-OH	+1		17±3 μM	41±5%
Ac-RKFNMKMI-OH	+2		3±1 μM	16±1%
Ac-RKFNMKAI-OH	+2		9±1 μM	61±2%
Ac-RKFNMAMI-OH	+1		94±9 μM	75±3%
Ac-RKFNAKMI-OH	+2		10±4 μM	66±3%
Ac-RKFAMKMI-OH	+2		1±0.1 μM	16±2%
Ac-RKANMKMI-OH	+2		10±1 μM	60±2%
Ac-MKMI-OH	0		ND	83±2%

A. IC_{50} last 5 ms summary

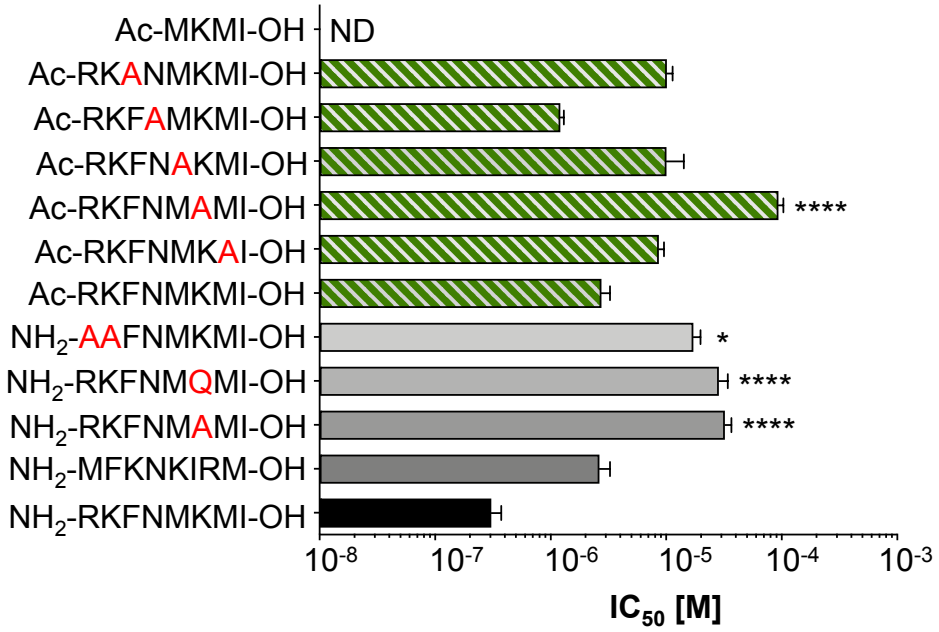

B. $_{inact}$ summary with 10 µM peptide

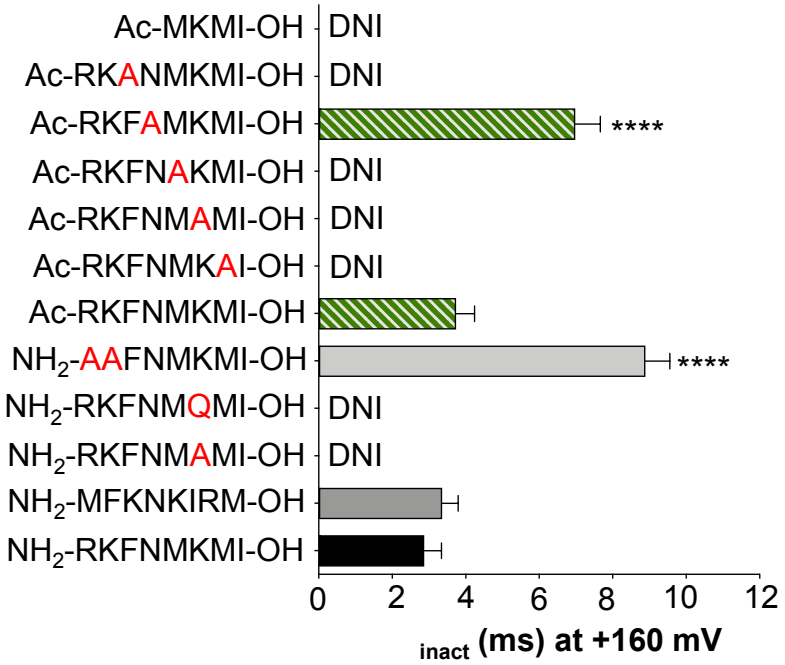

Figure 5.23: Comparison between variants of LINGO1 tail peptide on BK .
A Effect of LINGO tail peptides in the last 5 ms of the depolarising pulse, which shows IC_{50} values for LINGO1 and the variants of LINGO1 tail peptide (one-way ANOVA, * p<0.05, **** p<0.0001). **B** Mean inactivation time constant ($_{inact}$) of currents in the presence of 10 µM of LINGO1 and variants of LINGO1 tail peptide (one-way ANOVA, **** p<0.0001).

A. +100 mV summary

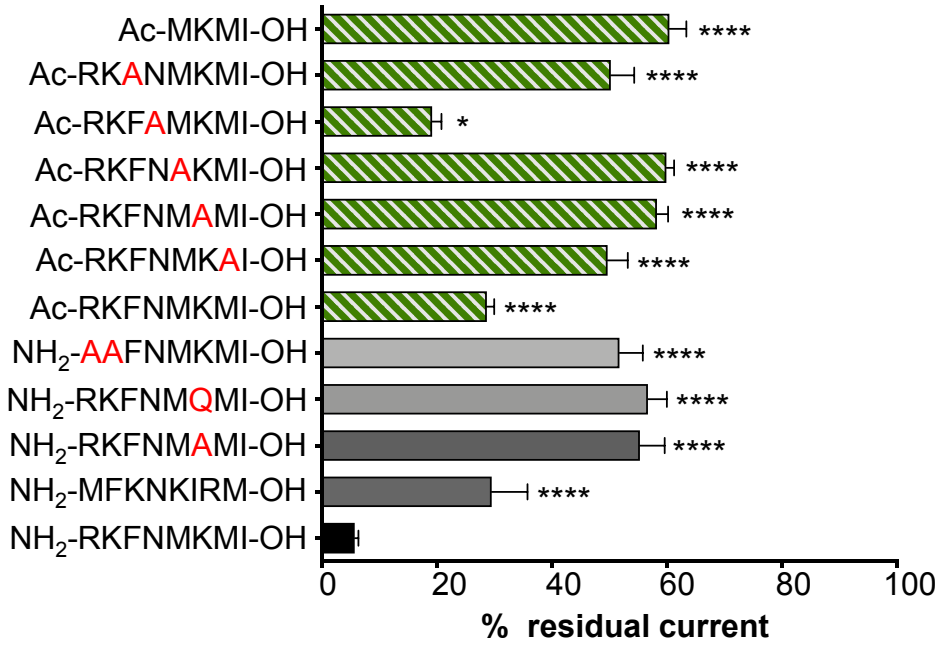

B. +200 mV summary

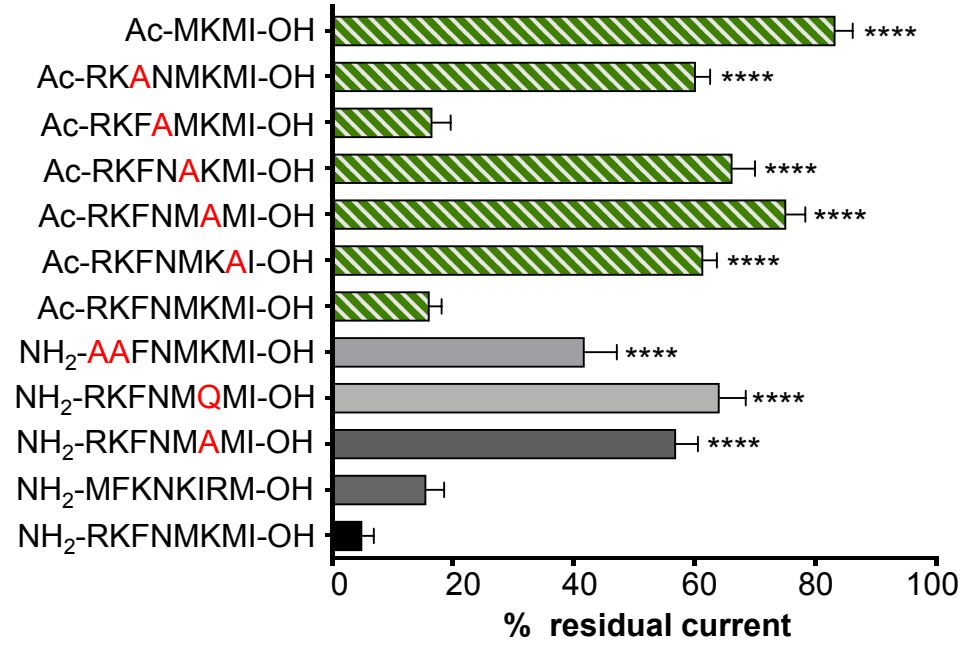

Figure 5.24: Comparison between variants of LINGO1 tail peptide on BK .
A Percentage of residual current measured in the last 5 ms at +100 mV and **B** at +200 mV in the presence of LINGO1 and variants of LINGO1 tail peptide (one-way ANOVA, * $p<0.05$, **** $p<0.0001$).

A. Summary of $_{inact}$ at +100 mV

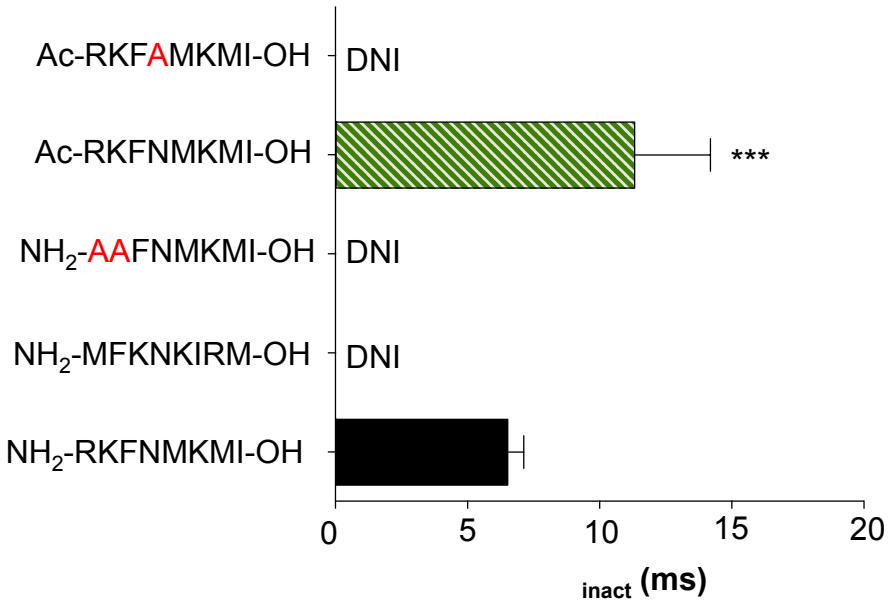

B. Summary of $_{inact}$ at +200 mV

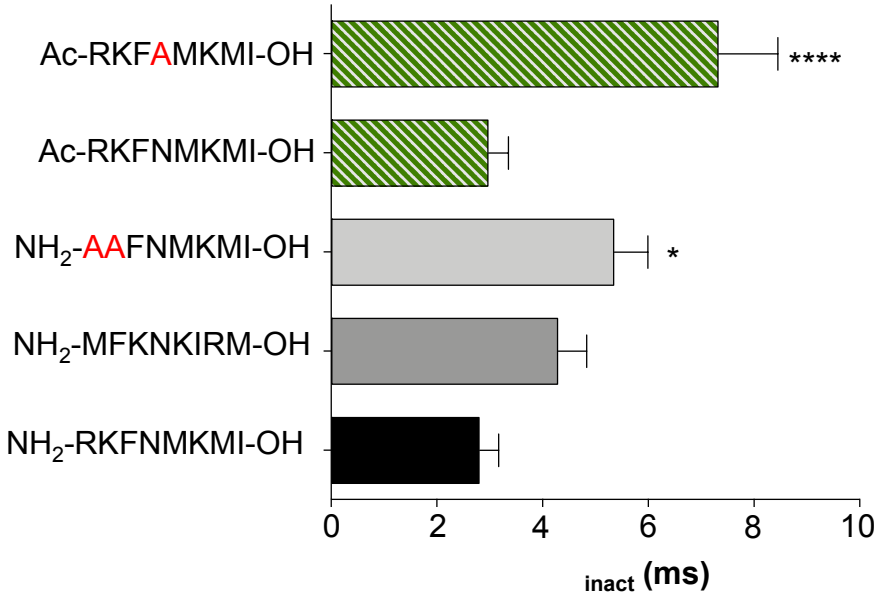

Figure 5.25: Comparison between variants of LINGO1 tail peptide on BK .
The rate of inactivation of BK currents was assessed by fitting the decay phase with a single exponential, the inactivation time constant ($_{inact}$) of currents **A** at +100 mV and **B** at +200 mV in the presence of 10 μM of LINGO1 and variants of LINGO1 tail peptide (one-way ANOVA, * p<0.05, ***p<0.001, **** p<0.0001).

Table 5.2 The effect of modifications of LINGO1 peptide on BK channels

Peptide	Net charge	Inactivation	IC_{50} (last 5 ms)	Residual current at +200 mV (last 5 ms)
NH_2-RKFNMKMI-OH	+3		308±60 nM	5±1%
Ac-RKFNMKMI-NH_2	+3		228±30 nM	3±0.1%
Ac-SSADAPRKFNMKMI-NH_2	+3		700±80 nM	2±0.2%
Ac-AKFNMKMI-NH_2	+2		2±1 μM	11±1%
Ac-RAFNMKMI-NH_2	+2		1±0.1 μM	16±3%
Ac-FNMKMI-NH_2	+1		5±1 μM	34±3%
Ac-AKFNMAMI-NH_2	+1		41±6 μM	86±2%
Ac-RAFNMAMI-NH_2	+1		92±10 μM	85±1%
Ac-AAFNMAMI-NH_2	0		ND	89±3%
Ac-RKFNMAAA-NH_2	+2		21±4 μM	69±3%
Ac-RKANMKMI-NH_2	+3		1±0.2 μM	12±2%
Ac-RKAAAKMI-NH_2	+3		3±0.3 μM	36±4%
NH_2-MFKNKIRM-OH	+3		3±1 μM	15±2%
NH_2-RKFNMAMI-OH	+2		32±4 μM	56±3%
NH_2-RKFNMQMI-OH	+2		28±6 μM	64±4%
NH_2-AAFNMKMI-OH	+1		17±3 μM	41±5%
Ac-RKFNMKMI-OH	+2		3±1 μM	16±1%
Ac-RKFNMKAI-OH	+2		9±1 μM	61±2%
Ac-RKFNMAMI-OH	+1		94±9 μM	75±3%
Ac-RKFNAKMI-OH	+2		10±4 μM	66±3%
Ac-RKFAMKMI-OH	+2		1±0.1 μM	16±2%
Ac-RKANMKMI-OH	+2		10±1 μM	60±2%
Ac-MKMI-OH	0		ND	83±2%

5.3 Discussion

In the present chapter we demonstrated the following results:

1. The position of the positively charged residues in the LINGO1 tail peptide may play an important role in binding and inactivating BK channels.
2. The reduction of net charge resulted in reduced efficacy of LINGO1 tail peptide to inactivate BK channels.
3. A number of uncharged residues in the LINGO1 tail peptide also play an important role in binding and inactivating BK channels.

A previous study by Murrell-Lagnado and Aldrich (1993a) on ShB 6-46 channels demonstrated that switching the positions of the acidic residues (E12 and D13) with the basic residues (K18 and K19) in the ShB peptide resulted in similar association and dissociation rate constants as the control ShB peptide. They further suggested that any of the charged residues within the C-terminal half of the ShB peptide would have a similar average probability of being oriented towards the binding site in ShB 6-46 channel.

In the present chapter, we first changed the order of the positively charged residues, by generating a scrambled NH_2-MFKNKIRM-OH peptide, which retained the net charge of +3. The time constant of inactivation with 10 M of this peptide was similar to amino free acid version of the WT LINGO1 peptide (Figure 5.23B) which perhaps suggested that the rate of the reaction affected by altering the position of the positively charged residues. However, this peptide inactivated BK currents only at higher concentrations, as evidenced by the rightward shift in IC_{50} values (Figure 5.23A), which perhaps indicated that the affinity of the peptide to the channel was reduced. During the application of 10 M NH_2-MFKNKIRM-OH peptide, the amount of sustained current at the end of the pulse was significantly higher at positive potentials (+100 mV and +200 mV: Figures 5.24A and B) when compared to WT peptide (NH_2-RKFNMKMI-OH), suggesting that the 'off-rate' with this peptide was increased. However, the time constant of inactivation was also significantly slower than WT peptide (Figures 5.25 A and B) which perhaps implied that the rate of the reaction was also decreased and both effects contributed to the rightward shift in IC_{50} values. These

data suggest that the net charge alone, although important, is not the sole determinant of the effectiveness of the LINGO1 peptide blocking.

We next examined the effect of replacing each positively charged residue with alanine, at R613, K614 and K618 in the LINGO1 peptide. With the NH_2-RKFNM**A**MI-OH peptide (net charge +2), we noticed four main effects, i) the inactivation was absent even at higher concentrations of the peptide, ii) there was a significant rightward shift in the IC_{50} values (Figure 5.23A), iii) the sustained current at the end of the pulse was significantly higher at positive potentials compared to the WT peptide (Figures 5.24A and B) and iv) currents were noisy in the presence of the peptide which perhaps indicated that the stability of the peptide binding was reduced. Similar effects were also observed with the replacement of a hydrophilic polar amino acid glutamine for K618 in the NH_2-RKFNM**Q**MI-OH peptide.

Interestingly, the replacement of R613 and K614 with alanine residues still resulted in inactivating BK currents (Figure 5.7), in contrast to the effect of removing the charge with the K618 mutant peptide (Figure 5.3). However, as shown in Figure 5.23B, the $_{inact}$ at +160 mV was significantly slower than that observed with the WT LINGO1 peptide, suggesting that the affinity (Murrell-Lagnado and Aldrich, 1993a; 1993b) of the block was reduced when these charges were neutralised. It is interesting to note that the apparent affinity of the NH_2-**AA**FNMKMI-OH peptide was reduced by a similar amount as the K618A mutant peptide (Figure 5.23A). This suggests that the charge and the position of K618 in the peptide are perhaps more important determinants of affinity and ability to inactivate the BK channel. Another interesting similarity between the effects of the two charge reduction peptides was that they were both less effective at maintaining block compared to the LINGO1 peptide. This was apparent when the proportion of current remaining at the end of the depolarising pulse to either +100 mV (Figure 5.24A) or +200 mV (Figure 5.24B) was compared. In the WT peptide, at +100 mV, 5±1% current remained at the end of the pulse, whereas in all of the 'charge reduced peptides', more than 50% of the peak current remained. These data suggest that the positively charged residues in the tail may also contribute to the stability of the block, once the block has

occurred. The noisy currents observed in the presence of these peptides (Figures 5.4B, 5.6B and 5.8B) are consistent with this suggestion.

Previously it has been shown that the net charge on Shaker ball peptides affected the association rates of the peptide with the Shaker channels. In 1993, a study by Murrell-Lagnado and Aldrich investigated the factors which determined the block and inactivation of ShB peptide on ShB 6-46 channels. It was observed that the peptide valence and the substitution of uncharged polar residues with charged residues, produced only small changes in the association rate constant of the peptide to the channel (Murrell-Lagnado and Aldrich, 1993a; 1993b).

In the previous chapter, we utilised acylated amide modifications of LINGO1 peptide and demonstrated that the positively charged residues along with the net positive charge of the peptide, played an important role in the LINGO1 peptide-mediated inactivation of BK channels. In the present chapter, we focussed on acylated free acid modifications of the LINGO1 peptide, where the R613 residue had an acylated (Ac) N-terminus and the I620 residue had a free acid (OH) at the end of the C-terminus. We adapted this modification in order to replicate the condition of the full-length LINGO1 protein and the effects of these peptides are summarised in Table 5.1. In addition, the effects of all the modifications of LINGO1 peptide on BK channels are summarised in Table 5.2.

The next modification was the reduction in the net positive charge from +3 to +2 by the addition of an acyl group at the N-terminus (Ac-RKFNMKMI-OH). This peptide did inactivate the BK currents, but it was less potent compared to the WT LINGO1 peptide, as evidenced by a rightward shift in the IC_{50} values (Figure 5.23A). However, the decay phase, when fitted with a single exponential, was similar to the WT peptide (Figure 5.23B), suggesting that reducing the net charge, by acylating the N-terminus of the tail, did not significantly reduce the rate of the ‘ ɵmeac. The amount of sustained current during the application of 10 M Ac-RKFNMKMI-OH peptide at the end of the pulse was also higher compared to the WT peptide at +100 mV and +200 mV (Figures 5.24A and B). The time constant of inactivation at +100 mV was significantly slower compared to WT peptide (Figures 5.25A). These results suggest that the reduction of net charge altered the efficacy of the LINGO1 peptide to inactivate BK channels.

Previous studies have demonstrated that the positively charged residues in the ShB peptide participated in long-range electrostatic interactions and in turn enhanced the concentration of peptide at its putative binding site in the ShB Δ6-46 channels (Murrell-Lagnado and Aldrich, 1993a; 1993b). In addition, Li and Aldrich (2006) demonstrated that both electrostatic and hydrophobic interactions were critical for binding of the enhanced ball peptide (EBP) in the BK channel pore. Our results from Chapter 4 also indicated that perhaps the charged and uncharged residues of the LINGO1 peptide participated in electrostatic and hydrophobic interactions with the residues in the BK channel pore to stabilise the binding of the peptide and thereby induce inactivation of BK currents.

We then further investigated the role of charged and uncharged residues with the acylated free acid modifications of LINGO1 peptide-mediated inactivation of BK channels. Interestingly, the replacement of F615, M617, K618 and M619 with alanine residues all resulted in similar effects. It is interesting to note that the replacement of the bulky phenylalanine at 615 or the sulphur containing methionine (M617 or M619) residues with less hydrophobic alanine residues abolished inactivation despite maintaining a net charge of +2. We noticed that these mutant peptides failed to induce inactivation even with higher concentrations of the peptide (Figures 5.11A, 5.13A, 5.15A and 5.19A). The IC_{50} values showed a significant rightward shift compared to 'control' Ac-RKFNMKMI-OH peptide (Figure 5.23A) suggesting that these peptides had an altered affinity to BK channels. Interestingly, in the presence of 10 M of all these mutant peptides the amount of sustained current was greater than 60% which was significantly higher than the control peptide (Figures 5.24A and B) indicating that the binding of these peptides was unstable, maybe due to the increased rate of 'off-rate'. These results suggest that the replacement of the F615, M617, K618 and M619 with alanine residues may block of the LINGO1 tail peptide in the BK channel pore. However, to confirm this additional single channel experiments will be required.

When we investigated the effect of the 4-residue Ac-MKMI-OH peptide, we noted that this peptide not only failed to induce inactivation of BK currents, but barely reduced BK current amplitude, even with 100 M of the peptide (Figure 5.21). It is clear from Figures 5.24A and B, that the amount of sustained current at the

end of the pulse was significantly higher at potentials positive to +100 mV compared to the control peptide. These results indicated that the binding of this peptide was more unstable, presumably as a result of a very large increase in ‘ e rf af o f t h é reaction. These results are also consistent with the idea that other charged and uncharged residues in the LINGO1 tail peptide may participate in hydrophobic and electrostatic interactions with the BK channel pore to induce inactivation of BK channels. The individual role of isoleucine at 620 in the LINGO1 tail peptide-mediated inactivation of BK channels remains to be elucidated.

Our results so far suggested that the replacement of F615, M617, K618 and M619 with alanine residues in the LINGO1 peptide abolished the inactivation of BK currents, suggesting that this region was critical for inactivation, even though a peptide of just the terminal four residues could not mimic inactivation. In our final modification, we attempted to investigate if any other residues were critical, and we examined the effects of replacing the asparagine at position 616 with alanine residue. With the Ac-RKF**A**MKMI-OH peptide, we noted that the peptide still inactivated BK channels, but showed a rightward shift in IC_{50} values (Figure 5.23A), indicative of a reduced binding affinity. The peptide also showed a slower time constant of inactivation than the Ac-RKFNMKMI-OH peptide (Figure 5.23B) s u g g e s t i n g - r t a h o f a h e ’ r e a c t i o n a l s o r e d u c e d. However, the sustained current that remained at the end of the pulse was similar to that of the Ac-RKFNMKMI-OH peptide (Figure 5.24B) s u g g e s t i n g - t h a t a e ’ t h e t reaction was unaffected with this peptide. This data suggested that although the substitution of N617 with alanine reduced the efficacy of LINGO1 tail peptide, its effects were better tolerated than substitutions closer to the C-terminus.

Murrell-Lagnado and Aldrich (1993a, 1993b) demonstrated that the hydrophobic residues in the N-terminal half of the ShB peptide were crucial for stabilising the bound peptide-channel complex and mainly influenced the dissociation or off-rates. In contrast, they demonstrated that the charged residues in the C-terminal half, influenced the association or on-rates of the ShB peptide in the pore of the ShBΔ6-46 channels. They suggested that these residues increased molecular encounters caused via long-range electrostatic interactions between the charged residues and the binding site in the ShBΔ6-46 channel pore. Thus, they

suggested that the electrostatic interactions may be involved in correctly orientating the peptide for binding. A previous study by Gonzalez-Perez *et al.* (2012) illustrated the importance of the orientation of the BK 3a peptide at inducing inactivation of BK channels. In their study, they examined the efficacy of the enantiomers of the 3a peptide and demonstrated that the D-enantiomer had a lower affinity than the L-enantiomer on BK channels. These data suggest that the binding of the inactivating peptides, such as the 3a peptide, to BK channels was stereospecific.

In the present chapter, we utilised the acylated free acid modifications of LINGO1 peptide which reduced the net charge of the peptide by 1. These untethered short chains of amino acids have more freedom in solution compared to the tethered LINGO1 protein and presumably can bind to the BK channels in more than one way. The reduction of net charge might affect the orientation and conformational folding of the LINGO1 peptide in solution, which in turn may result in reduced efficacy of the peptide to inactivate BK channels. These results perhaps suggest that the functional role of the charged residues of the LINGO1 peptide depend on their position within the peptide to mediate inactivation of BK channels.

6. The effects of LINGO1 tail peptide are reduced by mutations in the S6 helix of BK channels

6.1 Introduction

In the previous chapters, the data demonstrated that co-expression of LINGO1 with BK , or addition of LINGO1 tail peptide to WT BK channels, induced inactivation of BK channels and slowed their deactivation. This latter effect suggests that the LINGO1 tail peptide interferes with channel closing and may suggest that the tail peptide inserts itself into the channel pore. A similar mechanism of action has been proposed for both BK 2 and 3 subunits, as well as some K_V regulatory subunits (Wallner *et al*. 1999; Lingle *et al*. 2001; Li *et al*. 2016; Pisupati *et al*. 2018).

The QA ions are well-established cytosolic blockers of BK channels (Latorre *et al*. 2017). In 2001, Zhou *et al.* demonstrated that the binding site for the inactivation gate and the quaternary ammonium compounds was located in the hydrophobic central cavity and the inner pore of the KcsA K^+ channel, as illustrated in Figure 6.1.

Figure 6.1: Three-dimensional model of quaternary ammonium (QA) ions binding with KcsA K^+ channel. Ribbon diagram of two subunits of the KcsA channel are shown in beige and quaternary ammonium (QA) ions shown in stick format, below the K^+ ions (purple spheres, Adapted from Zhou *et al.* 2001 and Kutluay *et al*. 2005).

When QA was applied to excised patches expressing BK + 2 the rate of inactivation remained unchanged, suggesting that the inactivation induced by 2 subunits was independent of the site necessary for QA binding (Xia *et al*. 1999). Similarly, when 3b subunits were co-expressed with BK , they inactivated BK currents (Xia *et al*. 2000). Upon application of cytosolic blocker tetraethylammonium (TEA), this inactivation remained unchanged, suggesting that there was no competition between the 3b mediated inactivation and TEA (Xia *et al*. 2000) and consequently that their binding sites differed.

Similar studies have been carried out with a combination of enhanced ball peptide (EBP) and TBA to determine if they showed competition with the binding site to block BK channels and it was shown that the apparent rate of block of EBP was slowed down by TBA, suggesting that the binding site of EBP and TBA were common (Li and Aldrich, 2006).

In 1993, Murrell-Lagnado and Aldrich identified that ShB peptide binding to ShB 6-46 channels was significantly influenced by changes in the charged residues in the C-terminal and the hydrophobic residues in the N-terminal (Murrell-Lagnado and Aldrich, 1993a; 1993b). Thereafter, Li and Aldrich (2006) investigated if the charged residues present at the internal entrance to the BK channel pore played a role in the binding of EBP to the channels. The negatively charged residues E321 and E324 regulate the single channel conductance of BK channel through electrostatic interactions (Brelidze *et al.* 2003; Nimigean *et al*. 2003). Li and Aldrich (2006) also suggested that an electrostatic interaction occurred between the BK channel and the positively charged EBP, since the double mutant E321N:E324N showed ~10-fold reduction in the apparent affinity for the peptide.

In this study, we first examined if the LINGO1 tail peptide inactivation was altered in the presence of the QA, tetrapentylammoniumbromide (TPAB). Having established that the LINGO1 tail peptide competed with TPAB, we next examined if the negatively charged residues E321 and E324 in the intracellular pore and T287, situated deep within the pore of the BK channel, contributed to the inactivation induced by LINGO1 tail peptide.

6.2 Results

To test if the LINGO1 tail peptide inserted into the pore of the BK channel, we carried out a series of experiments in which the tail peptide was applied to the cytosolic surface of patches in the absence and presence of QA ions. These QA ions have been previously shown to bind in the deep pore region of K^+ channels (Zhou *et al*. 2001) and have been shown to compete with inactivating subunits of the mutant Shaker channels (Choi *et al*. 1991). Consequently, if LINGO1 and QA competed for the same site in the pore, we might expect that the apparent concentration of LINGO1 in the pore region would be reduced in the presence of QA. Since the time constant of inactivation of BK channels was dependent on the [LINGO1] (Figure 3.4), we would expect that the BK channels would inactivate more slowly in the presence of QA, if they compete for the same site. To test this, we bathed excised patches in 1 M $[Ca^{2+}]_i$ and stepped them from -60 mV to +160 mV before applying the amino, free acid version (NH_2-RKFNMKMI-OH) of the LINGO1 tail peptide. Figure 6.2A shows a typical example of the effect of 3 M LINGO1 tail peptide on BK currents, where the peak current (measured in the first 5 ms of the depolarising pulse) was reduced by 30% and the current inactivated with a time constant of 6 ms. The LINGO1 tail peptide was then washed out, prior to the application of 3 M TPAB, which itself reduced the BK current amplitude by ~30% (Figure 6.2B). When the tail peptide (3 M) was reintroduced, in the presence of 3 M TPAB, it still reduced BK current (by ~34%) and induced inactivation. However, when the inactivating current was fitted with a single exponential, the time constant of inactivation was slightly slower (9 ms). This effect is observed more easily in Figure 6.2C, where the currents in the presence of 3 M LINGO1 and 3 M LINGO1+3 M TPAB (red trace) were scaled in amplitude. In seven similar patches, TPAB (3 M) reduced the BK current amplitude by 27±3% (Figure 6.2D) and the time constant of inactivation slowed from 6.7±1 ms under control to 10±1 ms ($p<0.01$, paired t-test) in the presence of TPAB and LINGO1 tail peptide (Figure 6.2E). We also examined the effect of a higher concentration of TPAB (10 M), which reduced the BK current amplitude by 69±4% (Figure 6.3D, $p<0.0001$, one-way ANOVA) as shown in Figure 6.3B. In the continued presence of TPAB, LINGO1 tail peptide inactivated the channel

with a time constant of 25±2 ms, which was significantly slower than that observed in the absence of TPAB (Figure 6.3E, n=8, p<0.0001, paired t-test). This was clearly observed in Figure 6.3C, in which the currents in the presence of 3 M LINGO1 and 3 M LINGO1+10 M TPAB (red trace) were scaled in amplitude. Taken together, these results suggest that the LINGO1 tail peptide competes with TPAB for a common binding site and supports the idea that LINGO1 may induce inactivation by inserting into the pore region of the BK channel.

To examine if the peptide could insert itself into the open BK channel pore, we collaborated with Dr Irina Tikhonova (Q ueen's U niversityBelfast), who produced a homology model of the LINGO1 tail peptide and examined its ability to dock in the BK pore. This is shown in Figure 6.4 and illustrates that the LINGO1 tail peptide can insert itself, with the correct orientation, into the pore of the Ca^{2+} bound structure of a homology model of the human BK channel based on the *Aplysia* BK channel structure (5TJ6, Tao *et al*. 2017) as at the time of these experiments the human BK channel structure was not available. In this figure only three of the four BK subunits are shown (in red, green and gold) for clarity. The residues marked in white represent the two negatively charged BK glutamic acid residues (E) at position 321 and 324 of the S6 helices. The tail of LINGO1, shown as blue sticks, sits centrally in the pore and the last three residues of the C-terminus approached residue T287 (marked as sticks), which signified the internal entrance to the selectivity filter of the BK channel. Note the proximity of the four K^+ ions in the selectivity filter to the C-terminus end of LINGO1 tail peptide.

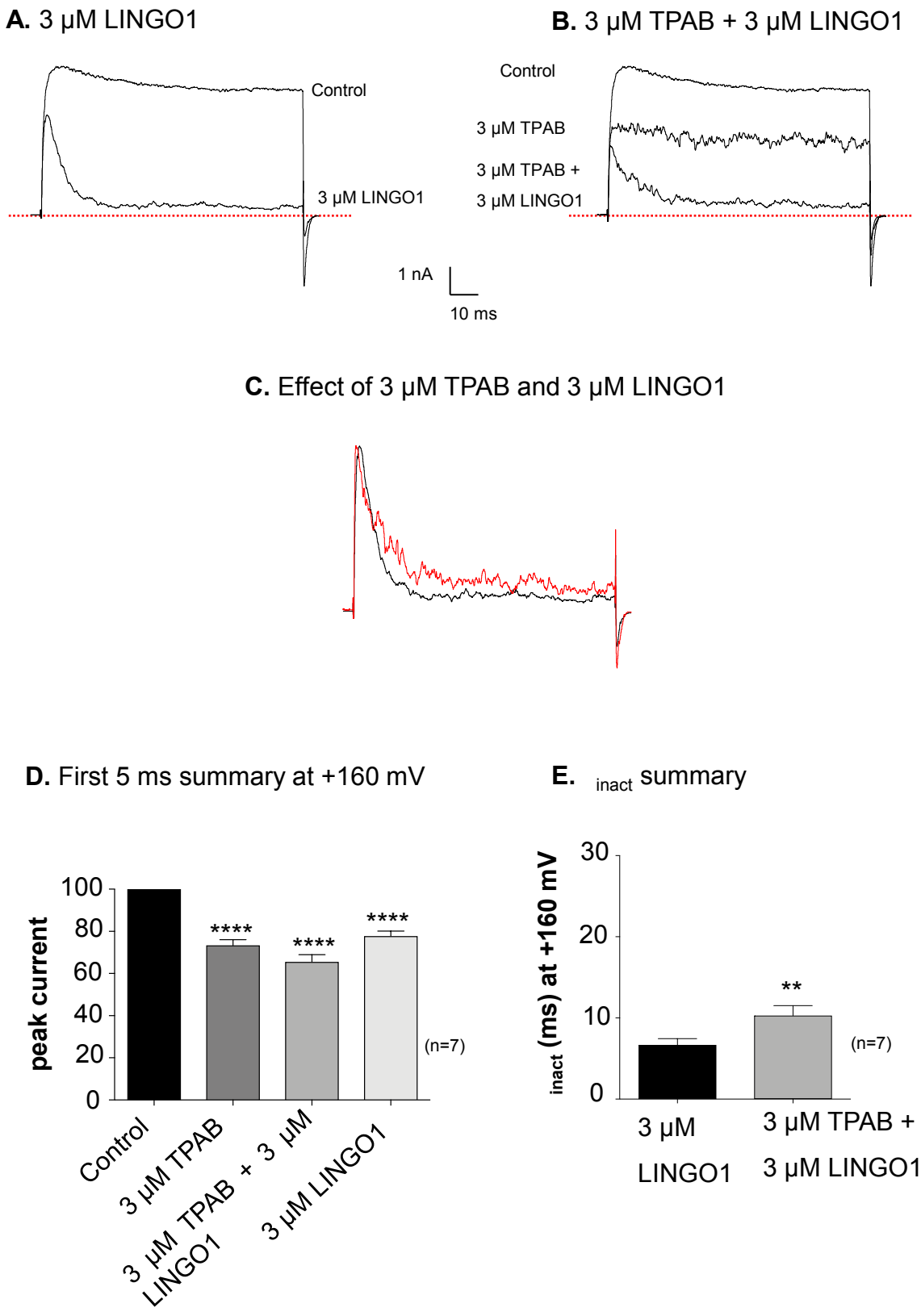

Figure 6.2: Combinative effect of TPAB and LINGO1 (NH_2-RKFNMKMI-OH) tail peptide on WT BK . Macroscopic BK currents evoked by a step from -60 mV to +160 mV in the presence of 3 µM LINGO1 (**A**), 3 µM TPAB and a combination of both (**B**). **C** Effect of 3 µM TPAB + 3 µM LINGO1 shown in scaled traces (red) and 3 µM LINGO1 (black trace). **D** Percentage of peak current in the first 5 ms of the depolarising pulse (n=7, one-way ANOVA, **** p<0.0001). **E** Mean inactivation time constant ($_{inact}$) of currents in the presence of 3 µM LINGO1 alone and a combination of 3 µM TPAB and 3 µM LINGO1 (n=7, paired t-test , ** p<0.01).

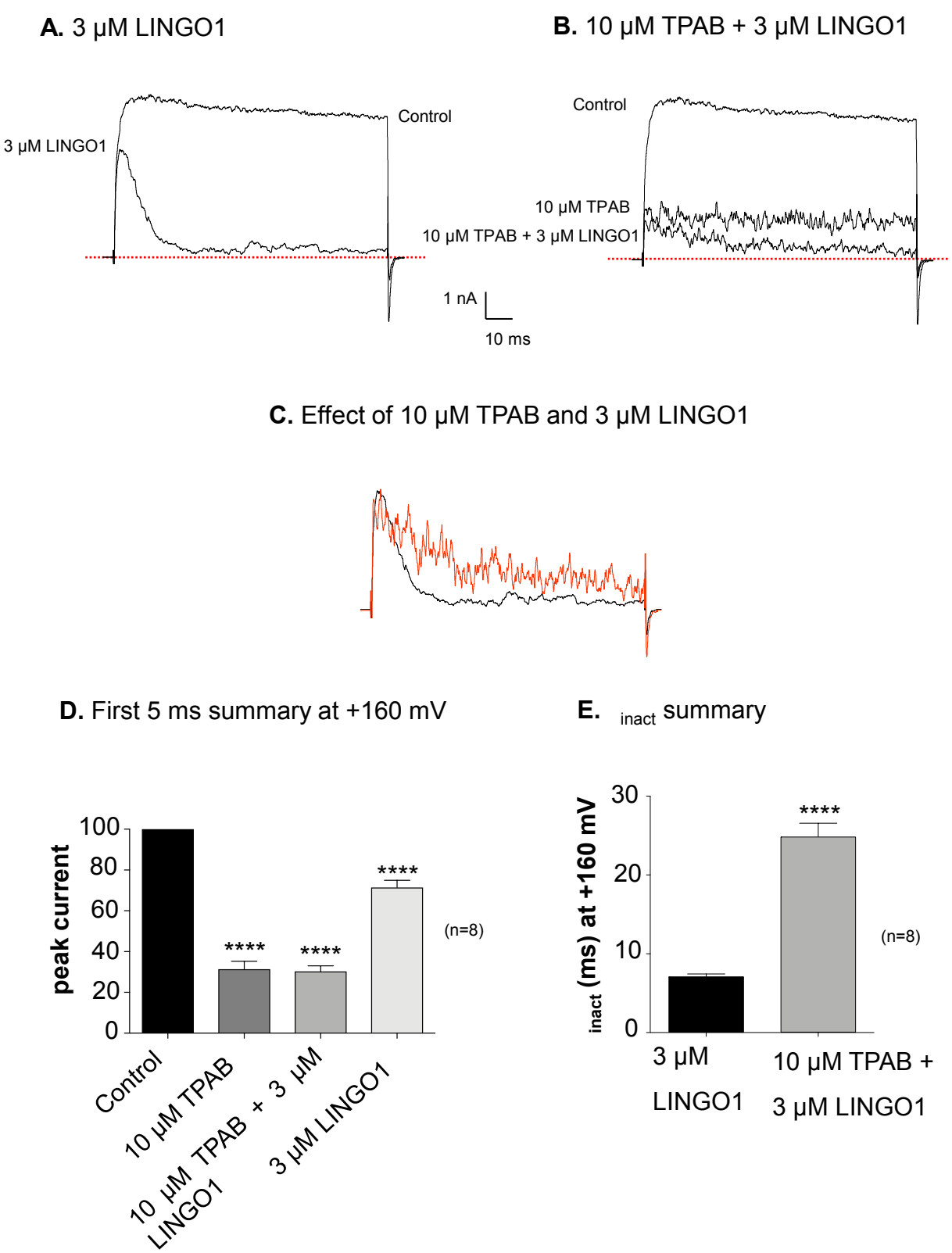

Figure 6.3: Combinative effect of TPAB and LINGO1 (NH_2-RKFNMKMI-OH) tail peptide on WT BK . Macroscopic BK currents evoked by a step from -60 mV to +160 mV in the presence of 3 µM LINGO1 (**A**), 10 µM TPAB and a combination of both (**B**). **C** Effect of 10 µM TPAB + 3 µM LINGO1 shown in scaled traces (red) and 3 µM LINGO1 (black trace). **D** Percentage of peak current in the first 5 ms of the depolarising pulse (n=8, one-way ANOVA, **** p<0.0001). **E** Mean inactivation time constant ($_{inact}$) of currents in the presence of 3 µM LINGO1 alone and a combination of 10 µM TPAB and 3 µM LINGO1 (n=8, paired t-test, **** p<0.0001).

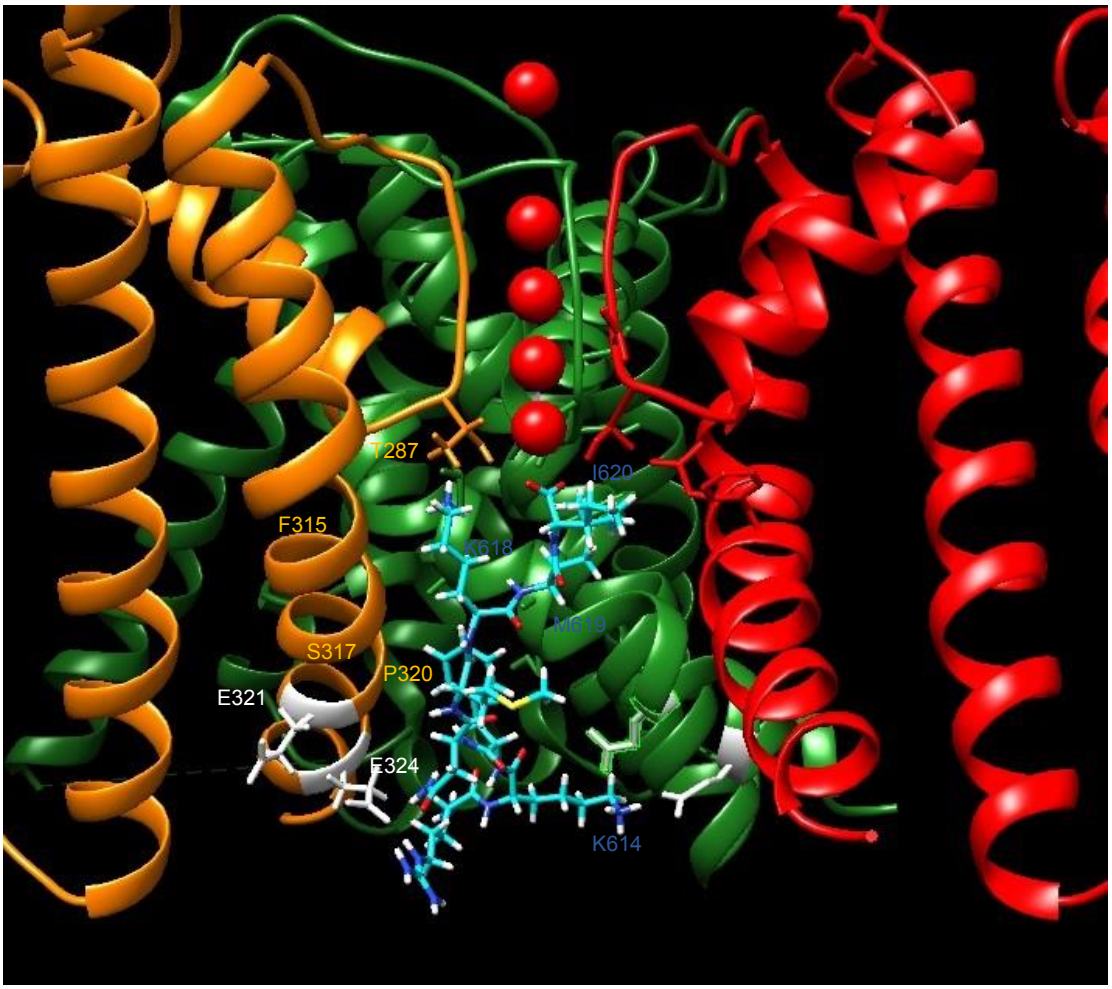

Figure 6.4: Chimera model of LINGO1 (NH_2-RKFNMKMI-OH) synthetic tail peptide docking into BK channel. Pore region of the human BK channel based on *Aplysia* BK channel (5TJ6) structure, of which only 3 of the four BK subunits are shown (red, green and gold). The residues marked in white represent the two negatively charged glutamic acid residues (E) at position 321 and 324 of the S6 helices. The tail of LINGO1 peptide (blue sticks), aligns in the pore and the last three residues of its C-terminus approach residue T287 (marked as sticks), which signifies the internal entrance to the selectivity filter of the BK channel. Note the proximity of the four K^+ ions in the selectivity filter, to the C-terminus end of LINGO1 tail peptide.

6.2.1 Effect of mutating negatively charged pore lining residues on the response to LINGO1 tail peptide

Based on the model shown in Figure 6.4, we identified a number of residues in the BK channel pore, that may interact with the tail of LINGO1 peptide. Firstly, we examined the effects of replacing the negatively charged E324 with an uncharged hydrophobic, alanine residue. Note that the large positively charged sidechain of K614 in LINGO1 tail peptide sits between the negatively charged sidechains of E321 and E324 of BK in subunit B shown in green.

The excised patches were held at -60 mV and currents were elicited by stepping to +160 mV in 1 M $[Ca^{2+}]_i$ before stepping down to -80 mV to evoke tail currents. Note that the E324A mutant activated ~–20 mV more negatively (compare Figures 3.5C and 6.6C) than WT BK , as shown previously by Tian *et al.* (2019). In this mutant, the LINGO1 peptide still caused inactivation and reduced the amplitude of the BK currents in a concentration-dependent manner (300 nM to 100 M) as shown in Figure 6.5A. When the IC_{50} values were calculated from currents measured in the first and last 5 ms of the depolarising pulses (white and black symbols respectively, Figure 6.5B), they yielded values of 14±1 μM and 1±0.4 M (n=6, $p<0.001$, paired t-test) respectively. The IC_{50} value recorded for the last 5 ms was approximately 3-fold higher than that recorded from WT BK channels ($p<0.05$, unpaired t-test) shown as a grey dotted line in Figure 6.5B. However, we noticed that the time constant of inactivation induced by 300 nM LINGO1 tail peptide appeared to be faster in this mutant than WT BK ($p<0.0001$, unpaired t-test), although there were no significant differences at any other concentrations (ns, one-way ANOVA). We next examined if the apparent voltage-dependence of block by the LINGO1 tail peptide was altered in the E324A mutant, by comparing families of currents generated by pulses up to +200 mV, in the absence and presence of 10 M LINGO1 tail peptide. As Figure 6.6B suggests, the tail peptide still inactivated the BK channels, but there was more residual current left at the end of each depolarising pulse. This was summarised for 8 similar experiments in Figure 6.6C where the normalised peak current was measured in the last 5 ms of each pulse before (open symbols) and after (closed symbols) application of the tail peptide. Note that these normalised currents activated at more negative potentials, compared to WT BK, as previously

demonstrated (Tian *et al.* 2019). A comparison of Figure 6.6C with the WT BK channels (Figure 3.5C), also showed that more residual current was present in the E324A mutant, in the presence of the peptide. For example, at +100 mV in WT BK, only 5±1% of current remained, compared to 21±3% in the E324A mutant ($p<0.01$, Mann-Whitney test). To analyse if the E324A mutant altered the apparent voltage-dependence of inactivation induced by the LINGO1 tail peptide, the decaying phase of the currents at each potential in Figure 6.6B was fitted with a single exponential and data from 8 such experiments was summarised in Figure 6.6D. We were unable to accurately fit the currents at potentials more negative to +120 mV, but at more positive potentials, the currents inactivated with time courses very similar to that observed with the WT BK channels (ns, one-way ANOVA).

A. E324A with LINGO1 *(NH_2-RKFNMKMI-OH)*

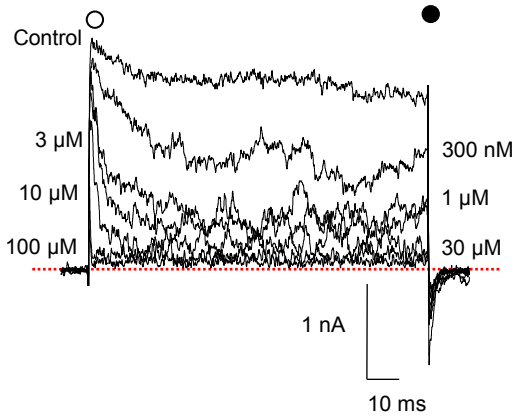

B. Summary

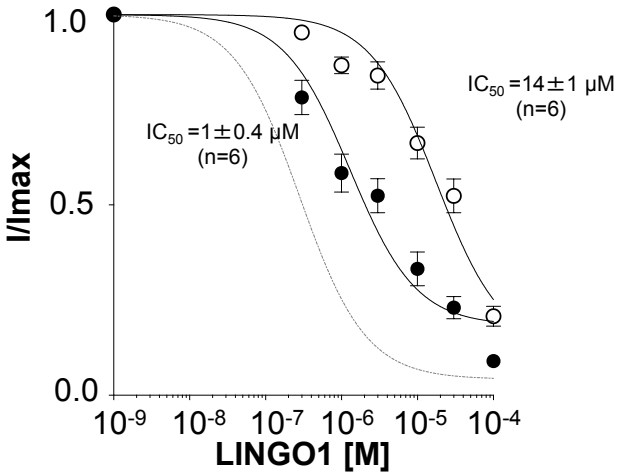

C. Summary of LINGO1 $_{inact}$

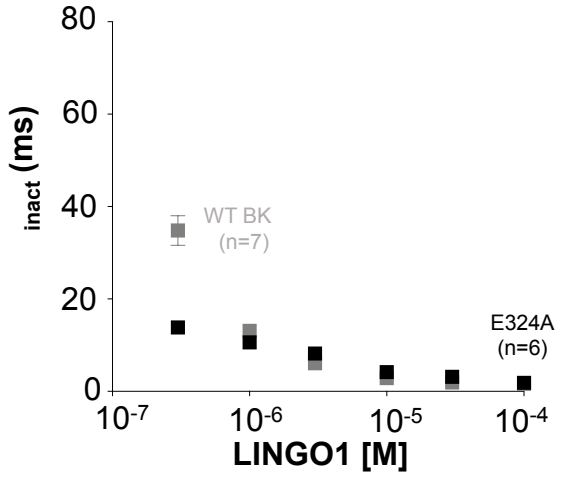

Figure 6.5: Concentration-dependent effect of LINGO1 (NH_2-RKFNMKMI-OH) tail peptide on E324A mutant BK .
A Representative concentration-dependent effect of LINGO1 tail peptide on HEK cells expressing E324A mutant BK currents. Currents were evoked by a step from -60 mV to +160 mV in the presence of 300 nM, 1, 3, 10, 30, 100 μM of LINGO1 tail peptide. **B** Summary concentration effect curve for the effect of LINGO1 tail peptide on E324A mutant BK currents (n=6). Data were fitted with the Hill-Langmuir equation (grey trace WT BK). **C** The rate of inactivation of BK currents was assessed by fitting the decay phase with a single exponential. The rate of inactivation increased with the concentration of LINGO1 tail peptide (grey squares WT BK).

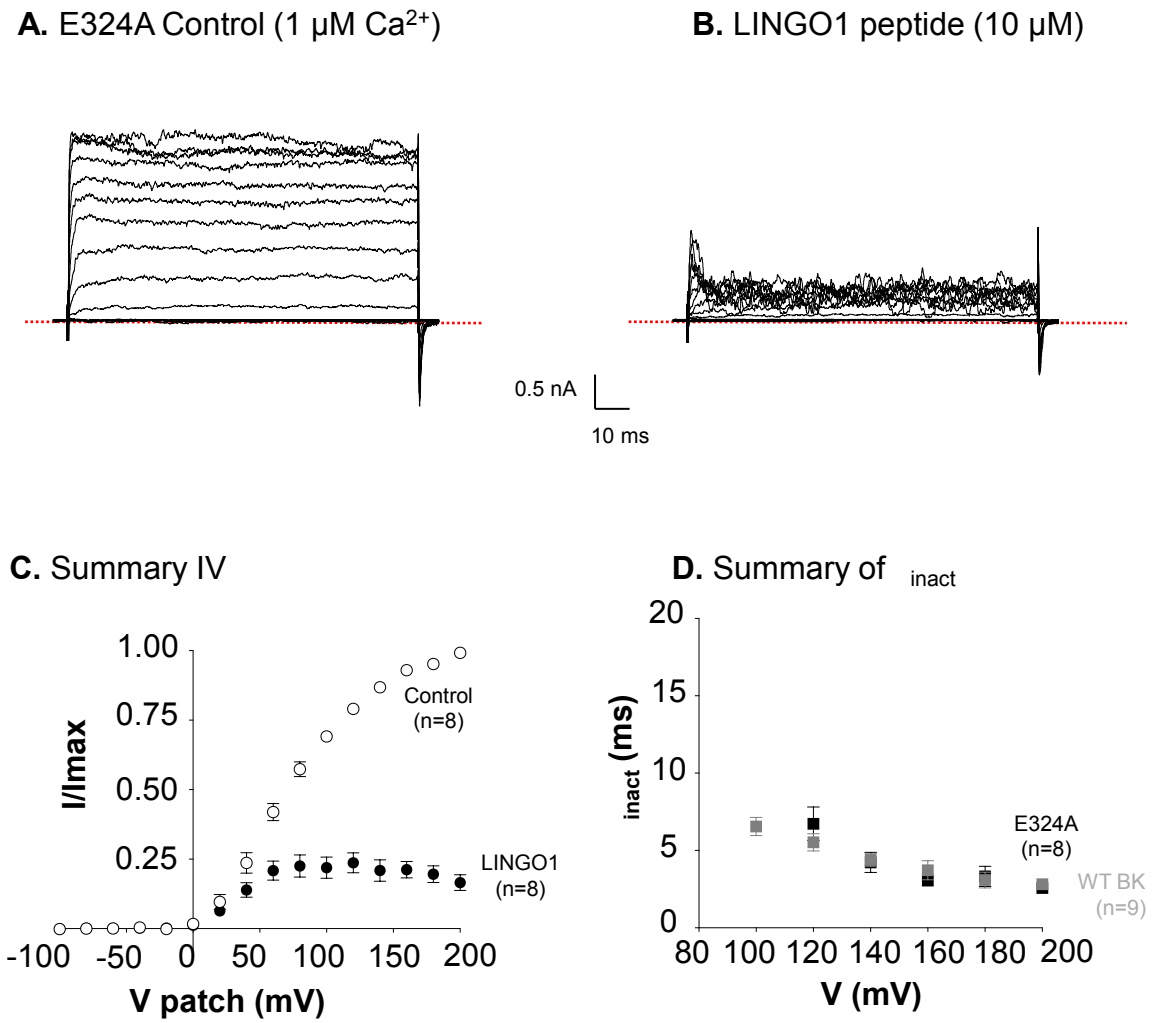

Figure 6.6: Voltage-dependence of LINGO1 (NH_2-RKFNMKMI-OH) tail peptide on E324A mutant BK .
A & **B** Macroscopic currents from inside-out patches expressing E324A mutant BK alone, show typical records in control (1 μM $[Ca^{2+}]_i$) and after application of 10 μM LINGO1 tail peptide. Patches were held at -60 mV and stepped from -100 mV to +200 mV in 20 mV increments and stepped back down to -80 mV to generate tail currents. **C** Summary of I/Imax measured in the last 5 ms of the pulse (n=8). **D** The rate of inactivation of BK currents was assessed by fitting the decay phase with a single exponential. The currents showed an apparent voltage-dependence at more positive potentials (grey squares WT BK).

6.2.2 Neutralisation of charge on E321 and E324 with an E321A:E324A double mutant reduces the effect of LINGO1 tail peptide on BK currents

Having established that neutralisation of E324 in BK reduced the ability of the tail peptide to block the BK current, we next examined the effect of neutralising both negative charges in this region of S6 helix by producing an E321A:E324A double mutant. Note that this mutant has previously been shown to cause a large leftward shift (–81 mV) in the activation $V_{1/2}$ as compared to WT channels (Tian *et al.* 2019) and this was evident in the summary IV curve shown in Figures 6.8A and C, where inward currents were apparent at negative membrane potentials. When we applied increasing concentrations of the LINGO1 tail peptide, it was clear that the peptide still induced inactivation, but its potency was reduced, as illustrated in Figure 6.7A. This was reflected in the summary data from 5 similar experiments in Figure 6.7B, in which the IC_{50} was determined from currents measured in the first 5 ms (open symbols) was 60±18 M and last 5 ms was 14±3 M of the depolarisation pulse (closed symbols). These values were not significantly different to each other (ns, paired t-test). However, the IC_{50} was approximately 14-fold higher than that determined for the E324A mutant ($p<0.001$, unpaired t-test) and 46-fold higher than that recorded in WT BK channels ($p<0.001$, unpaired t-test), shown as a grey dashed line in Figure 6.7B. However, as shown in Figure 6.7C, the rate of inactivation of the channels increased in a concentration-dependent manner. The rate of inactivation induced by the peptide appeared to be slower at concentrations >1 M in this mutant and it was statistically significant ($p<0.01$, one-way ANOVA). To determine if the E321A:E324A mutation altered the apparent voltage-dependence of LINGO1 tail peptide binding, we compared families of currents generated before and during the application of 10 M LINGO1. As Figure 6.8B suggests, 10 M of LINGO1 tail peptide induced inactivation but there was even more sustained current left at the end of the depolarisation pulse, when compared to the E324A mutant. This effect was summarised in Figure 6.8C, at +100 mV, 61±3% (n=5) of sustained current remained at the end of the pulse which was much higher than that observed with the E324A mutant (21±3%, $p<0.01$, Mann-Whitney test) and WT BK (5±1%, $p<0.001$, Mann-Whitney test). To assess how the rate of inactivation induced by 10 M peptide varied with voltage, the decay phase of the current at

each potential was fitted with a single exponential and the data from 5 experiments was summarised in Figure 6.8D. The time constant of inactivation of these currents was significantly slower compared to WT BK channels at all voltages measured ($p<0.001$, one-way ANOVA).

A. E321A:E324A with LINGO1 *(NH_2-RKFNMKMI-OH)*

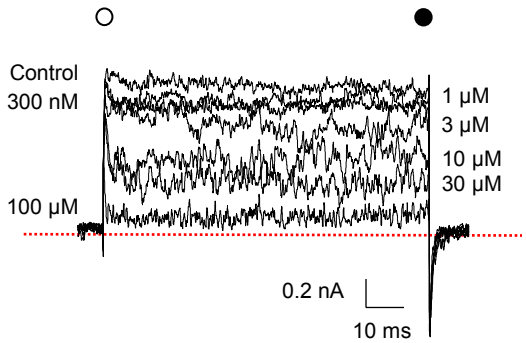

B. Summary

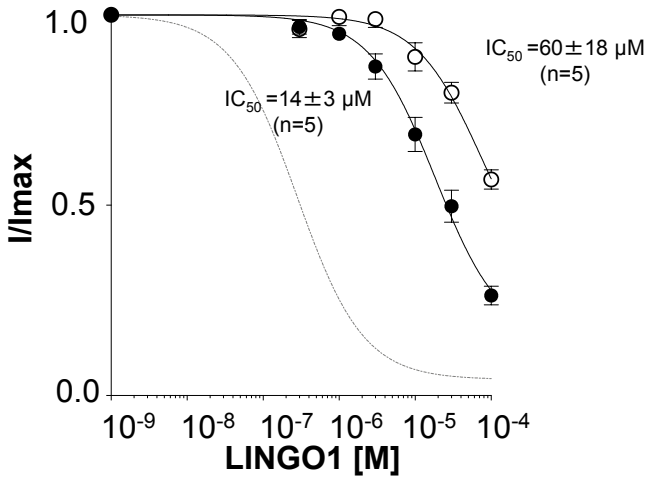

C. Summary of LINGO1 τ_{inact}

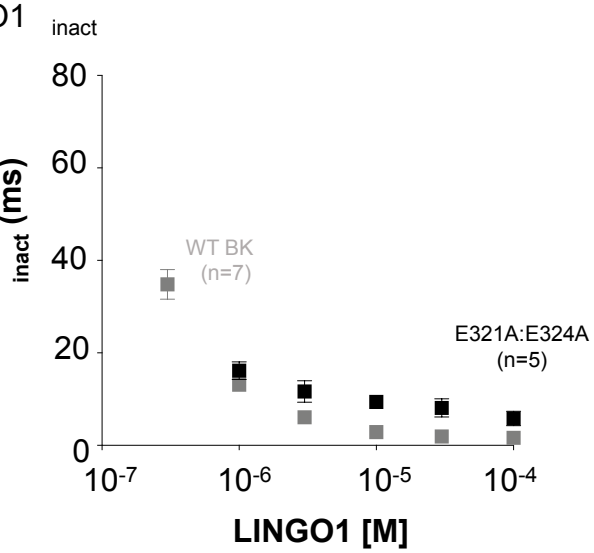

Figure 6.7: Concentration-dependent effect of LINGO1 (NH_2-RKFNMKMI-OH) tail peptide on E321A:E324A mutant BK .
A Representative concentration-dependent effect of LINGO1 tail peptide on HEK cells expressing E321A:E324A mutant BK currents. Currents were evoked by a step from -60 mV to +160 mV in the presence of 300 nM, 1, 3, 10, 30, 100 µM of LINGO1 tail peptide. **B** Summary concentration effect curve for the effect of LINGO1 tail peptide on E321A:E324A mutant BK currents (n=5). Data were fitted with the Hill-Langmuir equation (grey trace WT BK). **C** The rate of inactivation of BK currents was assessed by fitting the decay phase with a single exponential. The rate of inactivation increased with the concentration of LINGO1 tail peptide (grey trace WT BK).

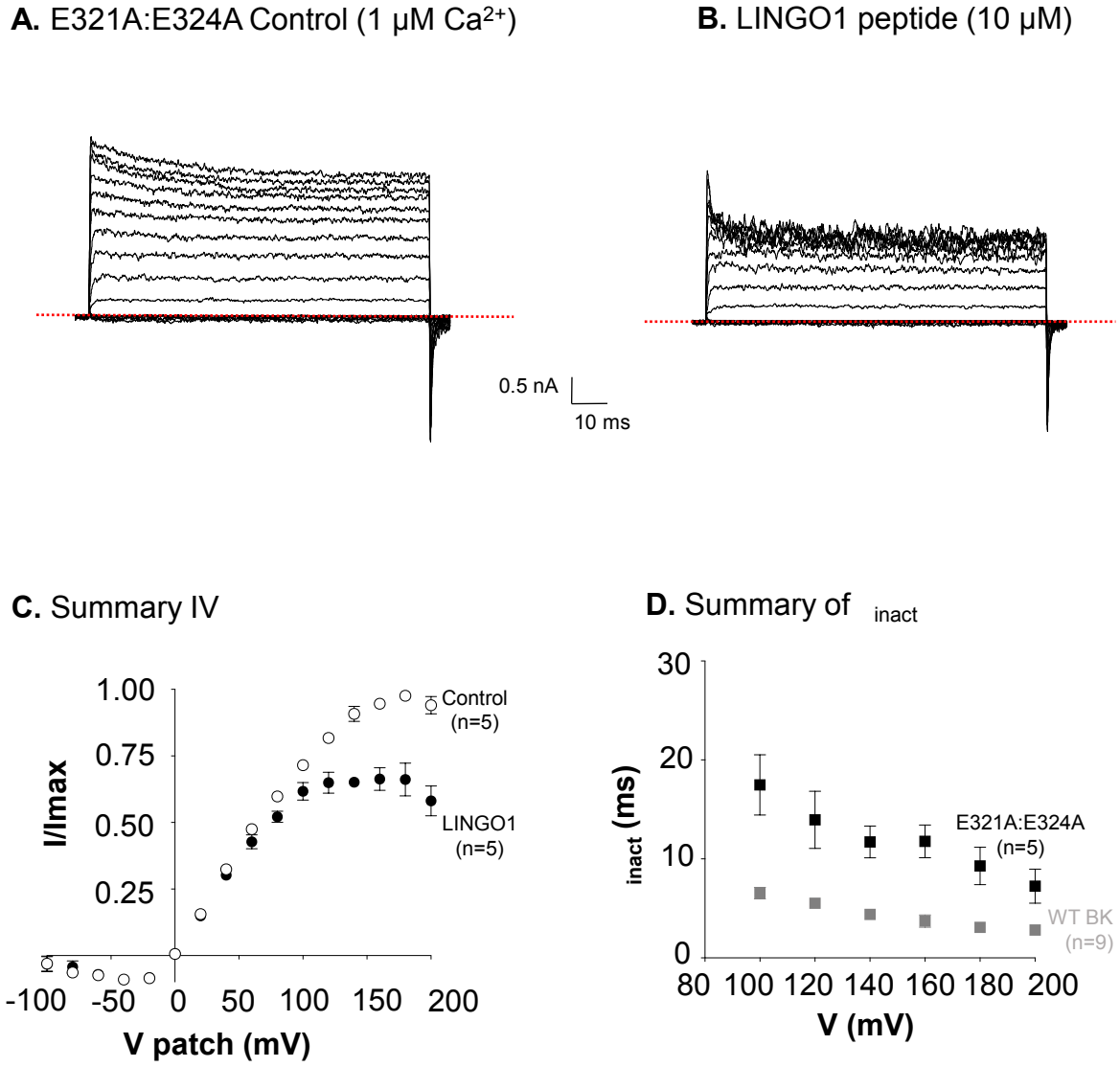

Figure 6.8: Voltage-dependence of LINGO1 (NH_2-RKFNMKMI-OH) tail peptide on E321A:E324A mutant BK .

A & **B** Macroscopic currents from inside-out patches expressing E321A:E324A mutant BK alone, show typical records in control (1 μM $[Ca^{2+}]_i$) and after application of 10 μM LINGO1 tail peptide. Patches were held at -60 mV and stepped from -100 mV to +200 mV in 20 mV increments and stepped back down to -80 mV to generate tail currents. **C** Summary of I/Imax measured in the last 5 ms of the pulse (n=5). **D** The rate of inactivation of BK currents was assessed by fitting the decay phase with a single exponential. The currents showed an apparent voltage-dependence at more positive potentials (grey squares WT BK).

6.2.3 Replacement of the negative charge on the E324 to a positive E324R mutation reduces the effect of LINGO1 tail peptide

As seen from Sections 6.2.1 and 6.2.2, neutralisation of glutamic acid residues by substitution with alanine residues in the S6 helix reduced LINGO1 tail peptide efficacy, perhaps suggesting a weakened electrostatic interaction between it and the BK channel pore. To test this further, we reversed the charge on E324 by producing an E324R mutant. As seen from Figure 6.9A, the LINGO1 tail peptide (300 nM to 100 M) still caused a concentration-dependent inactivation of the BK current. Figure 6.9B shows a summary of 6 experiments in which the IC_{50} was 38±14 μM when determined from currents in the first 5 ms (open symbols) and 18±2 μM in the last 5 ms (closed symbols) of the depolarising pulse (ns, paired t-test). This was approximately 60-fold higher than that observed with WT BK channels (grey dashed line, Figure 6.9B; $p<0.0001$, unpaired t-test). The currents at +160 mV inactivated with a $_{inact}$ of 12±1 ms in 10 M LINGO1 peptide, which was significantly slower than with that observed with the WT BK (3±1 ms) shown in grey ($p<0.0001$, unpaired t-test; Figure 6.9C). We next examined the voltage-dependence of the peptide block, by generating a family of currents by stepping from -100 mV to +200 mV in the absence and presence of 10 M LINGO1 tail peptide. Figure 6.10B shows that 56±3% of the current remained at the end of a depolarising pulse to +100 mV in the presence of 10 M LINGO1 peptide compared to WT BK channels ($p<0.0001$, Mann-Whitney test). Similar effects were observed in 8 different patches and the data are summarised in Figure 6.10C. When inactivating currents were fitted with a single exponential at potentials >+100 mV (Figure 6.10D), it was clear that the currents inactivated more slowly than WT BK channels, at all potentials measured ($p<0.01$, one-way ANOVA).

A. E324R with LINGO1 *(NH_2-RKFNMKMI-OH)*

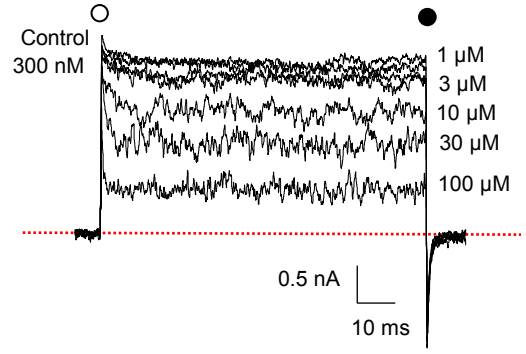

B. Summary

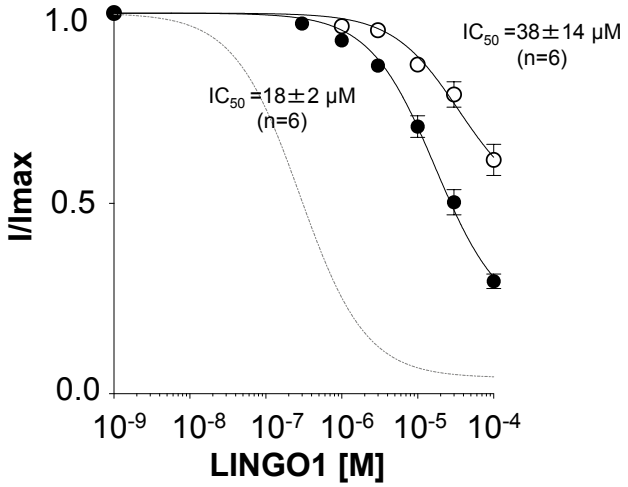

C. Summary of LINGO1 $_{inact}$

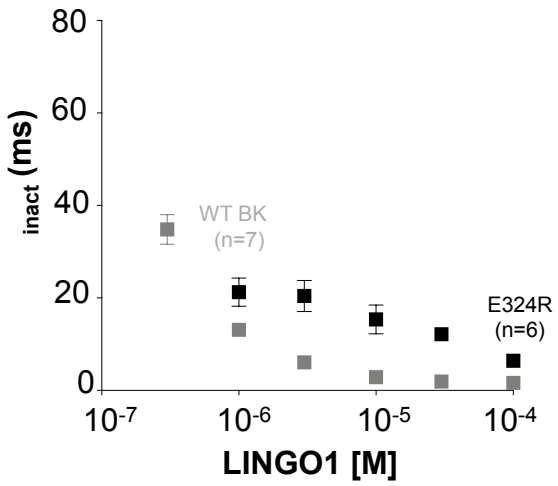

Figure 6.9: Concentration-dependent effect of LINGO1 (NH_2-RKFNMKMI-OH) tail peptide on E324R mutant BK .

A Representative concentration-dependent effect of LINGO1 tail peptide on HEK cells expressing E324R mutant BK currents. Currents were evoked by a step from -60 mV to +160 mV in the presence of 300 nM, 1, 3, 10, 30, 100 µM of LINGO1 tail peptide. **B** Summary concentration effect curve for the effect of LINGO1 tail peptide on E324R mutant BK currents (n=6). Data were fitted with the Hill-Langmuir equation (grey trace WT BK). **C** The rate of inactivation of BK currents was assessed by fitting the decay phase with a single exponential. The rate of inactivation increased with the concentration of LINGO1 tail peptide (grey trace WT BK).

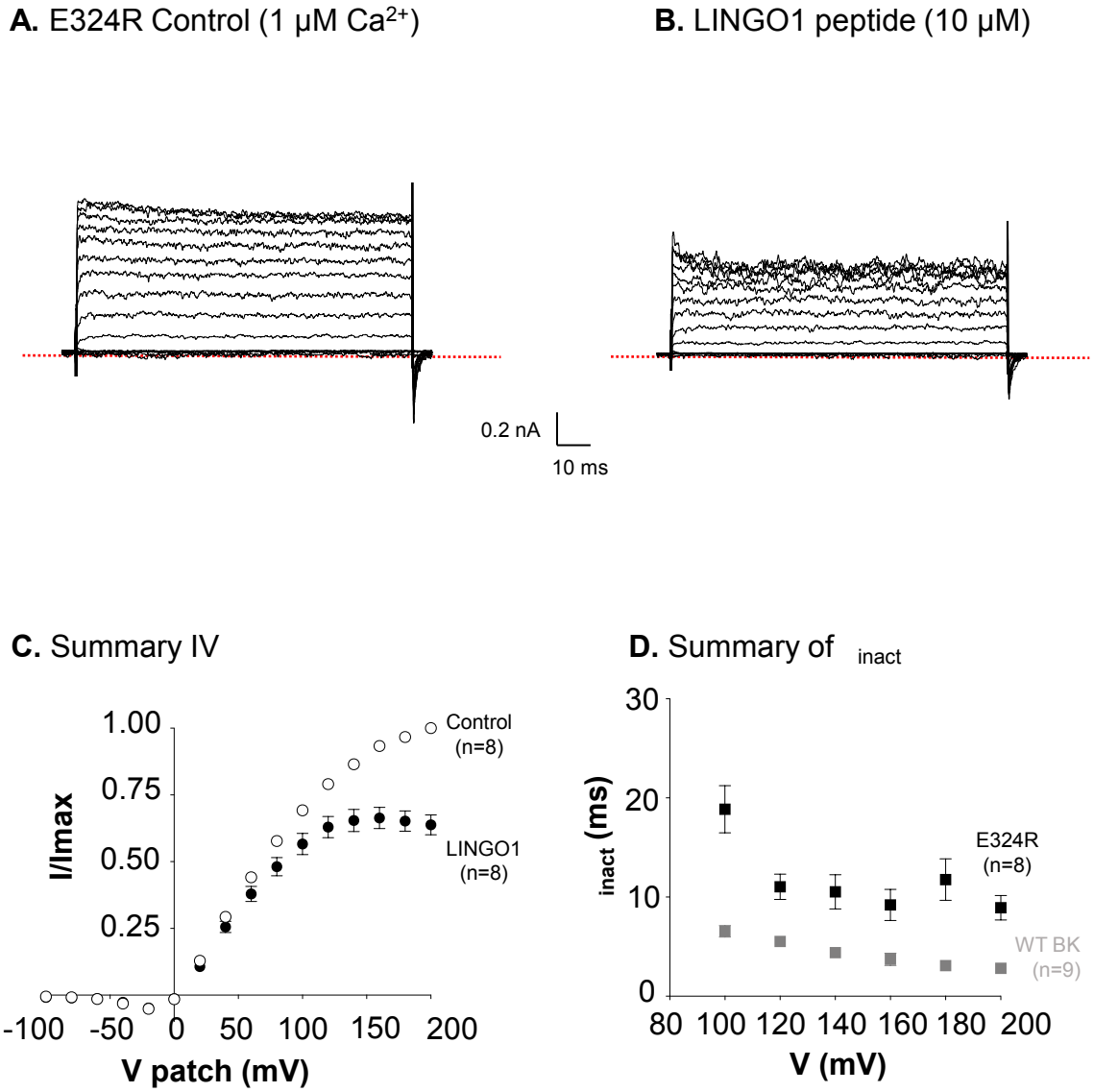

Figure 6.10: Voltage-dependence of LINGO1 (NH_2-RKFNMKMI-OH) tail peptide on E324R mutant BK .
A & **B** Macroscopic currents from inside-out patches expressing E324R mutant BK alone, show typical records in control (1 μM $[Ca^{2+}]_i$) and after application of 10 μM LINGO1 tail peptide. Patches were held at -60 mV and stepped from -100 mV to +200 mV in 20 mV increments and stepped back down to -80 mV to generate tail currents. **C** Summary of I/Imax measured in the last 5 ms of the pulse (n=8). **D** The rate of inactivation of BK currents was assessed by fitting the decay phase with a single exponential. The currents showed an apparent voltage-dependence at more positive potentials (grey squares WT BK).

6.2.4 A double E321R:E324R mutant reduces the effect of LINGO1 tail peptide

We next investigated the effect of a double charge reversal by generating an E321R:E324R mutant. Note that the E321R:E324R mutant has been previously shown to cause a large leftward shift (–67 mV) in the activation $V_{1/2}$ at 0 Ca^{2+}, compared to WT channels (Tian *et al.* 2019). LINGO1 tail peptide, when applied to excised patches in a concentration-dependent manner (300 nM to 100 M), still induced inactivation as shown in Figure 6.11A. Summary data from 8 similar experiments was shown in Figure 6.11B, in which an IC_{50} value of 44±8 μM was determined from the first 5 ms (open symbols) and 13±3 μM from the last 5 ms (closed symbols) of the depolarisation pulse ($p<0.01$, paired t-test). This effect was remarkably similar to the double charge neutralisation (E321A:E324A) mutant and appeared no more effective than the single E324R mutant (ns, one-way ANOVA). As Figure 6.11A shows, application of LINGO1 tail peptide still induced inactivation, albeit at higher concentrations. When inactivating currents were fitted with a single exponential (Figure 6.11C), the rate of inactivation was slower compared to that observed in WT BK with the peptide. For example, in 10 M LINGO1 tail peptide the $_{inact}$ at +160 mV was 10±1 ms in E321R:E324R mutant compared to 3±1 ms in WT ($p<0.0001$, unpaired t-test). When a family of currents were compared in the absence (Figure 6.12A) and presence of the 10 M LINGO1 tail peptide (Figure 6.12B), 53±1% of the residual current was left at the end of the pulse (+100 mV), which was very similar to the effects observed with both the E324R and the E321A:E324A mutants (ns, one-way ANOVA). Figure 6.12C shows summary IV curves from 8 similar experiments. The rate of inactivation was measured in 10 M LINGO1 tail peptide at different voltages and is summarised in Figure 6.12D and these were significantly slower than WT BK ($p<0.0001$, one-way ANOVA).

A. E321R:E324R with LINGO1 *(NH_2-RKFNMKMI-OH)*

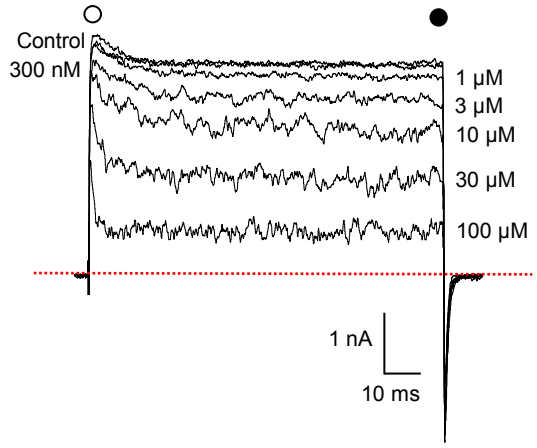

B. Summary

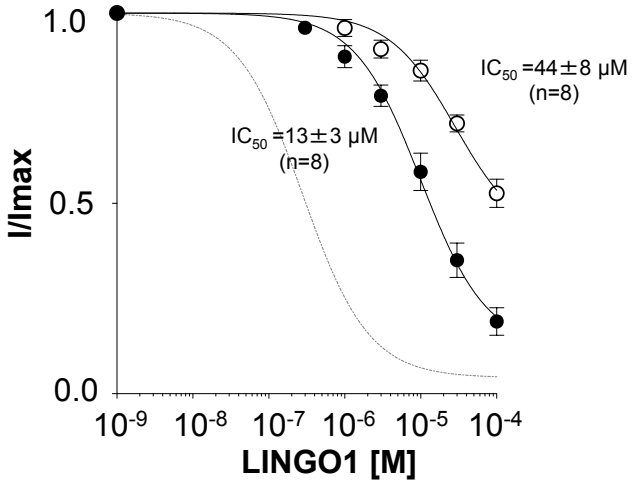

C. Summary of LINGO1 $_{inact}$

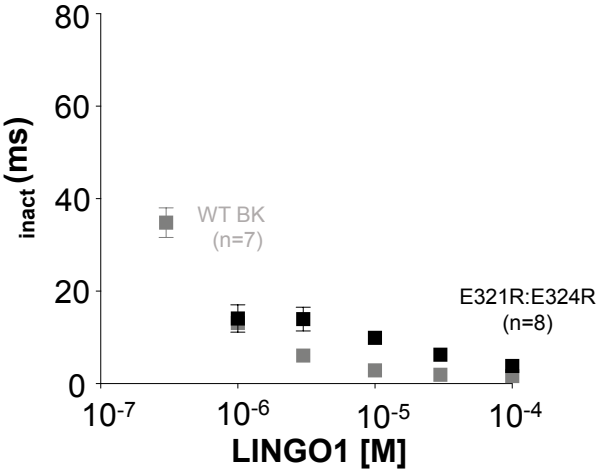

Figure 6.11: Concentration-dependent effect of LINGO1 (NH_2-RKFNMKMI-OH) tail peptide on E321R:E324R mutant BK .

A Representative concentration-dependent effect of LINGO1 tail peptide on HEK cells expressing E321R:E324R mutant BK currents. Currents were evoked by a step from -60 mV to +160 mV in the presence of 300 nM, 1, 3, 10, 30, 100 µM of LINGO1 tail peptide. **B** Summary concentration effect curve for the effect of LINGO1 tail peptide on E321R:E324R mutant BK currents (n=8). Data were fitted with the Hill-Langmuir equation (grey trace WT BK). **C** The rate of inactivation of BK currents was assessed by fitting the decay phase with a single exponential. The rate of inactivation increased with the concentration of LINGO1 tail peptide (grey trace WT BK).

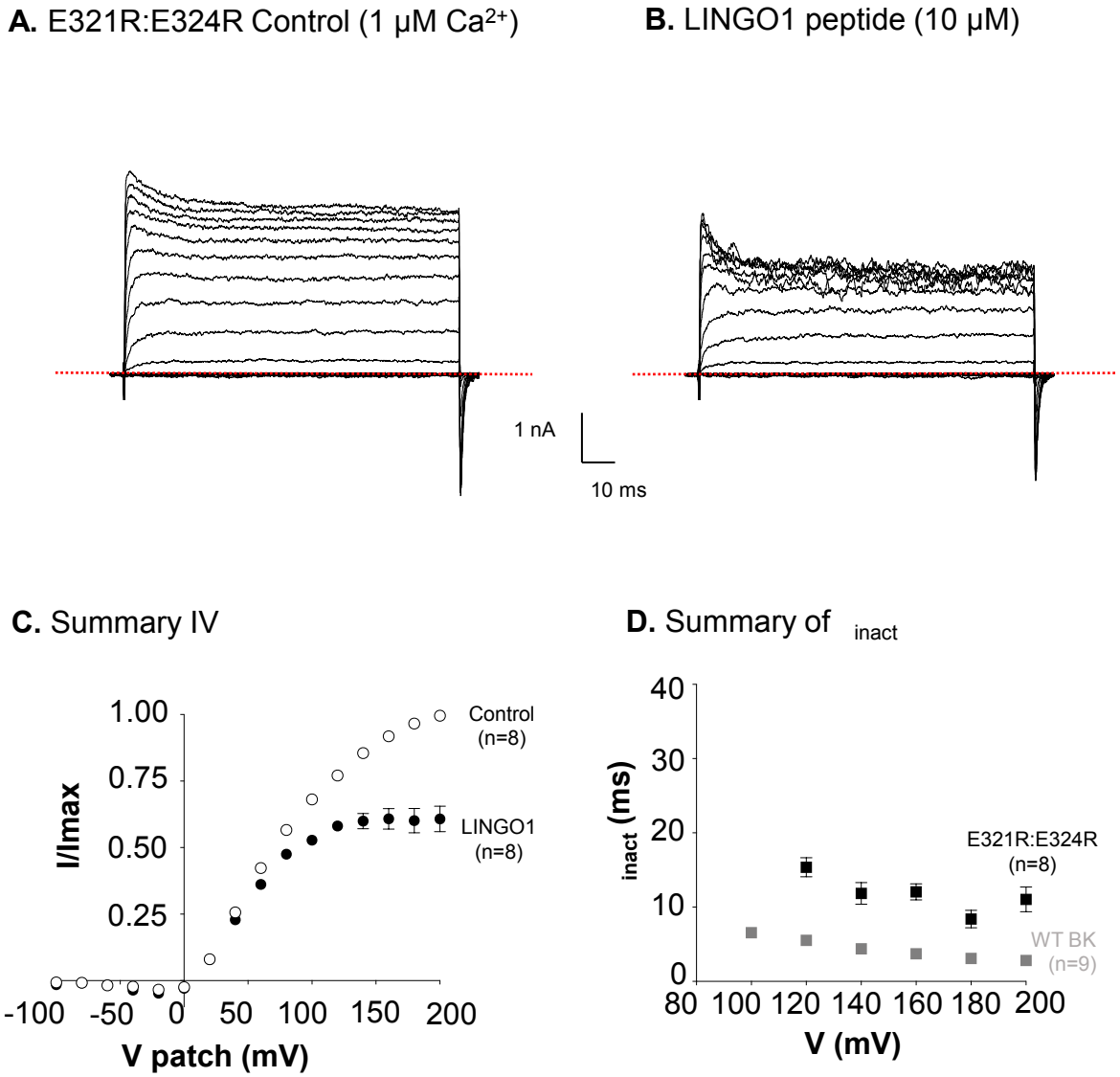

Figure 6.12: Voltage-dependence of LINGO1 (NH_2-RKFNMKMI-OH) tail peptide on E321R:E324R mutant BK .

A & **B** Macroscopic currents from inside-out patches expressing E321R:E324R mutant BK alone, show typical records in control (1 μM $[Ca^{2+}]_i$) and after application of 10 μM LINGO1 tail peptide. Patches were held at -60 mV and stepped from -100 mV to +200 mV in 20 mV increments and stepped back down to -80 mV to generate tail currents. **C** Summary of I/Imax measured in the last 5 ms of the pulse (n=8). **D** The rate of inactivation of BK currents was assessed by fitting the decay phase with a single exponential. The currents showed an apparent voltage-dependence at more positive potentials (grey trace WT BK).

6.2.5 Substitution of a hydrophilic amino acid T287 to hydrophobic alanine residue slightly alters the effect of LINGO1 tail peptide

According to the model shown in Figure 6.4, the tail of synthetic LINGO1 peptide (blue sticks), aligned in the pore and the last three residues of the C-terminus approached residue T287 (marked as sticks), which is positioned at the internal entrance to the selectivity filter of the BK channel. To investigate if this residue was important in LINGO1 inactivation, we replaced the polar, uncharged, hydrophilic amino acid T287 to a non-polar, uncharged, hydrophobic alanine residue and assessed the effect of LINGO1 peptide, using the protocols described previously. Figure 6.13A demonstrated that LINGO1 tail peptide still caused inactivation of the BK current in a concentration-dependent manner (300 nM to 30 M). As seen in Figure 6.13B, the IC_{50} obtained from currents in the first 5 ms (n=6) of the depolarising pulse was 3±1 µM and 370±70 nM in the last 5 ms (n=6, ns, paired t-test). This effect was similar to that observed with WT BK (ns, unpaired t-test). As shown in F igure 6 3A the peptide caused concentration-dependent inactivation (300 nM to 30 M) which was remarkably similar to that observed in the WT BK channel (ns, one-way ANOVA) and summarised in Figure 6.13C. We also examined the effects of the tail peptide on IVs in the absence (Figure 6.14A) and presence of 10 M LINGO1 tail peptide (Figure 6.14B) and noticed that 10±2% (n=6) of current remained at +200 mV in this mutant, compared to 5±1% of current in WT BK at the end of the depolarisation pulse ($p<0.05$, Mann-Whitney test, Figures 6.14B and C). The rate of inactivation at different voltages appeared similar to that observed with WT BK channels, as evidenced in Figure 6.14D (ns, one-way ANOVA) and suggests that the T287A had little effect on the interaction between LINGO1 and BK channels.

A. T287A with LINGO1 *(NH_2-RKFNMKMI-OH)*

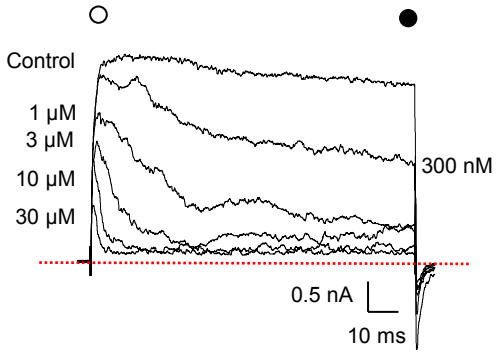

B. Summary

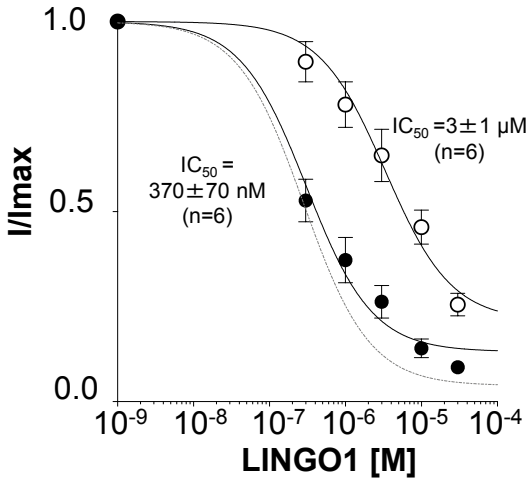

C. Summary of LINGO1 $_{inact}$

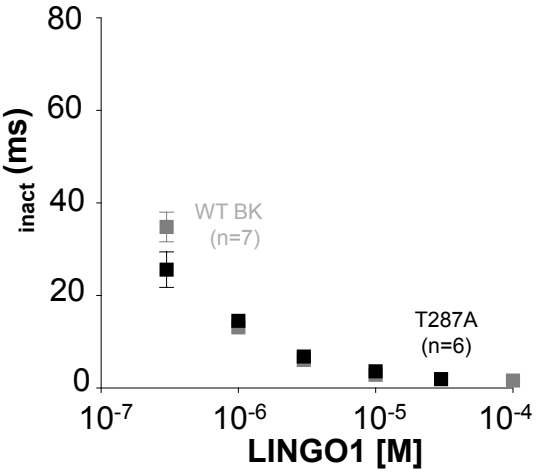

Figure 6.13: Concentration-dependent effect of LINGO1 (NH_2-RKFNMKMI-OH) tail peptide on T287A mutant BK .

A Representative concentration-dependent effect of LINGO1 tail peptide on HEK cells expressing T287A mutant BK currents. Currents were evoked by a step from -60 mV to +160 mV in the presence of 300 nM, 1, 3, 10, 30 µM of LINGO1 tail peptide. **B** Summary concentration effect curve for the effect of LINGO1 tail peptide on T287A mutant BK currents (n=6). Data were fitted with the Hill-Langmuir equation (grey trace WT BK). **C** The rate of inactivation of BK currents was assessed by fitting the decay phase with a single exponential. The rate of inactivation increased with the concentration of LINGO1 tail peptide (grey trace WT BK).

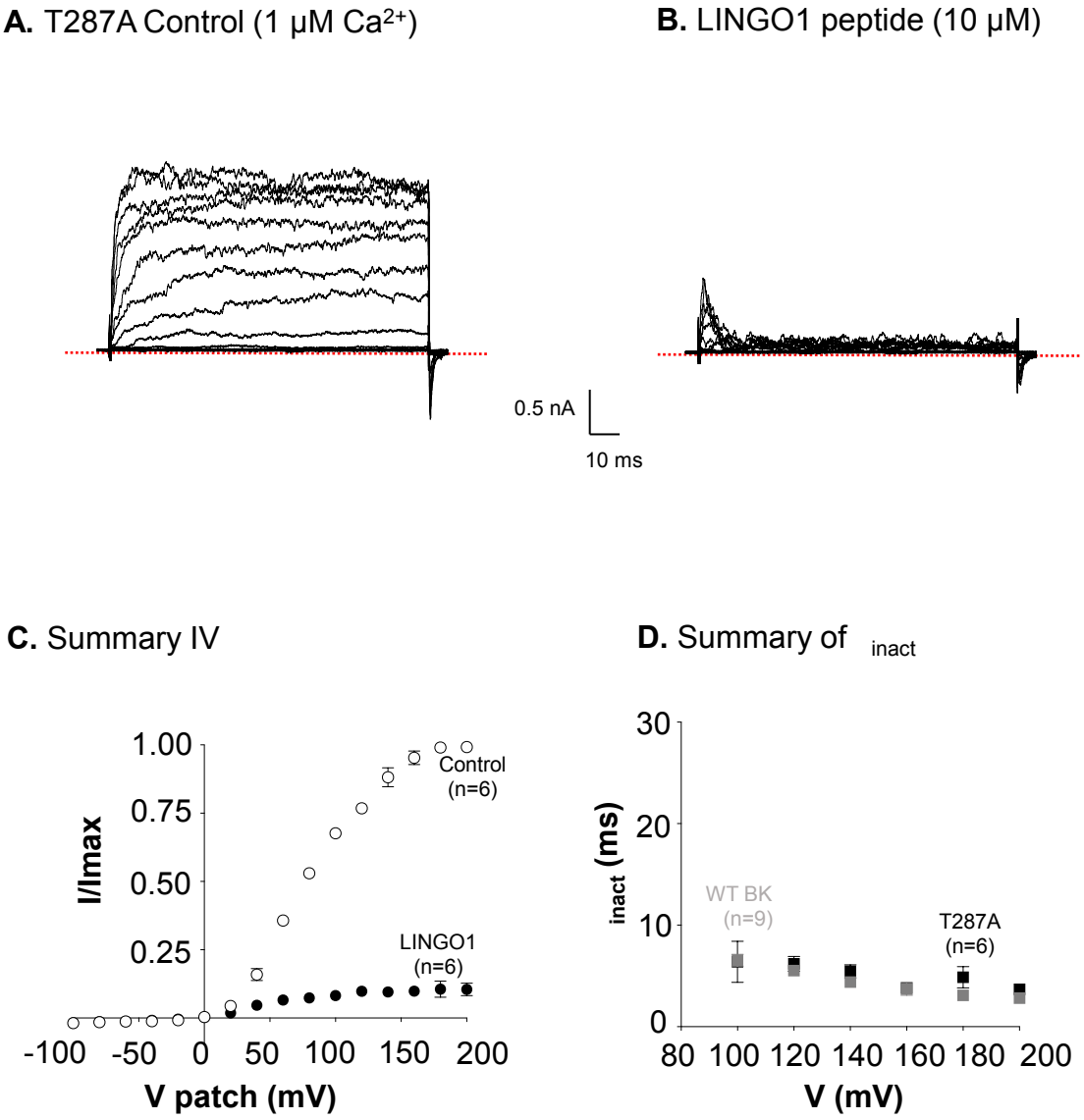

Figure 6.14: Voltage-dependence of LINGO1 (NH_2-RKFNMKMI-OH) tail peptide on T287A mutant BK .
A & **B** Macroscopic currents from inside-out patches expressing T287A mutant BK alone, show typical records in control (1 μM $[Ca^{2+}]_i$) and after application of 10 μM LINGO1 tail peptide. Patches were held at -60 mV and stepped from -100 mV to +200 mV in 20 mV increments and stepped back down to -80 mV to generate tail currents. **C** Summary of I/Imax measured in the last 5 ms of the pulse (n=6). **D** The rate of inactivation of BK currents was assessed by fitting the decay phase with a single exponential. The currents showed an apparent voltage-dependence at more positive potentials (grey trace WT BK).

Table 6.1 The effects of LINGO1 tail peptide on mutations in the S6 helix of BK channels

BK	Inactivation	IC_{50} (last 5 ms)	Residual current at +200 mV (last 5 ms)
WT		308±60 nM	5±1%
E324A		1±0.4 μM	16±2%
E321A:E324A		14±3 μM	58±5%
E324R		18±2 μM	63±3%
E321R:E324R		13±3 μM	60±4%
T287A		370 ±70 nM	10±2%

A. IC_{50} last 5 ms summary

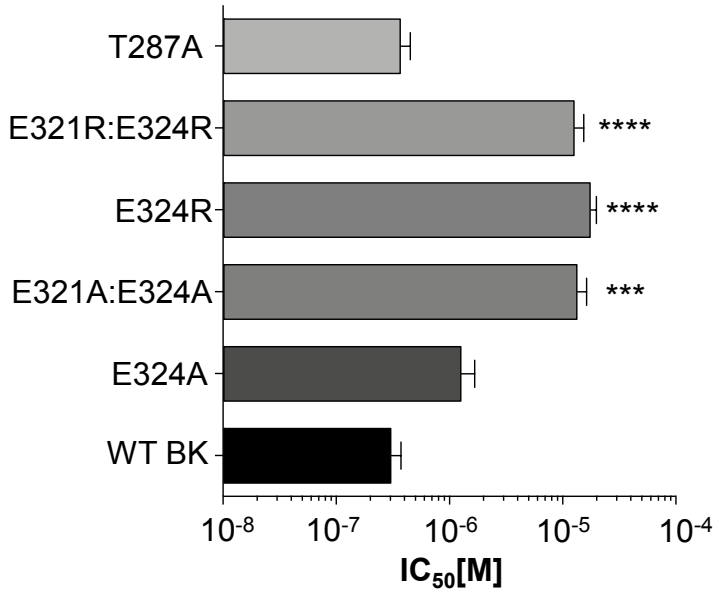

B. $_{inact}$ summary with 10 μM LINGO1 tail peptide

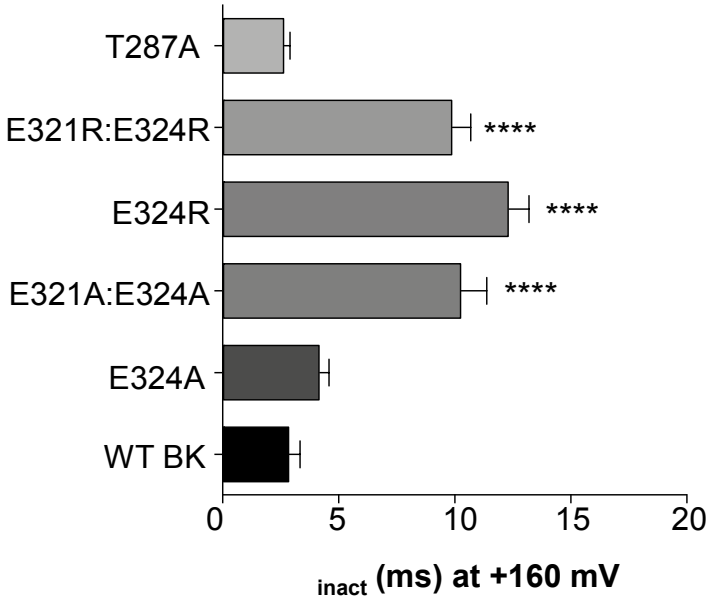

Figure 6.15: Comparison between BK mutants with the use of LINGO1 (NH_2-RKFNMKMI-OH) tail peptide.
A Effect of LINGO1 tail peptide on mutants of BK in the last 5 ms of the depolarising pulse, which shows IC_{50} values for LINGO1 in various BK mutants (one-way ANOVA, *** p<0.001, **** p<0.0001). **B** Mean inactivation time constant ($_{inact}$) of currents in mutants of BK in the presence of 10 μM LINGO1 tail peptide (one-way ANOVA, **** p<0.0001).

A. +100 mV summary

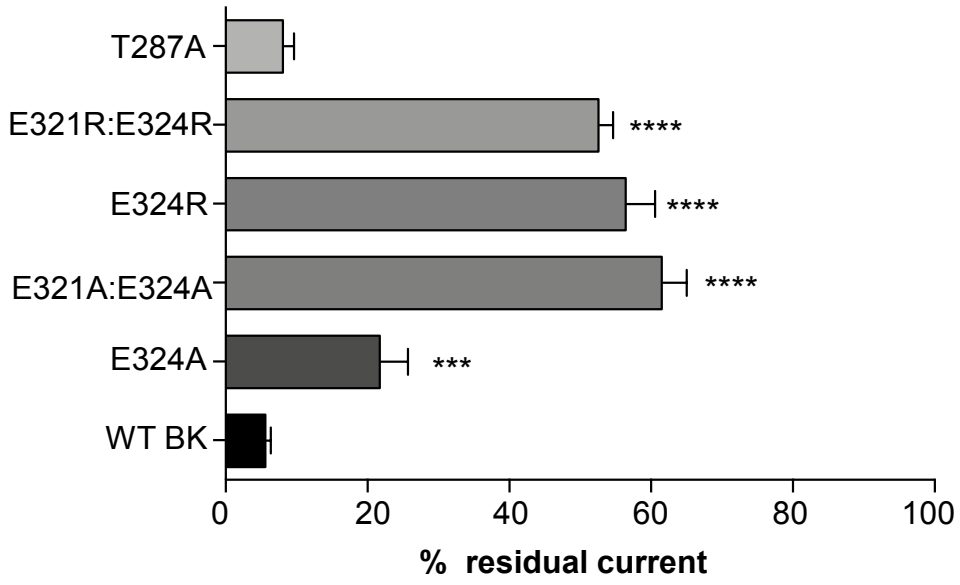

B. +200 mV summary

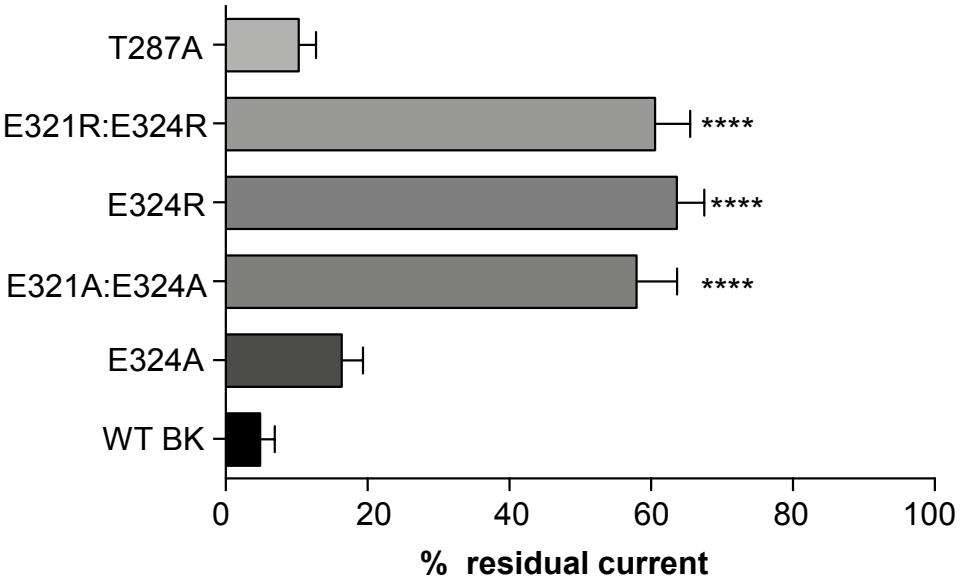

Figure 6.16: Comparison between BK mutants with the use of LINGO1 (NH_2-RKFNMKMI-OH) tail peptide.
A Percentage of residual current of BK mutants measured in the last 5 ms at +100 mV and **B** at +200 mV in the presence of LINGO1 tail peptide (one-way ANOVA, *** p<0.001, **** p<0.0001).

6.3 Discussion

The present chapter demonstrated the following:

1) LINGO1 peptide appears to insert itself into the pore of the BK channel since TPAB and LINGO1 appear to compete for a similar binding site.
2) The positively charged residues of LINGO1 tail peptide may interact with negatively charged residues in the S6 helix of the BK channel.

Previous literature demonstrated that the QA ions bind in the pore region of K^+ channels (Zhou *et al*. 2001). Li and Aldrich (2006) demonstrated that if the channel in an open-conformation state was blocked by an internal blocker, this blocker physically prevented the channel gate from closing. This was also observed at hyperpolarised membrane potentials, when a closed conformation of the channel was favoured (Li and Aldrich, 2006). In addition, these QA ions were shown to compete with the inactivating subunits of the mutant Shaker channel (Choi *et al.* 1991) and the inactivation mediated by 12 (1 subunit inactivation gate attached to 2 core) in mutant $K_v1.4$ subunits (Zhou *et al.* 2001). The mode of intact N-type inactivation of K^+ channels was proposed based on the mutational and structural experiments (Zhou *et al.* 2001; Li and Aldrich, 2006). This mechanism stated that the N-terminal acted as an extended peptide and wiggled into the pore, to bind in the hydrophobic central cavity, adjacent to the QA binding site (Zhou *et al.* 2001; Li and Aldrich, 2006).

In the present chapter, firstly, we investigated if LINGO1 tail peptide competes with TPAB. We used different concentrations of TPAB (3 M and 10 M) along with a steady concentration of LINGO1 tail peptide (3 M). We noticed that BK channels inactivated more slowly in the combined presence of TPAB and LINGO1 peptide (Figures 6.2 and 6.3), perhaps suggesting that, i) the peptide and TPAB compete for a common binding site in the pore of the BK channel or alternatively, ii) TPAB may occupy a site which may hinder the access of LINGO1 tail peptide to a different binding site.

Our observations are consistent with previous studies which demonstrated that a combination of 3 M EBP applied along with 500 M TBA, slowed the time constant of inactivation from 2.8 ms with EBP alone, to 5.6 ms in the presence of TBA and EBP (Li and Aldrich, 2006). Similarly, a combination of 1 mM TEA with 20 M ShB peptide resulted in ~2-fold increase in the time constant of decay of

the ShB 6-46 channels, suggesting that the ShB peptide also competed with the binding site of TEA (Murrell-Lagnado and Aldrich, 1993a). In addition, Wallner *et al.* (1999) demonstrated that intracellular application of 100 mM TEA along with 3 M BK 2 ball peptide, slowed the time constant of inactivation by ~2-fold, suggesting that the BK 2 ball peptide and TEA competed for a common binding site in the BK channel pore. Collectively, our results strongly suggest that the LINGO1 tail peptide and TPAB may compete for a similar binding site and supports the idea that the inactivation induced by LINGO1 may be caused by the peptide inserting deep into the BK pore.

Based on a homology model of the BK channel docked with the LINGO1 tail (Figure 6.4), we identified a number of residues in the BK channel pore, that may interact with the LINGO1 tail peptide. We produced a series of mutant BK channel constructs and examined the effect of the LINGO1 tail peptide on these mutants, which are summarised in Table 6.1. We started the mutagenesis experiments with the two negatively charged glutamate residues (E321, E324) situated at the C-terminal end of the S6 segment in the BK channels. Tian *et al.* (2019) demonstrated that at 0 Ca^{2+}, the mutations of either residue caused a significant leftward shift in the activation $V_{1/2}$, compared to WT BK channels. Their E324A mutant showed a leftward shift of –20 mV and the E321A:E324A mutant showed a –81 mV leftward shift, whereas a E321R:E324R mutant showed a –67 mV shift. In our first mutant, we replaced the negatively charged E324 with an uncharged hydrophobic alanine residue, which although induced inactivation, was less effective (Figure 6.15A). The decay phase of the currents, when fitted with a single exponential, was slower than WT BK (Figure 6.15B) indicating that the 'on rate' of the reaction also reduced (Murrell-Lagnado and Aldrich, 1993a; 1993b). In addition, the amount of sustained current remaining at the end of the pulse during the application of 10 M LINGO1 was higher than WT (Figures 6.16A and B), suggesting that the rate of the 'off reaction' was also affected by this BK channel mutant. Moreover, the currents recorded appeared noisy in the presence of LINGO1 peptide, possibly reflecting rather unstable binding of the peptide in the pore of the BK channel (Figure 6.5A).

Interestingly, the double charge neutralisation (E321A:E324A), single charge reversal (E324R) and the double charge reversal (E321R:E324R) mutants all

produced quantitatively similar effects with the LINGO1 peptide. We noticed with these mutants that the affinity of the LINGO1 peptide to the mutant channels was reduced compared to the WT BK channels, as evidenced by the rightward shift in IC_{50} values (Figure 6.15A). The time constant of inactivation with these mutants was slower compared to WT BK channels (Figure 6.15B) suggesting that the 'on-rate' of the peptide binding was reduced in all these mutants. Interestingly, in the presence of 10 M LINGO1 peptide, all of these mutants displayed ~60% of sustained current at the end of the depolarisation pulse which was significantly higher than WT BK (Figure 6.16). These data suggest that peptide binding to these channels was unstable, perhaps due to the increased rate of 'off-reaction'. Another similarity between these three mutants was that the currents appeared noisy in presence of the peptide, possibly due to the unstable binding of the tail peptide in the channel pore (Figures 6.7A, 6.9A and 6.11A). It should be noted that the K614 residue of LINGO1 peptide appeared to reside between the E321 and E324 residues in the model shown in Figure 6.4. Our results so far suggest that the single charge reversal mutant (E324R) produced similar effects to double charge neutralisation (E321A:E324A) mutant. The reduced effectiveness of the LINGO1 tail peptide may be due to unstable binding and perhaps suggests that there may be a possible electrostatic interaction between the positively charged residues of the tail peptide and the negatively charged residues in the BK channel pore. However, the effects of LINGO1 peptide on charge neutralisation and charge reversal mutants of E321 residue of the BK channel remain to be elucidated.

Previous studies have demonstrated that that the two negatively charged glutamates (E321, E324), located near the inner vestibule of the BK channel pore, participated in electrostatic interactions and contributed to the channel's large single channel conductance (Brelidze *et al.* 2003; Nimigean *et al*. 2003). These negative charges raise the apparent local $[K^+]$ ions near the inner vestibule of the pore, thereby increasing the conductance and a double mutation of these negative charges reduced channel conductance (Brelidze *et al.* 2003; Nimigean *et al*. 2003). Li and Aldrich (2006) demonstrated that the electrostatic and hydrophobic interactions of the enhanced ball peptide (EBP) with the negatively charged (E321 and E324) residues in the pore of the BK channel, were critical for binding of the ball peptide.

A recent study by Fan *et al.* (2020) revealed the cryo-EM structure of the prokaryotic MthK channel and demonstrated that the inactivating N-terminal peptide was bound to the channel in the open state. The positively charged residues in the N-terminal (R9, K10, R14, K17) interacted electrostatically with the negatively charged glutamate residues (E95 and E96) located at the bottom of the inner helices of the MthK channel. They also demonstrated that the binding of the peptide was stabilised due to hydrophobic interactions between the N-terminal peptide (V4, I5, I7 and I8) and (I84, F87, V91 and L95) the TM2 domain of the MthK channel. With the LINGO1 peptide we speculate that the positively charged residues (R613, K614 and K618) may perhaps interact electrostatically with the negatively charged E321 and E324 residues located near the inner vestibule of the BK channel pore. In addition, there perhaps may be hydrophobic interactions between the LINGO1 tail peptide (F615, M617, M619 and I620) and the BK channel pore (F315, S317, P320) which stabilise the peptide binding to the BK channel. However, to confirm this hypothesis, further experiments will clearly be required.

Interestingly, when the T287 residue, situated deep within the BK channel pore, was substituted with alanine, we noticed very little effect of this mutation on the tail peptide compared to WT BK (Figure 6.13A), as evidenced by the similar IC_{50} values and time constants of inactivation (Figures 6.15A and B). In fact, the only obvious change was a doubling of residual current (to ~10%) in this mutant compared to WT (Figures 6.14C and 6.16), indicating that this mutant only caused a small change in the stability of the block by the LINGO1 peptide.

Our results are consistent with experiments carried out by Li and Aldrich (2006) which demonstrated that the use of 100 M EBP on the E321N:E324N BK mutant showed <60% block by the peptide, whereas the WT channel showed a nearly complete block with 3 M EBP. This corresponded to a reduction in apparent affinity of ~2-orders of magnitude, compared to WT (Li and Aldrich, 2006). Similarly, at +100 mV, we observed, ~48% block by 10 M LINGO1 tail peptide on the E321R:E324R mutant (Figures 6.12B and 6.16) and ~39% block by 10 M LINGO1 tail peptide on the E321A:E324A mutant (Figures 6.8B and 6.16) at the end of the depolarisation pulse. In contrast, the WT BK channel showed

~95% block by 10 M LINGO1 tail peptide (Figures 3.5B and 6.16) at the end of the depolarisation pulse.

The inactivation of the ShB 6-46 channels is thought to occur via the movement of the N-terminal of the ShB peptide into the pore of the channel such that it obstructs the ion permeation pathway. This mechanism is called the ball-and-chain' inactivation or one-step inactivation (Bezanilla and Armstrong, 1977; Hoshi *et al.* 1990). A study published by Lingle *et al.* (2001) proposed that the inactivation of BK channels mediated by the BK 3b subunit involved two-steps, namely, the initial binding and then the block of BK channels. The first step in this mechanism involved the binding of the inactivation domain to the subunit in a non-blocking, or pre-inactivated site. The second step was the movement of the N-terminal inactivation domain into the pore of the BK channel, such that it obstructed the ion permeation pathway. However, the mechanism by which the LINGO1 protein mediates inactivation of BK channels remains to be elucidated.

Taken together, the data presented demonstrate that the affinity of the LINGO1 tail peptide to the pore of the BK channel was reduced in the E321 and E324 mutant constructs, suggesting a possible interaction between the negatively charged residues in the S6 helix of the BK channel and the positively charged residues of the LINGO1 tail peptide. However, this interpretation is open to the criticism that these experiments were carried out on an untethered short chain of amino acids, albeit with a sequence identical to that of the C-terminus of the LINGO1 protein. Nevertheless, these peptides will have more freedom in solution compared to tethered LINGO1 protein and it is possible that they can bind to the BK channels in more than one way. Future experiments will examine if the full-length LINGO1 protein, co-expressed with mutants of BK behaves in a similar manner to that of the LINGO1 tail peptide.

7. Conclusions and Future Directions

BK channels are widely expressed in excitable and non-excitable cells (Butler *et al*. 1993; Garcia-Calvo *et al.* 1994; Pallanck and Ganetzky, 1994). These channels consist of tetrameric subunits and the pharmacological and biophysiological functions of the channel are modulated by the association of auxiliary and subunits (Orio *et al.* 2002; Gessner *et al*. 2005; Latorre *et al.* 2017). Although all subunits modulate the biophysical properties of the BK channels, only the 2 and 3 subunits induced inactivation (Wallner *et al*. 1999; Xia *et al*. 2000). In contrast, the association of subunits did not induce inactivation of BK currents (Yan and Aldrich, 2012). The subunits are members of a much larger family of leucine rich repeat (LRR) proteins. Interestingly, LINGO (LRR and Ig domain-containing, Nogo Receptor-interacting) proteins, which belong to the LRRIG family, share some common structural features with the subunits, suggesting that they may be evolutionarily close to each other and recently, a study from our lab demonstrated that LINGO1 co-expression with BK resulted in rapid and complete inactivation of BK currents (Dudem *et al.* 2020).

Previous studies have demonstrated that the *LINGO1-4* subtypes are abundantly expressed in the CNS and are apparently absent in non-neuronal tissues (Homma *et al.* 2009; Mi *et al*. 2013). Although the expression of LINGO subtypes in different organs remains unknown, we demonstrated using RT-PCR experiments (Figure 3.3A) that *LINGO1-4* can be detected at the transcriptional level in murine brain and bronchus tissues. In addition, recent publicly available data suggests that LINGO1 protein is also found in the human lung and is abundantly expressed in the brain (https://www.proteinatlas.org/ENSG00000169783-LINGO1/tissue; Uhlén *et al.* 2015). This suggests that LINGO proteins may be expressed under normal conditions in both the human and murine brain and bronchus, although this will require further experimental confirmation using immunocytochemistry.

In Chapter 3, we assessed the effects of synthetic (amino free acid) tail peptides of LINGO proteins on BK channels and demonstrated that the LINGO1 tail peptide (NH_2-RKFNMKMI-OH) mimicked the inactivation of the full-length LINGO1 protein when co-expressed with BK channels. The application of

LINGO2 tail peptide (NH_2-RRFNMKMI-OH) also induced inactivation of BK channels. However, the LINGO4 tail peptide (NH_2-GNRVTAKLF-OH) did not induce inactivation of BK channels. This difference in effect perhaps may be due to the absence of the KMI motif in LINGO4 (Mi *et al*. 2013) or alternatively, the net charge of LINGO4 tail peptide.

In Chapter 4, we utilised the acylated amide modifications of LINGO1 to eliminate the charges at the N and C termini of the peptide. We demonstrated that the effects of acylated amidated versions of the LINGO1 peptide produced effects that were very similar to those obtained with the amino free acid version of the peptide. In addition, we found that the elongated LINGO1 peptide (14-residues) slightly reduced the efficacy of the peptide, although it was still able to inactivate BK channels. Importantly, the individual neutralisation of the R613 or K614 residues, reduced binding affinity of the peptide, suggesting that the net positive charge of the LINGO1 peptide affected its ability to bind and inactivate BK channels. Interestingly, the double neutralisation of the R613:K618 or K614: K618 abolished the inactivation mediated by the LINGO1 tail peptide and similar effects were observed when the three positively charged residues were neutralised. These data perhaps suggest that there may be an electrostatic interaction between the negatively charged E321, E324 residues at the base of the BK S6 helices (Brelidze *et al.* 2003; Nimigean *et al.* 2003) and the positively charged residues of LINGO1 peptide. These results also suggested that the position and charge at K618 residue in LINGO1 was essential for inactivation of BK currents, whereas the positive charges at R613 and K614 may play a role in maintaining the stability of the block by the LINGO1 tail peptide. However, to confirm this, additional co-expression experiments of the mutant full-length LINGO1 protein with BK will be required

Interestingly, the neutralisation of the KMI residues in the peptide failed to induce inactivation of the BK currents. These data suggest that the terminal three residues in LINGO1 are essential for inactivation and are in agreement with the results of Dudem *et al*. (2020) who demonstrated that the deletion of these three residues in the full-length LINGO1 protein (618-620) practically abolished inactivation.

In Chapter 5, we utilised the amino free acid version of LINGO1 tail peptide and demonstrated that the scrambled version of the tail peptide reduced the affinity of the peptide for the BK channel. Interestingly, the replacement of K618 with either polar or non-polar amino acid residues removed the ability of the peptide to inactivate BK currents. These data confirmed that the position of the positive charge (at K618) was crucial to mediate inactivation of BK channels. In contrast, the neutralisation of positive charges at R613 and K614 residues in the peptide still resulted in inactivation of BK channels, although the affinity of this peptide was reduced.

We also generated acylated free acid modifications of the LINGO1 tail peptide, where the R613 residue had an acylated (Ac) N-terminus and the I620 residue had a free acid (OH) at the end of the C-terminus, to mimic the condition of the full-length LINGO1 protein. With this modification the net charge of the tail peptide reduced to +2, and it only slightly altered the apparent affinity of the peptide for the BK channel. However, we noted that a peptide consisting of the final 4-residues of the C-terminus of the LINGO1 protein, failed to induce block or inactivation of BK currents (Figure 5.21), suggesting that this peptide did not possess the minimal essential structure to mimic inactivation, observed with the 8-residue peptide. Interestingly, we also noticed that the application of peptides in which F615, M617, K618 and M619 (Figures 5.19, 5.11, 5.13, 5.15, respectively) were replaced with alanine residues, failed to induce inactivation of BK channels, but did block them. These results perhaps suggest that the observed block induced by these mutant peptides was unstable due to the reduced electrostatic and hydrophobic interactions between the peptide and the channel. However, to confirm this, additional single channel experiments will be required. The individual role of isoleucine at 620 in the LINGO1 tail peptide-mediated inactivation of BK channels remains to be elucidated. Interestingly, the replacement of the asparagine at 616 with an alanine residue induced inactivation of BK currents although with a reduced affinity. These results suggest that the alterations to residues at this position were better tolerated than those closer to the C-terminus of the peptide. These results support the idea that the positive charges at residues R613, K614 and K618 in the LINGO1 tail peptide are necessary but not sufficient to confer inactivation of BK channels.

Future experiments will examine if these mutations in the full-length LINGO1 protein, co-expressed with BK behave in a similar manner to that of the LINGO1 tail peptide. The data so far suggests that the LINGO1 peptide-mediated inactivation of BK channels is dependent on a number of features. The essential components required for LINGO1 peptide-mediated inactivation of BK channels are highlighted in Figure 7.1.

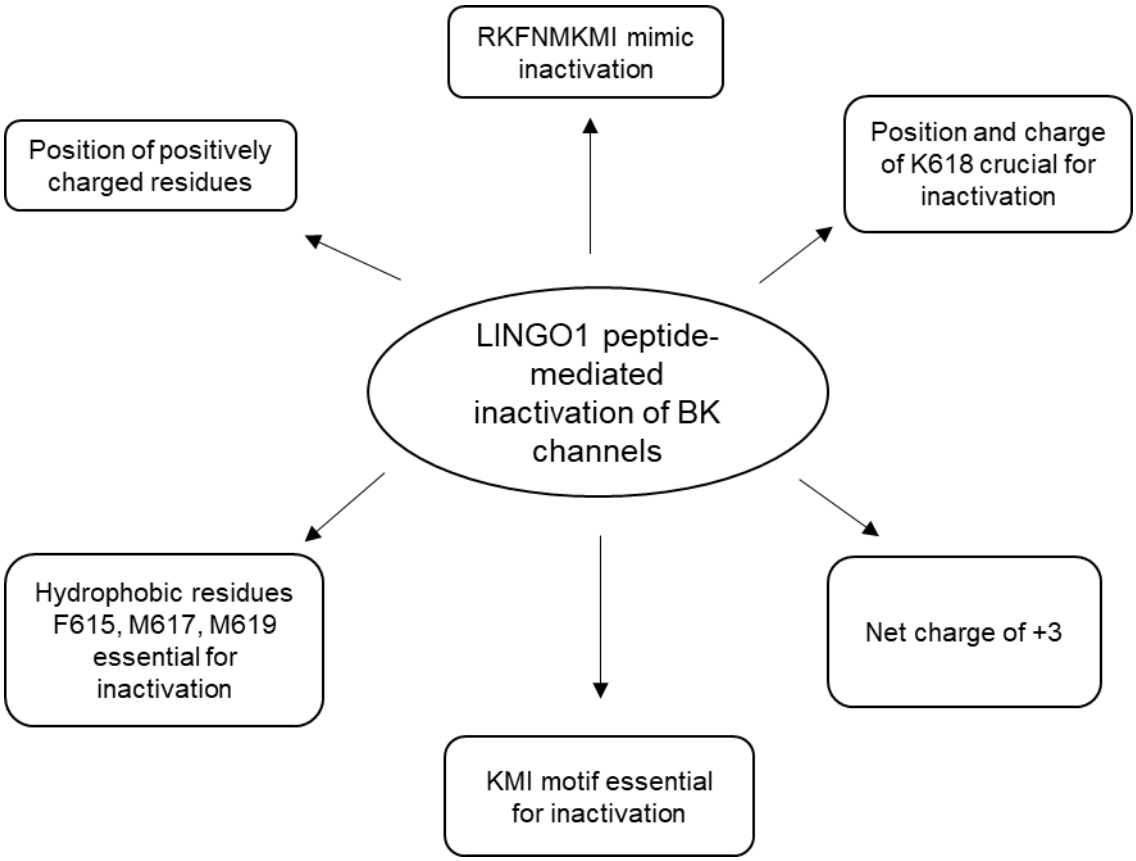

Figure 7.1: Schematic of LINGO1 peptide-mediated inactivation of BK channels.
The summary of LINGO1 peptide-mediated inactivation of BK channels. Each arrow depicts an essential component required for inactivation of BK channels.

The final results chapter demonstrated that the LINGO1 tail peptide appeared to insert itself in the pore of the BK channel, since the QA ion, TPAB and LINGO1 appear to compete for a common binding site. However, to confirm this, additional experiments involving application of TPAB to cells co-expressing full-length LINGO1 protein and BK will be required.

On the basis of the homology model (Figure 6.4) of the LINGO1 tail docked with the BK channel, we identified a number of residues in the BK channel pore, that may interact with the LINGO1 tail peptide. When the negative charge on the E324 was neutralised with an alanine residue, it altered the affinity of the LINGO1 tail peptide to the channel. Interestingly, the double charge neutralisation (E321A:E324A), single charge reversal (E324R) and the double charge reversal (E321R:E324R) mutants all produced quantitatively similar effects with the LINGO1 peptide. All of these mutants showed reduced affinity of the peptide to the mutant channels, suggesting that there may be a possible electrostatic interaction between the positively charged residues of the tail peptide with the negatively charged residues of the BK channel pore. However, the effects of LINGO1 peptide on charge neutralisation and charge reversal mutants of E321 residue of the BK channel remain to be elucidated.

Previous studies have reported that LINGO1 promotes the lysosomal degradation of -amyloid precursor protein (A PP) and carboxy-terminal fragment (CTF), in the presence of the -secretase inhibitor in cortical neurons (de Laat *et al.* 2015). Interestingly, LINGO1 expression was localised to intracellular puncta, possibly reflecting expression on intracellular membranous organelles, however, no cell-surface LINGO immunoreactivity was apparent in both mouse cerebellar granule neurons and cardiac myocytes (Meabon *et al.* 2015). In our recently published study, we have reported that both BK and LINGO1 localised to the cell membrane in HEK293 cells. Furthermore, it was demonstrated that LINGO1 supressed cell surface expression of BK channels (Dudem *et al.* 2020). The changes in distribution of BK on the HEK293 cell surface membrane and the mechanism by which LINGO1 suppresses expression of BK remain to be elucidated.

In addition, LINGO1 and BK proteins coimmunoprecipitated in both PD patients and age-matched control samples, suggesting that these proteins closely associated in the membranes of native human tissues (Dudem *et al.* 2020). However, additional research is required to elucidate if LINGO1 and BK proteins are associated in action potential firing patterns in neurons and other neuronal disorders like essential tremor, multiple sclerosis and chronic ataxia.

Furthermore, when we investigated the co-expression of LINGO1, BK , and either BK 1or BK 4 in HEK293 cells, it was observed that in the presence of either of the BK subunits, LINGO1 still inactivated BK channels although with a reduced rate of inactivation than BK :LINGO1 co-expression experiments (Dudem *et al.* 2020). However, additional research is required to elucidate if LINGO1 inactivation is affected by BK auxiliary subunits.

It is important to note that the interpretation of the experiments reported in this thesis is open to the criticism that they were carried out on an untethered, short chain of amino acids, albeit with a sequence identical to that of the C-terminus of the LINGO1 protein. Nevertheless, these peptides will have more freedom in solution compared to tethered LINGO1 protein and it is possible that they could bind to the BK channels in more than one configuration. It will therefore be necessary to carry out experiments with mutations in the full-length LINGO1 protein, co-expressed with BK , to determine if they behave in a similar manner to that of the LINGO1 tail peptide. However, the most direct way of examining which residues play an important role, would be to solve the cryo-EM structure of the LINGO1 protein docked in the BK channel open structure. However, we currently have no access to such facilities in Ireland.

In conclusion, the results of this thesis indicated that the last 8-residues of LINGO1 protein mimic the inactivation of the full-length LINGO1 protein, co-expressed with BK . In addition, the position of the positively charged K618 is crucial to mediate LINGO1 tail peptide inactivation of BK currents. Furthermore, it may be possible that the charged and uncharged residues of the LINGO1 tail peptide may participate in electrostatic and hydrophobic interactions with the charged and uncharged residues of the BK channel pore.

7.1 Future Directions

Although this thesis provides useful information about the LINGO1 tail peptide-mediated inactivation of BK channels, it is clear that additional research is required to elucidate the mechanism of its effects. Future experiments could be directed at:

1. Examining whether the other subtypes of LINGO proteins (LINGO2, LINGO3 and LINGO4) behave in a similar manner to those of the LINGO peptides utilised.
2. Examining whether the co-expression of BK with mutations of LINGO1 protein behave in a similar manner to those observed in LINGO1 mutant peptides.
3. Examining whether the co-expression of BK mutants with LINGO1 protein behave in a similar manner to those observed with LINGO1 peptide.
4. Investigating the mechanism of inactivation of BK channels (one-step or two-step binding) mediated by LINGO1 tail peptide and LINGO1 protein.
5. Identifying the potential interacting sites between the LINGO1 protein and the BK channel pore.
6. Investigating the possible involvement of negatively charged residues in S6 domain of BK channels on C-type inactivation.
7. Examining the protein expression of BK and LINGO1-4 subtypes in tracheal muscles and brain sections.

8. References

Adams, P.R., Constanti, A., Brown, D. A. Clark, R. B. (1982). Intracellular Ca^{2+} activates a fast voltage-sensitive K^+ current in vertebrate sympathetic neurones. *Nature, 296*(5859), 746-749.

Almassy, J., Begenisich, T. (2012). The LRRC26 protein selectively alters the efficacy of BK channel activators. *Molecular Pharmacology, 81(1),* 21 30.

Ansar, M., Riazuddin, S., Sarwar, M. T., Makrythanasis, P., Paracha, S. A., Iqbal, Z., Khan, J., Assir, M. Z., Hussain, M., Razzaq, A., Polla, D. L., Taj, A. S., Holmgren, A., Batool, N., Misceo, D., Iwaszkiewicz, J., de Brouwer, A. P. M., Guipponi, M., Hanquinet, S., Zoete, V., Santoni, F. A., Frengen, E., Ahmed, J., Riazuddin, S., van Bokhoven, H., Antonarakis, S. E. (2018). Biallelic variants in LINGO1 are associated with autosomal recessive intellectual disability, microcephaly, speech and motor delay. *Genetics in Medicine, 20*, 778-784.

Armstrong, C. M. and Gilly, W. F. (1992). Access resistance and space clamp problems associated with whole-cell patch clamping. *Methods in Enzymology, 207*, 100-122.

Armstrong, C. M., Bezanilla, F., Rojas, E. (1973). Destruction of sodium conductance inactivation in squid axons perfused with pronase. *The Journal of General Physiology,* 62, 375 391.

Bando, T., Sekine, K., Kobayashi, S., Watabe, A. M., Rump, A., Tanaka, M., Suda, Y., Kato, S., Morikawa, Y., Manabe, T., Miyajima, A. (2005). Neuronal leucine rich repeat protein 4 functions in hippocampus-dependent long-lasting memory. *Molecular and Cell Biology, 25*, 4166-4175.

Bao, L., Kaldany, C., Holmstrand, E. C, Cox, D. H. (2004). Mapping the BK_{Ca} $^{2+}$ -chains essential for Ca^{2+} sensing. *The Journal of General Physiology, 123*, 475 489.

high-affinity Ca^{2+} sensitivity. *The Journal of General Physiology, 120*, 173 189.

Bella, J., Hindle, K. L., McEwan, P. A., Lovell, S. C. (2008). The leucine-rich repeat structure. *Cell and Molecular Life Sciences, 65*, 2307 2333.

Bentzen, B. H., Nardi, A., Calloe, K., Madsen, L. S., Olesen, S. P., Grunnet, M. (2007). The small molecule NS11021 is a potent and specific activator of Ca^{2+}-activated big-conductance K^+ channels. *Molecular Pharmacology, 72*, 1033 1044.

Bentzen, B. H., Osadchii, O., Jespersen, T., Hansen, R. S., Olesen, S. P, Grunnet, M. (2009). Activation of big conductance Ca^{2+}-activated K^+ channels (BK) protects the heart against ischemia-reperfusion injury. *Pflügers Archiv: European Journal of Physiology, 457*, 979 988.

Berkefeld, H., Sailer, C. A., Bildl, W., Rohde, V., Thumfart, J. O., Eble, S., Klugbauer, N., Reisinger, E., Bischofberger, J., Oliver, D., Knaus, H. G., Schulte, U., Fakler, B. (2006). BK_{Ca}-Cav channel complexes mediate rapid and localized Ca^{2+}-activated K^+ signalling. *Science, 314*, 615-620.

Bermingham, J.R. Jr., Shearin, H., Pennington, J., O'Moore, J., Jaegle, M., Driegen, S., van Zon, A., Darbas, A., Ozkaynak, E., Ryu, E. J., Milbrandt, J., Meijer, D. (2006). The claw paw mutation reveals a role for Lgi4 in peripheral nerve development. *Nature Neuroscience, 9*, 76-84.

Bezanilla, F. and Armstrong, C. M. (1977). Inactivation of the sodium channel. I. Sodium current experiments. *Journal of General Physiology, 70,* 549 566.

Bian, S., Favre, I., Moczydlowski, E. (2001). Ca^{2+}-binding activity of a COOH-terminal fragment of the Drosophila BK channel involved in Ca^{2+}-dependent activation. *Proceedings of the National Academy of Sciences of the USA, 98*, 4776 4781.

Blanc, E., Romi-Lebrun, R., Bornet, O., Nakajima, T., Darbon, H. (1998). Solution structure of two new toxins from the venom of the Chinese scorpion Buthus martensi Karsch blockers of potassium channels. *Biochemistry, 37,* 12412 12418.

Blatz, A. L. and Magleby, K. L. (1984). Ion conductance and selectivity of single calcium-activated potassium channels in cultured rat muscle. *The Journal of General Physiology, 84*, 1 23.

Bocksteins, E. (2016). Kv5, Kv6, Kv8, and Kv9 subunits: No simple silent bystanders. *The Journal of General Physiology, 147*(2), 105-125.

Bolton, T. B. and Imaizumi, Y. (1996). Spontaneous transient outward currents in smooth muscle cells. *Cell Calcium, 20*, 1411 1452.

Brayden, J. E., Nelson, M. T. (1992). Regulation of arterial tone by activation of calcium-dependent potassium channels. *Science, 256*(5056), 532-535.

Brelidze, T. I. and Magleby, K. L. (2005). Probing the Geometry of the Inner Vestibule of BK Channels with Sugars. *The Journal of General Physiology, 126*(2), 105 121.

Brelidze, T. I., Niu, X., Magleby, K. L. (2003). A ring of eight conserved negatively charged amino acids doubles the conductance of BK channels and prevents inward rectification. *Proceedings of the National Academy of Sciences of the USA, 100*, 9017 9022.

Brenner, R., Jegla, T. J., Wickenden, A., Liu, Y., Aldrich, R. W. (2000a). Cloning and functional characterization of novel large conductance calcium-activated potassium channel beta subunits, hKCNMB3 and hKCNMB4. *Journal of Biological Chemistry, 275* ,6453 6461.

Brenner, R., Perez, G. J., Bonev, A. D., Eckman, D. M., Kosek, J. C., Wiler, S. W., Patterson, A. J., Nelson, M. T., Aldrich, R. W. (2000b). Vasoregulation by the beta1 subunit of the calcium-activated potassium channel. *Nature, 407*, 870 876.

Bruening-Wright, A., Lee, W. S., Adelman, J.P., Maylie, J. (2007). Evidence for a deep pore activation gate in small conductance Ca^{2+}-activated K^+ channels. *The Journal of General Physiology*, *130*, 601 610.

Buckley, C., Williams, J., Munteanu, T., King, M., Park, S. M., Meredith, A. L., Lynch, T. (2020). Status Dystonicus, Oculogyric Crisis and Paroxysmal Dyskinesia in a 25 Year-Old Woman with a Novel KCNMA1 Variant, K457E. *Tremor and Other Hyperkinetic Movements*, *10(1),* 1 6.

Budelli, G., Geng, Y., Butler, A., Magleby, K. L., Salkoff, L. (2013). Properties of Slo1 K^+ channels with and without the gating ring. *Proceedings of the National Academy of Sciences of the USA, 110(41)*, 16657 16662.

Bukiya, A. N., Singh, A. K., Parrill, A. L., Dopico, A. M. (2011). The steroid interaction site in transmembrane domain 2 of the large conductance, voltage- and calcium-gated potassium (BK) channel accessory beta1 subunit. *Proceedings of the National Academy of Sciences of the USA*,*108(50)*, 20207 20212.

Butler, A., Tsunoda, S., McCobb, D. P., Wei, A., Salkoff L. (1993). mSlo, a Complex Mouse Gene Encoding "Maxi" Calcium-Activated Potassium Channels. *Science, 261*, 221-224.

Cai, Z., Xu, C., Xu, Y., Lu, W., Chi, C. W., Shi, Y., Wu, J. (2004). Solution structure of BmBKTx1, a new BKCa1 channel blocker from the Chinese scorpion Buthus martensi Karsch. *Biochemistry, 43*(13), 3764-3771.

Carrasquel-Ursulaez, W., Contreras, G. F., Sepulveda, R. V., Aguayo, D., Gonzalez-Nilo, F., Gonzalez, C., Latorre, R. (2015). Hydrophobic interaction between contiguous residues in the S6 transmembrane segment acts as a stimuli integration node in the BK channel. *The Journal of General Physiology*, *145*, 61-74.

Castillo, J. P., Sanchez-Rodriguez, J. E., Hyde, H. C., Zaelzer, C. A., Aguayo, D., Sepulveda, R. V., Luk, L. Y., Kent, S. B., Gonzalez-Nilo, F. D., Bezanilla, F., Latorre, R. (2016). Beta1-subunit-induced structural rearrangements of the Ca^{2+}-and voltage-activated K^+ (BK) channel. *Proceedings of the National Academy of Sciences of the USA, 113*, E3231 3239.

Cha, A. and Bezanilla, F. (1997). Characterizing Voltage-Dependent Conformational Changes in the Shaker K^+ Channel with Fluorescence. *Neuron, 19,* 1127 1140.

Chen, C. Y. (2017). Patch Clamp Technique and Applications. In: Jue T. (eds) Modern Tools of Biophysics. *Handbook of Modern Biophysics, Springer, New York, (5),* 49-64.

Chen, X., Yan, J., Aldrich, R. W. (2014). BK channel opening involves side-chain reorientation of multiple deep-pore residues. *Proceedings of the National Academy of Sciences of the USA*, *111*, E79 E88.

Cheng, H., Lederer, M. R., Lederer, W. J., Cannell, M. B. (1996). Calcium sparks and $[Ca^{2+}]_i$ waves in cardiac myocytes. *American Journal of Physiology: Cell Physiology, 270,* C148 C159.

Cheng, H., Lederer, W. J., Cannell, M. B. (1993). Calcium sparks: elementary events underlying excitation-contraction coupling in heart muscle. *Science, 262*, 740 744.

Chester, N. and Marshak, D. R. (1993). Dimethyl sulfoxide-mediated primer Tm reduction: a method for analyzing the role of renaturation temperature in the polymerase chain reaction. *Analytical Biochemistry, 209*, 284-290.

Choi, K. L., Aldrich, R.W., Yellen, G. (1991). Tetraethylammonium blockade distinguishes two inactivation mechanisms in voltage-activated K^+ channels. *Proceedings of the National Academy of Sciences of the USA, 88*, 5092-5095.

Cole, K. S. (1949). Dynamic electrical characteristics of the squid axon membrane. *Archives des Sciences Physiologiques, 3*, 253--258.

Contreras, G. F., Castillo, K., Enrique, N., Carrasquel-Ursulaez, W., Castillo, J. P., Milesi, V., Neely, A., Alvarez, O., Ferreira, G., González, C., Latorre, R. (2013). A BK (Slo1) channel journey from molecule to physiology. *Channels (Austin), 7*(6), 442 458.

Cox, D. H., Cui, J., Aldrich, R. W. (1997). Allosteric gating of a large conductance Ca-activated K^+ channel. *The Journal of Physiology*, *110*, 257 281.

Crest, M., Jacquet, G., Gola, M., Zerrouk, H., Benslimane, A., Rochat, H., Mansuelle, P., Martin-Eauclaire, M. F. (1992). Kaliotoxin, a novel peptidyl inhibitor of neuronal BK-type Ca(2+)-activated K+ channels characterized from Androctonus mauretanicus mauretanicus venom. *Journal of Biological Chemistry, 267*(3), 1640-1647.

Cui, J. and Aldrich, R. W. (2000). Allosteric linkage between voltage and Ca^{2+}-dependent activation of BK-type mslo1 K^+ channels. *Biochemistry 39,*15612 15619.

Cui, J., Cox, D.H. and Aldrich, R.W. (1997). Intrinsic Voltage Dependence and Ca^{2+} Regulation of mslo Large Conductance Ca-activated K^+ Channels. *The Journal of General Physiology, 109,* 647 673.

de Laat, R., Meabon, J. S., Wiley, J. C., Hudson, M. P., Montine, T. J., & Bothwell, M. (2015). LINGO-1 promotes lysosomal degradation of amyloid- *Pathobiology of aging and age related diseases, 5*, 25796.

de Wit, J., Hong, W., Luo, L., Ghosh, A. (2011). Role of leucine-rich repeat proteins in the development and function of neural circuits. *Annual Review of Cell and Developmental Biology, 27*, 697 729.

Delay, C., Tremblay, C., Brochu, E., Paris-Robidas, S., Emond, V., Rajput, A. H., Rajput, A., Calon, F. E. (2014). Increased LINGO1 in the Cerebellum of Essential Tremor Patients. *Movement Disorders, 29(13),* 1637 1647.

Denson, D. D., Wang, X., Worrell, R. T, Eaton, D. C. (2000). Effects of fatty acids on BK channels in GH3 cells. *American Journal of Physiology-Cell Physiology*, *279*, C1211 C1219.

Di Resta, C. and Becchetti, A. (2010). Introduction to Ion Channels. In: Becchetti A. and Arcangeli, A. (eds) Integrins and Ion Channels. *Advances in Experimental Medicine and Biology*, *674*. Springer, New York, NY.

Diaz, L., Meera, P., Amigo, J., Stefani, E., Alvarez, O., Toro, L., Latorre, R. (1998). Role of the S4 segment in a voltage-dependent calcium-sensitive potassium (hSlo) channel. *The Journal of Biological Chemistry, 273,* 32430 32436.

Dick, G. M., Rossow, C. F., Smirnov, S., Horowitz, B., Sanders, K. M. (2001). Tamoxifen activates smooth muscle BK channels through the regulatory beta 1 subunit. *Journal of Biological Chemistry, 276*, 34594 34599.

Dolan, J., Walshe, K., Alsbury, S., Hokamp, K., O'Keeffe, S., Okafuji, T., Miller, S. F. C., Tear, G., Mitchell, K. J. (2007). The extracellular Leucine-Rich Repeat superfamily; a comparative survey and analysis of evolutionary relationships and expression patterns. *BioMed Central Genomics, 8,* 320.

Doyle, D. A., Morais Cabral, J., Pfuetzmer, R. A., Kuo, A., Gulbis, J. M., Cohen, S.L., Chait, B. T., MacKinnon R. (1998). The Structure of the Potassium Channel: Molecular Basis of K^+ Conduction and Selectivity. *Science, 280*(5360), 69-77.

Dudem, S. (2019). Effects of GoSLo-SR family of ion channel modulators on BK and K_V7 channels [unpublished]. PhD thesis, Dundalk Institute of Technology.

Dudem, S., Large, R. J., Kulkarni, S., McClafferty, H., Tikhonova, I. G., Sergeant, G. P., Thornbury, K. D., Shipston, M J., Perrino, B. A., Hollywood M. A. (2020). LINGO1 is a novel regulatory subunit of large conductance, Ca^{2+}-activated potassium channels. *Proceedings of the National Academy of Sciences of the USA, 117*(4), 2194-2200.

Dworetzky, S. I., Boissard, C. G., Lum-Ragan, J. T., McKay, M. C., Post-Munson, D. J., Trojnacki, J. T., Chang, C. P, Gribkoff, V. K. (1996). Phenotypic alteration of a human BK (hSlo) channel by hSlobeta subunit co-expression: changes in blocker sensitivity, activation/relaxation and inactivation kinetics, and protein kinase A modulation. *Journal of Neuroscience, 16*, 4543 4550.

Egland, K. A., Liu, X. F., Squires, S., Nagata, S., Man, Y. G., Bera, T. K., Onda, M., Vincent, J. J., Strausberg, R. L, Lee, B., Pastan, I. (2006). High expression of a cytokeratin-associated protein in many cancers. *Proceedings of the National Academy of Sciences of the USA*, *103*, 5929 5934.

Evanson, K. W., Bannister, J. P., Leo, M. D., Jaggar, J. H. (2014). LRRC26 is a functional BK channel auxiliary gamma subunit in arterial smooth muscle cells. *Circulation Research, 115*, 423 431.

Fakler, B., Adelman, J. P. (2008). Control of KCa channels by calcium nano/microdomains. *Neuron, 59*, 873 881.

Fan, C., Sukomon, N., Flood, E., Rheinberger, J., Allen, T. W., Nimigean, C. M. (2020). Ball-and-chain inactivation in a calcium-gated potassium channel. *Nature*, *580(7802),* 288-293.

Fernandez-Fernandez, J. M., Tomas, M., Vazquez, E., Orio, P., Latorre, R., Senti, M., Marrugat, J., Valverde, M. A. (2004). Gain-of-function mutation in the KCNMB1 potassium channel subunit is associated with low prevalence of diastolic hypertension. *Journal of Clinical Investigation, 113*, 1032 1039.

Flynn, G. E. and Zagotta, W. N. (2001). Conformational changes in S6 couple to the opening of cyclic nucleotide-gated channels. *Neuron 30*, 689 698.

Fodor, A. A. and Aldrich, R. W. (2006). Statistical Limits to the Identification of Ion Channel Domains by Sequence Similarity. *The Journal of General Physiology, 127*(6), 755 766.

Frey, B. and Suppman, B. (1995). Demonstration of the Expand™
Fidelity and Higher Yields with a lacI-based PCR Fidelity Assay. *Biochemica, 2*, 34-35.

Fu, Q. L., Hu, B., Wu, W., Pepinsky, R. B., Mi, S., So, K. F. (2008). Blocking LINGO-1 function promotes retinal ganglion cell survival following ocular hypertension and optic nerve transection. *Investigative Ophthalmology and Visual Science, 49(3),* 975-985.

Galvez, A., Gimenez-Gallego, G., Reuben, J. P., Roy-Contancin, L., Feigenbaum, P., Kaczorowski, G. J., Garcia, M. L. (1990). Purification and characterization of a unique, potent, peptidyl probe for the high conductance calcium-activated potassium channel from venom of the scorpion Buthus tamulus. *Journal of Biological Chemistry, 265*(19), 11083-11090.

Gan, G., Yi, H., Chen, M., Sun, L., Li, W., Wu, Y., Ding, J. (2008). Structural basis for toxin resistance of beta4-associated calcium-activated potassium (BK) channels. *Journal of Biological Chemistry, 283*, 24177 24184.

Garcia-Calvo, M., Knaus, H. G., McManus, O. W., Giangiacomo, K. L., Kaczorowski, G. J. and Garcia, M. L. (1994). Purification and Reconstitution of the High-conductance, Calcium activated Potassium Channel from Tracheal Smooth Muscle. *Journal of Biological Chemistry, 269*(1), 676-682.

Garcia-Valdes, J., Zamudio, F. Z., Toro, L., Possani, L. D. (2001). Slotoxin, alphaKTx1.11, a new scorpion peptide blocker of MaxiK channels that differentiates between alpha and alpha+beta (beta1 or beta4) complexes. *FEBS Letters, 505*, 369 373.

Geng, Y., Niu, X., and Magleby, K. L. (2011). Low resistance, large dimension entrance to the inner cavity of BK channels determined by changing side-chain volume. *The Journal of General Physiology, 137*, 533 548.

Gessner, G., Schonherr, K., Soom, M., Hansel, A., Asim, M., Baniahmad, A., Derst, C., Hoshi, T., Heinemann, S. H. (2005). BK_{Ca} channels activating at resting potential without calcium in LNCaP prostate cancer cells. *Journal of Membrane Biology, 208*, 229 240.

ourke, S. T. (2006). Large-conductance, calcium-activated potassium channels: structural and functional implications. *Pharmacology & Therapeutics,110*, 103 116.

Goldklang, M. P., Perez-Zoghbi, J. F, Trischler, J., Nkyimbeng, T., Zakharov, S. I., Shiomi, T.,

asthma using a single small molecule with anti-inflammatory and BK channel-activating properties. *FASEB Journal, 27*, 4975 4986.

González, C., Baez-Nieto, D., Valencia, I., Oyarzún, I., Rojas, P., Naranjo, D., Latorre, R. (2012). K^+ channels: function-structural overview. *Comprehensive Physiology,2*(3), 2087-2149.

Gonzalez-Perez, V. and Lingle, C. J. (2019). Regulation of BK Channels by Beta and Gamma Subunits. *Annual Review of Physiology 81,* 113 137.

Gonzalez-Perez, V., Zeng, X. H., Henzler-Wildman, K., Lingle, C. J. (2012). Stereospecific binding of a disordered peptide segment mediates BK channel inactivation. *Nature, 485(7396),* 133 136.

Griguoli, M., Sgritta, M., Cherubini, E. (2016). Presynaptic BK channels control transmitter release: physiological relevance and potential therapeutic implications. *The Journal of Physiology, 594(13),* 3489 3500.

Grizel, A. V., Glukhov, G. S., Sokolova, O. S. (2014). Mechanisms of activation of voltage-gated potassium channels. *Acta naturae, 6*(4), 10-26.

Grover G. J. and Garlid K. D. (2000). ATP-sensitive potassium channels: a review of their cardioprotective pharmacology. *The Journal of Molecular Cell Cardiology, 32*, 677 695.

Grunnet, M., and Kaufmann, W. A. (2004). Coassembly of big conductance Ca2+- activated K+ channels and L-type voltage-gated Ca2+ channels in rat brain. *Journal of Biological Chemistry, 279*, 36445 36453.

Guan, X., Li, Q., Yan, J. (2017). Relationship between auxiliary gamma subunits and mallotoxin on BK channel modulation. *Science Reports, 7(42240),* 1-10.

Haines, B. P., & Rigby, P. W. J. (2008). Expression of the Lingo/LERN gene family during mouse embryogenesis. *Gene Expression Patterns, 8(2),* 79 86.

Hamill, O. P., Marty, A., Neher, E., Sakmann, B., Sigworth, F. J. (1981). Improved patch-clamp techniques for high-resolution current recording from cells and cell-free membrane patches. *Pflügers Archiv European Journal of Physiology, 391*, 85 100.

Hanahan, D. (1983). Studies on transformation of Escherichia coli with plasmids. *The Journal of Molecular Biology, 166*(4), 557 580.

Hansel, N. N., Pare, P. D., Rafaels, N., Din D. D., Sanford, A., Daley, D., Vergara, C., Huang, L., Elliot, W. M., Pascoe, C. D., Arsenault, B. A., Postma, D. S., Boezen, H. M., Bosse, Y., van den Berge, M., Hiemstra, P. S., Cho, M. H., Litonjua A. A., Sparrow, D., Ober, C., Wise R. A., Connet, J., Neptune, E. R., Beaty, T. H., Ruczinski, I., Mathias, R. A., Barnes, K. C. (2015). Genome-wide Association Study Identification of Novel Loci Associated with Airway Responsiveness in Chronic Obstructive Pulmonary Disease. *American Journal of Respiratory Cell and Molecular Biology, 53*(2), 226-234.

Haug, T., Olcese, R., Toro, L., Stefani, E. (2004). Regulation of K^+ flow by a ring of negative charges in the outer pore of BK_{Ca} channels. Part II: Neutralization of aspartate 292 reduces long channel openings and gating current slow component. *The Journal of General Physiology, 124,* 185 197.

Herrington, J., Solaro, C. R., Neely, A., Lingle, C. J. (1995). The suppression of Ca^{2+}- and voltage dependent outward K^+ current during mAChR activation in rat adrenal chromaffin cells. *Journal of Physiology, 485,* 297 318.

Hicks, G. A. and Marrion, N. V. (1998). Ca^{2+} dependent inactivation of large conductance Ca^{2+}-activated K^+ (BK) channels in rat hippocampal neurones produced by pore block from an associated particle. *Journal of Physiology, 508,* 721 734.

Hille, B. (2001). Ion channels of excitable membranes. 3rd edition. *Sunderland: Sinauer associates.*

Hite, R. K., Tao, X., MacKinnon, R. (2017). Structural basis for gating the high-conductance Ca^{2+}-activated K^+ channel. *Nature, 541*, 52 57.

Hodgkin, A. L., Huxley, A. F. (1952). A quantitative description of membrane current and its application to conduction and excitation in the nerve. *The Journal of Physiology, 117*(4), 500-544.

Homma, S., Shimada, T., Hikake, T., Yaginuma, H. (2009). Expression pattern of LRR and Ig domain-containing protein (LRRIG protein) in the early mouse embryo. *Gene Expression Patterns, 9*(1), 1 26.

Horrigan, F. T. (2012). Conformational coupling in BK potassium channels. *The Journal of General Physiology, 140*(6), 625-634.

Horrigan, F. T., Aldrich, R. W. (1999). Allosteric voltage gating of potassium channels II. Mslo channel gating charge movement in the absence of Ca^{2+}. *The Journal of General Physiology, 114,* 305 336.

Horrigan, F. T., Aldrich, R. W. (2002). Coupling between voltage sensor activation, Ca^{2+} binding and channel opening in large conductance (BK)potassium channels. *The Journal of General Physiology, 120*, 267 305.

Horrigan, F. T., Cui, J., Aldrich, R. W. (1999). Allosteric voltage gating of potassium channels I. Mslo ionic currents in the absence of Ca^{2+}. *The Journal of General Physiology, 114,* 277 304.

Hoshi, T., Tian, Y., Xu, R., Heinemann, S. H., Hou, S. (2013a). Mechanism of the modulation of BK potassium channel complexes with different auxiliary subunit compositions by the omega-3 fatty acid DHA. *Proceedings of the National Academy of Sciences of the USA, 110*, 4822 4827.

Hoshi, T., Wissuwa, B., Tian, Y., Tajima N., Xu, R., Bauer, M., Heinemann, S. H., Hou, S. (2013b). Omega-3 fatty acids lower blood pressure by directly activating large-conductance Ca^{2+} dependent K^+ channels. *Proceedings of the National Academy of Sciences of the USA, 110*, 4816 4821.

Hoshi, T., Zagotta, W. N., Aldrich, R. W. (1990). Biophysical and molecular mechanisms of Shaker potassium channel inactivation. *Science, 250,* 533 538.

Hou, P., Zeng, W., Gan, G., Lv, C., Guo, X., Zhang, Z., Liu, H., Wu, Y., Yao, J., Wei, A. D., Wang, S., Ding, J. (2013). Inter- / subunits coupling mediating pre-inactivation and augmented activation of BK_{Ca}(2). *Scientific reports, 3(1666),* 1-8.

Hu, H., Shao, L. R., Chavoshy, S., Gu, N., Trieb, M., Behrens, R., Laake, P., Pongs, O., Knaus, H. G., Ottersen, O. P., Storm, J. F. (2001). Presynaptic Ca^{2+}-activated K^+ channels in glutamatergic hippocampal terminals and their role in spike repolarization and regulation of transmitter release. *Journal of Neuroscience, 21*, 9585 9597.

Hu, L., Shi, J., Ma, Z., Krishnamoorthy, G., Sieling, F., Zhang, G., Horrigan, F. T., Cui, J. (2003). Participation of the S4 voltage sensor in the $Mg2^{+}$-dependent activation of large conductance (BK) K^{+} channels. *Proceedings of the National Academy of Sciences of the USA, 100*, 10488 10493.

Hu, Y., Yang, G., Xiao, X., Liu, L., Li, T. (2014). BK_{Ca} opener, NS1619 pretreatment protects against shock-induced vascular hyporeactivity through PDZ-Rho GEF-RhoA-Rho kinase pathway in rats. *Journal of Trauma and Acute Care Surgery, 76*, 394 401.

Huang, C. W., Huang, C. C., Wu, S. N. (2007). Activation by zonisamide, a newer antiepileptic drug, of large-conductance calcium-activated potassium channel in differentiated hippocampal neuron-derived H19-7 cells. *Journal of Pharmacology and Experimental Therapeutics, 321*, 98 106.

Inoue, H., Lin, L., Lee, X., Shao, Z., Mendes, S., Snodgrass-Belt, P., Sweigard, H., Engber, T., Pepinsky, B., Yang, L., Beal, M. F., Mi, S., Isacson, O. (2007). Inhibition of the leucine-rich repeat protein LINGO-1 enhances survival, structure, and function of dopaminergic neurons in *Proceedings of the National Academy of Sciences of the USA, 104(36),* 14430 14435.

Inoue, H., Nojima, H., Okayama, H. (1990). High efficiency transformation of Escherichia coli with plasmids. *Gene, 96*, 23-28.

Islas, L. D., Sigworth, F. J. (1999). Voltage Sensitivity and Gating Charge in Shaker and Shab Family Potassium Channels. *The Journal of General Physiology, 114,* 723-741.

Jaggar, J. H., Porter, V. A., Lederer, W. J., Nelson, M. T. (2000). Calcium sparks in smooth muscle. *American Journal of Physiology: Cell Physiology, 278,* C235-C256.

Javaherian, A. D., Yusifov, T., Pantazis, A., Franklin, S., Gandhi, C. S., Olcese, R. (2011). Metal-driven operation of the human large-conductance voltage- and Ca^{2+}-dependent potassium channel (BK) gating ring apparatus. *Journal of Biological Chemistry, 286*, 20701 20709.

Ji, B., Li, M., Wu, W. T., Yick, L. W., Lee, X., Shao, Z., Wang, J., So, K. F., McCoy, J. M., Pepinsky, R. B., Mi, S., Relton, J. K. (2006). LINGO-1 antagonist promotes functional recovery and axonal sprouting after spinal cord injury. *Molecular and Cellular Neuroscience, 33*(3), 311 320.

Ji, Y., Wei, Y., Park, J., Hung, L., Y., Young, T., Herbine, K., Oniskey, T., Pastore, C., Nieves, W., Somsouk, M., Herbert, D. R. (2019). TFF3 is a ligand for LINGO2 that de-represses EGFR to control disease outcome during colitis and gastrointestinal nematode infection. *BioRxiv, 469700*, 1-17.

Jiang, Y., Lee, A., Chen, J., Cadene, M., Chait, B. T., MacKinnon, R. (2002b). The open pore conformation of potassium channels. *Nature, 417*, 523 526.

Jiang, Y., Lee, A., Chen, J., Cadene, M., Chait, B.T., MacKinnon, R. (2002a). Crystal structure and mechanism of a calcium-gated potassium channel. *Nature 417*, 515-522.

Jiang, Y., Pico, A., Cadene, M., Chait, B. T., MacKinnon, R. (2001). Structure of the RCK Domain from the E. coli K^+ Channel and Demonstration of Its Presence in the Human BK Channel. *Neuron, 29*, 593 601.

Kajava, A. V. (1998). Structural diversity of leucine-rich repeat proteins. *Journal of Molecular Biology, 277,* 519 527.

Kielian, T. (2009). Overview of Toll-like receptors in the CNS. *Current Topics in Microbiology and Immunology, 336*, 1 14.

King, J. T., Lovell, P. V., Rishniw, M., Kotlikoff, M. I., Zeeman, M. L., McCobb, D. P. (2006). Beta2 and beta4 subunits of BK channels confer differential sensitivity to acute modulation by steroid hormones. *Journal of Neurophysiology, 95*, 2878-2888.

Kiraly, I., Pataricza, J., Bajory, Z., Simonsen, U., Varro, A., Papp, J. G., Pajor, L., Kun, A. (2013). Involvement of large-conductance Ca^{2+}-activated K^+ channels in both nitric oxide and endothelium-derived hyperpolarization-type relaxation in human penile small arteries. *Basic and Clinical Pharmacology and Toxicology,113*, 19 24.

Kis, A., Krick, S., Baumlin, N., Salathe, M. (2016). Airway Hydration, Apical K^+ Secretion, and the Large-Conductance, Ca^+-activated and Voltage-dependent Potassium (BK) Channel. *Annals of the American Thoracic Society, 13(2),* 163-168.

Knaus, H. G., Folander, K., Garcia-Calvo, M., Garcia, M. L., Kaczorowski, G. J., Smith, M., Swanson, R. (1994a). Primary sequence and immunological characterization of beta-subunit of high conductance Ca^{2+}-activated K^+ channel from smooth muscle. *Journal of Biological Chemistry, 269*, 17274 17278.

Knaus, H. G., Garcia-Calvo, M., Kaczorowski, G. J., Garcia, M. L. (1994b). Subunit composition of the high conductance calcium-activated potassium channel from smooth muscle, a representative of the mSlo and slowpoke family of potassium channels. *Journal of Biological Chemistry, 269*, 3921 3924.

Knaus, H. G., Schwarzer, C., Koch, R. O., Eberhart, A., Kaczorowski, G. J., Glossmann, H., Wunder, F., Pongs, O., Garcia, M. L., Sperk, G. (1996). Distribution of high-conductance Ca(2+)- activated K+ channels in rat brain: targeting to axons and nerve terminals. *Journal of Neuroscience, 16*, 955 963.

Kobe, B. and Kajava, A.V. (2001). The leucine-rich repeat as a protein recognition motif. *Current Opinion in Structural Biology, 11*, 725 732.

Kobe, B., and Deisenhofer, J. (1993). Crystal structure of porcine ribonuclease inhibitor, a protein with leucine-rich repeats. *Nature, 366*, 751 756.

Koval, O. M., Fan, Y. R., Brad, S. (2007). A Role for the S0 Transmembrane Segment in Voltage-dependent Gating of BK Channels. *The Journal of General Physiology, 129*(3), 209-220.

Kun, A., Matchkov, V. V., Stankevicius, E., Nardi, A., Hughes, A. D., Kirkeby, H. J., Demnitz, J., Simonsen, U. (2009). NS11021, a novel opener of large-conductance Ca^{2+}-activated K^+ channels, enhances erectile responses in rats. *British Journal of Pharmacology, 158*, 1465 1476.

Kutluay, E., Roux, B., Heginbotham, L. (2005). Rapid Intracellular TEA Block of the KcsA Potassium Channel. *Biophysical Journal, 88*, 1018 1029.

La Fuente, J. M., Fernandez, A., Cuevas, P., Gonzalez-Corrochano, R., Chen, M. X., Angulo, J. (2014). Stimulation of large-conductance calcium-activated potassium channels inhibits neurogenic contraction of human bladder from patients with urinary symptoms and reverses acetic acid-induced bladder hyperactivity in rats. *European Journal of Pharmacology, 735*, 68 76.

Large, R. J., Kshatri, A., Webb, T. I., Roy, S., Akande, A., Bradley, E., Sergeant, G. P., Thornbury, K. D., McHale, N. G., Hollywood, M. A. (2015). Effects of the novel BK (KCa1.1) channel opener GoSlo-SR-5- *British Journal of Pharmacology, 172(10),* 2544-2556.

Latorre, R. and Brauchi, S. (2006). Large conductance Ca^{2+}-activated K^+ (BK) channel: Activation by Ca^{2+} and voltage. *Biological Research, 39*, 385-401.

Latorre, R., Castillo, K., Carrasquel-Ursulaez, W., Sepulveda, R. V., Gonzalez-Nilo, F., Gonzalez, C., Alvarez, O. (2017). Molecular Determinants of BK Channel Functional Diversity and Functioning. *Physiology Reviews, 97*, 39 87.

Layne, J. J., Nausch, B., Olesen, S. P., Nelson, M. T. (2010). BK channel activation by NS11021 decreases excitability and contractility of urinary bladder smooth muscle. *American Journal of Physiology-Lung Cellular and Molecular Physiology, 298*, R378 R384.

Ledwell, J, L., Aldrich, R. W. (1999). Mutations in the S4 Region Isolate the Final Voltage-dependent Cooperative Step in Potassium Channel Activation. *The Journal of General Physiology, 113*, 389-414.

Lee, U. S., Cui, J. (2010). BK channel activation: Structural and functional insights. *Trends in Neuroscience, 33*(9), 425-423.

Li, Q., Fan, F., Kwak, H. R., Yan, J. (2015). Molecular basis for differential modulation of BK channel voltage-dependent gating by auxiliary gamma subunits. *Journal of General Physiology, 145*, 543 554.

Li, Q., Li, Y., Wei, H., Pan, H. M., Vouga, A. G., Rothberg, B. S., Wu, Y., Yan, J. (2018). Molecular determinants of Ca2+ sensitivity at the inter subunit interface of the BK channel gating ring. *Scientific reports, 8(509)*, 1-9.

Li, Q., Yan, J. (2016). Modulation of BK Channel Function by Auxiliary Beta and Gamma Subunits. *International Review of Neurobiology,* 128, 51 90.

Li, W., Aldrich, R. W. (2004). Unique inner pore properties of BK channels revealed by quaternary ammonium block. *The Journal of General Physiology, 124*, 43 57.

Li, W., Aldrich, R. W. (2006). State-dependent Block of BK Channels by Synthesized Shaker Ball Peptides. *The Journal of General Physiology, 128*(4), 423-441.

Li, Z. W., Ding, J. P., Kalyanaraman, V., Lingle, C. J. (1999). RINm5f cells express inactivating BK channels whereas HIT cells express non inactivating BK channels. *Journal of Neurophysiology, 81*, 611 624.

Lingle, C.J., Zeng, X-H., Ding, J.-P., Xia, X-M. (2001). Inactivation of BK Channels Mediated by the NH_2 -Step Mechanism:Possible Separation of Binding and Blockade. *The Journal of General Physiology, 117*(6), 583-606.

Lippiat, J. D., Standen, N. B., Davies, N. W. (2000). A residue in the intracellular vestibule of the pore is critical for gating and permeation in Ca^{2+} -activated K^+ (BK_{Ca}) channels. *The Journal of Physiology, 529*, 131 138.

Liu, G., Niu, X., Wu, R. S., Chudasama, N., Yao, Y., Jin, X., Weinberg, R., Zakharov, S. I., Motoike, H., Marx, S.O., Karlin, A. (2010). Location of modulatory b subunits in BK potassium channels. *The Journal of General Physiology*, *135*, 449 459.

Liu, G., Zakharov, S. I., Yang, L., Wu, R. S., Deng, S. X., Landry, D. W., Karlin, A., Marx, S. O. (2008). Locations of the beta1 transmembrane helices in the BK potassium channel. *Proceedings of the National Academy of Sciences of the USA, 105*, 10727 10732.

Liu, H. W., Hou, P. P., Guo, X. Y., Zhao, Z. W., Hu, B., Li, X., Wang, L. Y., Ding, J. P., Wang, S. (2014). Structural basis for calcium and magnesium regulation of a large conductance calcium- ts. *Journal of Biological Chemistry, 289(24),* 16914-16923.

Liu, R., Zhang, Z., Liu, H., Hou, P., Lang, J., Wang, S., Yan, H., Li, P., Huang, Z., Wu, H., Rong, M., Huang, J., Wang, H., Lv, L., Qiu, M., Ding, J., Lai, R. (2013). Human beta-defensin 2 is a novel opener of Ca^{2+}-activated potassium channels and induces vasodilation and hypotension in monkeys. *Hypertension, 62*, 415 425.

Liu, Y. C., Lo, Y. K., Wu, S. N. (2003). Stimulatory effects of chlorzoxazone, a centrally acting muscle relaxant, on large conductance calcium-activated potassium channels in pituitary GH3 cells. *Brain Research, 959*, 86 97.

Liu, Z. W., Li, L. J., Liu, C. G. (2000). Analysis of P/N Leak Subtraction of pClamp Acquisition Software. *Acta Physiologica Sinica, 52(5),* 440-443.

Long, H., Sabatier, C., Ma, L., Plump, A., Yuan, W., Ornitz, D. M., Tamada, A., Murakami, F., Goodman, C. S., Tessier-Lavigne, M. (2004). Conserved roles for Slit and Robo proteins in midline commissural axon guidance. *Neuron, 42*, 213-223.

Long, S. B., Campbell, E. B., MacKinnon, R. (2005). Crystal Structure of a mammalian Voltage-Dependent Shaker Family K^+ Channel. *Science, 309*, 897-902.

Long, S. B., Tao, X., Campbell, E. B. MacKinnon, R. (2007). Atomic structure of a voltage-dependent K+ channel in a lipid membrane-like environment. *Nature, 450*, 376 382.

Lu, Z., Klem, A. M., Ramu, Y. (2001). Ion conduction pore is conserved among potassium channels. *Nature, 413*, 809-813.

Lu, Z., Klem, A. M., Ramu, Y. (2002). Coupling between Voltage Sensors and Activation Gate in Voltage-gated K^+ Channels. *The Journal of General Physiology*, *120*(5), 663-676.

Ma, Z., Lou, X. J., Horrigan, F. T. (2006). Role of Charged Residues in the S1 S4 Voltage Sensor of BK Channels. *The Journal of General Physiology, 127*(3)*,* 309-328.

Majercak, J., Ray, W. J., Espeseth, A., Simon, A., Shi, X. P., Wolffe, C., Getty, K., Marine, S., Stec, E., Ferrer, M., Strulovici, B., Bartz, S., Gates, A., Xu, M., Huang, Q., Ma, L., Shughrue, P., Burchard, J., Colussi, D., Pietrak, B., Kahana, J., Beher, D., Rosahl, T., Shearman, M., Hazuda, D., Sachs, A. B., Koblan, K. S., Seabrook, G. R., Stone, D. J. (2006). LRRTM3 promotes processing of amyloid-precursor protein by BACE1 and is a positional candidate gene for late-*Proceedings of the National Academy of Sciences of the USA*, *103*, 17967 72.

Mandai, K., Guo, T., Hillaire, C. S, Meabon, J. S., Kanning, K. C., Bothwell, M., Ginty, D. D. (2009). LIG Family Receptor Tyrosine Kinase-Associated Proteins Modulate Growth Factor Signals during Neural Development. *Neuron, 63(5),* 614-627.

Mandel, M., Higa, A. (1970). Calcium-dependent bacteriophage DNA infection. *The Journal of Molecular Biology*, *53*(1), 159 162.

Mannuzzu, L. M., Moronne, M. M., Isacoff, E. Y. (1996). Direct Physical Measure of Conformational Rearrangement Underlying Potassium Channel Gating. *Science, 271*, 213-216.

Manzanares, D., Krick, S., Baumlin, N., Dennis, J. S., Tyrrell, J., Tarran, R., Salathe, M. (2015). Airway surface dehydration by growth factor TGF- in cystic fibrosis is due to decreased function of a voltage-dependent potassium channel and can be rescued by the drug pirfenidone. *Journal of Biological Chemistry, 290*, 25710 25716.

Manzanares, D., Srinivasan, M., Salathe, S.T., Ivonnet, P., Baumlin, N., Dennis, J. S., Conner, G. E., Salathe, M. (2014). IFN-gamma-mediated reduction of large-conductance, Ca^{2+} activated, voltage-dependent K^+ (BK) channel activity in airway epithelial cells leads to mucociliary dysfunction. *American Journal of Physiology-Lung Cellular and Molecular Physiology, 306*, L453 L462.

Marmont, G. (1949). Studies on the axon Membrane; a new method. *Journal of Cell Physiology, 34*(3), 351-382.

Marshall, D. L., Vatanpour, H., Harvey, A. L., Boyot, P., Pinkasfeld, S., Doljansky, Y., Bouet, F., Ménez, A. (1994). Neuromuscular effects of some potassium channel blocking toxins from the venom of the scorpion Leiurus quinquestriatus hebreus. *Toxicon, 32*(11), 1433-1443.

Martinez-Espinosa, P. L., Yang, C., Gonzalez-Perez, V., Xia, X. M., Lingle, C. J. (2014). Knockout of the BK 2 subunit abolishes inactivation of BK currents in mouse adrenal chromaffin cells and results in slow-wave burst activity. *Journal of General Physiology, 144*, 275 295.

Matsunami, N., Hadley, D., Hensel, C. H., Christensen, G. B., Kim, C., Frackelton, E., Thomas, K., da Silva, R. P., Stevens, J., Baird, L., Otterud, B., Ho, K., Varvil, T., Leppert, T., Lambert, C. G., Leppert, M., Hakonarson, H. (2013). Identification of rare recurrent copy number variants in high-risk autism families and their prevalence in a large ASD population. *PloS one, 8(1)*, e52239, 1-14.

Matsushima, N. and Miyashita, H. (2012). Leucine-Rich Repeat (LRR) Domains Containing Intervening Motifs in Plants. *Biomolecules*, *2*, 288-311.

McGee, A. W., Yang, Y., Fischer, Q. S., Daw, N. W., Strittmatter, S. M. (2005). Experience-driven plasticity of visual cortex limited by myelin and Nogo receptor. *Science, 309*, 2222-2226.

McManus, O. B., Harris, G. H., Giangiacomo, K. M., Feigenbaum, P., Reuben, J. P., Addy, M. E., Burka, J. F., Kaczorowski, G. J., Garcia, M. L. (1993). An activator of calcium-dependent potassium channels isolated from a medicinal herb. *Biochemistry, 32*, 6128 6133.

McManus, O. B., Helms, L. M., Pallanck, L., Ganetzky, B., Swanson, R., Leonard, R. J. (1995). Functional role of the beta subunit of high conductance calcium-activated potassium channels. *Neuron, 14*, 645 650.

McManus, O. B., Magleby, K. L. (1991). Accounting for the Ca^{2+}-dependent kinetics of single large-conductance Ca^{2+}-activated K^{+} channels in rat skeletal muscle. *The Journal of Physiology*, *443*, 739 777.

Meabon, J. S., De Laat, R., Ieguchi, K., Wiley, J. C., Hudson, M. P., & Bothwell, M. (2015). LINGO-1 protein interacts with the p75 neurotrophin receptor in intracellular membrane compartments. *The Journal of biological chemistry, 290*(15), 9511 9520.

Meera, P., Wallner, M., Song, M., Toro, L. (1997). Large conductance voltage- and calcium-dependent K+ channel, a distinct member of voltage-dependent ion channels with seven N-terminal transmembrane segments (S0-S6), an extracellular N terminus, and an intracellular (S9-S10) C terminus. *Proceedings of the National Academy of Sciences of the USA, 94*(25), 14066 14071.

Meredith, A. L., Thorneloe, K. S., Werner, M. E., Nelson, M. T., Aldrich, R. W. (2004). Overactive bladder and incontinence in the absence of the BK large conductance Ca2-activated K channel. *Journal Of Biological Chemistry*, *279*, 36746-36752.

Mi, S., Hu, B., Hahm, K., Luo, Y., Kam Hui, E. S., Yuan, Q., Wong, W. M., Wang, L., Su, H., Chu, T. H., Guo, J., Zhang, W., So, K. F., Pepinsky, B., Shao, Z., Graff, C., Garber, E., Jung, V., Wu, E. X., Wu, W. (2007). LINGO-1 antagonist promotes spinal cord remyelination and axonal integrity in MOG-induced experimental autoimmune encephalomyelitis. *Nature Medicine, 13*(10), 1228 1233.

Mi, S., Lee, X., Shao, Z., Thill, G., Ji, B., Relton, J., Levesque, M., Allaire, N., Perrin, S., Sands, B., Crowell, T., Cate, R. L., McCoy, J. M., Pepinsky, R. B. (2004) LINGO-1 is a component of the Nogo-66 receptor/p75 signaling complex. *Nature Neuroscience, 7*(3), 221 228.

Mi, S., Miller, R. H., Lee, X., Scott, M. L., Shulag-Morskaya, S., Shao, Z., Chang, J., Thill, G., Levesque, M., Zhang, M., Hession, C., Sah, D., Trapp, B., He, Z., Jung, V., McCoy, J. M., Pepinsky, R. B. (2005). LINGO-1 negatively regulates myelination by oligodendrocytes. *Nature Neuroscience, 8*, 745-751.

Mi, S., Miller, R. H., Tang, W., Lee, X., Hu, B., Wu, W., Zhang, Y., Shields, C. B., Zhang, Y., Miklasz, S., Shea, D., Mason, J., Franklin, R. J., Ji, B., Shao, Z., Chédotal, A., Bernard, F., Roulois, A., Xu, J., Jung, V., Pepinsky B. (2009). Promotion of central nervous system remyelination by induced differentiation of oligodendrocyte precursor cells. *Annals of Neurology, 65*(3) 304 315.

Mi, S., Pepinsky, R. B., Cadavid, D. (2013). Blocking LINGO-1 as a Therapy to Promote CNS Repair: From Concept to the Clinic. *CNS Drugs, 27*, 493 503.

Miller, C., Moczydlowski, E., Latorre, R., Phillips, M. (1985). Charybdotoxin, a protein inhibitor of single Ca^{2+}-activated K^+ channels from mammalian skeletal muscle. *Nature, 313*, 316 318.

Miranda, P., Contreras, J. E., Plested, A. J., Sigworth, F. J., Holmgren, M., Giraldez, T. (2013). State dependent FRET reports calcium- and voltage-dependent gating-ring motions in BK channels. *Proceedings of the National Academy of Sciences of the USA*,*110*, 5217 5222.

Miranda, P., Holmgren, M., Giraldez, T. (2018). Voltage-dependent dynamics of the BK channel cytosolic gating ring are coupled to the membrane-embedded voltage sensor. *eLife, 7*, e40664, 1-18.

Morimoto, T., Sakamoto, K., Sade, H., Ohya, S., Muraki, K., Imaizumi, Y. (2007). Voltage-sensitive oxonol dyes are novel large-conductance Ca^{2+}-activated K^+ channel activators selective for beta1 and beta4 but not for beta2 subunits. *Molecular Pharmacology*, *71*, 1075 1088.

Morrow, J. P., Zakharov, S. I., Liu, G., Yang, L., Sok, A. J., Marx, S. O. (2006). Defining the BK channel domains required for beta1-subunit modulation. *Proceedings of the National Academy of Sciences of the USA, 103*(16), 5096 5101.

Mosyak, L., Wood, A., Dwyer, B., Buddha, M., Johnson, M., Aulabaugh, A., Zhong, X., Presman, E., Benard, S., Kelleher, K., Wilhelm, J., Stahl, M. L., Kriz, R, Gao, Y., Cao, Z., Ling, H-P., Pangalos, M. N., Walsh, F. S., Somers, W. S. (2006). The Structure of the Lingo-1 Ectodomain, a Module Implicated in Central Nervous System Repair Inhibition. *Journal of Biological Chemistry, 281*(47), 36378 36390.

Murrell-Lagnado, R. D. and Aldrich R. W. (1993a). Interactions of amino terminal domains of Shaker K channels with a pore blocking site studied with synthetic peptides. *Journal of General Physiology, 102*, 949-975.

Murrell-Lagnado, R. D. and Aldrich R. W. (1993b). Energetics of Shaker K channels block by inactivation peptides. *Journal of General Physiology, 102*(6), 977-1003.

, P. (2011). Targeting BK (big potassium) channels in epilepsy. *Expert Opinions on Therapeutic Targets, 15*, 1283 1295.

Nardi, A., Calderone, V., Chericoni, S., Morelli, I. (2003). Natural modulators of large-conductance calcium-activated potassium channels. *Planta Medica,* 69, 885-892.

Neher, E. (1992). Correction for liquid junction potentials in patch clamp experiments. *Methods in Enzymology*, 207 123-131.

Neher, E. and Sakmann, B. (1976). Single- channel currents recorded from membrane of denervated frog muscle fibres. *Nature, 260*(5554), 799-802.

Nelson, M. T., Cheng, H., Rubart, M., Santana, L. F., Bonev, A. D., Knot, H. J., Lederer, W. J. (1995). Relaxation of arterial smooth muscle by calcium sparks. *Science, 270*, 633 637.

Nichols, C. G. and Lopatin, A. N. (1997). Inward Rectifier Potassium Channels. *Annual Review of Physiology, 59*, 171 91.

Nilius, B., Droogmans, G. (2001). Ion channels and their functional role in vascular endothelium. *Physiological reviews, 81*(4), 1415-1459.

Nimigean, C. M., Chappie, J. S., Miller C. (2003). Electrostatic tuning of ion conductance in potassium channels. *Biochemistry (Moscow), 42*, 9263 9268.

Niu, X., Qian, X., Magleby, K, L. (2004). Linker-gating ring complex as passive spring and Ca^{2+} dependent machine for a voltage- and Ca^{2+} -activated potassium channel. *Neuron, 42*,745 756.

Nurnberger, T., Brunner, F., Kemmerling, B., Piater, L. (2004). Innate immunity in plants and animals: striking similarities and obvious differences. *Immunological Reviews, 198,* 249-266.

Ohyanagi, T. and Matsushima, N. (1997). Classification of tandem leucine-rich repeats within a great variety of proteins. *FASEB Journal*, *11*, A949.

Okun, E., Griffioen, K. J., Lathia, J. D., Tang, S-C., Mattson, M. P., Arumugam, T. V. (2009). Toll-like receptors in neurodegeneration. *Brain Research Reviews, 59*, 278 292.

Olesen, S. P., Munch, E., Watjen, F., Drejer, J. (1994). NS 004 an activator of Ca2+-dependent K+ channels in cerebellar granule cells. *NeuroReport, 5*, 1001 1004.

Orio, P., Rojas, P., Ferreira, G., Latorre, R. (2002). New disguises for an old channel: MaxiK channel beta-subunits. *News in Physiological Sciences, 17,* 156-171.

Pallanck, L., Ganetzky, B. (1994). Cloning and characterization of human and mouse homologs of the Drosophila calcium-activated potassium channel gene, slowpoke. *Human Molecular Genetics, 3,* 1239 1243.

Pantazis, A. and Olcese, R. (2012). Relative transmembrane segment rearrangements during BK channel activation resolved by structurally assigned fluorophore quencher pairing. *The Journal of General Physiology, 140*(2), 207 218.

Pantazis, A., Kohanteb, A. P., Olcese, R. (2010). Relative motion of transmembrane segments S0 and S4 during voltage sensor activation in the human BK_{Ca} channel. *The Journal of General Physiology,136*(6), 645-657.

Pepinsky, R. B., Arndt, J. W., Quan, C., Gao, Y., Quintero-Monzon, O., Lee, X., Mi, S. (2014). Structure of the LINGO-1-Anti-LINGO-1 Li81 Antibody Complex Provides Insights into the Biology of LINGO-1 and the Mechanism of Action of the Antibody Therapy. *Journal of Pharmacology and Experimental Therapeutics, 350*(1), 110 123.

Petkov, G. V. (2014). Central role of the BK channel in urinary bladder smooth muscle physiology and pathophysiology. *American Journal of Physiology-Regulatory, Integrative and Comparative Physiology, 307*, R571 R584.

Pisupati, A., Mickolajczyk, K.J., Horton, W., van Rossum, D.B., Anishkin, A., Chintapalli, S.V., Li, X., Chu-Luo, J., Busey, G., Hancock, W.O., Jegla, T. (2018). The S6 gate in regulatory K_v6 subunits restricts heteromeric K^+ channel stoichiometry. *The Journal of General Physiology, 150* (12) 1702-1721.

Quirk, J. C. and Reinhart, P. H. (2001). Identification of a Novel Tetramerization Domain in Large Conductance K_{Ca} Channels. *Neuron, 32*(11), 13-23.

Revermann, M., Neofitidou, S., Kirschning, T., Schloss, M., Brandes, R. P., Hofstetter, C. (2014). Inhalation of the BK(Ca)-opener NS1619 attenuates right ventricular pressure and improves oxygenation in the rat monocrotaline model of pulmonary hypertension. *PloS One, 9*, e86636.

Robitaille, R., Garcia, M. L., Kaczorowski, G. J., Charlton, M. P. (1993). Functional colocalization of calcium and calcium-gated potassium channels in control of transmitter release. Neuron, 11(4), 645-655.

Romi-Lebrun, R., Lebrun, B., Martin-Eauclaire, M. F., Ishiguro, M., Escoubas, P., Wu, F. Q., Hisada, M., Pongs, O., Nakajima, T. (1997). Purification, characterization, and synthesis of three novel toxins from the Chinese scorpion Buthus martensi, which act on K+ channels. *Biochemistry, 36*(44), 13473-13482.

Rothberg, B. S. and Magleby, K. L. (1999). Gating kinetics of single large- conductance Ca^{2+}-activated K^+ channels in high Ca^{2+} suggest a two-tiered allosteric gating mechanism. *The Journal of Physiology*, *114*, 93 124.

Rothberg, B. S. and Magleby, K. L. (2000). Voltage and Ca^{2+} activation of single large-conductance Ca^{2+}- activated K^+ channels described by a two-tiered allosteric gating mechanism. *The Journal of Physiology*, *116*, 75 100.

Roy, S., Large, R. J., Akande, A. M., Kshatri, A., Webb, T. I., Domene, C., Sergeant, G. P., McHale, N. G., Thornbury, K. D., Hollywood, M. A. (2014). Development of GoSlo-SR-5-69, a potent activator of large conductance Ca^{2+}-activated K^+ (BK) channels. *European Journal of Medicinal Chemistry, 75,* 426-437.

Roy, S., Morayo Akande, A., Large, R. J., Webb, T. I., Camarasu, C., Sergeant, G. P., McHale, N. G., Thornbury, K. D., Hollywood, M. A. (2012). Structure-activity relationships of a novel group of large-conductance Ca^{2+}-activated K^+ (BK) channel modulators: the GoSlo-SR family. *ChemMedChem, 7*, 1763 1769.

Saha, N., Kolev, M., Nikolov, D. B. (2014). Structural features of the Nogo receptor signaling complexes at the neuron/myelin interface. *Neural Regeneration Research, 87*, 1 7.

Sailer, C. A., Kaufmann, W. A., Kogler, M., Chen, L., Sausbier, U., Ottersen, O, P., Ruth, P., Shipston, M, J., Knaus, H, G. (2006). Immunolocalization of BK channels in hippocampal pyramidal neurons. *European Journal of Neuroscience*, *24*, 442 454.

Salkoff, L., Butler, A., Ferreira, G., Santi, C. and Wei, A. (2006). High-conductance potassium channels of the SLO family. *Nature Reviews Neuroscience, 7,* 921 931.

Sausbier, M., Hu, H., Arntz, C., Feil, S., Kamm, S., Adelsberger, H. (2004). Cerebellar ataxia and Purkinje cell dysfunction caused by Ca2+-activated K+ channel deficiency. *Proceedings of the National Academy of Sciences of the USA, 101*, 9474 9478.

Savalli, N., Kondratiev, A., Toro, L., Olcese, R. (2006). Voltage-dependent conformational changes in human Ca^{2+-} and voltage-activated K^+ channel, revealed by voltage-clamp fluorometry. *Proceedings of the National Academy of Sciences of the USA, 103*(33), 12619 12624.

Savalli, N., Pantazis, A., Yusifov, T., Sigg, D., Olcese, R. (2012). The contribution of RCK domains to human BK channel allosteric activation. *Journal of Biological Chemistry*, *287*, 21741 21750.

Schoenmakers, T. J., Visser, G. J., Flik, G., Theuvenet, A. P. (1992). CHELATOR: an improved method for computing metal ion concentrations in physiological solutions. *Biotechniques, 6*, 870-879.

Schreiber, M. and Salkoff, L. (1997). A novel calcium-sensing domain in the BK channel. *Biophysical Journal, 73*, 1355 1363.

Schreiber, M., Wei, A., Yuan, A., Gaut, J., Saito, M., Salkoff, L. (1998). Slo3, a Novel pH-sensitive K^+ Channel from Mammalian Spermatocytes. *The Journal of Biological Chemistry, 273*(6), 3509-3516.

Seiler, S. and Widme, H. R. (2015). Nogo-A and its functions beyond axonal inhibition: the controversial role of Nogo-A in Parkinson's disease. *Neural Regeneration Research, 10*(8), 1223 1224.

Shi, J., Krishnamoorthy, G., Yang, Y., Hu, L., Chaturvedi, N., Harilal, D., Qin, J., Cui. J. (2002). Mechanism of magnesium activation of calcium-activated potassium channels. *Nature, 418*, 876 880.

Solaro, C. R. and Lingle, C. J. (1992). Trypsin-sensitive, rapid inactivation of a calcium-activated potassium channel. *Science, 257,* 1694 1698.

Solaro, C. R., Ding, J. P., Li, Z. W., Lingle, C. J. (1997). The cytosolic inactivation domains of BK_i channels in rat chromaffin cells do not behave like simple, open-channel blockers. *Biophysical Journal, 73*, 819 830.

Soler-Llavina, G. J., Chang, T. H., Swartz, K. J. (2006). Functional Interactions at the Interface between Voltage-Sensing and Pore Domains in the Shaker K_v Channel. *Neuron, 52*, 623 634.

Soroka, V., Kolkova, K., Kastrup, J., Diederichs, K., Breed, J., Kiselyov, V., Poulsen, F., Larsen, I., Welte, W., Berezin, V., Bock, E., Kasper, C. (2003). Structure and Interactions of NCAM Ig1-2-3 Suggest a Novel Zipper Mechanism for Homophilic Adhesion. *Structure, 11*, 1291 1301.

Sousa, I., Clark, T. G., Holt, R., Pagnamenta, A. T., Mulder, E. J., Ruud B Minderaa, R. B., Bailey, A. J., Battaglia, A., Klauck, S. M., Poustka, F., Monaco, A. P. (2010). Polymorphisms in leucine-rich repeat genes are associated with autism spectrum disorder susceptibility in populations of European ancestry. *Molecular Autism, 1*(7), 1-14.

Swensen, A. M., and Bean, B. P. (2003). Ionic mechanisms of burst firing in dissociated Purkinje neurons. *Journal of Neuroscience, 23*, 9650 9663.

Tao, J., Zhou, Z. L., Wu, B., Shi, J., Chen, X. M., Ji, Y. H. (2014). Recombinant expression and functional characterization of martentoxin: a selective inhibitor for BK channel (alpha + beta4). *Toxins (Basel), 6,* 1419 1433.

Tao, X. and MacKinnon, R. (2019). Molecular structures of the human Slo1 K^+ channel in complex with b4. *eLife, 8*, e51409-51436.

Tao, X., Hite, R. K., MacKinnon, R. (2017). Cryo-EM structure of the open high-conductance Ca^{2+} -activated K^+ channel. *Nature, 541*, 46-51.

Tian, C., Zhu, R., Zhu, L., Qiu, T., Cao, Z., Kang, T. (2014). Potassium Channels: Structures, Diseases, and Modulators. *Chemical Biology and Drug Design. 83*, 1-26.

Tian, Y., Heinemann, S. H., Hoshi, T. (2019). Large-conductance Ca^{2+}- and voltage-gated K^+ channels form and break interactions with membrane lipids during each gating cycle. *Proceedings of the National Academy of Sciences of the USA, 116*(17), 8591 8596.

Tristani-Firouzi, M., Chen, J., Sanguinetti, M. C. (2002). Interactions between S4-S5 Linker and S6 Transmembrane Domain Modulate Gating of HERG K^+ Channels. *The Journal of Biological Chemistry, 277*(21), 18994-19000.

Uebele, V. N., Lagrutta, A., Wade, T., Figueroa, D. J., Liu, Y., McKenna, E., Austin, C. P., Bennet, P. B., Swanson R. (2000). Cloning and functional expression of two families of -subunits of the large conductance calcium-activated K^+ channel. *Journal of Biological Chemistry, 275* (30), 23211-23218.

Uhlén, M., Fagerberg, L., Hallström, B. M., Lindskog, C., Oksvold, P., Mardinoglu, A., Sivertsson, A., Kampf, C., Sjöstedt, E., Asplund, A., Olsson, I., Edlund, K., Lundberg, E., Navani, S., Szigyarto, C. A., Odeberg, J., Djureinovic, D., Takanen, J. O., Hober, S., Alm, T., Edqvist, P. H., Berling, H., Tegel, H., Mulder, J., Rockberg, J., Nilsson, P., Schwenk, J. M., Hamsten, M., Feilitzen, K. V., Forsberg, M., Persson, L., Johansson, F., Zwahlen, M., Heijne, G. V., Nielsen, J., Pontén, F. (2015). Tissue-based map of the human proteome. *Science, 347(6220),* 1260419 (1-9).

Valverde, M. A., Rojas, P., Amigo, J., Cosmelli, D., Orio, P., Bahamonde, M. I., Mann, G. E., Vergara, C., Latorre, R. (1999). Acute activation of Maxi-K channels (hSlo) by estradiol binding to the beta subunit. *Science, 285*, 1929 1931.

Vilariño-Güell, C., Wider, C., Ross, O. A., Jasinska-Myga, B., Kachergus, J., Cobb, S. A., Soto-Ortolaza, A. I., Behrouz, B., Heckman, M. G., Diehl, N. N., Testa, C. M., Wszolek, Z. K., Uitti, R. J., Jankovic, J., Louis, E. D., Clark, L. N., Rajput, A., & Farrer, M. J. (2010). LINGO1 and LINGO2 variants are associated with essential tremor and Parkinson disease. *Neurogenetics, 11(4)*, 401 408.

Vouga, A. G., Rockman, M. E., Yan, J., Jacobson, M. A., Rothberg, B. S. (2021). State-dependent inhibition of BK channels by the opioid agonist loperamide. *Journal of General Physiology, 153*(9), e202012834.

Wallner, M., Meera, P., Toro, L. (1996). Determinant for b-subunit regulation in high-conductance voltage-activated and Ca^{2+}-sensitive K^+ channels: An additional transmembrane region at the N terminus. *Proceedings of the National Academy of Sciences of the USA, 93*, 14922 14927.

Wallner, M., Meera, P., Toro, L. (1999). Molecular basis of fast inactivation in voltage and Ca^{2+} activated K^+ channels: a transmembrane beta-subunit homolog. *Proceedings of the National Academy of Sciences of the USA, 96*, 4137 4142.

Wang, B., Brenner, R. (2006). An S6 mutation in BK channels reveals beta1 subunit effects on intrinsic and voltage-dependent gating. *The Journal of General Physiology, 128*, 731 744.

Wang, J., Shen, B., Guo, M., Lou, X., Duan, Y., Cheng, X. P., Teng, M., Niu, L., Liu, Q., Huang, Q., Hao, Q. (2005). Blocking effect and crystal structure of natrin toxin, a cysteine-rich secretory protein from Naja atra venom that targets the BKCa channel. *Biochemistry, 44*(30), 10145-10152.

Wang, L. and Sigworth, F. J. (2009). Structure of the BK potassium channel in a lipid membrane from electron cryomicroscopy. *Nature, 461*, 292-295.

Webster, S. M., DelCamino, D., Dekker, J. P., Yellen, G. (2004). Intracellular gate opening in Shaker K^+ channels defined by high-affinity metal bridges. *Nature, 428,* 864 868.

Wei, A., Jegla, T., Salkoff, L. (1996). Eight potassium channel families revealed by the C. elegans genome project. *Neuropharmacology, 35*(7), 805-829.

Weiger, T. M., Holmqvist, M. H, Levitan, I. B., Clark, F. T., Sprague, S., Huang, W. J., Ge, P., Wang, C., Lawson, D., Jurman, M. E., Glucksmann, M. A., Silos-Santiago, I., DiStefano, P. S., Curtis, R. (2000). A novel nervous system beta subunit that downregulates human large conductance calcium-dependent potassium channels. *Journal of Neuroscience, 20*, 3563 3570.

Wilkens, C. M. and Aldrich, R. W. (2006). State-independent block of BK channels by an intracellular quaternary ammonium. *The Journal of General Physiology*, *128*, 347 364.

Wu, R. S., Chudasama, N., Zakharov, S. I., Doshi, D., Motoike, H., Liu, G., Yao, Y., Niu, X., Deng, S. X., Landry, D. W., Karlin, A., Marx, S. O. (2009). Location of the b4 transmembrane helices in the BK potassium channel. *The Journal of Neuroscience, 29*, 8321 8328.

Wu, R. S., Liu, G., Zakharov, S. I., Chudasama, N., Motoike, H., Karlin, A., Marx, S. O. (2013). Positions of b2 and b3 subunits in the large-conductance calcium- and voltage-activated BK potassium channel. *The Journal of General Physiology, 141*, 105 117.

Wu, S. N., Liu, S. I., Huang, M. H. (2004). Cilostazol, an inhibitor of type 3 phosphodiesterase, stimulates large-conductance, calcium-activated potassium channels in pituitary GH3 cells and pheochromocytoma PC12 cells. *Endocrinology, 145*, 1175 1184.

Wu, Y. W., Prakash, K. M., Rong, T. Y., Li, H. H., Xiao, Q., Tan, L. C., Au, W. L., Ding, J. Q., Chen, S. D., Tan, E. K. (2011). Lingo2 variants associated with essential tremor and *Human Genetics, 129*, 611 615.

Wu, Y., Xiong, Y., Wang, S., Yi, H., Li, H., Pan, N., Horrigan, F. T., Ding, J. (2009). Intersubunit coupling in the pore of BK channels. *The Journal of Biological Chemistry, 284*, 23353 23363.

Wu, Y., Yang, Y., Ye, S., Jiang, Y. (2010). Structure of the Gating Ring from the Human High-conductance Ca^{2+}-gated K^+ Channel. *Nature, 466*(7304), 393 397.

Xia, X. M., Ding, J. P., Lingle, C. J. (1999). Molecular basis for the inactivation of Ca^{2+}- and voltage-dependent BK channels in adrenal chromaffin cells and rat insulinoma tumor cells. *Journal of Neuroscience, 19*, 5255 5264.

Xia, X. M., Ding, J. P., Lingle, C. J. (2003). Inactivation of BK channels by the NH2 terminus of the beta2 auxiliary subunit: an essential role of a terminal peptide segment of three hydrophobic residues. *Journal of General Physiology, 121*,125 148.

Xia, X. M., Ding, J. P., Zeng, X. H., Duan, K. L., Lingle, C. J. (2000). Rectification and rapid activation at low Ca^{2+} of Ca^{2+} -activated, voltage-dependent BK currents: consequences of rapid inactivation by a novel beta subunit. *Journal of Neuroscience, 20*, 4890 4903.

Xia, X. M., Zeng, X., Lingle, C. J. (2002). Multiple regulatory sites in large-conductance calcium activated potassium channels. *Nature, 418*, 880 884.

Yan, J. and Aldrich, R. W. (2010). LRRC26 auxiliary protein allows BK channel activation of resting voltage without calcium. *Nature, 466*(7305), 513-516.

Yan, J. and Aldrich, R. W. (2012). BK potassium channel modulation by leucine-rich repeat containing proteins. *Proceedings of the National Academy of Sciences of the USA*, *109*(20), 7917-7922.

Yang, H., Shi, J., Zhang, G., Yang, J., Delaloye, K., Cui, J. (2008). Activation of Slo1 BK channels by Mg^{2+} coordinated between the voltage sensor and RCK1 domains. *Nature Structural and Molecular Biology, 15,* 1152 1159.

Yang, H., Zhang, G., Cui, J. (2015). BK channels: multiple sensors, one activation gate. *Frontiers in physiology, 6*, 1-16.

Yang, J., Krishnamoorthy, G., Saxena, A., Zhang, G., Shi, J, Yang, H., Delaloye, K., Sept, D., Cui, J. (2010). An Epilepsy/Dyskinesia-Associated Mutation Enhances BK Channel Activation by Potentiating Ca^{2+} Sensing. *Neuron, 66,* 871 883.

Yang, Y., Li, P. Y., Cheng, J., Mao, L., Wen, J., Tan, X. Q., Liu, Z. F, Zeng, X. R. (2013). Function of BK_{Ca} channels is reduced in human vascular smooth muscle cells from Han Chinese patients with hypertension. *Hypertension, 61*, 519 525.

Yao, J., Chen, X., Li, H., Zhou, Y., Yao, L., Wu, G., Chen, X., Zhang, N., Zhou, Z., Xu, T., Wu, H., Ding, J. (2005). BmP09, a "long chain" scorpion peptide blocker of BK channels. *Journal of Biological Chemistry, 280*(15),14819-14828.

Yazdani, M., Zhang, G., Jia, Z., Shi, J., Cui, J., Chen, J. (2020). Nonspecific Membrane Interactions Can Modulate BK Channel Activation. *bioRxiv,* 936161-936196.

Yin, W. and Hu, B. (2014). Knockdown of Lingo1b protein promotes myelination and oligodendrocyte differentiation in zebrafish. *Experimental Neurology, 251*, 72-83.

Yu, M., Liu, S. L., Sun, P. B., Pan, H., Tian, C. L., Zhang, L. H. (2016). Peptide toxins and small-molecule blockers of BK channels. *Acta Pharmacologica Sinica, 37*(1), 56 66.

Yuan, P., Leonetti, M. D., Hsiung, Y., MacKinnon, R. (2012). Open structure of the Ca^{2+} gating ring in the high-conductance Ca^{2+}-activated K^{+} channel. *Nature, 481*, 94 97.

Yuan, P., Leonetti, M. D., Pico, A R., Hsiung, Y., MacKinnon, R. (2010). Structure of the Human BK Channel Ca^{2+}-Activation Apparatus at 3.0 Å Resolution. *Science, 329*, 182-186.

Yusifov, T., Javaherian, A. D., Pantazis, A., Gandhi, C. S., Olcese, R. (2010). The RCK1 domain of the human BK_{Ca} channel transduces Ca^{2+} binding into structural rearrangements. *The Journal of General Physiology*, *136*, 189 202.

Yusifov, T., Savalli, N., Gandhi, C. S., Ottolia, M., Olcese, R. (2008). The RCK2 domain of the human BK_{Ca} channel is a calcium sensor. *Proceedings of the National Academy of Sciences of the USA*, *105*, 376 381.

Zagotta, W. N., Hoshi, T., Aldrich R. W. (1990). Restoration of inactivation in mutants of Shaker potassium channels by a peptide derived from ShB. *Science, 250*, 568-571.

Zakharov, S. I., Morrow, J. P., Liu, G., Yang, L., Marx, S. O. (2005). Activation of the BK (SLO1) potassium channel by mallotoxin. *Journal Of Biological Chemistry*, *280(35)*, 30882 30887.

Zhang, G., Geng, Y., Jin, Y., Shi, J., McFarland, K., Magleby, K. L., Salkoff, L., Cui, J. (2017). Deletion of cytosolic gating ring decreases gate and voltage sensor coupling in BK channels. *Journal of General Physiology, 149(3)*, 373-387.

Zhang, G., Huang, S. Y., Yang, J., Shi, J., Yang, X., Moller, A., Zou, X., Cui, J. (2010). Ion sensing in the RCK1 domain of BK channels. *Proceedings of the National Academy of Sciences of the USA, 107*(43), 18700-18705.

Zhang, J., Yan, J. (2014). Regulation of BK channels by auxiliary gamma subunits. *Frontiers in Physiology, 5*(401)*,* 1-7.

Zhang, Y.Y., Han, X., Liu, Y., Chen, J., Hua, L., Ma, Q., Huang, Y. Y. X., Tang, Q. Y., Zhang, Z. (2018). +mRNA expression of LRRC55 protein (leucine-rich repeat-containing protein 55) in the adult mouse brain. *PLOS ONE, 13*(1), 1-10.

Zhou, M., Morais-Cabral, J. H., Mann, S., & MacKinnon, R. (2001). Potassium channel receptor site for the inactivation gate and quaternary amine inhibitors. *Nature, 411*(6838), 657 661.

Zhou, Y, Lingle, C. J. (2014). Paxilline inhibits BK channels by an almost exclusively closed-channel block mechanism. *Journal of General Physiology, 144*(5), 415-440.

Zhou, Y., Xia, X. M., Lingle, C. J. (2011). Cysteine scanning and modification reveal major differences between BK channels and K_V channels in the inner pore region. *Proceedings of the National Academy of Sciences of the USA*, *108*,12161-12166.

Zullo, K. M., Ji, Y., Wei, Y., Herbine, K., Maloney, N., Cohen, R., Pastore, C., Samsouk, M., Srivatsa, S., Hung, L. Y., Kohanski, M. H., Cohen, N. A., Herbert, D. R. (2018). LINGO3 interacts with Trefoil factor 2 to enforce mucosal barrier integrity and drive tissue repair during colitis. *BioRxiv, 469684,* 1-20.